frontiers | Research Topics

# Radiotherapy for brain metastases

**Edited by**
Xiangpan Li, Meng Xu Welliver and Yirui Zhai

**Published in**
Frontiers in Oncology

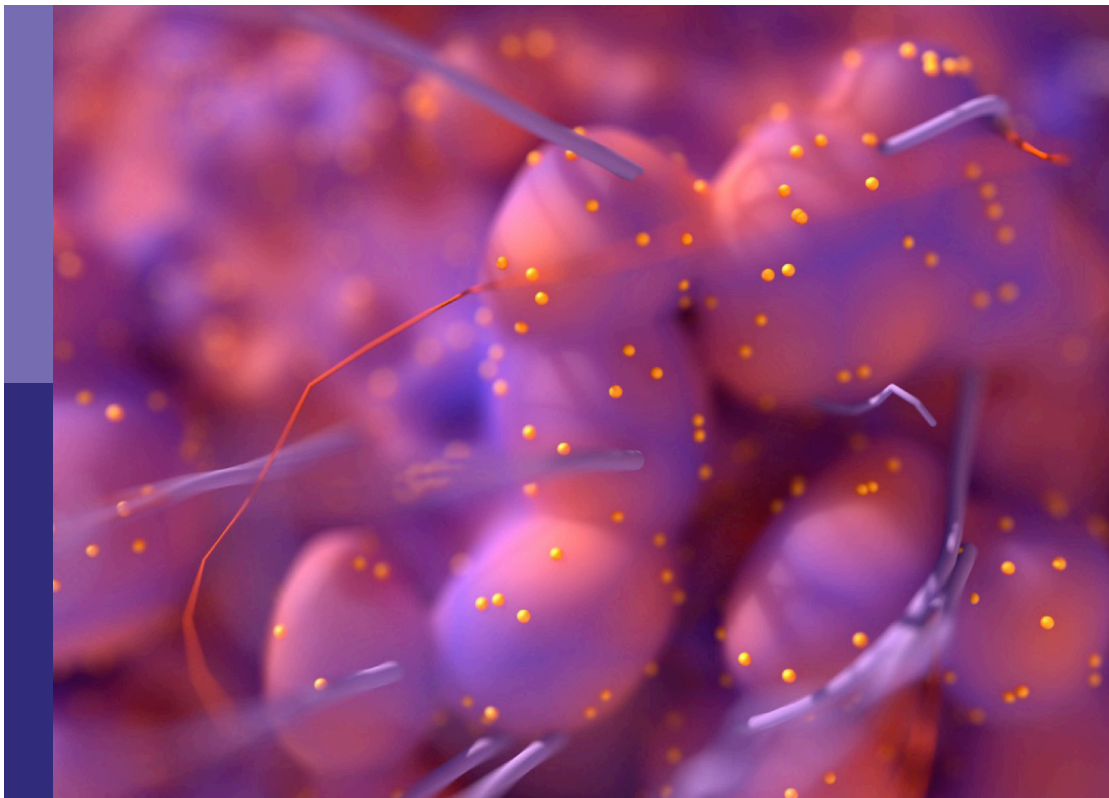

ISSN 1664-8714
ISBN 978-2-8325-5682-5
DOI 10.3389/978-2-8325-5682-5

## About Frontiers

Frontiers is more than just an open access publisher of scholarly articles: it is a pioneering approach to the world of academia, radically improving the way scholarly research is managed. The grand vision of Frontiers is a world where all people have an equal opportunity to seek, share and generate knowledge. Frontiers provides immediate and permanent online open access to all its publications, but this alone is not enough to realize our grand goals.

## Frontiers journal series

The Frontiers journal series is a multi-tier and interdisciplinary set of open-access, online journals, promising a paradigm shift from the current review, selection and dissemination processes in academic publishing. All Frontiers journals are driven by researchers for researchers; therefore, they constitute a service to the scholarly community. At the same time, the *Frontiers journal series* operates on a revolutionary invention, the tiered publishing system, initially addressing specific communities of scholars, and gradually climbing up to broader public understanding, thus serving the interests of the lay society, too.

## Dedication to quality

Each Frontiers article is a landmark of the highest quality, thanks to genuinely collaborative interactions between authors and review editors, who include some of the world's best academicians. Research must be certified by peers before entering a stream of knowledge that may eventually reach the public - and shape society; therefore, Frontiers only applies the most rigorous and unbiased reviews. Frontiers revolutionizes research publishing by freely delivering the most outstanding research, evaluated with no bias from both the academic and social point of view. By applying the most advanced information technologies, Frontiers is catapulting scholarly publishing into a new generation.

## What are Frontiers Research Topics?

Frontiers Research Topics are very popular trademarks of the *Frontiers journals series*: they are collections of at least ten articles, all centered on a particular subject. With their unique mix of varied contributions from Original Research to Review Articles, Frontiers Research Topics unify the most influential researchers, the latest key findings and historical advances in a hot research area.

Find out more on how to host your own Frontiers Research Topic or contribute to one as an author by contacting the Frontiers editorial office: frontiersin.org/about/contact

# Radiotherapy for brain metastases

**Topic editors**

Xiangpan Li — Renmin Hospital of Wuhan University, China

Meng Xu Welliver — Mayo Clinic, United States

Yirui Zhai — Chinese Academy of Medical Sciences and Peking Union Medical College, China

**Citation**

Li, X., Welliver, M. X., Zhai, Y., eds. (2024). *Radiotherapy for brain metastases*. Lausanne: Frontiers Media SA. doi: 10.3389/978-2-8325-5682-5

# Table of contents

frontiers | Frontiers in Oncology

TYPE Methods
PUBLISHED 30 June 2023
DOI 10.3389/fonc.2023.1216852



OPEN ACCESS

EDITED BY
Xiangpan Li,
Renmin Hospital of Wuhan University, China

REVIEWED BY
Feifei Teng,
Shandong University Cancer Center, China
Qinyong Hu,
Renmin Hospital of Wuhan University, China

*CORRESPONDENCE
Weiyu Shen
nblhlswy@163.com

†These authors have contributed equally to this work

RECEIVED 04 May 2023
ACCEPTED 14 June 2023
PUBLISHED 30 June 2023

CITATION
Chen T, Tang M, Zhou Y, Wang Z, Li S, Wang H, Lu Y, Wang J and Shen W (2023) Pretreatment lymphocyte-to-monocyte ratio as a prognostic factor and influence on dose-effect in fractionated stereotactic radiotherapy for oligometastatic brain metastases in non-small cell lung cancer patients. *Front. Oncol.* 13:1216852. doi: 10.3389/fonc.2023.1216852



# Pretreatment lymphocyte-to-monocyte ratio as a prognostic factor and influence on dose-effect in fractionated stereotactic radiotherapy for oligometastatic brain metastases in non-small cell lung cancer patients

Tian Chen[1†], Mengqiu Tang[1†], Yang Zhou[2], Zhepei Wang[3], Shiwei Li[4], Hongcai Wang[4], Yangfang Lu[1], Jinguo Wang[1] and Weiyu Shen[5*]

[1]Department of Radiation Oncology, Ningbo Medical Center Lihuili Hospital, Ningbo University, Ningbo, China, [2]Department of Ningbo Institute of Innovation for Combined Medicine and Engineering, Ningbo Medical Center Lihuili Hospital, Ningbo University, Ningbo, China, [3]Department of Neurosurgery, Ningbo First Hospital, Ningbo Hospital of Zhejiang University, Ningbo, China, [4]Department of Neurosurgery, Ningbo Medical Center Lihuili Hospital, Ningbo University, Ningbo, China, [5]Department of Thoracic Surgery, Ningbo Medical Center Lihuili Hospital, Ningbo University, Ningbo, China

**Background:** Studies on the prognostic factors for patients with brain oligo-metastasis treated with fractionated stereotactic radiotherapy (FSRT) usually focus on the size of metastatic tumor and radiation dose. Some inflammatory indicators have predictive value in non-small cell lung cancer (NSCLC) with brain metastasis receiving stereotactic radiotherapy. However, the prognostic value of inflammatory indicators in NSCLC patients with brain oligo-metastasis treated with FSRT, and their effect on radiotherapy dose is unknown.

**Methods:** A total of 95 advanced NSCLC patients with brain oligo-metastasis who had undergone FSRT treatment at Ningbo Medical Center Lihuili Hospital between January 2015 and April 2022 were enrolled into the study. Neutrophil to lymphocyte ratio (NLR), platelet lymphocyte ratio (PLR), lymphocyte to monocyte ratio (LMR), tumor diameter and biologically effective dose (BED10) were analyzed using Chi-square test. Univariate and multivariate Cox regressions were used to identify predictors of survival.

**Results:** Tumor diameter (< 2 cm), BED10 (≥ 48Gy) and LMR (≥ 4) were found to be independently associated with good intracranial local control survival (i-LCS) through multivariate analysis. The median i-LCS was longer in patients with 2 independent risk factors (tumor diameter ≥ 2 and LMR < 4) administered with BED10 > 53.6Gy compared with patients administered with BED10 ≤ 53.6Gy (20.7 months vs 12.0 months, $P$ = 0.042). LMR ≥ 4 ($P$ = 0.019) and positivity for driver gene mutations ($P$ = 0.011) were independently associated with better overall survival (OS).

**Conclusions:** LMR is an independent prognostic factor of i-LCS and OS in NSCLC patients with brain oligo-metastasis treated with FSRT. Patients with tumor diameter ≥ 2 and LMR < 4 should be treated with BED10 greater than 53.6Gy.

KEYWORDS

lymphocyte to monocyte ratio (LMR), biologically effective dose (BED), brain oligo-metastasis, fractionated stereotactic radiotherapy (FSRT), intracranial local control survival (i-LCS)

# Background

Brain metastases are the most common intracranial tumors in adult accounting for about 20-40 percent (1). Lung cancer is the most common primary malignant tumor that results in the brain metastases, with non-small cell lung cancer (NSCLC) accounting for more than 60 percent of the lung tumors (1, 2). The prognoses of patients with brain metastases arising from NSCLC varies greatly with the median survival time ranging from 6.9 to 46.8 months (3). Several high-technique models, such as diagnosis-specific graded prognostic assessment (DS-GPA), Graded Prognostic Assessment for Lung Cancer Using Molecular Markers (Lung-molGPA), score index for radiosurgery (SIR), and basic score for brain metastases (BSBM), are used to evaluate the prognosis of NSCLC patients (3–6), but the techniques are ineffective in evaluating the prognosis of NSCLC patients with brain oligo-metastasis treated with fractionated stereotactic radiotherapy (FSRT). FSRT has a higher local control rate and fewer side effects than stereotactic radiosurgery (SRS) therapy and has thus been widely used in the clinic. Compared with SRS therapy, FSRT showed a different biological effectiveness. For example, hypoxic tumor cells may survive after SRS, but FSRT, which is based on the principle of reoxidation, has better control rate in tumor (7), suggesting that the SIR model might not apply to the FSRT patients. There is need to identify prognostic factors for NSCLC patients with brain oligo-metastasis receiving FSRT therapy. Current studies on prognostic factors for oligo-metastasis patients treated with FSRT focus on the size of metastatic tumor and radiation dose. However, there is still no standard evaluation method for tumor size, radiation dose and fractionation scheme, with different studies suggesting different radiotherapy biologically effective dose (BED) (8–10). Therefore, there is need to develop and enhance predictive indexes indicating the efficacy and survival of NSCLC patients with brain oligo-metastasis receiving FSRT.

Since the discovery of the relationship between inflammation and cancer in 1863 by R Virchow (11), inflammatory indicators such as neutrophil-lymphocyte ratio (NLR), platelet to lymphocyte ratio (PLR), lymphocyte to monocyte ratio (LMR), regulatory T cells and peripheral memory CD4+ T cell, have been used in predicting efficacy and survival in different kinds of cancer (12–16). Inflammatory indicators have also been associated with prognosis of surgery, chemotherapy, targeted therapy, immunotherapy (17–20), and curative effect of radiotherapy (21, 22). In our previous study, we demonstrated that NLR, PLR and LMR constitute a simple and effective prediction index, in locally advanced esophageal cancer treated with surgery, and radiotherapy and in NSCLC treated with anti-vascular targeted therapy (23, 24). Several studies have also demonstrated the predictive value of some inflammatory indicators in NSCLC patients with brain metastasis receiving SRS therapy (25, 26). Although FSRT is similar to radiosurgery, the predictive value of inflammatory indicators in NSCLC patients with brain oligo-metastasis treated with FSRT and their effect on radiotherapy dose is unknown.

This study is a retrospective analysis of the association between inflammatory indicators (NLR, PLR and LMR) and the local control rate and survival of NSCLC patients with brain oligo-metastasis treated with FSRT, and their effect on radiotherapy dose.

# Materials and methods

## Patient selection

This was a retrospective study involving NSCLC patients with oligometastatic brain metastases who had been treated with FSRT at Ningbo Medical Center Lihuili Hospital between January 2015 and January 2022. The inclusion criteria was as follows: (i) pathological findings of metastatic or recurrent NSCLC; (ii) 3 or less brain metastases; (iii) FSRT used to treat brain metastases; (iv) availability of results for routine blood tests carried out two weeks prior to treatment. The exclusion criteria was as follows: (i) co-administration of FSRT and targeted drugs (osimertnib, almonertinib, furmonertinib, alectinib) during the stable disease stage; (ii) assessable focus was treated with FSRT previously; (iii) lack of relevant hematological data within 2 weeks prior to FSRT treatment; (iv) in an acute infection state when obtaining blood inflammation indicators; (v) absence of efficacy evaluation and follow-up information. In the end, 95 patients were enrolled into the study.

## Fractionated stereotactic radiotherapy technique

The FSRT treatment plan was based on the preference of the attending physician because the tumors were located near or within a critical structure. The head was first immobilized with an aquaplast, and then a computed tomography (CT) scan with intravenous contrast was acquired to plan radiotherapy. Fusing magnetic resonance (MR) T1-weighted imaging with CT images within two weeks of treatment planning. In CT and MR images, the gross tumor volume (GTV) was defined as the contrast medium-enhancing tumor, the clinical target volume (CTV) represented the GTV, while the planning target volume (PTV) was considered as CTV plus a 2-4mm margin. A single split dose of FSRT was set from 3.5-7Gy. Approximately 90% of the maximum dose was applied to the peripheral area, and 95% of the PTV was covered by the peripheral dose. Radiation therapy was administered 5 times a week. We evaluated the dose response of various FSRT fractionation schedules according to a biologically effective dose using an alpha/beta ratio of 10 (BED10) as a measure of the biological effectiveness of the treatment.

## Analysis of laboratory parameters

The following hematology indexes were evaluated up to 2 weeks prior to FSRT: neutrophil count ($\times 10^9$/L), platelet count ($\times 10^9$/L), lymphocyte count ($\times 10^9$/L) and monocytes count ($\times 10^9$/L). NLR was defined as the neutrophil count divided by the lymphocyte count. Similarly, PLR was the ratio of the platelet count to the lymphocyte count, LMR was the ratio of the lymphocyte count to the monocytes count. The cutoff values were defined as 5, 180 and 4 for NLR, PLR, and LMR, respectively (25, 27–29). For tumor diameter, the cut off value was 2cm (median tumor diameter), and for BED 10, the cut off value was 48 Gy.

## Outcome evaluation and statistics

Taking brain enhanced MR re-examination after FSRT in 1-2 months, subsequently checking per 2-3 months, checking enhanced MR immediately at the appearance of intracranial hypertension or neuropsychiatric symptoms. Intracranial local control (i-LC) was defined as no significant increase in the size tumor lesion treated with FSRT on follow-up MR. Intracranial local control survival (i-LCS) was the primary end point of assessment. It was defined as the time from the start of radiation therapy to the time enlargement of the tumor treated with FSRT was observed. Overall survival (OS) was calculated from the date of initiation of FSRT to the time of death from any reason or last time of follow up. OS was the secondary end point of assessment.

The statistical analyses were performed using a social science statistical software package, version 26.0 (SPSS Inc., Chicago, IL, US). Chi-squared tests were used to analyze categorical variables. A Kaplan-Meier survival curve was plotted and compared with a log-rank-test curve. Factors for survival were identified using univariate and multivariate Cox regression analyses. Statistical significance was deemed to be a $P$-value < 0.05.

# Results

## Patient characteristics and curative effect

The median age of the study participants was 63 years (range from 37 to 79 years).Adenocarcinoma was the most common type of cancer (n = 79, 83.2%), with 13 patients having squamous cell carcinomas, 2 patients having poorly differentiated carcinoma, and 1 patient having large cell carcinoma. Only 11 patients had karnofsky performance status (KPS) scores less than 80, while the rest had scores greater than or equal to 80. The maximum diameter of intracranial metastases ranged from 0.6 to 6.4cm, with a median diameter of 2.0cm. A total of 38 patients (40.0%) had confirmed EGFR mutations, 3 patients (5.1%) had ALK rearrangement and one patient had MET-14 jumping mutation. Most of the patients had no history of brain radiotherapy (n = 84, 88.4%). The median BED10 was 53.6Gy (range from 37.5 to 85.1 Gy) and the number of splits was 5-18. The detailed information of patient characteristics and baseline data are shown in Table 1.

The follow-up time ranged from 3.0 to 37.7 months, with a median of 20.6 months. The local control rates at 6 and 12 months were 82.9% and 66.5%, respectively. The median i-LCS and OS were 15.8 months and 19.4 months, respectively. (Figure S1A, B).

## Factors associated with intracranial local control survival and their effect on radiotherapy dose

Univariate analyses found that tumor diameter, BED10, PLR and LMR were significant risk factors for i-LCS. Other factors including age, gender, number of brain metastases and presence of extracranial metastasis at diagnosis were not associated with i-LCS in univariate analyses (Table 2). Median i-LCS was significantly shorter in patients with tumor diameter ≥ 2 cm, compared to patients with smaller tumors (13.7 months vs. 31.5 months, HR: 2.595, 95% CI: 1.417-4.750, P = 0.002) (Figure 1A). Median i-LCS was significantly longer in patients with BED10 ≥ 48Gy, compared to patients with less BED10 (17.0 months vs 5.5 months, HR: 0.241, 95% CI: 0.124-0.468, $P$ = 0.001) (Figure 1B). Median i-LCS was significantly longer among patients with PLR ≥ 180, compared to patients with lower values (10.7 months vs 16.5 months, HR: 2.023, 95% CI: 1.116-3.669, $P$ = 0.020) (Figure 1C). Median i-LCS was significantly longer in patients with LMR ≥ 4, compared to patients with lower values (not reached vs 14.0 months, HR: 0.306, 95% CI: 0.147-0.636, $P$ = 0.001) (Figure 1D). The results of multivariate analysis demonstrated that tumor diameter (< 2 cm), BED10 (≥ 48Gy) and LMR (≥ 4) were independently associated with good i-LCS (Table 3).

We then evaluated the effect of the independent prognostic factors on radiotherapy among the patients with BED10 ≥ 48Gy. In total, 49 patients had BED10 ≥ 48Gy, with the median BED10 being

10.3389/fonc.2023.1216852

TABLE 1 Basic characteristics of non-small cell lung cancer patients with oligometastatic brain metastases.

| Characteristics | Patients (%) |
|---|---|
| Age (years) | |
| Median | 63 years |
| Range | 37-79 |
| < 65 | 55 (57.9%) |
| ≥ 65 | 40 (42.1%) |
| Gender | |
| Male | 45 (47.4%) |
| Female | 50 (52.6%) |
| Karnofsky performance status (%) | |
| ≥ 80 | 84 (88.4%) |
| < 80 | 11 (11.6%) |
| Histologic subtype | |
| Adenocarcinoma | 79 (83.2%) |
| Squamous cell carcinoma | 13 (13.7%) |
| Other | 3 (3.1%) |
| Driver gene mutation | |
| Positive | 42 (44.2%) |
| Negative or unknown | 53 (55.8%) |
| Number of brain metastases | |
| 1 | 71 (74.7%) |
| 2-3 | 24 (25.3%) |
| Localization of brain metastases | |
| Supratentorial | 81 (85.3%) |
| Infratentorial | 14 (14.7%) |
| CNS treatment before FSRT | |
| None | 84 (88.4%) |
| WBRT | 4 (4.2%) |
| FSRT not in this location of metastases | 7 (7.4%) |
| Extracranial metastases | |
| Yes | 74 (77.9%) |
| No | 21 (22.1%) |
| Maximum diameter of brain metastases (cm) | |
| Median | 2.0 |
| Range | 0.6-6.4 |
| >2 | 44 (46.3%) |
| ≥2 | 51 (53.7%) |
| BED10 of FSRT (Gy) | |
| Median | 53.6 |
| Range | 37.5-85.1 |
| >48 | 16 (16.8%) |
| 48-53.6 | 50 (52.6%) |
| <53.6 | 29 (30.6%) |
| NLR | |
| Median | 2.75 |
| Range | 0.78-9.25 |
| >5 | 70 (73.7%) |
| ≥5 | 25 (26.3%) |
| PLR | |
| Median | 152.00 |
| Range | 52.38-698.00 |
| >180 | 65 (68.4%) |
| ≥180 | 30 (31.6%) |
| LMR | |
| Median | 2.57 |
| Range | 0.83-16.00 |
| >4 | 67 (70.5%) |
| ≥4 | 28 (29.5%) |

*(Continued)*

TABLE 1 Continued

FSRT fractionated stereotactic radiotherapy, WBRT whole brain radiation therapy, BED10 biologically effective dose (α/β = 10), NLR neutrophil to lymphocyte ratio, PLR platelet lymphocyte ratio, LMR lymphocyte to monocyte ratio.

53.6Gy. Surprisingly, in patients with 2 independent risk factors (tumor diameter ≥ 2 and LMR < 4), the i-LCS was longer in patients with BED10 greater than 53.6Gy, compared to patients with BED10 less than 53.6Gy (20.7 months vs 12.0 months, HR: 0.290, 95% CI: 0.082-1.030, $P$ = 0.042) (Figure 2A). There was no significant difference in i-LCS among patients with different BED10 values and with only 1 independent risk factor ($P$ = 0.101, Figure 2B)

## Factors associated with overall survival

Results of univariate analysis revealed that driver gene mutations, PLR< 180 and LMR ≥ 4 were associated with better OS, but not BED10 (Table 2). Patients positive for driver gene mutations had longer median OS than patients negative for driver gene mutations or with unknown mutations (30.0 months vs 15.0 months, HR: 0.417, 95% CI: 0.226-0.769, $P$ = 0.005) (Figure 3A). The median OS of patients with PLR <180 was significantly shorter compared to patients with higher values (14.8 months vs 20.5 months, HR: 1.856, 95% CI: 1.024-3.366, $P$ = 0.042) (Figure 3B). The median OS of patients with LMR ≥ 4 was significantly longer compared to patients with lower values (32.4 months vs 16.8 months, HR: 0.408, 95% CI: 0.197-0.843, $P$ = 0.015) (Figure 3C).

10.3389/fonc.2023.1216852

TABLE 2 Univariate analysis of factors associated with intracranial local control survival and overall survival.

| Prognostic factors | Intracranial local control survival | | | Overall survival | | |
|---|---|---|---|---|---|---|
| | HR | 95% CI | *P*-value | HR | 95% CI | *P*-value |
| Age (years) | | | | | | |
| < 65 | 1 | | | 1 | | |
| ≥ 65 | 0.948 | 0.536-1.677 | 0.855 | 0.891 | 0.497-1.596 | 0.698 |
| Gender | | | | | | |
| Female | 1 | | | 1 | | |
| Male | 0.981 | 0.558-1.724 | 0.946 | 1.185 | 0.673-2.086 | 0.557 |
| KPS (%) | | | | | | |
| < 80 | 1 | | | 1 | | |
| ≥ 80 | 0.689 | 0.321-1.477 | 0.339 | 1.260 | 0.498-3.188 | 0.626 |
| Histologic subtype | | | | | | |
| Adenocarcinoma | 1 | | | 1 | | |
| Others | 1.627 | 0.785-3.370 | 0.191 | 1.811 | 0.920-3.564 | 0.086 |
| Driver gene mutation | | | | | | |
| Negative or unknown | 1 | | | 1 | | |
| Positive | 0.675 | 0.384-1.188 | 0.173 | 0.417 | 0.226-0.769 | 0.005 |
| Number of brain metastases | | | | | | |
| 1 | 1 | | | 1 | | |
| 2-3 | 0.851 | 0.457-1.584 | 0.611 | 0.887 | 0.475-1.657 | 0.707 |
| Localization of brain metastases | | | | | | |
| Supratentorial | 1 | | | 1 | | |
| Infratentorial | 1.127 | 0.501-2.535 | 0.773 | 0.447 | 0.138-1.447 | 0.179 |
| CNS treatment before FSRT | | | | | | |
| None | 1 | | | 1 | | |
| RT | 0.636 | 0.251-1.611 | 0.340 | 0.457 | 0.141-1.478 | 0.191 |
| Extracranial metastases | | | | | | |
| No | 1 | | | 1 | | |
| Yes | 0.876 | 0.464-1.654 | 0.683 | 1.073 | 0.544-2.117 | 0.840 |
| Maximum diameter of brain metastases (cm) | | | | | | |
| < 2 | 1 | | | 1 | | |
| ≥ 2 | 2.595 | 1.417-4.750 | 0.002 | 1.265 | 0.719-2.225 | 0.414 |
| BED10 of FSRT (Gy) | | | | | | |
| < 48 | 1 | | | 1 | | |
| ≥ 48 | 0.241 | 0.124-0.468 | 0.001 | 0.903 | 0.421-1.937 | 0.793 |
| NLR | | | | | | |
| < 5 | 1 | | | 1 | | |
| ≥ 5 | 1.104 | 0.592-2.056 | 0.756 | 1.261 | 0.678-2.343 | 0.464 |
| PLR | | | | | | |

*(Continued)*

TABLE 2 Continued

| Prognostic factors | Intracranial local control survival | | | Overall survival | | |
|---|---|---|---|---|---|---|
| | HR | 95% CI | *P*-value | HR | 95% CI | *P*-value |
| < 180 | 1 | | | 1 | | |
| ≥ 180 | 2.023 | 1.116-3.669 | 0.020 | 1.856 | 1.024-3.366 | 0.042 |
| LMR | | | | | | |
| < 4 | 1 | | | 1 | | |
| ≥ 4 | 0.306 | 0.147-0.636 | 0.001 | 0.408 | 0.197-0.843 | 0.015 |

HR hazard ratio, CI confidence interval, KPS karnofsky performance status, CNS central nervous system, FSRT fractionated stereotactic radiotherapy, RT radiotherapy, BED10 biologically effective dose ($\alpha/\beta$ = 10), NLR neutrophil to lymphocyte ratio, PLR platelet to lymphocyte ratio, LMR lymphocyte to monocyte ratio

Multivariate analysis demonstrated that LMR ≥ 4 and presence of driver gene mutations were independently associated with better OS (Table 3).

## Discussion

To our knowledge, this is the first study to evaluate the predictive value of inflammatory indicators in NSCLC patients with brain oligo-metastasis treated with FSRT. Our results showed that, in addition to tumor diameter and BED 10, LMR (an inflammatory indicator), was also an independent prognostic factor for i-LCS. Tumor diameter and BED10 had previously been identified as prognostic factors for i-LCS (9, 30, 31), but our study is the first to identify LMR value as an independent prognostic factor. Anna Cho et al. (25) reported that NLR, PLR and LMR were independent prognostic factors of overall survival in NSCLC patients with brain metastases after Gamma Knife Radiosurgery. However, Aijie Li et al. (32) proposed that LMR was the only independent prognostic factor of overall survival in NSCLC patients with brain metastases. The differences in these finding could be due to differences in the study population. The participants in our study were all NSCLC patients with oligometastatic brain metastases who had undergone FSRT treatment. We found that LMR as the only inflammatory indicator that acted as an independent prognostic factor of overall survival, although PLR was identified as prognostic factor during univariate analysis but was negative in multivariable analysis. Therefore LMR ≥ 4 is an excellent independent prognostic factor for i-LCS and overall survival in NSCLC patients with oligometastatic brain metastases treated with FSRT. We also found that positivity for driver gene mutations was an independent prognostic indicator of overall survival, which was consistent with the findings of Aijie Li et al. (32). The reason why driver gene mutations were independent prognostic indicators of overall survival but not i-LCS may be attributed to the overall poor extracranial control rate in patients negative for driver gene mutations, which leads to the death from extracranial lesions.

It is generally acknowledged that the cut-off value of LMR is 4 (25, 26), which was confirmed in our study. There is no consensus on the cut-off value of tumor diameter. Some articles indicate that the cut-off value of tumor diameter is 1cm in brain metastases receiving radiosurgery (33), and 2cm or 3cm in brain metastases receiving FSRT (34, 35). The i-LCS was significantly better in patients with lower cut-off value. Our results showed the cut-off value was 2cm demarcated by the median value. The median i-LCS was just 13.7 months in patients with tumors above 2cm but was as long as 31.5 months in patients with tumors below 2 treated with FSRT. The effective radiation dose for clinical application is still controversial. It is generally agreed that the radiation dose cut-off value for SRS treatment in brain metastases is 18Gy, with local control deteriorating significantly in patients receiving the dose below 18Gy (36). The use of BED is determining the curative effect of SRS is debatable (37), but is usually applied in determining the curative effect of FSRT treatment. Several divide-up radiotherapy plans have been suggested (8–10). One review summarized and compared the curative effect of different BED values, and concluded that BED12 values greater than 40Gy (which equals to BED10 greater than 48Gy) achieved a higher local control rate (38). Another study showed the 1 year local control rate was 100% for BED10 greater than 48Gy but was only 33% for BED10 less that 48Gy in treating postoperative metastasis tumor bed using FSRT (39). Thus it is generally believed the cut-off value of BED10 is 48Gy. In our study, we found that the median i-LCS of patients who received BED10 greater than 48Gy was significantly longer than for patient who received less BED10 (17.0 months vs 5.5 months). Results from multivariate analysis indicated the BED10 was an independent prognostic factor of i-LCS. Samuel R et al. (34) assessed if enhancement of BED value improved i-LCS, and found that enhancing BED10 value did not improve i-LCS in patients with a tumor diameter of more than 3cm. However, we found that administration of BED 10 greater than 53.6Gy improved the i-LCS of patients with two independent risk factors (tumor diameter ≥ 2 and LMR < 4), but had no benefit in the patients with 1 or no independent risk factor. The difference in findings may be because the study by Samuel R et al. enrolled patients with only 1 independent risk factor (tumor diameter ≥3cm) and did not screen the patients for obstinate resistance to radiotherapy. Unlike their results, this study analyzed the LMR value below 4 as the other independent risk factor. Thus got benefit by improving BED value in patients simultaneously possessed two independent risk factors (tumor diameter ≥ 2 and LMR < 4) equivalent to possessing obstinate resistance to radiotherapy.

Neutrophils inhibit immune functions and induce resistance to chemoradiotherapy by secreting cytokines and chemokines (13, 40,

10.3389/fonc.2023.1216852

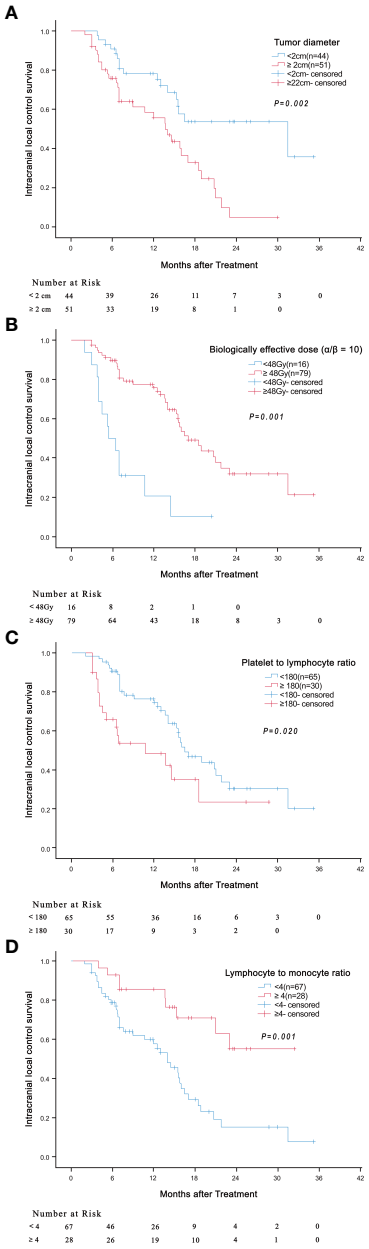


FIGURE 1
Association of tumor diameter (≥ 2cm versus < 2cm) ((**A**) *P* = 0.002), BED10 (≥ 48Gy versus < 48Gy) ((**B**) *P* = 0.001), PLR (≥ 180 versus < 180) ((**C**) *P* = 0.020) and LMR (≥ 4 versus < 4) ((**D**) *P* = 0.001) with intracranial local control survival.

41). Platelets are a critical source of cytokines, such as transforming growth factor-β, platelet-derived growth factor, and vascular endothelial growth factor (VEGF), which induce angiogenesis and cell invasion (42, 43). Moreover, lymphocytes can produce several cytokines, including IFN-γ and perforin, to prevent tumor development and induce apoptosis in cancer cells (36). Monocytes are innate immune cells that play important roles in tumor progression, invasion and metastasis and can be grouped into macrophages and myeloid-derived suppressor cells (44, 45). These findings from literature suggest that NLR, PLR and LMR have potential roles as prognostic factors in tumor development and

TABLE 3 Multivariate analysis of factors associated with intracranial local control survival and overall survival.

| Prognostic factors | Intracranial local control survival | | | Overall survival | | |
|---|---|---|---|---|---|---|
| | HR | 95% CI | *P*-value | HR | 95% CI | *P*-value |
| Maximum diameter of brain metastases (< 2cm *vs* ≥ 2cm) | 1.945 | 1.041-3.636 | 0.037 | / | / | / |
| BED10 of FSRT (< 48Gy *vs* ≥48Gy) | 0.268 | 0.130-0.553 | 0.001 | / | / | / |
| PLR (< 180 *vs* ≥ 180) | 1.369 | 0.716-2.618 | 0.342 | 1.476 | 0.800-2.723 | 0.212 |
| LMR (< 4 *vs* ≥ 4) | 0.365 | 0.171-0.776 | 0.009 | 0.414 | 0.198-0.864 | 0.019 |
| Driver gene mutation (negative or unknown *vs* positive) | / | / | / | 0.442 | 0.236-0.828 | 0.011 |

BED10 biologically effective dose (α/β = 10), FSRT fractionated stereotactic radiotherapy, PLR platelet to lymphocyte ratio, LMR lymphocyte to monocyte ratio

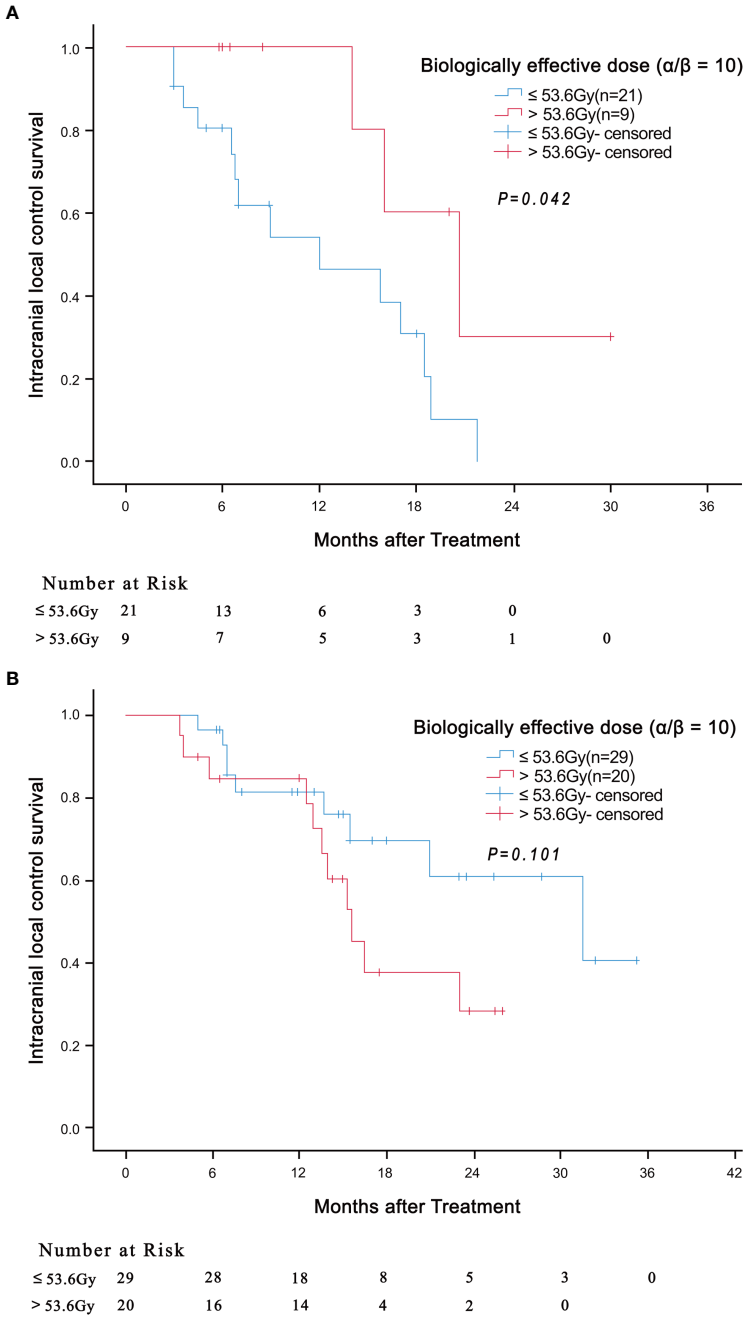


FIGURE 2
Association of BED10 (> 53.6Gy versus ≤ 53.6Gy) with intracranial local control survival in patients with 2 independent risk factors (tumor diameter ≥ 2 and LMR < 4) ((**A**) $P$ = 0.042) and in patients with only 1 independent risk factor ((**B**) $P$ = 0.101).

treatment. In our study, we found that LMR but not NLR was a prognostic factor in the NSCLC patients with oligometastatic brain metastases receiving FSRT treatment. The difference between the two factors could be due to the effect of glucocorticoids. Glucocorticoids are usually administered to reduce the intracranial pressure before radiation therapy once the diagnosis of brain metastasis has been confirmed. The use of glucocorticoids can affect neutrophil counts which affects NLR value resulting in a negative result. It is also possible that NLR has no prognostic value in patients receiving FSRT treatment.

There are some limitations in our study. First, this was a retrospective study involving a small sample from a single center, which may have caused analytical bias. Second, the lack of follow-up data for different treatments before and after the radiotherapy may have influenced the analysis. Third, adverse reactions such as acute cerebral edema and radionecrosis are difficult to detect and were not

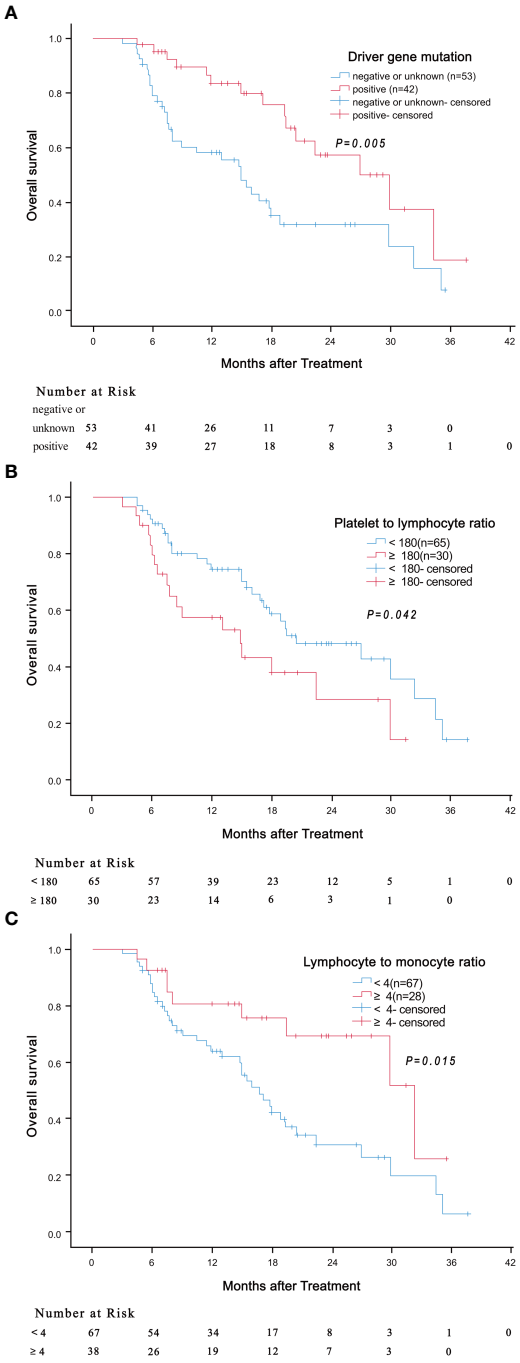


FIGURE 3
Association of driver gene mutation (**A**, *P* = 0.005), PLR (**B**, *P* = 0.042) and LMR (**C**, *P* = 0.015) with overall survival.

reported during follow-up, thus adverse reactions analysis could not be carried out. Fourthly, selection bias may have been present despite the strict inclusion criteria, and thus the findings need to be validated in future prospective studies. Fifth, a part of patients from our study had been pronounced dead because of the extracranial lesions before the intracranial lesions, and this point was linked to the end of intracranial follow-up which resulted in attrition bias. Therefore, there is need for multi-center prospective randomized clinical trials with large sample size to validate the prognostic value of LMR in NSCLC patients with oligometastatic brain metastases treated with FSRT and its effect on radiotherapy dose.

## Conclusions

LMR is a prognostic factor for i-LCS and OS in NSCLC patients with oligometastatic brain metastases treated with FSRT. The basic dose for BED10 was greater that 48Gy, but should be increased to greater than 53.6Gy in patients with tumor diameter ≥ 2 and LMR < 4.

## Data availability statement

The raw data supporting the conclusions of this article will be made available by the authors, without undue reservation.

## Ethics statement

The studies involving human participants were reviewed and approved by Ningbo Medical Center Lihuili Hospital ethics committee. Written informed consent for participation was not required for this study in accordance with the national legislation and the institutional requirements. Written informed consent was not obtained from the individual(s) for the publication of any potentially identifiable images or data included in this article.

## Author contributions

TC and WS contributed to the conception and design of the study. TC and MT wrote the article together. SL, YL, and JW contributed to the acquisition and analysis of the data. YZ, ZW, and HW participated in revising of the article. All authors contributed to the article and approved the submitted version.

## Funding

This work was supported by the Ningbo Clinical Research Center for thoracic and breast neoplasms (grant number 2021L002), the National Natural Science Foundation of China (grant number 21906014) and the Ningbo Medical and Health Leading Academic Discipline Project (grant number 2022-F04).

## Conflict of interest

The authors declare that the research was conducted in the absence of any commercial or financial relationships that could be construed as a potential conflict of interest.

## Publisher's note



## Supplementary material

The Supplementary Material for this article can be found online at: https://www.frontiersin.org/articles/10.3389/fonc.2023.1216852/full#supplementary-material

SUPPLEMENTARY FIGURE 1
Curves of intracranial local control survival **(A)** and overall survival **(B)**.

## References

1. Patchell RA. The management of brain metastases. *Cancer Treat Rev* (2003) 29 (6):533–40. doi: 10.1016/s0305-7372(03)00105-1

2. Wu YL, Planchard D, Lu S, Sun H, Yamamoto N, Kim DW, et al. Pan-Asian adapted clinical practice guidelines for the management of patients with metastatic non-small-cell lung cancer: a CSCO-ESMO initiative endorsed by JSMO, KSMO, MOS, SSO and TOS. *Ann Oncol* (2019) 30(2):171–210. doi: 10.1093/annonc/mdy554

3. Sperduto PW, Yang TJ, Beal K, Pan H, Brown PD, Bangdiwala A, et al. Estimating survival in patients with lung cancer and brain metastases: an update of the graded prognostic assessment for lung cancer using molecular markers (Lung-molGPA). *JAMA Oncol* (2017) 3(6):827–31. doi: 10.1001/jamaoncol.2016.3834

4. Sperduto PW, Kased N, Roberge D, Xu Z, Shanley R, Luo X, et al. Summary report on the graded prognostic assessment: an accurate and facile diagnosis-specific tool to estimate survival for patients with brain metastases. *J Clin Oncol* (2012) 30 (4):419–25. doi: 10.1200/JCO.2011.38.0527

5. Lorenzoni J, Devriendt D, Massager N, David P, Ruíz S, Vanderlinden B, et al. Radiosurgery for treatment of brain metastases: estimation of patient eligibility using three stratification systems. *Int J Radiat Oncol Biol Physics* (2004) 60(1):218–24. doi: 10.1016/j.ijrobp.2004.02.017

6. Franzin A, Snider S, Picozzi P, Bolognesi A, Serra C, Vimercati A, et al. Evaluation of different score index for predicting prognosis in gamma knife radiosurgical treatment for brain metastasis. *Int J Radiat Oncol Biol Physics* (2009) 74(3):707–13. doi: 10.1016/j.ijrobp.2008.08.062

7. Van De Voorde L, Vanneste B, Houben R, Damen P, van den Bogaard J, Lammering G, et al. Image-guided stereotactic ablative radiotherapy for the liver: a safe and effective treatment. *Eur J Surg Oncol* (2015) 41(2):249–56. doi: 10.1016/j.ejso.2014.10.053

8. Ishihara T, Yamada K, Harada A, Isogai K, Tonosaki Y, Demizu Y, et al. Hypofractionated stereotactic radiotherapy for brain metastases from lung cancer: evaluation of indications and predictors of local control. *Strahlentherapie Und Onkol* (2016) 192(6):386–93. doi: 10.1007/s00066-016-0963-2

9. Loo M, Clavier JB, Attal Khalifa J, Moyal E, Khalifa J. Dose-response effect and dose-toxicity in stereotactic radiotherapy for brain metastases: a review. *Cancers* (2021) 13(23):6086. doi: 10.3390/cancers13236086

10. Musunuru HB, Witt JS, Yadav P, Francis DM, Kuczmarska-Haas A, Labby ZE, et al. Impact of adjuvant fractionated stereotactic radiotherapy dose on local control of brain metastases. *J Neuro-Oncol* (2019) 145(2):385–90. doi: 10.1007/s11060-019-03308-7

11. Balkwill F, Mantovani A. Inflammation and cancer: back to virchow? *Lancet (London England)* (2001) 357(9255):539–45. doi: 10.1016/S0140-6736(00)04046-0

12. Zhang X, Hu D, Lin X, Zhang H, Xia Y, Lin J, et al. Prognostic value of an inflammation-related index in 6,865 Chinese patients with postoperative digestive tract cancers: the FIESTA study. *Front Oncol* (2019) 9:427. doi: 10.3389/fonc.2019.00427

13. Guthrie GJ, Charles KA, Roxburgh CS, Horgan PG, McMillan DC, Clarke SJ. The systemic inflammation-based neutrophil-lymphocyte ratio: experience in patients with cancer. *Crit Rev Oncol/Hematol* (2013) 88(1):218–30. doi: 10.1016/j.critrevonc.2013.03.010

14. Templeton AJ, Ace O, McNamara MG, Al-Mubarak M, Vera-Badillo FE, Hermanns T, et al. Prognostic role of platelet to lymphocyte ratio in solid tumors: a systematic review and meta-analysis. *Cancer Epidemiol Biomarkers Prev* (2014) 23 (7):1204–12. doi: 10.1158/1055-9965.EPI-14-0146

15. Liu C, Sun B, Hu X, Zhang Y, Wang Q, Yue J, et al. Stereotactic ablative radiation therapy for pulmonary recurrence-based oligometastatic non-small cell lung cancer: survival and prognostic value of regulatory T cells. *Int J Radiat Oncol Biol Physics* (2019) 105(5):1055–64. doi: 10.1016/j.ijrobp.2019.08.012

16. Liu C, Hu Q, Xu B, Hu X, Su H, Li Q, et al. Peripheral memory and naïve T cells in non-small cell lung cancer patients with lung metastases undergoing stereotactic body radiotherapy: predictors of early tumor response. *Cancer Cell Int* (2019) 19:121. doi: 10.1186/s12935-019-0839-5

17. Lang C, Egger F, Alireza Hoda M, Saeed Querner A, Ferencz B, Lungu V, et al. Lymphocyte-to-monocyte ratio is an independent prognostic factor in surgically treated small cell lung cancer: an international multicenter analysis. *Lung Cancer (Amsterdam Netherlands)* (2022) 169:40–6. doi: 10.1016/j.lungcan.2022.05.010

18. Tada T, Kumada T, Hiraoka A, Michitaka K, Atsukawa M, Hirooka M, et al. Neutrophil-to-lymphocyte ratio is associated with survival in patients with unresectable hepatocellular carcinoma treated with lenvatinib. *Liver Int* (2020) 40 (4):968–76. doi: 10.1111/liv.14405

19. Yao Y, Yuan D, Liu H, Gu X, Song Y. Pretreatment neutrophil to lymphocyte ratio is associated with response to therapy and prognosis of advanced non-small cell lung cancer patients treated with first-line platinum-based chemotherapy. *Cancer Immunol Immunother* (2013) 62(3):471–9. doi: 10.1007/s00262-012-1347-9

20. Peng L, Wang Y, Liu F, Qiu X, Zhang X, Fang C, et al. Peripheral blood markers predictive of outcome and immune-related adverse events in advanced non-small cell lung cancer treated with PD-1 inhibitors. *Cancer Immunol Immunother* (2020) 69 (9):1813–22. doi: 10.1007/s00262-020-02585-w

21. Sebastian NT, Raj R, Prasad R, Barney C, Brownstein J, Grecula J, et al. Association of pre- and posttreatment neutrophil-lymphocyte ratio with recurrence and mortality in locally advanced non-small cell lung cancer. *Front Oncol* (2020) 10:598873. doi: 10.3389/fonc.2020.598873

22. Ng SP, Bahig H, Jethanandani A, Sturgis EM, Johnson FM, Elgohari B, et al. Prognostic significance of pre-treatment neutrophil-to-lymphocyte ratio (NLR) in patients with oropharyngeal cancer treated with radiotherapy. *Br J Cancer* (2021) 124(3):628–33. doi: 10.1038/s41416-020-01106-x

23. Wang C, Tong J, Tang M, Lu Y, Liang G, Zhang Z, et al. Pretreatment neutrophil-to-Lymphocyte ratio and platelet-to-Lymphocyte ratio as prognostic factors and reference markers of treatment options for locally advanced squamous cell carcinoma located in the middle and upper esophagus. *Cancer Manage Res* (2021) 13:1075–85. doi: 10.2147/CMAR.S294344

24. Chen T, Song C, Liang G, Xu X, Wang C, Zhang Z, et al. Neutrophil-to-Lymphocyte ratio, platelet-to-Lymphocyte ratio, and their variations as a basis for a prediction model in advanced NSCLC patients receiving anlotinib. *Dis Markers* (2022) 2022:5879137. doi: 10.1155/2022/5879137

25. Cho A, Untersteiner H, Hirschmann D, Fitschek F, Dorfer C, Rössler K, et al. Pre-radiosurgery leucocyte ratios and modified glasgow prognostic score predict survival in non-small cell lung cancer brain metastases patients. *J Neuro-Oncol* (2021) 151(2):257–65. doi: 10.1007/s11060-020-03660-z

26. Cho A, Kranawetter B, Untersteiner H, Khalaveh F, Dorfer C, Rössler K, et al. Neutrophil-to-Lymphocyte ratio is superior to other leukocyte-based ratios as a prognostic predictor in non-small cell lung cancer patients with radiosurgically treated brain metastases under immunotherapy or targeted therapy. *World Neurosurg* (2021) 151:e324–e31. doi: 10.1016/j.wneu.2021.04.033

27. Mandaliya H, Jones M, Oldmeadow C, Nordman II. Prognostic biomarkers in stage IV non-small cell lung cancer (NSCLC): neutrophil to lymphocyte ratio (NLR), lymphocyte to monocyte ratio (LMR), platelet to lymphocyte ratio (PLR) and advanced lung cancer inflammation index (ALI). *Trans Lung Cancer Res* (2019) 8(6):886–94. doi: 10.21037/tlcr.2019.11.16

28. Gu X, Sun S, Gao XS, Xiong W, Qin S, Qi X, et al. Prognostic value of platelet to lymphocyte ratio in non-small cell lung cancer: evidence from 3,430 patients. *Sci Rep* (2016) 6:23893. doi: 10.1038/srep23893

29. Cao D, Xu H, Xu X, Guo T, Ge W. A reliable and feasible way to predict the benefits of nivolumab in patients with non-small cell lung cancer: a pooled analysis of 14 retrospective studies. *Oncoimmunology* (2018) 7(11):e1507262. doi: 10.1080/2162402X.2018.1507262

30. Matsuyama T, Kogo K, Oya N. Clinical outcomes of biological effective dose-based fractionated stereotactic radiation therapy for metastatic brain tumors from non-small cell lung cancer. *Int J Radiat Oncol Biol Physics* (2013) 85(4):984–90. doi: 10.1016/j.ijrobp.2012.09.008

31. Redmond KJ, Gui C, Benedict S, Milano MT, Grimm J, Vargo JA, et al. Tumor control probability of radiosurgery and fractionated stereotactic radiosurgery for brain metastases. *Int J Radiat Oncol Biol Physics* (2021) 110(1):53–67. doi: 10.1016/j.ijrobp.2020.10.034

32. Li A, Mu X, He K, Wang P, Wang D, Liu C, et al. Prognostic value of lymphocyte-to-monocyte ratio and systemic immune-inflammation index in non-small-cell lung cancer patients with brain metastases. *Future Oncol (London England)* (2020) 16(30):2433–44. doi: 10.2217/fon-2020-0423

33. Chang EL, Hassenbusch SJ3rd, Shiu AS, Lang FF, Allen PK, Sawaya R, et al. The role of tumor size in the radiosurgical management of patients with ambiguous brain metastases. *Neurosurgery* (2003) 53(2):272–80. doi: 10.1227/01.neu.0000073546.61154.9a

34. Marcrom SR, McDonald AM, Thompson JW, Popple RA, Riley KO, Markert JM, et al. Fractionated stereotactic radiation therapy for intact brain metastases. *Adv Radiat Oncol* (2017) 2(4):564–71. doi: 10.1016/j.adro.2017.07.006

35. Kwon AK, Dibiase SJ, Wang B, Hughes SL, Milcarek B, Zhu Y. Hypofractionated stereotactic radiotherapy for the treatment of brain metastases. *Cancer* (2009) 115 (4):890–8. doi: 10.1002/cncr.24082

36. Shiau CY, Sneed PK, Shu HK, Lamborn KR, McDermott MW, Chang S, et al. Radiosurgery for brain metastases: relationship of dose and pattern of enhancement to local control. *Int J Radiat Oncol Biol Physics* (1997) 37(2):375–83. doi: 10.1016/s0360-3016(96)00497-x

37. Brown JM, Koong AC. High-dose single-fraction radiotherapy: exploiting a new biology? *Int J Radiat Oncol Biol Phys* (2008) 71(2):324–5. doi: 10.1016/j.ijrobp.2008.02.003

38. Wiggenraad R, Verbeek-de Kanter A, Kal HB, Taphoorn M, Vissers T, Struikmans H. Dose-effect relation in stereotactic radiotherapy for brain metastases. a systematic review. *Radiother Oncol* (2011) 98(3):292–7. doi: 10.1016/j.radonc.2011.01.011

39. Kumar AMS, Miller J, Hoffer SA, Mansur DB, Coffey M, Lo SS, et al. Postoperative hypofractionated stereotactic brain radiation (HSRT) for resected brain metastases: improved local control with higher BED(10). *J Neuro-Oncol* (2018) 139(2):449–54. doi: 10.1007/s11060-018-2885-6

40. Diakos CI, Charles KA, McMillan DC, Clarke SJ. Cancer-related inflammation and treatment effectiveness. *Lancet Oncol* (2014) 15(11):e493–503. doi: 10.1016/S1470-2045(14)70263-3

41. Powell DR, Huttenlocher A. Neutrophils in the tumor microenvironment. *Trends Immunol* (2016) 37(1):41–52. doi: 10.1016/j.it.2015.11.008

42. Schumacher D, Strilic B, Sivaraj KK, Wettschureck N, Offermanns S. Platelet-derived nucleotides promote tumor-cell transendothelial migration and metastasis *via* P2Y2 receptor. *Cancer Cell* (2013) 24(1):130–7. doi: 10.1016/j.ccr.2013.05.008

43. Yun SH, Sim EH, Goh RY, Park JI, Han JY. Platelet activation: the mechanisms and potential biomarkers. *BioMed Res Int* (2016) 2016:9060143. doi: 10.1155/2016/9060143

44. Marvel D, Gabrilovich DI. Myeloid-derived suppressor cells in the tumor microenvironment: expect the unexpected. *J Clin Invest* (2015) 125(9):3356–64. doi: 10.1172/JCI80005

45. Liu C, Li X, Huang Q, Zhang M, Lei T, Wang F, et al. Single-cell RNA-sequencing reveals radiochemotherapy-induced innate immune activation and MHC-II upregulation in cervical cancer. *Signal Transduction Targeted Ther* (2023) 8(1):44. doi: 10.1038/s41392-022-01264-9

frontiers | Frontiers in Oncology

TYPE Original Research
PUBLISHED 15 September 2023
DOI 10.3389/fonc.2023.1245506



OPEN ACCESS

EDITED BY
Xiangpan Li,
Renmin Hospital of Wuhan University, China

REVIEWED BY
Feng Liu,
Central South University, China
Jing Yu,
Wuhan University, China
Chengcheng Fan,
Affiliated Cancer Hospital of Zhengzhou University, China

*CORRESPONDENCE
Lujun Zhao
zhaolujun@tjmuch.com
Ping Wang
wangping@tjmuch.com

†These authors have contributed equally to this work

RECEIVED 23 June 2023
ACCEPTED 02 August 2023
PUBLISHED 15 September 2023

CITATION
Xu L, Zhang K, Han H, Sun H, Yuan Y, Wang J, Zhao L and Wang P (2023) Low radiotherapy dose is suitable for brain metastases in SCLC compared with high dose.
*Front. Oncol.* 13:1245506.
doi: 10.3389/fonc.2023.1245506



# Low radiotherapy dose is suitable for brain metastases in SCLC compared with high dose

Liming Xu[1†], Kunning Zhang[1†], Haonan Han[2†], Han Sun[3], Yajing Yuan[4], Jun Wang[1,5], Lujun Zhao[1*] and Ping Wang[1*]

[1]Department of Radiation Oncology, Tianjin Medical University Cancer Institute and Hospital, National Clinical Research Center for Cancer, Key Laboratory of Cancer Prevention and Therapy, Tianjin's Clinical Research Center for Cancer, Tianjin, China, [2]Hubei Key Laboratory of Tumor Microenvironment and Immunotherapy, College of Basic Medical Sciences, China Three Gorges University, Yichang, China, [3]Department of Radiation Oncology, Cancer Center/National Clinical Research, Center for Cancer/Cancer Hospital & Shenzhen Hospital, Chinese Academy of Medical Sciences and Peking Union Medical College, Shenzhen, China, [4]Department of Anesthesia, Tianjin Medical University Cancer Institute and Hospital, National Clinical Research Center for Cancer, Key Laboratory of Cancer Prevention and Therapy, Tianjin's Clinical Research Center for Cancer, Tianjin, China, [5]Department of Radiation Oncology, Tianjin Cancer Hospital Airport Hospital, Tianjin, China

**Objective:** This study was designed to evaluate the suitable radiotherapy dose in SCLC patients with BM.

**Methods:** A retrospective analysis was performed among 121 patients on the prognosis of BM of SCLC who were admitted to our hospital from 2013 to 2023. They all received first line chemotherapy. 80 patients of them received TRT after chemotherapy. The Chi square method was used to compare the categorical data. Univariate survival analysis was estimated by Kaplan Meier method and the logrank was used to compare survival curves between groups. A multivariate prognostic analysis was made by the Cox proportional hazard model. The iOS and iLC of two groups of low dose and high dose were analyzed after propensity score matching (PSM).

**Results:** In all the patients, the median follow-up time was 18.6 months (range 6.30~85.7), the 2-year iOS and iLC rates were 15.4% and 70.3%, respectively, and cerebral necrosis occurred in 2 patients. In univariate analysis related to iOS, extracranial disease control (p=0.023), higher DS-GPA (≥2) (p=0.016), immunotherapy (p=0.049), low-dose(p=0.030), and WBRT+SIB (p=0.009) were significantly associated with an increase in survival rate. After PSM, the 2-year iOS of low dose (n=49) was significantly higher than that of high dose (n=49) (P=0.025), while the 2-year iLC was not significantly improved (P=0.267). In DS-GPA < 2 subgroup, the iOS of low dose group was significantly higher than that of high dose group (p=0.019). In the DS-GPA ≥ 2 subgroup, the 2-year iLC of the low dose group was significantly inferior than that of the high dose group (p=0.044).

**Conclusions:** The iLC was improved along with increasing radiotherapy dose, but high dose had inferior iOS compared to low dose, while there were not significantly improving iLC when radiotherapy BED >56Gy. But in patients with DS-GPA≥2 subgroup, high dose brought better iLC benefits.

KEYWORDS

carcinoma, brain metastases, small cell lung cancer, radiotherapy, prognosis

# Introduction

Lung cancer is the second most common cancer worldwide. It is the most common cancer in men and the second most common cancer in women. There were more than 2.2 million new cases of lung cancer in 2020 (1). Small cell lung cancer (SCLC) is a high-grade neuroendocrine tumor characterized by rapid growth, early metastatic spread, and initial responsiveness to therapy. It represents about 15% of all lung cancers. Approximately 18% of the patients were found to have BM at the time of diagnosis. In approximately 33% of the cases, these BM did not cause symptoms. More than 50% will develop BM within 2 years (2). BM were found to have a negative effect on survival in patients with SCLC. The median survival time after BM was 8.7 months and 3-year OS rate was 15.0%, the median survival time of patients without BM was 20.1 months and 3-year OS was 33.4% (P=0.014) (3, 4). Patients with BM were subsequently treated with palliative therapy. The standard treatment for SCLC BM is still WBRT, with an overall effective rate (ORR) of approximately 50% -80% (5). Magnetic resonance imaging (MRI) is a more sensitive technique to detect BM, In the MRI era, the estimated prevalence of BM increased by 14% (6). Patients with asymptomatic BM by MRI were more detected, and had a better prognosis (7). In our previous clinical studies, we have found that WBRT combined with radiation boost can improve the overall survival (OS) of SCLC patients with BM (8). However, the suitable radiotherapy dose of BM and efficacy are not very clear. This article analyzes the efficacy and safety of low dose or high dose in SCLC patients with BM retrospectively, in order to optimize WBRT+ suitable radiation boost dose for SCLC patients with BM.

# Materials and methods

## Inclusion criteria

We retrospectively analyzed the clinical characteristics of SCLC BM patients who received brain radiation therapy from 2013 to 2023. All patients received treatment from Tianjin Cancer Institute and Hospital. This study was approved by the ethics committee of Tianjin Medical University Cancer Hospital. This research on patient services in our hospital was an analysis of patients' medical data, which did not involve human experiments or compensation. The Tianjin Medical University Cancer Hospital approved the study data collection from the hospital information system. It is typically diagnosed in small biopsies or cytology specimens, demonstrating neuroendocrine features of SCLC (9). All clinical data of patients are from outpatient or inpatient clinical records. The patient underwent standardized physical examinations, including CT scans of the neck, chest, and abdomen, brain MRI, as well as ECT or PET/CT. ES-SCLC was defined in this study depending on the staging system of the Veterans Administration Lung Study Group, (VALG).

## Initial treatment strategy

All patients underwent chemotherapy and/or combined concurrent radiotherapy/sequential TRT. Chemotherapy strategies: The etoposide(100 mg from days 1 to 5) with either cisplatin (30 mg/m from days 1 to 3) or carboplatin (500 mg for day 1) (platinum–etoposide) as the first-line chemotherapy regimen. The median chemotherapy cycles are 6 (range 2-6). TRT strategies: The tumor and metastatic lymph nodes were defined as the GTV. The CTV encompassed the tumor bed after chemotherapy, and the draining area of metastatic lymph nodes before chemotherapy, which was expanded from the GTV by a 5 mm uniform margin. The PTV was evenly extended 0.5 to 1cm uniform margin on the basis of CTV. The prescription dose was 50-63Gy in 25-30 fractions, 1.8-2.1 Gy per fraction at one fraction per day. All patients were treated WBRT with radiation boost by IMRT or SRS. The WBRT plus a radiation boost strategy: WBRT was performed with 6 MV photon beams using opposed lateral fields (90° and 270°) with a total dose of 30 Gy (3 Gy per fraction administered in 10 fractions at one fraction per day). The SRS was administered using a Cyberknife (Accuracy, Sunnyvale,California, USA) or X-knife after the WBRT in 56 patients. The GTV encompassed contrast-enhancing tumor on MRI and were reviewed by the radiation oncologist and the neurosurgeon based on the tumor volume, tumor location, and neurological symptoms. The PTV was defined as the 1 to 2 mm margin to the GTV. The administered radiation dose was 8.5-19 Gy in 1-3fractions with 6.3-18.0 Gy per fraction and one fraction per day(BED=10.3-29.9Gy). The IMRT simultaneous integrated boost WBRT (WBRT-SIB) was administered in 65 patients. The GTV was contoured based on the tumor from contrast-enhanced MRI scans. The PTV of brain

metastases (PTVbm) was defined as the 3mm margin to the GTV with the dose of 35-50 Gy in 10 fractions with 3.5-5 Gy per fraction and one fraction per day. In general, we treated BMs less than 10 mm in maximum diameter with a prescription of 50 Gy (BED=75Gy); BMs larger than 10 mm but smaller than 30 mm with 40 Gy(BED=56Gy); and BMs larger than 30mm and less than 40 mm with 35Gy(BED=47.25Gy). The prescription of dose fractionation was consistent with previous clinical trials (10, 11). The PTV was expanded from the contour of the brain by the 3mm uniform margin with the dose of 30 Gy in 10 fractions with 3 Gy per fraction and one fraction per day.

## Efficacy evaluation, follow-up and side effects

Acute toxicity reactions are classified according to CTCAE version 5.0, and late toxicity is classified according to RTOG standards. Evaluate the efficacy of solid tumors according to RECIST 1.1. Repeat the baseline assessment every two cycles and every 6-8 weeks after treatment interruption until the disease progresses. Intracranial overall survival (iOS)is defined as the period from the start of BM diagnosis by imaging (MRI or enhanced CT) until the event occurs or the last follow-up. Intracranial local control survival (iLC) is defined as the time from the start of BM diagnosis by imaging (MRI or enhanced CT) until the first event of intracranial local failure.

## Statistical analysis

All survival analyses were conducted using the Kaplan Meier method. Compare survival curves between different groups using logarithmic rank test and use $\chi^2$ test and compare classified data. Cox proportional hazard regression model was used for Multivariate analysis of survival rate. Two groups of patients were subjected in a 1:1 ratio by PSM to analyze and control the confounding variables, including diagnosis-specific Graded Prognostic Assessment (DS-GPA) score, number of intracranial metastases, maximum diameter of metastases, and progression of extracranial diseases. In this study, the p-values were all one-way tests, and there was a statistically significant difference between groups when $p<0.05$. All analyses were conducted using SPSS software version 25.0.

# Result

## Clinical features

The patient characteristics of 121 patients were shown in Table 1. The majority of patients are male (n=100, 82.6%). The median age is 61 years (range 18-83 years). Most patients have severe smoking (smoking index ≥ 400, n=90,74.4%). Most patients have a superior Karnofsky performance status (KPS) score (KPS score ≥ 80, n=107, 88.4). The most common metastatic organs are as follows: 40 cases

TABLE 1 Distribution of the 121 patients' treatment and clinical characteristics.

| Characteristic | Number | Ratio (%) |
|---|---|---|
| Age (yrs) | | |
| **<65 yrs** | 86 | 71.1 |
| **≥65 yrs** | 35 | 28.9 |
| Gender | | |
| **male** | 100 | 82.6 |
| **female** | 21 | 17.4 |
| Smoke index | | |
| **≥400** | 90 | 74.4 |
| **<400** | 31 | 25.6 |
| Family history of tumors | | |
| **No** | 97 | 80.2 |
| **Yes** | 24 | 19.8 |
| Weight loss | | |
| **>5%** | 96 | 79.3 |
| **≤5%** | 25 | 20.7 |
| KPS | | |
| **≥80** | 107 | 88.4 |
| **<80** | 14 | 11.6 |
| **Thoracic radiation therapy dose** | | |
| **<50Gy** | 12 | 9.9 |
| **≥50Gy** | 68 | 56.2 |
| Stage | | |
| **LS-SCLC** | 67 | 55.4 |
| **ES-SCLC** | 54 | 44.6 |
| Number of BMs | | |
| **1** | 51 | 42.1 |
| **2-3** | 62 | 51.2 |
| **>3** | 8 | 6.6 |
| Maximum diameter of the largest tumor(cm) | | |
| **≤ 2.0** | 76 | 62.8 |
| **> 2.0** | 45 | 37.2 |
| Interval from diagnosis of SCLC to BMs (mths) | | |
| **≤ 10** | 63 | 52.1 |
| **> 10** | 58 | 47.9 |
| Extracranial disease control status | | |
| **Yes** | 40 | 33.1 |
| **No** | 81 | 66.9 |

*(Continued)*

TABLE 1 Continued

| Characteristic | Number | Ratio (%) |
|---|---|---|
| **(Diagnosis-specific Graded Prognostic Assessment) DS-GPA** | | |
| <2 | 31 | 25.6 |
| ≥2 | 90 | 74.4 |
| Immunotherapy (ICI) | | |
| **Yes** | 14 | 11.6 |
| **No** | 107 | 88.4 |
| Targeted therapy (anti-angiogenic therapy) | | |
| **Yes** | 5 | 4.1 |
| **No** | 116 | 95.9 |
| Brain radiotherapy | | |
| **WBRT+SIB** | 66 | 54.5 |
| **WBRT+SBRT** | 55 | 45.5 |
| Radiotherapy dose (BED) | | |
| **low-dose (BED ≤ 56Gy)** | **65** | **48.1** |
| **high-dose (BED>56Gy)** | **56** | **51.9** |

(33.1%) had bone metastasis; 21 cases (17.4%) had distant lymph node metastasis; 20 cases (16.5%) had lung metastasis; 15 cases (12.4%) had pleural metastasis; 14 cases (11.6%) had adrenal metastasis; Liver metastasis occurred in 12 cases (10.0%). Most patients received more than 4 cycles of chemotherapy (n=115, 95.0%). 86 patients (71.1%) responded to chemotherapy. Only 14 patients received immunotherapy (immune checkpoint inhibitors, ICIs), and 5 patients received treatment with arotinib.

## Survival and side effects

The median follow-up time was 18.6 months (ranging from 6.30 to 85.7months) with 2 patients lost to follow-up. The 2-year incidence of iOS and iLC was 15.4% and 70.3%, respectively (Figure 1). 92 patients died of disease progression, 1 patient died of radiation pneumonia, and 2 patients developed radiation brain necrosis. A few of patients have experienced treatment related toxic side effects, mainly including nausea, vomiting, dizziness, headache, leukopenia, radiation brain necrosis, etc. (The side effects of the low dose group and the high dose group are shown in Table 2).

Assess the predictive significance of patient and disease characteristics for iOS. Due to the small number (only 5) patients who were treated with arotinib, this factor is not suitable for analysis. In univariate analysis related to iOS, extracranial disease control (p=0.023), higher DS-GPA (≥2) (p=0.016), immunotherapy (p=0.049), low dose (p=0.030), and WBRT+SIB (p=0.009) were significantly associated with an increase in survival rate (Table 3). Age, gender, weight loss, smoking history, TRT dosage, and the time interval for BM after diagnosis were not significantly observed in staging and the number of brain metastases (all factors p>0.05). Multivariate covariates analysis of factors related to iOS were further analyzed with p<0.05 in univariate Cox regression model analysis. The extracranial progress control (p=0.049) and higher DS-GPA (≥2) (p=0.014) can significantly improve iOS by multivariate analysis (Table 3). However, there was no significant difference in immunotherapy, BM radiotherapy strategy and radiotherapy dose (p>0.05 for all factors).

## Comparison of survival between the low dose group and the low dose group

This study divided 121 patients into two groups according to BM radiotherapy, with 65 receiving low dose treatment and 56 receiving high dose. As shown in Table 4, compared to the low dose group, the high dose group had more patients with more weight loss >5%(9.2%vs33.9%, p=0.001), a smaller maximum diameter of BMs (53.8%vs73.2%, p=0.022), longer interval from diagnosis of SCLC to BMs (36.9% vs69.6%, p=0.000)and SRS (1.5%vs96.4%, p=0.000), which resulted in an imbalance between the two groups, and there was no significant difference in other baseline characteristics between the two treatment groups. Because the difference between SIB and SRS was too significant, and the majority of the low dose group had SIB and the majority of high dose group had SBRT, so the brain radiotherapy strategy factor was excluded. After a 1:1 PSM analysis, the baseline characteristics of the two groups of patients were well balanced (Table 5). The low dose group (n=49) was significantly superior than that of the high dose group (n=49) about the 2-year iOS (47.1% vs 30.7%, P=0.025), while there was no increasing significantly about the 2-year iLC in high dose(65.3% vs 91.9%, P=0.267) (Figure 2).

Further analysis was conducted on the prognosis of the low and high dose groups in different DS-GPA scores. It was found that in the GPA<2 subgroup, the 2-year iOS in the low dose group was significantly superior than that in the high dose group (65.3% and 25.0%, respectively, at, p=0.019), while in the DS-GPA ≥ 2 subgroup, there was no significant difference between the low dose group and high dose group (31.6% and 28.8%, respectively, p=0.502); in the DS-GPA<2 subgroup, there was no significant difference between the low dose group and high dose group in the 2-year iLC (100% and 100%, respectively). In the DS-GPA ≥ 2 subgroup, the 2-year iLC of the low dose group was significantly inferior than that of the high dose group (52.2% and 91.7%, respectively, p=0.044) (Figure 3).

# Discussion

In this study, we conducted a further study about radiotherapy dose in SCLC patients with BMs. Our previous studies have confirmed that WBRT with additional radiation boost is more effective than the WBRT alone group in prolonging the survival of SCLC patients with BMs (12). On this basis, we further investigate the different radiotherapy dose in brain metastases: low dose and high dose, which have effects on iOS, iLC, and radiotherapy side effects. The results showed that there was no

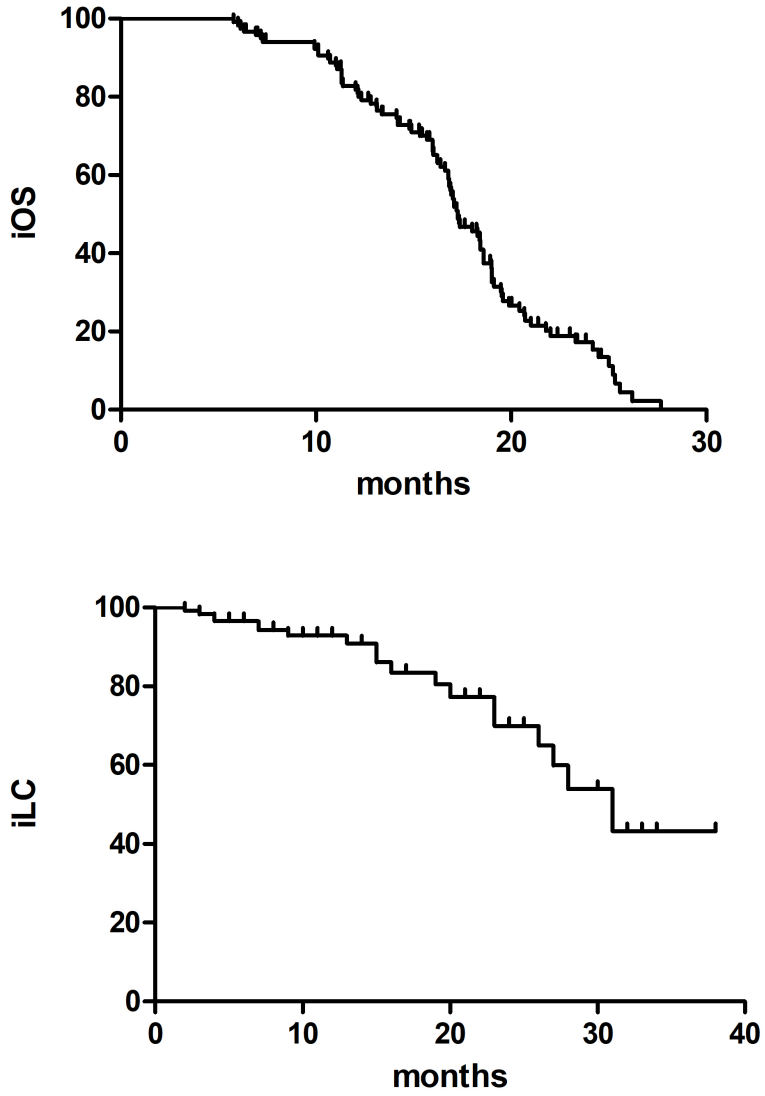


FIGURE 1
The iOS and iLC in 121 SCLC BM patients.

TABLE 2 Adverse reactions of 98 patients of SCLC with BMs in t in two treatment groups after PSM matching.

| Adverse reactions | Low dose (49) | | High dose (49) | | P value |
|---|---|---|---|---|---|
| | 1 or 2 (%) | 3 (%) | 1 or 2 (%) | 3 (%) | |
| **Weakness** | **8** | **3** | **8** | **2** | **0.550** |
| **Headache** | **15** | **10** | **19** | **9** | **0.379** |
| **Dizziness** | **12** | **8** | **10** | **8** | **0.520** |
| **Nausea** | **20** | **7** | **19** | **7** | **0.483** |
| **Vomit** | **4** | **0** | **3** | **0** | |
| **Fever** | **1** | **0** | **0** | **0** | |
| **Leukopenia** | **20** | **5** | **18** | **5** | **0.581** |
| **Thrombocytopenia** | **2** | **0** | **2** | **1** | |

*(Continued)*

TABLE 2 Continued

| Adverse reactions | Low dose (49) | | High dose (49) | | P value |
|---|---|---|---|---|---|
| | 1 or 2 (%) | 3 (%) | 1 or 2 (%) | 3 (%) | |
| **Radiation dermatitis** | **2** | **0** | **2** | **0** | **0.167** |
| **Disorders of consciousness** | **0** | **0** | **0** | **0** | |
| **Radiation brain necrosis** | **1** | **0** | **0** | **1** | **0.500** |

TABLE 3 121 patients' clinical and treatment characteristics and survival-related factors on iOS in univariate and multivariate analysis.

| Characteristic | univariate analysis | | | | multivariate analysis | | | |
|---|---|---|---|---|---|---|---|---|
| | HR | 95% CI | | P value | HR | 95% CI | | P value |
| **Age (<65 yrs v.s.≥65 yrs)** | **0.580** | **0.361** | **0.933** | **0.055** | | | | |
| **Gender(male v.s.female)** | **0.951** | **.526** | **1.721** | **0.869** | | | | |
| **Smoke index (≥400v.s. <400)** | **0.872** | **0.536** | **1.419** | **0.582** | | | | |
| **Family history of tumors (no v.s.yes)** | **1.310** | **0.786** | **2.182** | **0.301** | | | | |
| **Weight loss (>5%v.s.≤5%)** | **0.939** | **0.542** | **1.628** | **0.824** | | | | |
| **Karnofsky scoring (≥80v.s. <80)** | **0.807** | **0.427** | **1.526** | **0.510** | | | | |
| **Thoracic radiation therapy dose (≥50Gyv.s.<50Gy)** | **0.919** | **0.450** | **1.875** | **0.816** | | | | |
| **Stage [LS (limited stage) vs. ES (extensive stage)]** | **1.301** | **0.851** | **1.990** | **0.224** | | | | |
| **Number of BMs (1v.s.2-3v.s.>3)** | **1.159** | **0.802** | **1.675** | **0.432** | | | | |
| **Maximum diameter of the largest tumor (cm) (≤ 2.0v.s.> 2.0)** | **0.976** | **0.636** | **1.498** | **0.912** | | | | |
| **Interval from diagnosis of SCLC to BMs (mths) (≤ 9v.s> 9)** | **0.878** | **0.576** | **1.338** | **0.545** | | | | |
| **Extracranial disease control status (yes v.s. no)** | **1.723** | **1.077** | **2.756** | **0.023** | **1.628** | **1.001** | **2.648** | **0.049** |
| **Diagnosis-specific Graded Prognostic Assessment (DS-GPA) (<2 v.s.≥2)** | **0.522** | **0.307** | **0.886** | **0.016** | **0.508** | **0.296** | **0.873** | **0.014** |
| **Immunotherapy (no v.s.yes )** | **0.444** | **0.193** | **1.020** | **0.049** | **0.492** | **0.206** | **1.175** | **0.110** |
| **brain metastasis (BM) Radiotherapy [whole brain radiotherapy (WBRT)+simultaneous integrated boost (SIB) v.s.WBRT+stereotactic radiosurgery (SRS)]** | **0.563** | **0.367** | **0.863** | **0.009** | **0.268** | **0.035** | **2.075** | **0.207** |
| **Radiotherapy dose (low-dose v.s.high dose)** | **1.607** | **1.048** | **2.465** | **0.030** | **0.438** | **0.056** | **3.407** | **0.430** |

TABLE 4 Distribution of the 121 patients' treatment and clinical characteristics in two treatment groups.

| Characteristic | Low dose (n=65) (%) | High dose (n=56)(%) | P value |
|---|---|---|---|
| **Age (<65 yrs)** | **67.7%** | **75.0%** | **0.377** |
| **Gender(male)** | **84.6%** | **80.4%** | **0.537** |
| **Smoke index≥400** | **83.1%** | **74.5%** | **0.189** |
| **Family history of tumors (yes)** | **24.6%** | **14.3%** | **0.116** |
| **Weight loss >5%(yes)** | **9.2%** | **33.9%** | **0.001** |
| **Karnofsky scoring≥80** | **86.2%** | **91.1%** | **0.399** |
| **Thoracic radiation therapy dose ≥50Gy** | **79.2%** | **87.5%** | **0.263** |
| **Stage [limited stagesmall cell lung cancer (LS-SCLC)]** | **50.8%** | **60.7%** | **0.181** |
| **Number of brain metastasis (BMs)** | | | **0.306** |
| **1** | **44.6%** | **39.3%** | |

*(Continued)*

TABLE 4 Continued

| Characteristic | Low dose (n=65) (%) | High dose (n=56)(%) | P value |
|---|---|---|---|
| 2-3 | 46.2% | 57.1% | |
| >3 | 9.2% | 3.6% | |
| Diagnosis-specific Graded Prognostic Assessment (DS-GPA) (<2) | 32.3% | 17.9% | 0.053 |
| Maximum diameter of the largest tumor(≤2.0cm) | 53.8% | 73.2% | 0.022 |
| Interval from diagnosis of SCLC to BMs (>10 mths) | 36.9% | 69.6% | 0.000 |
| Extracranial disease control status (yes) | 61.5% | 73.2% | 0.173 |
| whole brain radiotherapy (WBRT)+stereotactic radiosurgery (SRS) | 1.5% | 96.4% | 0.000 |

significant difference in the side effects of different radiotherapy dose (Table 2). After PSM matching, the 2-year iOS of the low dose group was significantly superior than that of the high dose group. Further analysis revealed that in the DS-GPA<2 subgroup, the iOS in the low dose group was significantly superior than that in the high dose group; In subgroups of DS-GPA ≥ 2, the iLC in the high dose group was significantly superior than that in the low dose group.

More than 50% of SCLC patients may have BMs during the disease developing, and the prognosis is poor after the occurrence of BM. The treatment of BM in SCLC patients is different from other solid tumors because SCLC is a very aggressive, poorly differentiated, and high-grade neuroendocrine carcinoma (13). Even in patients with stage I-III SCLC who received surgical resection, the cumulative incidence of brain metastases was as high as 30% (14). According to the time of BMs to initial diagnosis, clinical manifestations of BMs (synchronous and asynchronous BM), BM treatment plans are different. In addition, the radiotherapy strategy also considers the patient's extracranial disease control status. Considering the high frequency of intracranial recurrence, SRS or surgical treatment SRS for limited BM from SCLC is not a standard of care. However, more evidence suggests that SBRT alone is feasible for treating BM in SCLC patients. However, in a large multicenter analysis, it was found that compared to SRS alone, WBRT improved TTP (HR 0.38, p<0.001), but did not significantly improve OS (median OS, 6.5 [SRS] vs 5.2 months [WBRT], p=0.003) (15).

Several clinical studies have reported the role of WBRT plus boost radiotherapy in the treatment of BM. Andrews et al (16) recruited 331 patients with 1-3 BMs, and found that WBRT combined with SRS significantly improved the 1-year local control of intracranial metastasis (82% vs 71%, p=0.013) compared with WBRT alone. In addition, compared to WBRT alone, WBRT+SRS improved the survival of patients with single BM, with a median OS of 4.9 months and 6.5 months, respectively (p=0.039) (15). The recent report showed that WBRT+SRS

TABLE 5 Distribution of the 98 patient treatment and clinical characteristics in two treatment groups after PSM matching.

| Characteristic | low dose(%) | high dose(%) | P value |
|---|---|---|---|
| Age (<65 yrs) | 71.4% | 79.6% | 0.241 |
| Gender(male) | 87.8% | 77.6% | 0.143 |
| Smoke index≥400 | 80.0% | 70.8% | 0.217 |
| Family history of tumors (yes) | 24.5% | 12.2% | 0.096 |
| Weight loss >5%(no) | 18.4% | 28.6% | 0.170 |
| KPS≥80 | 83.7% | 91.8% | 0.187 |
| TRT dose ≥50Gy | 77.3% | 85.4% | 0.302 |
| Stage (LS-SCLC) | 51.0% | 67.3% | 0.075 |
| Number of BMs | | | 0.206 |
| 1 | 49.0% | 40.8% | |
| 2-3 | 42.9% | 57.1% | |
| >3 | 8.2% | 2.0% | |
| GPA (<2) | 30.6% | 16.3% | 0.176 |
| Maximum diameter of the largest tumor(≤2.0cm) | 59.2% | 71.4% | 0.144 |
| Interval from diagnosis of SCLC to BMs (≤10 mths) | 51.0% | 65.3% | 0.110 |
| Extracranial disease control status (yes) | 77.6% | 83.7% | 0.305 |

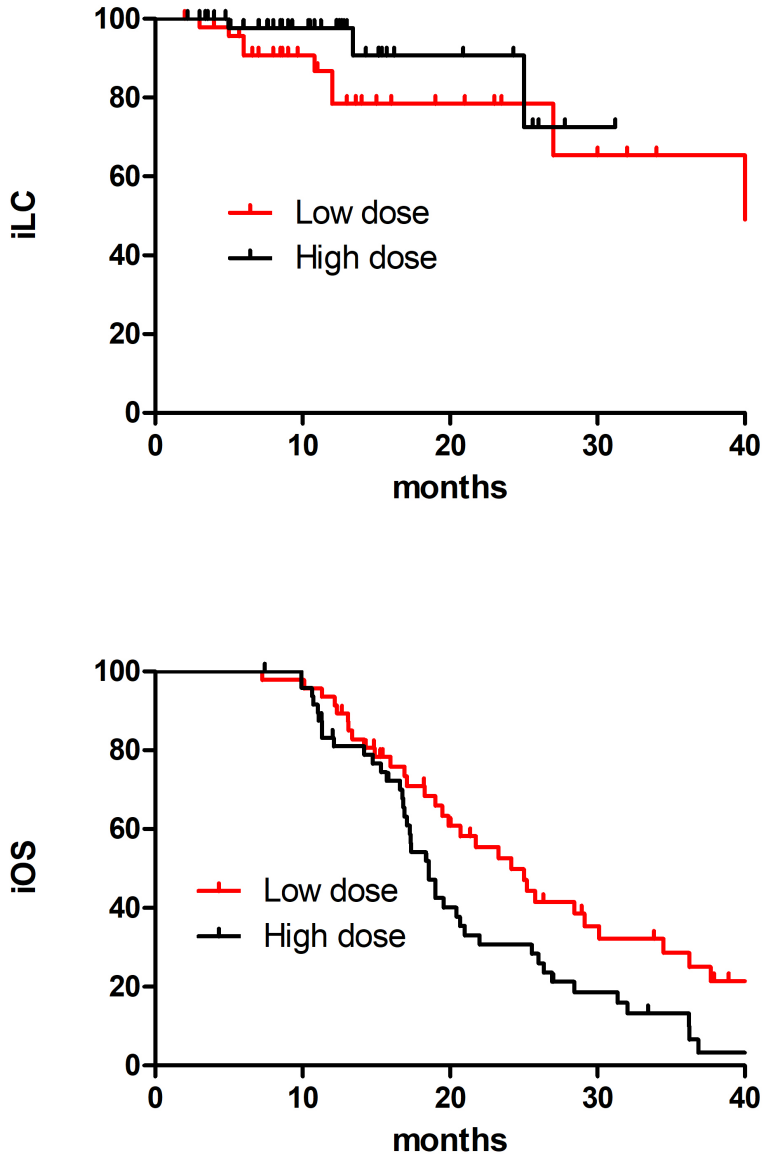


FIGURE 2
The iOS and iLC in 96 SCLC BM patients in low dose and high dose after PSM matching.

significantly improved the OS in the DS-GPA 2.5-4.0 subgroup, with median OS of 16.7 months and 10.6 months, respectively (p=0.04) (15, 17, 18).

In previous studies, some prognostic factors such as KPS, age, extracranial disease control status, and number of BM were identified in SCLC patients with BM. In this study, by univariate and multivariate analysis, extracranial disease control, and the higher DS-GPA were significantly related to the superior of OS. In addition, although the number of immunotherapy cases is relatively small, OS is still significantly affected by immunotherapy in univariate analysis.

With the promotion of SCLC comprehensive treatment and the application of immunotherapy, the OS of SCLC patients has significantly improved, reaching over 12 months. Therefore, the radiotherapy strategies for BM need further study. A meta-analysis showed that for patients with BM receiving SRS, when the BED was 40, 50, and 60Gy, 1-year iLC were 73%, 78%, and 84%, respectively, and 2-year iLC were 62%, 69%, and 81%, respectively (19). The iLC was improved along with increasing radiotherapy dose. A multi-center retrospective study reported that BED dose >50.7Gy was associated with improved OS in patients with BM (23.3 months vs. 8.2 months, $p < 0.01$) (20). Another retrospective study suggested that the BED >47.4Gy brain radiotherapy can improve OS and iPFS (21). This study mainly compared the impact on prognosis with different radiotherapy dose, and the results showed that high dose had inferior iOS compared to low dose, while there were not significantly improving in iLC when BED >56Gy. This may be related to the low GPA score, large BM, multiple BM in the high group (22–24). However, there was no significant difference in clinical characteristic distribution after PSM in this study, indicating that low dose had a survival advantage for BM patients. Based on the classification of DS-GPA, we further analyzed the prognosis of different DS-GPA scores in the low and high dose groups. We found that in the GPA<2

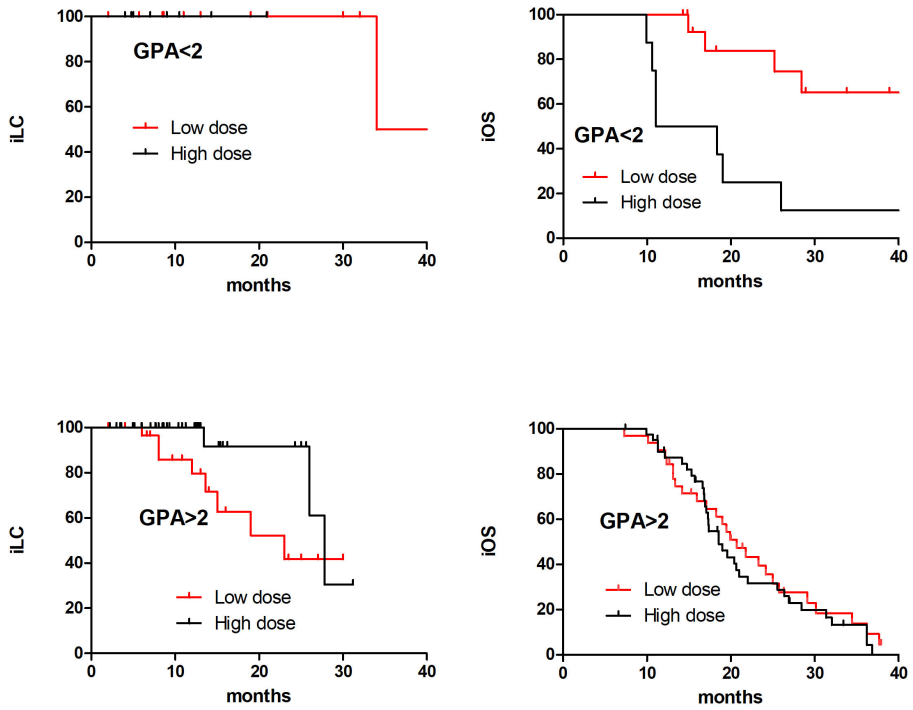


FIGURE 3
The iOS and iLC in 98 SCLC BM patients with different DS-GPA scores in low dose and high dose after PSM matching.

subgroup, the iOS in the low dose group was significantly superior than that in the high dose group; in subgroups with GPA ≥ 2, the iLC in the high dose group was significantly superior than that in the low dose group. This inconsistent phenomenon suggested that the role of chemotherapy and immunity may be more important for SCLC patients with BM in the GPA<2 subgroup.

This study has the following limitations. Firstly, this study is a retrospective analysis, and the distribution of clinical features is not very uniform. Secondly, this is a small sample retrospective study with choice bias, which should be verified by further prospective cohort study.

## Conclusions

To our knowledge, this is the first retrospective study to evaluate WBRT with different radiotherapy boost approaches (SIB and SRS) in SCLC patients with BM. Our study found that the iLC was improved along with increasing radiotherapy dose, but high dose had inferior iOS compared to low dose, while there were not significantly improving iLC when BED >56Gy. In patients with GPA≥2 subgroup, high dose brought better iLC benefits. This surprising result suggested that the iLC was not improved iOS along with increasing radiotherapy dose when the radiotherapy dose reached to a certain extent, which needed further observed.

## Data availability statement

The original contributions presented in the study are included in the article/supplementary material. Further inquiries can be directed to the corresponding authors.

## Ethics statement

The studies involving humans were approved by The ethics committee of Tianjin Medical University Cancer Hospital. The studies were conducted in accordance with the local legislation and institutional requirements. Written informed consent for participation was not required from the participants or the participants' legal guardians/next of kin in accordance with the national legislation and institutional requirements.

## Author contributions

LX, KZ and HH performed data acquisition, the statistical analysis and drafted the manuscript, the three authors contributed equally to the study. HS and YY performed data acquisition and the statistical analysis. JW, LZ and PW critically reviewed the manuscript. All authors contributed to the article and approved the submitted version.

## Funding

This study was supported by the National Natural Science Foundation of China (No.81502656 and No. 81501140).

## Conflict of interest

The authors declare that the research was conducted in the absence of any commercial or financial relationships that could be construed as a potential conflict of interest.

## Publisher's note



## References

1. Thai AA, Solomon BJ, Sequist LV, Gainor JF, Heist RS. Lung cancer. *Lancet* (2021) 398(10299):535–54. doi: 10.1016/S0140-6736(21)00312-3

2. Rong YT, Zhu YC, Wu Y. A novel nomogram predicting cancer-specific survival in small cell lung cancer patients with brain metastasis. *Transl Cancer Res* (2022) 11 (12):4289–302. doi: 10.21037/tcr-22-1561

3. Wu Q, Chen M, Peng F, Zhang Q, Kong Y, Bao Y, et al. A study of the prognosis of patients with limited-stage small cell lung cancer who did or did not receive prophylactic cranial irradiation after effective chemoradiotherapy. *Front Oncol* (2023) 13:1118371. doi: 10.3389/fonc.2023.1118371

4. Wang C, Mu S, Yang X, Li L, Tao H, Zhang F, et al. Outcome of immune checkpoint inhibitors in patients with extensive-stage small-cell lung cancer and brain metastases. *Front Oncol* (2023) 13:1110949. doi: 10.3389/fonc.2023.1110949

5. Zhou G, Zhang Z, Yu P, Geng-Oses R, Wang G, Ma W, et al. Predictive value of clinical characteristics on risk and prognosis of synchronous brain metastases in small-cell lung cancer patients: A population-based study. *Cancer Med* (2023) 12(2):1195–203. doi: 10.1002/cam4.4978

6. Seute T, Leffers P, Ten Velde GP, Twijnstra A. Detection of brain metastases from small cell lung cancer: consequences of changing imaging techniques (CT versus MRI). *Cancer* (2008) 112(8):1827–34. doi: 10.1002/cncr.23361

7. Zhou S, Ren F, Li C, Meng X, Huang Z. Efficacy and safety of immune checkpoint inhibitors plus anlotinib in small cell lung cancer with brain metastases: a retrospective, multicentre study. *J Neurooncol* (2022) 160(3):631–42. doi: 10.1007/s11060-022-04182-6

8. Sun H, Xu L, Wang Y, Zhao J, Xu K, Qi J, et al. Additional radiation boost to whole brain radiation therapy may improve the survival of patients with brain metastases in small cell lung cancer. *Radiat Oncol* (2018) 13(1):250. doi: 10.1186/s13014-018-1198-4

9. Gay CM, Stewart CA, Park EM, Diao L, Groves SM, Heeke S, et al. Patterns of transcription factor programs and immune pathway activation define four major subtypes of SCLC with distinct therapeutic vulnerabilities. *Cancer Cell* (2021) 39(3):346–60 e7. doi: 10.1016/j.ccell.2020.12.014

10. Chia B SH, Leong JY, Ong A LK, Lim C, Poon SH, Chua MLK, et al. Randomised prospective phase II trial in multiple brain metastases comparing outcomes between hippocampal avoidance whole brain radiotherapy with or without simultaneous integrated boost: HA-SIB-WBRT study protocol. *BMC Cancer* (2020) 20(1):1045. doi: 10.1186/s12885-020-07565-y

11. Qing D, Zhao B, Zhou YC, Zhu HL, Ma DY. Whole-brain radiotherapy plus sequential or simultaneous integrated boost for the treatment of a limited number of brain metastases in non-small cell lung cancer: A single-institution study. *Cancer Med* (2020) 9(1):238–46. doi: 10.1002/cam4.2696

12. Rieken S. Stereotactic radiosurgery for patients with small-cell lung cancer brain metastases. *Lancet Oncol* (2022) 23(7):832–3. doi: 10.1016/S1470-2045(22)00301-1

13. Gaebe K, Li AY, Park A, Parmar A, Lok BH, Sahgal A, et al. Stereotactic radiosurgery versus whole brain radiotherapy in patients with intracranial metastatic disease and small-cell lung cancer: a systematic review and meta-analysis. *Lancet Oncol* (2022) 23(7):931–9. doi: 10.1016/S1470-2045(22)00271-6

14. Rittberg R, Banerji S, Kim JO, Rathod S, Dawe DE. Treatment and prevention of brain metastases in small cell lung cancer. *Am J Clin Oncol* (2021) 44(12):629–38. doi: 10.1097/COC.0000000000000867

15. Rusthoven CG, Yamamoto M, Bernhardt D, Smith DE, Gao D, Serizawa T, et al. Evaluation of first-line radiosurgery vs whole-brain radiotherapy for small cell lung cancer brain metastases: the FIRE-SCLC cohort study. *JAMA Oncol* (2020) 6(7):1028–37. doi: 10.1001/jamaoncol.2020.1271

16. Andrews DW, Scott CB, Sperduto PW, Flanders AE, Gaspar LE, Schell MC, et al. Whole brain radiation therapy with or without stereotactic radiosurgery boost for patients with one to three brain metastases: phase III results of the RTOG 9508 randomized trial. *Lancet* (2004) 363(9422):1665–72. doi: 10.1016/S0140-6736(04)16250-8

17. Rodriguez DE Dios N, Counago F, Murcia-Mejia M, Rico-Oses M, Calvo-Crespo P, Samper P, et al. Randomized phase III trial of prophylactic cranial irradiation with or without hippocampal avoidance for small-cell lung cancer (PREMER): A GICOR-GOECP-SEOR study. *J Clin Oncol* (2021) 39(28):3118–27. doi: 10.1200/JCO.21.00639

18. Schunn F, Koerber S. Prophylactic cranial irradiation with or without hippocampal avoidance for small-cell lung cancer (PREMER)- a randomized phase III trial. *Strahlenther Onkol* (2022) 198(3):319–21. doi: 10.1007/s00066-021-01899-7

19. Baliga S, Garg MK, Fox J, Kalnicki S, Lasala PA, Welch MR, et al. Fractionated stereotactic radiation therapy for brain metastases: A systematic review with tumour control probability modelling. *Br J Radiol* (2017) 90(1070):20160666. doi: 10.1259/bjr.20160666

20. Casanova N, Mazouni Z, Bieri S, Combescure C, Pica A, Weber DC. Whole brain radiotherapy with a conformational external beam radiation boost for lung cancer patients with 1-3 brain metastasis: A multi institutional study. *Radiat Oncol* (2010) 5:13. doi: 10.1186/1748-717X-5-13

21. Lagerwaard FJ, van der Hoorn EA, Verbakel WF, Haasbeek CJ, Slotman BJ, Senan S. Whole-brain radiotherapy with simultaneous integrated boost to multiple brain metastases using volume tric modulated Arc therapy. *Int J Radiat Oncol Biol Phys* (2009) 75(1):253–9. doi: 10.1016/j.ijrobp.2009.03.029

22. Lin B, Huang D, Du H, Fan J, Zhang Y, Feng G, et al. Whole-brain radiation therapy with simultaneous integrated boost versus whole-brain radiation therapy plus stereotactic radiosurgery for the treatment of brain metastasis from lung cancer. *Front Oncol* (2021) 11:631422. doi: 10.3389/fonc.2021.631422

23. Chia BSH, Leong JY, Ong ALK, Lim C, Poon SH, Chua MLK, et al. Randomised prospective phase II trial in multiple brain metastases comparing outcomes between hippocampal avoidance whole brain radiotherapy with or without simultaneous integrated boost: HA-SIB-WBRT study protocol. *BMC Cancer* (2020) 20(1):1045. doi: 10.1186/s12885-020-07565-y

24. Bailleux C, Eberst L, Bachelot T. Treatment strategies for breast cancer brain metastases. *Br J Cancer* (2021) 124(1):142–55. doi: 10.1038/s41416-020-01175-y

frontiers | Frontiers in Oncology

TYPE Original Research
PUBLISHED 22 September 2023
DOI 10.3389/fonc.2023.1220047



OPEN ACCESS

EDITED BY
Xiangpan Li,
Renmin Hospital of Wuhan University, China

REVIEWED BY
Guixiang Liao,
Jinan University, China
Mirek Fatyga,
Mayo Clinic Arizona, United States

*CORRESPONDENCE
Ling Yuan
hnhnyl@126.com

RECEIVED 10 May 2023
ACCEPTED 04 September 2023
PUBLISHED 22 September 2023

CITATION
Dong X, Wang K, Yang H, Li Y, Hou Y, Chang J and Yuan L (2023) Choice of radiotherapy modality for the combined treatment of non-small cell lung cancer with brain metastases: whole-brain radiation therapy with simultaneous integrated boost or stereotactic radiosurgery.
*Front. Oncol.* 13:1220047.
doi: 10.3389/fonc.2023.1220047



# Choice of radiotherapy modality for the combined treatment of non-small cell lung cancer with brain metastases: whole-brain radiation therapy with simultaneous integrated boost or stereotactic radiosurgery

Xiaotao Dong, Kunlun Wang, Hui Yang, Yan Li, Yanqi Hou, Jiali Chang and Ling Yuan*

Department of Radiation Oncology Affiliated Cancer Hospital of Zhengzhou University, Zhengzhou, Henan, China

**Purpose:** To compare Whole-brain radiation therapy with simultaneous integrated boost (WBRT+SIB) to stereotactic radiosurgery (SRS)for non-small cell lung cancer (NSCLC)with brain metastases (BMs)in terms of overall survival (OS), intracranial progression-free-survival(iPFS), toxicity and objective response rate (ORR)

**Methods:** A retrospective review was performed in our hospital of 90 patients diagnosed with NSCLC- BM who received either SRS (n = 48) or WBRT+SIB (n = 42) from January 2016 to January 2022. 76 (84.44%) patients received systemic drug therapy after radiotherapy, including chemotherapy(n=53), targeted therapy(n=40), immunotherapy(n=23), and anti-vascular drug therapy(n=45). OS and iPFS were estimated by the Kaplan-Meier method and compared using the log-rank test. Univariate and Multivariate analysis of the prognostic factors was performed using the Cox proportional hazard regression model.

**Results:** The WBRT+SIB cohort had a longer median iPFS (20.0 versus (VS) 12.0 months, P = 0.0069) and a similar median OS (32.0 vs 28.0 months, P = 0.195) than the SRS cohort. Intracranial objective response rates in WBRT +SIB and SRS cohorts were 76.19% and 70.09%, respectively (P = 0.566). Disease control rates were 88.09% and 83.33%, respectively (P = 0.521). Multivariate analysis showed that WBRT+SIB is the only factor affecting iPFS(hazard ratio (HR):0.597 {95% confidence interval(CI):0.370-0.966}, P=0.035). Sex, Liver metastasis and Lymph node metastasis are risk factors for NSCLC-BM.

**Conclusion:** In the context of systemic drug therapy, WBRT+SIB may have better intracranial local control than SRS in NSCLC-BM patients.

KEYWORDS

**brain metastasis, simultaneous integrated boost, stereotactic radiosurgery, non-small cell lung cancer, combined therapy, radiotherapy**

# 1 Introduction

Among the most common cancers, lung cancer ranks first in cancer-associated death worldwide. More than 80% of lung cancer patients are non-small cell lung cancer (NSCLC). Brain metastases (BMs) from NSCLC represent an unmet need of increasing relevance as their incidence is rising considerably. Early use of magnetic resonance imaging/positron emission tomography-computed tomography (MRI/PET-CT) and improvements in therapies for systemic disease and ageing populations are contributing factors to this increasing incidence. The treatment of NSCLC-BM patients was always the hotspot of study. Neurosurgical resection is usually reserved for patients with good performance status, low-burden oligometastatic disease, and controlled extracranial/primary disease. Radiotherapy and drug therapy remain the primary treatment for many BM patients (1). The conventional view is that anti-tumor drugs are subject to the central nervous system (CNS) barrier (blood-brain barrier/blood-tumor barrier). However, Several studies have shown that novel drugs, such as three generations-targeted drugs and immune checkpoint inhibitors (ICIs), can achieve effective therapeutic concentrations in the CNS (2, 3). In addition, Radiation has synergistic effects with the drugs mentioned above (4–9). However, the local control (LC) rate is still unsatisfactory when treated with Whole- Brain Radiation Therapy/Stereotactic radiosurgery (WBRT/SRS) alone. WBRT with Simultaneous Integrated Boost (SIB) can enhance the intracranial control more than WBRT (10, 11), and SIB has the biological advantage of dose fractionation. One of the critical unanswered questions in the BM therapy field is the choice of radiotherapy mode under the principle of drug combined with radiation. It is unclear whether WBRT + SIB can improve efficacy and reduce toxicity compared with SRS. This study aimed to research the efficacy of these two conventional radiotherapy modalities WBRT+SIB and SRS, and investigate the prognostic factors, providing a reference for establishing the best strategy for treating NSCLC-BM.

# 2 Materials and methods

The clinical data of NSCLC-BM patients who underwent radiotherapy in the Affiliated Cancer Hospital of Zhengzhou University from January 2016 to January 2022 were retrospectively analyzed. This study was approved by the ethics committees of the Affiliated Cancer Hospital of Zhengzhou University & Henan Cancer Hospital, Zhengzhou, China. Due to the retrospective nature of the study and because no patient specimens were used, the requirement for informed consent was waived by the ethics committees. The inclusion criteria were as follows:(1) all included patients were confirmed by pathological diagnosis with primary lung cancer. (2) brain metastases were confirmed by CT scan or MRI. (3) radiotherapy, including WBRT +SIB or SRS and (4) clinical data integrity. The exclusion criteria were as follows: (1) received BM resection (2) small cell lung cancer (3) meningeal metastases. Finally, 90 patients were enrolled in this study. We collected baseline characteristics about the patients, including age, gender, BM numbers and the longest diameter, clinicopathological type,BMI, Distant metastatic status other than the brain(Liver,Bone, Lymph node and Contralateral lung), Common geriatric diseases such as hypertension and Glycuresis, Karnofsky performance status (KPS), radiotherapy modality, extracranial metastasis status, and post-radiotherapy treatment including chemotherapy, targeted therapy, immunotherapy, and anti-angiogenic drugs therapy. Besides, radiotherapy dose, start and end time of radiotherapy, date of intracranial progression and date of death, and radiotherapy-related toxicity were also collected.

## 2.1 Radiotherapy strategy

Radiotherapy was administered using WBRT+SIB or SRS. Patients were placed in the supine position. The head was immobilized with a thermoplastic mask; Enhanced CT was performed to localize the scan from the cranial vault to the cricoid cartilage with a layer thickness of 2 mm. The localization images were transmitted to the ECLIPSE planning system and fused with brain MRI images. Outline the target area on the ECLIPSE system. The gross tumor volume (GTV) was the metastases visible on the image, the clinical target volume (CTV) was the whole brain, GTV and CTV were exenterated 2 mm as the planning gross tumor volume (P-GTV) and clinical gross tumor volume(P-CTV). Besides, Outline the relevant organs at risk (e.g., optic nerve, optic cross, eye, crystal, brainstem, hippocampus, etc.) Radiotherapy schedule: IMRT 6MV-Xray P-CTV: 30Gy/3Gy/10f, P-GTV: 45Gy/4.5Gy/10f. 5 treatments per week (Mon-Fri). The prescribed dose of SRS varies according to the longest BM diameter (16-24Gy).

## 2.2 Follow-up

Data was obtained from inpatient medical records, and follow-up data was obtained by contacting patients by phone, home visits, or questionnaires. A complete inpatient medical record was available for each patient. Clinical efficacy and adverse effects were evaluated, and the final results were based on the data from the last follow-up visit.

## 2.3 Endpoint

The primary endpoint was Overall Survival (OS) and Intracranial Progression-free Survival(iPFS), while the secondary endpoint was the objective intracranial response. Objective response rate (ORR) = the number of (CR+PR) cases/total cases × 100%, and disease control rate (DCR) = the number of (CR+PR +SD) cases/total cases × 100%. iPFS was the time from radiotherapy to intracranial progression or patient death. OS was defined as the time from the start of radiotherapy to death or the last follow-up (2023.01.01). Progression was defined as >20% increase in BM diameter or new BM on imaging brain CT/MRI according to RECIST 1.1 criteria. Imaging evaluation of brain CT/MRI was

performed monthly until the third month and reviewed every three months afterwards.

## 2.4 Statistical analysis

R studio (version 4.2.3) and SPSS Statistics software, version 26.0 (IBM Corporation, Armonk, NY, United States), were used for the analysis in this study. The cardinality test was used to compare the two groups' differences in categorical variables, objective response rates, and toxicity. Kaplan-Meier method was used to analyze the iPFS and OS of the two groups and plot survival curves, and the log-rank test was used for different assessments. Univariate and Multivariate analyses used COX proportional risk regression models to estimate prognosis-related independent factors. After univariate analysis, clinical factors with $P < 0.20$ were included in the Multivariate Cox proportional risk regression model for analysis, reporting hazard ratio (HR) and 95% confidence interval (CI). All tests were performed bilaterally. $P < 0.05$ was considered statistically significant.

# 3 Results

## 3.1 Baseline characteristics

This study included 2963 patients with NSCLC-BM who were treated at the Affiliated Cancer Hospital of Zhengzhou University from January 2016 to January 2022, of whom 145 received WBRT, 32 received WBRT+SRS, 30 underwent neurosurgery, and 7 patients had missing data. Only 90 patients (42 underwent WBRT+SIB and 48 underwent SRS) were included in the study (Figure 1). The mean age of the total population was 60.1 years old (range 32-77 years),62 patients (68.89%) were ≤65 years old, 55 patients (61.11%) were male, 75 patients (83.33%) were adenocarcinoma and 40 cases had gene mutation (31 were EGFR +,7 were ALK+, and 2 were ROS1+), 73(81.11%) patients with KPS ≥70. The proportion of patients with single BM was significantly higher in the SRS group than in the WBRT+SIB group (16.67% vs 56.25%, $P < 0.05$). 76 patients (84.44%) received drug therapy after radiotherapy, of which 55 patients (61.11%%) received chemotherapy, 40 patients (44.44%) received targeted therapy, 23 patients (25.56%) received immunotherapy, and 45 patients (50.0%) received anti-angiogenic drugs. Other distant metastatic organs other than brain metastases, 35(38.9%) patients had liver metastases, 34(37.8%) had distant lymph node metastases, 27 (30.0%) had contralateral lung metastases, and 27(30.0%) had bone metastases. All baseline patient characteristics are shown in Table 1.

## 3.2 Prognostic information

The median follow-up time was 38.0 months (range 2.0-80.0 months). The median iPFS of enrolled patients was 15.0 months (95% CI: 10.2-19.7 months) median OS was 29.0 months (95% CI: 24.3-33.7 months) (Figure 2). As of the last follow-up, there were 31 and 45 cases of intracranial progression or death in the WBRT+SIB and SRS groups, respectively.

## 3.3 Subgroup analysis

Except for the number of BMs ($P < 0.001$), there were no significant differences in other baseline characteristics between the two cohorts. Overall mortality was 54.7% in the WBRT+SIB cohort and 62.5% in the SRS cohort. Median iPFS was significantly longer in the WBRT+SIB cohort than in the SRS cohort (20.0 vs. 12.0

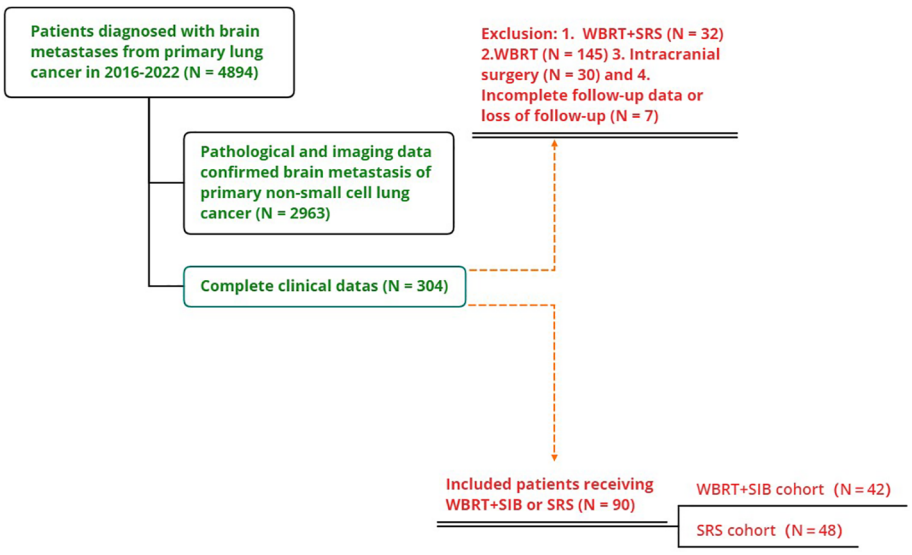


FIGURE 1
The flowchart of the database filtering process.

TABLE 1 Patients characteristics.

| | WBRT+SIB(N=42) | SRS(N=48) | Pvalue |
|---|---|---|---|
| Median age and range | 59(32-77) | 62(42-76) | |
| Age | | | |
| ≤65 | 34(80.95%) | 28(58.33%) | 0.084 |
| >65 | 8 (19.05%) | 20(41.67%) | |
| Sex | | | 0.773 |
| Male | 17(40.48%) | 18(37.50%) | |
| Female | 25(59.52%) | 30(62.50%) | |
| BMI | | | 0.756 |
| ≤23.9 | 36(85.71%) | 40(83.3%) | |
| >23.9 | 6(14.29%) | 8(16.7%) | |
| Number of BM | | | P<0.005 |
| 1 | 7 (16.67%) | 27(56.25%) | |
| >1 | 35(83.33%) | 21(43.75%) | |
| Diameter of the largest BM | | | 0.245 |
| ≤3cm | 34(80.95%) | 43(89.58%) | |
| >3cm | 8 (19.05%) | 5 (10.42%) | |
| Histological status | | | 0.257 |
| Squamous cell | 5(11.90%) | 10(20.83%) | |
| Adenocarcinoma | 37(88.10%) | 38(79.17%) | |
| Surgery before RT | | | 0.488 |
| No | 30(71.43%) | 31(64.58%) | |
| Yes | 12(28.57%) | 17(35.42%) | |
| KPS | | | 0.297 |
| <70 | 6(14.29%) | 11(22.92%) | |
| ≥70 | 36(85.71%) | 37(77.08%) | |
| Hypertension | | | 0.215 |
| No | 19(45.24%) | 28(58.33%) | |
| Yes | 23(55.76%) | 20(41.67%) | |
| Glycuresis | | | 0.027 |
| No | 29(69.04%) | 22(45.83%) | |
| Yes | 13(30.96%) | 26(54.17%) | |
| Liver metastasis | | | 0.563 |
| No | 27(64.29%) | 28(58.33%) | |
| Yes | 15(35.71%) | 20(41.67%) | |
| Lymph metastasis | | | 0.706 |
| No | 27(64.29%) | 29(60.42%) | |
| Yes | 15(35.71%) | 19(39.58%) | |

*(Continued)*

TABLE 1 Continued

| | WBRT+SIB(N=42) | SRS(N=48) | Pvalue |
|---|---|---|---|
| Contralateral lung metastasis | | | 0.782 |
| No | 30(71.42%) | 33(68.75%) | |
| Yes | 12(28.58%) | 15(31.25%) | |
| Bone metastasis | | | 0.461 |
| No | 31(73.81%) | 32(66.67%) | |
| Yes | 11(26.19%) | 16(33.33%) | |
| Chemotherapy after RT | | | 0.753 |
| No | 18(42.86%) | 19(39.58%) | |
| Yes | 24(57.14%) | 29(60.42%) | |
| Target therapy after RT | | | 0.571 |
| No | 22(52.38%) | 28(58.33%) | |
| Yes | 20(47.62%) | 20(41.67%) | |
| Immunotherapy after RT | | | 0.722 |
| No | 32(76.19%) | 35(72.92%) | |
| Yes | 10(23.81%) | 13(27.08%) | |
| Anti-angiogenic drug therapy after RT | | | 0.673 |
| No | 20(52.38%) | 25(60.42%) | |
| Yes | 22(47.62%) | 23(39.58%) | |

WBRT+SIB, Whole- Brain Radiation Therapy with Simultaneous Integrated Boost; SRS, Stereotactic Radiosurgery; BM, brain metastasis; RT, Radiotherapy; BMI, Body mass index.

months,P= 0.0069, Figure 3), and median OS was also longer in the WBRT+SIB cohort (32.0 vs. 28.0 months P = 0.19, Figure 3), though, the difference in OS was not statistically significant.

## 3.4 Univariate/multivariate analysis

In univariate analysis, radiotherapy modality (P = 0.010) had the predictive value for iPFS. Histological status, Liver metastasis, Lymph node metastasis, BMI and Hypertension had the predictive value for OS. Factors which P ≤ 0.2 in univariate analysis were included in multifactorial analysis, Cox regression model analysis showed that the only independent prognostic factor for iPFS was Treatment group (Table 2). Sex, Liver metastasis and Lymph node metastasis are risk factors for NSCLC-BM (Table 3).

## 3.5 Intracranial objective response rate

The WBRT+SIB and SRS groups had similar objective intracranial remission rates (objective response rate (ORR): 76.19% vs. 70.09%, P = 0.566) (disease control rate (DCR): 88.09% vs. 83.33%, P = 0.521) The brain CT/MRI at the third month after radiotherapy showed 2 cases of complete response (CR), 30 cases of partial response (PR), 5 cases of stable disease (SD), and 5 cases of progressive disease (PD) in the WBRT+SIB group and 1 case of CR, 33 cases of PR, 6 cases of SD, and 8 cases of PD in the SRS group (Table 4).

## 3.6 Toxicity

Post-radiotherapy-related toxicity according to the RTOG standard mainly included Nausea and vomiting, Leukopenia, Thrombocytopenia and CNS symptoms (including speech impairment, impaired consciousness, drowsiness, etc.) Acute radiation injury and late radiation injury as well as injury grading are shown in (Table 5).

# 4 Discussion

This single-center retrospective study aimed to compare the effects of two radiotherapy modalities, WBRT+SIB and SRS, for the treatment of NSCLC-BM, with the primary study endpoints of iPFS and OS. The study results showed that compared to SRS, iPFS was significantly improved in the WBRT+SIB group (20.0 vs. 12.0 months, P = 0.0069). The difference in OS was not statistically significant (32.0 vs. 28.0 months, P = 0.19); patients with adenocarcinoma only tended to benefit in OS and iPFS compared to squamous cell carcinoma, but not statistically significant. The two groups had no significant difference in the current objective intracranial remission rate (76.19% vs. 70.09%, P = 0.566).

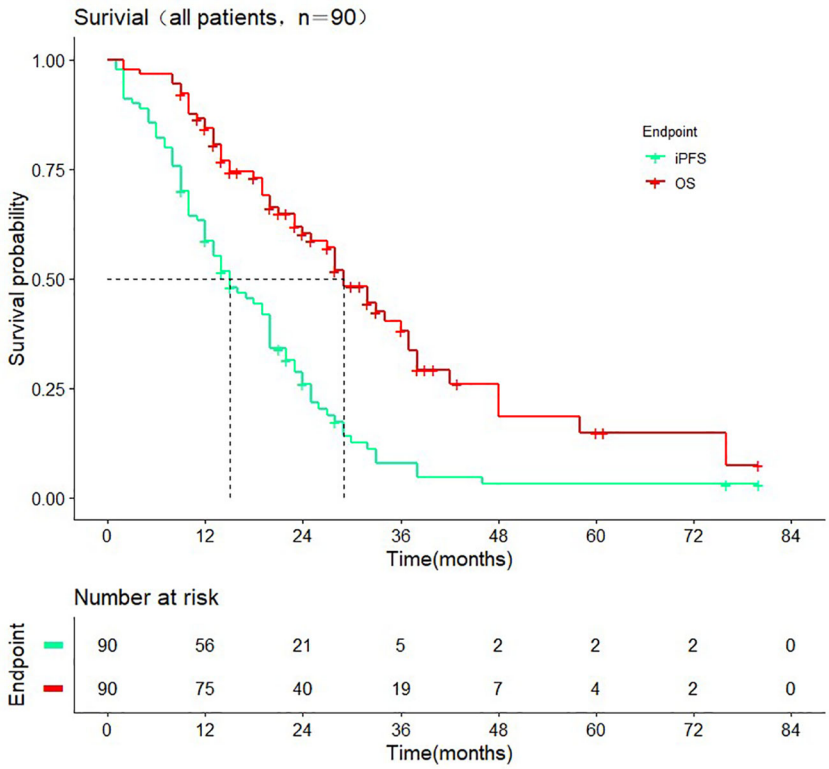


FIGURE 2
Intracranial progression-free-survival and overall survival in all patients.

Current studies suggest that OS in patients with BMs under systemic therapy no longer appears to be limited by the control of intracranial lesions but instead had a more significant relationship with systemic disease progression (12). Our results also support the above view. In addition, we found relevant factors affecting OS of NSCLC-BM, including lymph node metastasis, bone metastasis, and hypertension.

The choice of radiotherapy modality when treating different kinds of BM patients is an issue that requires careful consideration. Yamamoto et al. (13) found that after SRS treatment, patients in the BM number 2-4 and 5-10 groups had the same OS. No difference in OS was found between BM number ≥10 and 2-9 groups (14). More and more evidence showed that SRS should no longer be limited to the number of BM. WBRT tends to withdraw from the mainstream of

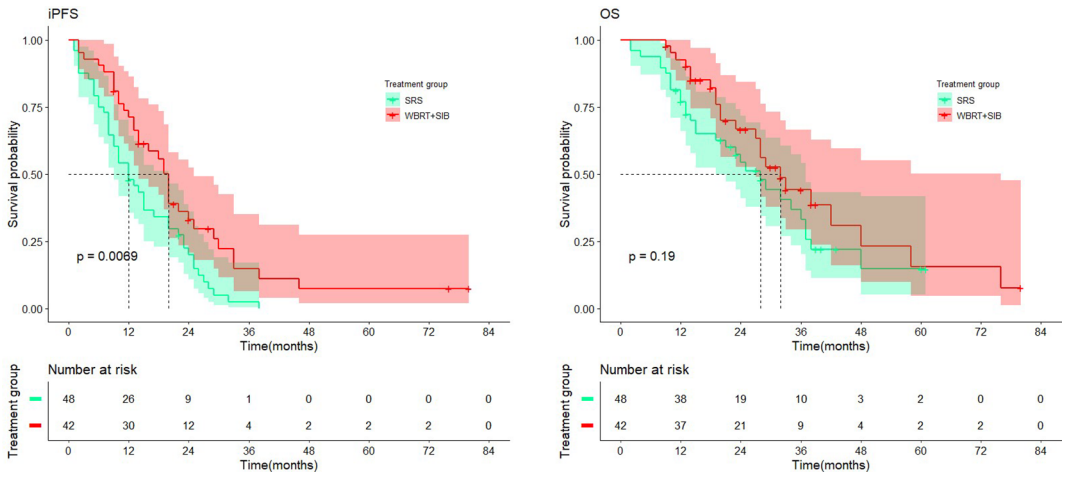


FIGURE 3
Comparison of intracranial progression-free-survival and overall survival in treatment cohort.

TABLE 2 Survival-related factors on iPFS in univariate/multivariate analysis.

| | ◆Univariate analysis | | | | ○Multivariate analysis | | | |
|---|---|---|---|---|---|---|---|---|
| | Pvalue | HR | Lower | Upper | Pvalue | HR | Lower | Upper |
| Sex(Male vsFemale) | 0.679 | 1.104 | 0.692 | 1.760 | | | | |
| Treatment group(WBRT+SIB vs SRS) | **0.010** | 0.544 | 0.342 | 0.863 | **0.023** | 0.564 | 0.345 | 0.922 |
| Age(>65 vs ⩽65) | **0.075** | 1.528 | 0.959 | 2.436 | 0.579 | 1.154 | 0.695 | 1.915 |
| Histological status(Adenocarcinoma vs Squamous cell) | **0.112** | 0.610 | 0.331 | 1.122 | 0.554 | 0.824 | 0.434 | 1.564 |
| Diameter of largest BM(>3cm vs⩽3cm) | 0.738 | 0.897 | 0.472 | 1.702 | | | | |
| Surgery before RT(Yes vs No) | 0.520 | 1.167 | 0.729 | 1.870 | | | | |
| Chemotherapy after RT(Yes vs No) | 0.673 | 1.104 | 0.697 | 1.748 | | | | |
| Target therapy after RT(Yes vs No) | 0.874 | 1.037 | 0.663 | 1.622 | 0.231 | 1.352 | 0.826 | 2.214 |
| Immunotherapy after RT(Yes vs No) | 0.499 | 1.195 | 0.714 | 2.000 | 0.246 | 0.720 | 0.414 | 1.254 |
| Anti angiogenic drug therapy after RT(Yes vs No) | 0.440 | 1.199 | 0.756 | 1.903 | | | | |
| KPS(⩾70 vs <70) | 0.631 | 0.875 | 0.508 | 1.508 | | | | |
| Liver metastasis(Yes vs No) | **0.070** | 1.524 | 0.966 | 2.407 | | | | |
| Lymph node metastasis(Yes vs No) | 0.324 | 1.257 | 0.798 | 1.980 | | | | |
| Contralateral lung metastasis(Yes vs No) | **0.070** | 0.627 | 0.378 | 1.040 | | | | |
| Bone metastasis(Yes vs No) | 0.493 | 1.193 | 0.720 | 1.976 | | | | |
| BMI(⩾23.9 vs <23.9) | 0.280 | 0.703 | 0.371 | 1.333 | | | | |
| Hypertension(Yes vs No) | 0.301 | 0.788 | 0.501 | 1.238 | | | | |
| Glycuresis(Yes vs No) | 0.316 | 1.257 | 0.804 | 1.965 | | | | |

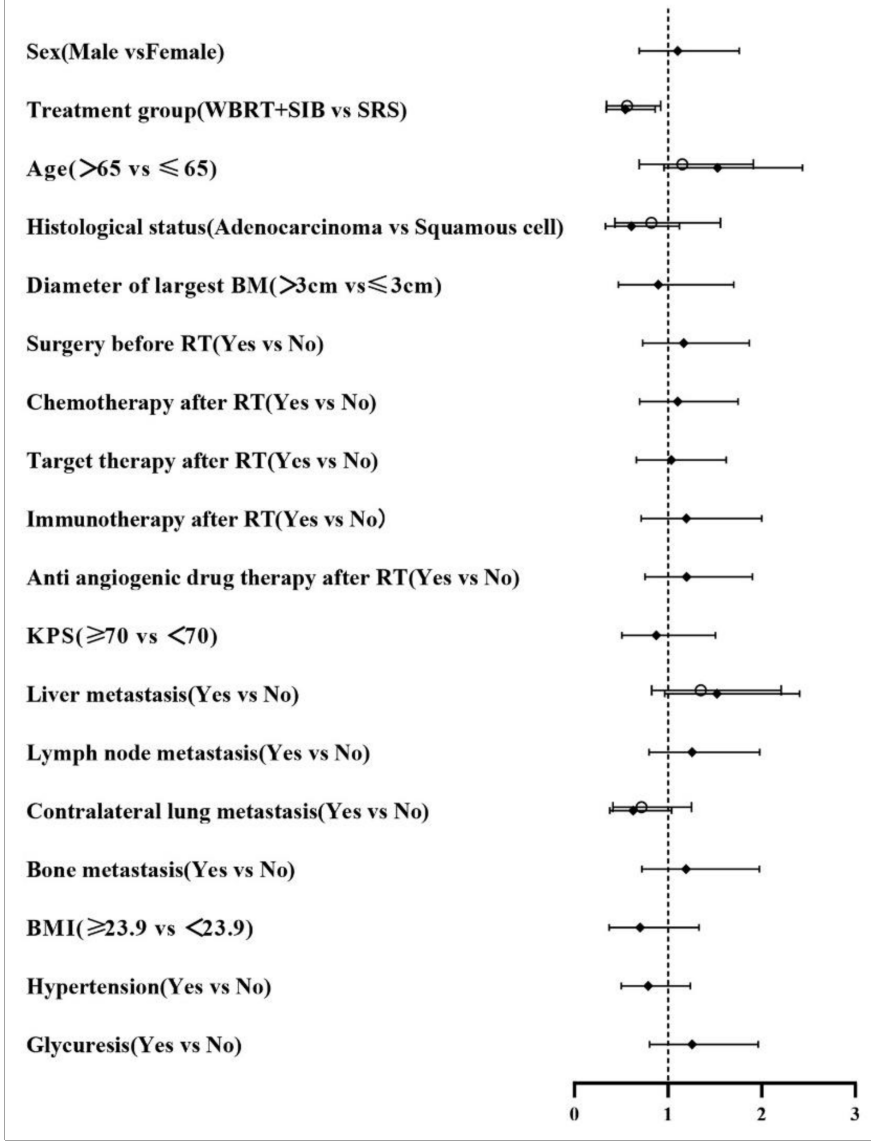


WBRT+SIB, Whole- Brain Radiation Therapy with Simultaneous Integrated Boost; SRS, Stereotactic Radiosurgery; BM, brain metastasis; RT, Radiotherapy; KPS, Karnofsky; BMI, Body mass index.
Significance in bold was P < 0.2 in univariate analysis. In multivariate analysis, significance in bold is P< 0.05.





10.3389/fonc.2023.1220047

TABLE 3 Survival-related factors on OS in univariate/multivariate analysis.

| | ◆Univariate analysis | | | | ○Multivariate analysis | | | |
|---|---|---|---|---|---|---|---|---|
| | Pvalue | HR | Lower | Upper | Pvalue | HR | Lower | Upper |
| Sex(Male vsFemale) | **0.062** | 1.761 | 0.973 | 3.187 | **0.020** | 2.138 | 1.129 | 4.052 |
| Treatment group(WBRT+SIB vs SRS) | 0.204 | 0.700 | 0.403 | 1.214 | | | | |
| Age(>65 vs ⩽65) | 0.066 | 1.678 | 0.967 | 2.913 | | | | |
| Histological status(Adenocarcinoma vs Squamous cell) | **0.010** | 0.411 | 0.208 | 0.811 | 0.059 | 0.496 | 0.240 | 1.026 |
| Diameter of largest BM(>3cm vs⩽3cm) | 0.980 | 0.990 | 0.444 | 2.207 | | | | |
| Surgery before RT(Yes vs No) | 0.496 | 0.814 | 0.450 | 1.473 | | | | |
| Chemotherapy after RT(Yes vs No) | 0.347 | 0.768 | 0.443 | 1.331 | | | | |
| Target therapy after RT(Yes vs No) | 0.484 | 0.823 | 0.478 | 1.418 | | | | |
| Immunotherapy after RT(Yes vs No) | 0.264 | 0.673 | 0.337 | 1.347 | | | | |
| Anti angiogenic drug therapy after RT(Yes vs No) | 0.445 | 0.803 | 0.457 | 1.410 | | | | |
| KPS(⩾70 vs <70) | 0.524 | 0.810 | 0.424 | 1.549 | | | | |
| Liver metastasis(Yes vs No) | **<0.001** | 3.084 | 1.768 | 5.328 | **0.001** | 2.924 | 1.535 | 5.568 |
| Lymph node metastasis(Yes vs No) | **0.043** | 1.757 | 1.019 | 3.029 | **0.015** | 2.080 | 1.156 | 3.745 |
| Contralateral lung metastasis(Yes vs No) | **0.082** | 0.552 | 0.282 | 1.078 | 0.912 | 0.960 | 0.464 | 1.985 |
| Bone metastasis(Yes vs No) | **0.078** | 1.693 | 0.942 | 3.044 | 0.134 | 1.670 | 0.853 | 3.267 |
| BMI(⩾23.9 vs <23.9) | **0.045** | 1.961 | 1.015 | 3.786 | 0.921 | 1.039 | 0.488 | 2.212 |
| Hypertension(Yes vs No) | **0.019** | 0.510 | 0.291 | 0.894 | 0.088 | 0.580 | 0.310 | 1.085 |
| Glycuresis(Yes vs No) | 0.278 | 1.354 | 0.783 | 2.342 | | | | |

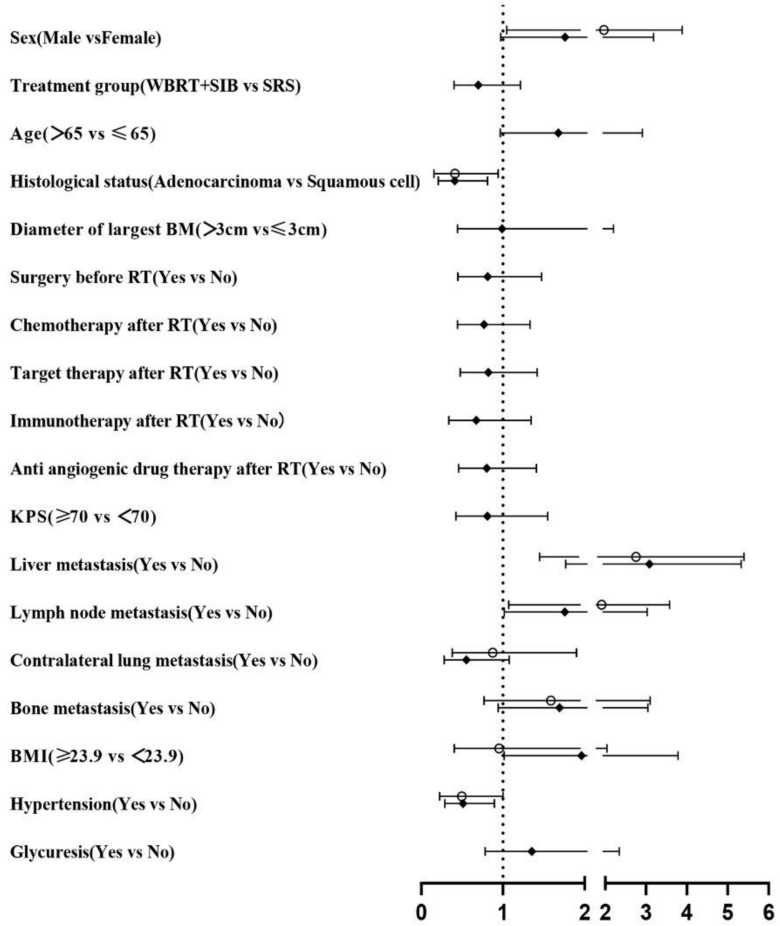


WBRT+SIB, Whole- Brain Radiation Therapy with Simultaneous Integrated Boost; SRS, Stereotactic Radiosurgery; BM, brain metastasis; RT, Radiotherapy; KPS, Karnofsky; BMI, Body mass index.
Significance in bold was P < 0.2 in univariate analysis. In multivariate analysis, significance in bold is P< 0.05.





10.3389/fonc.2023.1220047

TABLE 4 Overall response.

| | WBRT+SIB | SRS | Pvalue |
|---|---|---|---|
| ORR | 32(76.19%) | 34(70.09%) | 0.566 |
| DCR | 37(88.09%) | 40(83.33%) | 0.521 |
| CR | 2 (4.76%) | 1 (2.08%) | |
| PR | 30(71.43%) | 33(68.75%) | |
| SD | 5 (11.90%) | 6 (12.50%) | |
| PD | 5 (11.90%) | 8 (16.67%) | |

WBRT+SIB, Whole- Brain Radiation Therapy with Simultaneous Integrated Boost; SRS, Stereotactic Radiosurgery; ORR, objective response rate; DCR, disease control rate; CR, complete response; PR, partial response; SD, stable disease; PD, progressive disease.

BM radiotherapy. What is more, WBRT is associated with poor cognitive function and decreased quality of survival. Theoretically, Radiation alters CNS barrier permeability in a time-dose-dependent manner (15–18). WBRT has a stronger ability to open up drug delivery barriers in the CNS than SRS, so it, combined with drugs, is more effective in treatment. Considering the long-term radiotherapy toxicity associated with WBRT, studies on Hippocampal Avoidance-Whole Brain Radiotherapy with simultaneous integrated boost(HA-WBRT+SIB)are increasing (19). Due to the highly economical and technical barriers of SRS/HA-WBRT+SIB, it i urgent to promote research on WBRT+SIB as a cost-effective approach.

The studies by Rodrigues et al. (20) and Du et al. (21) only included patients who received chemotherapy after radiotherapy

TABLE 5 Comparison of adverse events in treatment cohort.

| | | Grade | WBRT+SIB (n=42) | SRS(n=48) |
|---|---|---|---|---|
| Acute radiation injury | Nausea/vomiting | 0 | 19 | 27 |
| | | 1 | 14 | 11 |
| | | 2 | 7 | 9 |
| | | 3 | 2 | 1 |
| | | 4 | 0 | 0 |
| | Leukopenia | 0 | 27 | 32 |
| | | 1 | 10 | 7 |
| | | 2 | 5 | 8 |
| | | 3 | 0 | 1 |
| | | 4 | 0 | 0 |
| | Thrombocytopenia | 0 | 34 | 39 |
| | | 1 | 7 | 7 |
| | | 2 | 1 | 2 |
| | | 3 | 0 | 0 |
| | | 4 | 0 | 0 |
| | CNS symptoms | 0 | 33 | 37 |
| | | 1 | 6 | 7 |
| | | 2 | 2 | 4 |
| | | 3 | 1 | 0 |
| | | 4 | 0 | 0 |
| Late radiation injury | CNS symptoms | 0 | 22 | 35 |
| | | 1 | 12 | 10 |
| | | 2 | 5 | 2 |
| | | 3 | 2 | 1 |
| | | 4 | 1 | 0 |
| | | 5 | 0 | 0 |

WBRT+SIB, Whole- Brain Radiation Therapy with Simultaneous Integrated Boost; SRS, Stereotactic Radiosurgery; CNS, central nervous system.

and did not count patients treated with targeted drugs and ICIs. To be more clinically relevant, 84.44% of the included patients in our study were treated with scientific systemic drug therapy, including chemotherapy, targeted therapy, immunotherapy, anti-angiogenic drugs therapy, and supportive therapy after radiotherapy. Small cell lung cancer was also not included in this study. All these made the included patients have longer iPFS and OS (Figure 2). In general, the use of targeted drugs and ICIs is associated with a better prognosis. Although not indicated in the figure, we found that whether the patients received ICIs or targeted therapy iPFS (ICIs compared cohort: p = 0.49 Targeted therapy compared cohort: p = 0.84) and OS (ICIs compared cohort: p = 0.25 Targeted therapy cohort: p = 0.48) were not statistically different (Supplementary Figures 1–4). 78% of patients who did not receive targeted therapy received other drugs. In ICIs compared cohort, this rate was 94%. Other drugs may have obscured the survival benefit of single targeted drugs or ICIs therapy. We may conclude that WBRT +SIB is preferable to SRS under the standard treatment mode of radiotherapy plus drugs for NSCLC-BM patients. Regarding radiotherapy-related toxicity, a prospective study by Zhong et al. (22) demonstrated the safety and efficacy of WBRT+SIB, which was similar to the results of the radiotherapy-related toxicity assessment in this study, i.e., no significant difference was seen between WBRT +SIB and SRS in recent radiotherapy-related toxicity.

A study from the SEER database of lung cancer by Hao (23) et al. showed that distant liver/bone/lymph node metastases, higher T and N stages were risk factors for NSCLC-BM. Our study only found that Sex, Liver metastasis and Lymph node metastasis were independent prognostic factors for NSCLC-BM. Considering that the participants in our study all received brain radiotherapy, this may account for the difference between our conclusion and Hao et al. Further studies are needed to confirm our conclusions.

This study has several limitations; First, as a retrospective study, we were biased and enrolled a small number of patients. Then, our study lacked drug side effects (e.g.,immune-related adverse events, Bleeding risk, skin reactions, etc.) and did not document the long-term cognitive function and quality of life changes in patients after treatment. Moreover, most patients received multiple drug combinations after radiotherapy, which may have masked the effect of single drug classes on survival.

In conclusion, the results of this study suggest that Radiotherapy modality is a crucial and independent prognostic factor in patients with NSCLC-BM, and WBRT+SIB seems to be associated with a more favorable prognosis compared to SRS. Presently, the treatment of drugs such as mannitol and hormone to reduce the toxicity of radiotherapy is more and more standardized, and the probability of short-term toxicity is less and less. Although not described in detail in this study, we must consider the question of long-term cognitive function and quality of life decline associated with WBRT. Although there is no difference in OS between WBRT+SIB and SRS, as we all know. Compare to WBRT+SIB,Whether the advantages of repeatability and security of SRS can offset the disadvantages of economy and technology still, need to be considered comprehensively. In the future, we should focus on finding a balance in treating BM by making trade-offs between intracranial control, management of systemic progression, and neurocognitive decline in patients. However, prospective, large-sample randomized controlled trials are needed to validate our results.

## Data availability statement

The original contributions presented in the study are included in the article/Supplementary Material. Further inquiries can be directed to the corresponding author.

## Ethics statement

The studies involving humans were approved by The Affiliated Cancer Hospital of Zhengzhou University. The studies were conducted in accordance with the local legislation and institutional requirements. The ethics committee/institutional review board waived the requirement of written informed consent for participation from the participants or the participants' legal guardians/next of kin because This study was approved by the ethics committees of the Affiliated Cancer Hospital of Zhengzhou University & Henan Cancer Hospital, Zhengzhou, China. Due to the retrospective nature of the study and because no patient specimens were used, the requirement for informed consent was waived by the ethics committees.

## Author contributions

XD and LY designed this study and analyzed the data. XD collected the data and wrote the manuscript. HY, YH, JC and YL assisted in collecting data and correcting the manuscript. All authors contributed to the article and approved the submitted version.

## Funding

This study was supported by Science and Technology Department, Henan Province (grant numbers: SB201901113 and 192102310048).

## Conflict of interest

The authors declare that the research was conducted in the absence of any commercial or financial relationships that could be construed as a potential conflict of interest.

## Publisher's note

All claims expressed in this article are solely those of the authors and do not necessarily represent those of their affiliated organizations, or those of the publisher, the editors and the

reviewers. Any product that may be evaluated in this article, or claim that may be made by its manufacturer, is not guaranteed or endorsed by the publisher.

## Supplementary material

The Supplementary Material for this article can be found online at: https://www.frontiersin.org/articles/10.3389/fonc.2023.1220047/full#supplementary-material

SUPPLEMENTARY FIGURE 1
Comparison of intracranial progression-free-survival in ICIs compared cohort. ICIs, immune checkpoint inhibitors.

SUPPLEMENTARY FIGURE 2
Comparison of intracranial progression-free-survival in targeted therapy compared cohort.

SUPPLEMENTARY FIGURE 3
Comparison of overall survival in ICIs compared cohort. ICIs, immune checkpoint inhibitors.

SUPPLEMENTARY FIGURE 4
Comparison of overall survival in targeted therapy compared cohort.

## References

1. Soffietti R, Abacioglu U, Baumert B, Combs SE, Kinhult S, Kros JM, et al. Diagnosis and treatment of brain metastases from solid tumors: Guidelines from the European Association of Neuro-Oncology (EANO). *Neuro Oncol* (2017) 19(2):162–74. doi: 10.1093/neuonc/now241

2. Soria JC, Ohe Y, Vansteenkiste J, Reungwetwattana T, Chewaskulyong B, Lee KH, et al. Osimertinib in untreated EGFR-mutated advanced non-small-cell lung cancer. *N Engl J Med* (2018) 378(2):113–25. doi: 10.1056/NEJMoa1713137

3. Yang G, Xing L, Sun X. Navigate towards the immunotherapy era: Value of immune checkpoint inhibitors in non-small cell lung cancer patients with brain metastases. *Front Immunol* (2022) 13:852811. doi: 10.3389/fimmu.2022.852811

4. Deng X, Zheng Z, Lin B, Su H, Chen H, Fei S, et al. The efficacy and roles of combining temozolomide with whole brain radiotherapy in protection neurocognitive function and improvement quality of life of non-small-cell lung cancer patients with brain metastases. *BMC Cancer* (2017) 17(1):42. doi: 10.1186/s12885-016-3017-3

5. Zhuang H, Yuan Z, Wang J, Zhao L, Pang Q, Wang P. Phase II study of whole brain radiotherapy with or without erlotinib in patients with multiple brain metastases from lung adenocarcinoma. *Drug Des Devel Ther* (2013) 7:1179–86. doi: 10.2147/DDDT.S53011

6. Welsh JW, Komaki R, Amini A, Munsell MF, Unger W, Allen PK, et al. Phase II trial of erlotinib plus concurrent whole-brain radiation therapy for patients with brain metastases from non-small-cell lung cancer. *J Clin Oncol* (2013) 31(7):895–902. doi: 10.1200/JCO.2011.40.1174

7. Magnuson WJ, Lester-Coll NH, Wu AJ, Yang TJ, Lockney NA, Gerber NK, et al. Management of brain metastases in tyrosine kinase inhibitor-naïve epidermal growth factor receptor-mutant non-small-cell lung cancer: A retrospective multi-institutional analysis. *J Clin Oncol* (2017) 35(10):1070–7. doi: 10.1200/JCO.2016.69.7144

8. Scoccianti S, Olmetto E, Pinzi V, Osti MF, Di Franco R, Caini S, et al. Immunotherapy in association with stereotactic radiotherapy for non-small cell lung cancer brain metastases: Results from a multicentric retrospective study on behalf of AIRO. *Neuro Oncol* (2021) 23(10):1750–64. doi: 10.1093/neuonc/noab129

9. Metro G, Gili A, Signorelli D, De Toma A, Garaffa M, Galetta D, et al. Upfront pembrolizumab as an effective treatment start in patients with PD-L1 ≥ 50% non-oncogene addicted non-small cell lung cancer and asymptomatic brain metastases: An exploratory analysis. *Clin Transl Oncol* (2021) 23(9):1818–26. doi: 10.1007/s12094-021-02588-8

10. Rades D, Janssen S, Bajrovic A, Khoa MT, Veninga T, Schild SE. A matched-pair analysis comparing whole-brain radiotherapy with and without a stereotactic boost for intracerebral control and overall survival in patients with one to three cerebral metastases. *Radiat Oncol* (2017) 12(1):69. doi: 10.1186/s13014-017-0804-1

11. Popp I, Rau S, Hintz M, Schneider J, Bilger A, Fennell JT, et al. Hippocampus-avoidance whole-brain radiation therapy with a simultaneous integrated boost for multiple brain metastases. *Cancer* (2020) 126(11):2694–703. doi: 10.1002/cncr.32787

12. Ramos A, Giantini-Larsen A, Pannullo SC, Brandmaier A, Knisely J, Magge R, et al. A multidisciplinary management algorithm for brain metastases. *Neurooncol Adv* (2022) 4(1):vdac176. doi: 10.1093/noajnl/vdac176

13. Yamamoto M, Serizawa T, Shuto T, Akabane A, Higuchi Y, Kawagishi J, et al. Stereotactic radiosurgery for patients with multiple brain metastases (JLGK0901): A multi-institutional prospective observational study. *Lancet Oncol* (2014) 15(4):387–95. doi: 10.1016/S1470-2045(14)70061-0

14. Yamamoto M, Kawabe T, Sato Y, Higuchi Y, Nariai T, Watanabe S, et al. Stereotactic radiosurgery for patients with multiple brain metastases: A case-matched study comparing treatment results for patients with 2-9 versus 10 or more tumors. *J Neurosurg* (2014) 121(Suppl):16–25. doi: 10.3171/2014.8.GKS141421

15. Lamba N, Wen PY, Aizer AA. Epidemiology of brain metastases and leptomeningeal disease. *Neuro Oncol* (2021) 23(9):1447–56. doi: 10.1093/neuonc/noab101

16. Lemasson B, Serduc R, Maisin C, Bouchet A, Coquery N, Robert P, et al. Monitoring blood-brain barrier status in a rat model of glioma receiving therapy: Dual injection of low-molecular-weight and macromolecular MR contrast media. *Radiology* (2010) 257(2):342–52. doi: 10.1148/radiol.10092343

17. Erel-Akbaba G, Carvalho LA, Tian T, Zinter M, Akbaba H, Obeid PJ, et al. Radiation-induced targeted nanoparticle-based gene delivery for brain tumor therapy. *ACS Nano* (2019) 13(4):4028–40. doi: 10.1021/acsnano.8b08177

18. Qin DX, Zheng R, Tang J, Li JX, Hu YH. Influence of radiation on the blood-brain barrier and optimum time of chemotherapy. *Int J Radiat Oncol Biol Phys* (1990) 19(6):1507–10. doi: 10.1016/0360-3016(90)90364-P

19. Chia B, Leong JY, Ong ALK, Lim C, Poon SH, Chua MLK, et al. Randomised prospective phase II trial in multiple brain metastases comparing outcomes between hippocampal avoidance whole brain radiotherapy with or without simultaneous integrated boost: HA-SIB-WBRT study protocol. *BMC Cancer* (2020) 20(1):1045. doi: 10.1186/s12885-020-07565-y

20. Rodrigues G, Zindler J, Warner A, Bauman G, Senan S, Lagerwaard F. Propensity-score matched pair comparison of whole brain with simultaneous in-field boost radiotherapy and stereotactic radiosurgery. *Radiother Oncol* (2013) 106(2):206–9. doi: 10.1016/j.radonc.2012.10.014

21. Du TQ, Li X, Zhong WS, Tian JD, Zhao YX, Liu D. Brain metastases of lung cancer: Comparison of survival outcomes among whole brain radiotherapy, whole brain radiotherapy with consecutive boost, and simultaneous integrated boost. *J Cancer Res Clin Oncol* (2021) 147(2):569–77. doi: 10.1007/s00432-020-03359-8

22. Zhong J, Waldman AD, Kandula S, Eaton BR, Prabhu RS, Huff SB, et al. Outcomes of whole-brain radiation with simultaneous in-field boost (SIB) for the treatment of brain metastases. *J Neurooncol* (2020) 147(1):117–23. doi: 10.1007/s11060-020-03405-y

23. Hao Y, Li G. Risk and prognostic factors of brain metastasis in lung cancer patients: A Surveillance, Epidemiology, and End Results population–based cohort study. *Eur J Cancer Prev* (2023) 32(5):498–511. doi: 10.1097/CEJ.0000000000000790

frontiers | Frontiers in Oncology

TYPE Original Research
PUBLISHED 22 November 2023
DOI 10.3389/fonc.2023.1290434



OPEN ACCESS

EDITED BY
Xiangpan Li,
Renmin Hospital of Wuhan University, China

REVIEWED BY
Raees Tonse,
Baptist Hospital of Miami, United States
Yvonne Dzierma,
Saarland University Hospital, Germany

*CORRESPONDENCE
Fangyu Liu
liufangyu_30@163.com

†These authors have contributed equally to this work

RECEIVED 07 September 2023
ACCEPTED 06 November 2023
PUBLISHED 22 November 2023

CITATION
Liu F, Peng Y, Li Q, Zhang Q, Shi H, Qie S and Zhang R (2023) Feasibility of flattening filter free beams for hippocampal avoidance whole-brain radiotherapy: a dosimetric and radiobiological analysis. *Front. Oncol.* 13:1290434. doi: 10.3389/fonc.2023.1290434



# Feasibility of flattening filter free beams for hippocampal avoidance whole-brain radiotherapy: a dosimetric and radiobiological analysis

Fangyu Liu[1,2*†], Yu Peng[1†], Qian Li[1], Qianru Zhang[3], Hongyun Shi[1], Shuai Qie[1] and Ruohui Zhang[4]

[1]Department of Radiotherapy, Affiliated Hospital of Hebei University, Baoding, Hebei, China, [2]School of Nuclear Science and Technology, School of Energy and Power Engineering, Xi'an Jiaotong University, Xi'an, Shaanxi, China, [3]Department of Pediatrics, Affiliated Hospital of Hebei University, Baoding, Hebei, China, [4]Department of Radiotherapy, The Fourth Hospital of Hebei Medical University, Shijiazhuang, Hebei, China

**Objectives:** The purpose of this study is to evaluate the potential of the flattening filter free (FFF) mode of a linear accelerator for patients with hippocampal avoidance whole-brain radiotherapy (HA-WBRT) by comparison with flattened beams (FF) technique in the application of volumetric modulated arc therapy (VMAT) and intensity modulated radiation therapy (IMRT) using dosimetric and radiobiological indexes based on the volume of hippocampus and target.

**Methods:** 2 VMAT- and 2 IMRT- plans were optimized in Eclipse planning system with 2 different delivery modes (6 MV standard vs. 6 MV FFF) for each of 25 patients. Dose distributions of the target and organs at risk (OARs), normal tissue complication probability (NTCP) of the hippocampus, monitor units, treatment time and quality assurance results were evaluated to compare the normal and FFF beam characteristics by Wilcoxon matched-pair signed-rank test with a significance level of 0.05.

**Results:** VMAT-FFF provided the significantly best homogeneity and conformity of the target, delivered the lowest dose to hippocampus and the other OARs, and led to the lowest NTCP of the hippocampus among all modalities, which has the potential to alleviate neurocognitive decline after WBRT. IMRT-FFF reduced the dose to the lens with similar dose distributions of the target compared with IMRT-FF, whereas the lower dose to the hippocampus was achieved using the conventional beams. The monitor units were obviously increased by 19.2% for VMAT and 33.8% for IMRT, when FFF beams w ere used. The removal of flattening filter for IMRT resulted in a 26% reduction in treatment time, but VMAT had the similar treatment time for the two modes owing to the limitation of gantry rotation speed. Gamma analysis showed an excellent agreement for all plans at 3%/2 mm, and no statistical differences were found between FF and FFF.

**Conclusion:** In conclusion, this study suggests that FFF mode is feasible and advantageous in HA-WBRT and VMAT-FFF is the optimal solution in terms of dose distribution of the target, OARs sparing, NTCP of the hippocampus and delivery efficiency compared to the other three techniques. Additionally, the advantages of the FFF technique for VMAT are more prominent in cases with small hippocampal volumes.

KEYWORDS

flattening filter free, hippocampal avoidance, whole-brain radiation therapy, volumetric modulated arc therapy, intensity modulated radiation therapy, normal tissue complication probability

## 1 Introduction

Brain metastases represent an important clinical problem, accounting for approximately 25–45% of cancer patients, which cause significant morbidity and mortality, and management focuses on improving survival and optimizing quality of life. Whole-brain radiation therapy (WBRT) is usually the primary treatment option for patients with brain metastases, controlling macroscopic and microscopic tumor deposits within the affected area. However, it is reported that WBRT can cause long-term serious and irreversible toxic effects, including neurocognitive deterioration, leukoencephalopathy, cerebellar dysfunction and dementia, potentially compromising patients' quality of life (1–3). In the last few decades, it has already been proven that hippocampus is crucial to memory function (4). Furthermore, recent studies have indicated that the neurocognitive decline (short and long-term memory loss and cognitive impairment) is strongly associated with radiation-induced injury to the neural stem cells in the subgranular zone of the hippocampi (5, 6).

With innovative techniques for planning and delivering WBRT, such as volumetric modulated arc therapy (VMAT) and helical tomotherapy, allowing a better sparing of organs at risk (OARs), it is possible to selectively spare sensitive brain regions, such as the hippocampus, while maintaining uniform dose delivery to the remaining brain. Hence, hippocampal avoidance (HA) during whole brain radiotherapy (HA-WBRT) has become an emerging strategy that is expected to mitigate the neurocognitive side effects by reducing the dose to the hippocampus. Recently, results of the phase II Radiation Therapy Oncology Group (RTOG) 0933 study showed evidence of improvements in neurocognitive outcomes compared to conventional WBRT for patients with multiple brain metastases (7). Nevertheless, the studies employing HA-WBRT generally exclude the region within 5 mm of the hippocampus, which may pose the risk of diminishing the clinical benefit of WBRT if the metastases are located in the spared region. Ghia et al. reported that the incidence of metastases within 5 mm of the hippocampus was very low (3.3%), which shows that the risks of HA-WBRT may be overestimated (8).

Intensity modulated radiation therapy (IMRT) has been used as a practical delivery method for HA-WBRT based on RTOG 0933 guidelines, whereas VMAT technique, which is based on simultaneous optimization of multi-leaf collimator (MLC) shapes, dose rate, and gantry rotation speed to achieve the desired dose distribution, have shown superior dosimetric performance and shorter treatment time compared with conventional IMRT (9–11). Despite these efforts, recent survey results indicated relatively low rates of utilization of HA-WBRT, which may result from the complexity of the treatment planning process owing to the anatomical shape and location of the hippocampus, the lack of dosimetry and physics support, and the suitability of patients.

To further improve the delivery efficiency, flattening-filter-free (FFF) technique has become increasingly popular due to its higher dose rates. As a result, the treatment delivery time can be reduced greatly, which is essential in improving patient comfort and limiting uncertainty of delivered dose related to intra-fraction motion (12). Hence, the FFF technique is particularly appealing for delivering stereotactic radiotherapy and has demonstrated great advantages due to significantly reducing treatment time without compromising the target coverage and organs at risk sparing (13–16). Furthermore, the removal of flattening filter is shown to have lower out-of-field dose on account of the diminution of head scatter and residual electron contamination in comparison to flattening-filtered (FF) mode (17). Patients may benefit from reduced exposure of healthy tissue to scattered doses outside the X-ray field. Dosimetric benefits of FFF also include less penumbra and MLC leakage (18). Therefore, FFF beams may offer a better solution in sparing the hippocampus and other OARs for HA-WBRT, in the hope of improving neurocognitive function impairment. With the advent of clinical FFF-linac, the planning studies of FFF mode have been carried out in various common cancer sites, such as prostate (19), hypopharynx (20), and breast (21). However, to the best of our knowledge, no investigation has been previously implemented for the dosimetric and radiobiological comparison of HA-WBRT using VMAT and IMRT with and without flattening filter.

The aim of this present study is to provide the first systematic clinical information on the application of the FFF irradiation mode in whole brain radiation therapy with hippocampal avoidance and evaluate whether the FFF mode is feasible and advantageous with respect to plan quality, delivery time and normal tissue complication probability (NTCP) for impaired neurocognitive function as compared to the flattening filter irradiation mode in VMAT and IMRT. Furthermore, considering the special anatomical

location of the hippocampus, as well as the correlation between the performance of the FFF technique and the target volume, the impacts of hippocampal and target volumes on the differences between FFF beams and FF beams are also discussed.

# 2 Materials and methods

## 2.1 CT simulation and treatment preparation

With approval from our institutional review board, a total of 25 patients, who were diagnosed with brain metastases and underwent whole-brain radiation therapy with hippocampal avoidance at the Affiliated Hospital of Hebei University, were included and replanned in this retrospective study. The median age of the patients was 63 years (range: 37-76). Non-contrast computed tomography (CT) images for planning were obtained for all patients positioned supine and immobilized by means of a thermoplastic body mask using a large aperture 16 rows spiral CT of GE Medical System with 2.5 mm slice thickness. The DICOM images were then electronically sent to the Eclipse treatment planning system (Varian Medical Systems, Palo Alto, CA).

A gadolinium-enhanced, T1-weighted, three-dimensional spoiled gradient echo axial Magnetic Resonance Imaging (MRI) was acquired using a 1.5-T magnetic resonance scanner (Siemens AG, Munich, Germany) with 1.5 mm slice thickness for each patient. CT and MRI were rigidly co-registered by using an Eclipse mutual information algorithm. The hippocampus was manually contoured by an experienced radiation oncologist using the RTOG 0933 atlas as reference. According to the volume of the hippocampi (range: 1.12 $cm^3$ - 4.59 $cm^3$), the patients were divided into three groups for subsequent volume-based analysis, as Group 1 (1 $cm^3$< hippocampi ≤ 2 $cm^3$), Group 2 (2 $cm^3$< hippocampi ≤ 3 $cm^3$), Group 3 (3 $cm^3$< hippocampi ≤ 4.59 $cm^3$). The hippocampal avoidance zone (HAZ) was created using a 5-mm volumetric expansion of the hippocampi to account for necessary dose fall-off between the hippocampi and the target. The following volumes of interest were also delineated: clinical target volume (CTV, CTV was defined as the whole brain parenchyma), lens, optic nerve and optic chiasm. The planning target volume (PTV) was constructed by expanding the CTV by 3 mm in all directions. The planning target volume with hippocampal avoidance (PTV-HA) used for dose optimization was generated by subtracting the HAZ from PTV. For the other grouping method, all patients were stratified in three groups according to the volume of PTV-HA (range: 1098.3 $cm^3$ - 2056.8 $cm^3$): Group 4 (1000 $cm^3$< PTV-HA ≤ 1568.2 $cm^3$), Group 5 (1568.2 $cm^3$< PTV-HA ≤ 1867.9 cm3), Group 6 (1867.9 $cm^3$< PTV-HA ≤ 2056.8 $cm^3$).

## 2.2 Linear accelerator

The treatment planning was implemented using Varian Trilogy linear accelerator (Varian Medical Systems, Palo Alto, CA, USA), which has the flattened as well as unflattened beams and is equipped with 120 Millennium multi-leaf collimator leaves. The leaf width is 5 mm in the central 20-cm part of the field and 10 mm in the outer 2×10 cm. Removing the flattening filter from the beam path increases the dose rate up to 1400 MU/min for 6 MV but decreases the beam quality index (TPR20/10: 6 MV 0.669, 6 MV (FFF) 0.629).

## 2.3 Treatment planning setup

Four different plans were optimized for each patient based on Eclipse treatment planning system using intensity-modulated radiotherapy and volumetric modulated arc therapy with 6 MV photon beams with flattening filter or without, in the following referred to as IMRT-FF, IMRT-FFF, VMAT-FF and VMAT-FFF plans. The maximum dose rate was adopted to leave the highest degree of freedom in the optimization process, which was 600 MU/min for FF beams, and 1400 MU/min for FFF beams. For IMRT, the dose rate is always maintained at the maximum during dose delivery. However, due to mechanical motion speed restrictions, the maximum dose rate will not be applied throughout the VMAT process. The total dose prescribed was 30 Gy delivered in 10 fractions to the PTV-HA for all the studied cases. The IMRT plans were realized by sliding window dynamic delivery method and consisted of seven equispaced beams with gantry angles of 204°, 256°, 308°, 0°, 52°, 104° and 156°. The collimator was angled to 0° in IMRT plans. To reduce treatment time and the possibility of operating errors, the couch angles of all fields were set to 0° instead of the noncoplanar beam arrangement recommended by RTOG. The VMAT plans were generated using RapidArc technique with two coplanar arcs as clockwise arc 181°–179° and anti-clockwise arc 179°–181°. Gantry spacing between two control points was 4°. In addition, to reduce the MLC tongue-and-groove leaves' leakage, the collimator angle was set to 30 degrees for the first clockwise arc and the collimator of the second anti-clockwise arc was 330 degrees (22). For all plans, the isocenter was located centrally in the PTV-HA based on beam's eye view graphic. All plans utilized the Photon Optimizer (Version 13.6.23, Varian, Palo Alto, CA, USA) to optimize the intensity map for IMRT and determine the optimal combination of beam weight and shape for VMAT. The constraints for target and OARs were matched to RTOG 0933 planning requirements (see Table 1 for the RTOG criteria). Identical dose volume objectives and weights were used for optimization of four plans for each patient to make the results

TABLE 1 Dosimetric compliance criteria for hippocampal sparing in RTOG 0933.

| Parameter | Dose constraints |
|---|---|
| PTV-HA | $D_{2\%} \leq 37.5$ Gy ($D_{2\%} \leq 40$ Gy is allowed)<br>$D_{98\%} \geq 25$ Gy and $V_{30} \geq 90\%$ |
| Hippocampus | $D_{100\%} \leq 9$ Gy ($D_{100\%} \leq 10$ Gy is allowed)<br>$D_{max} \leq 16$ Gy ($D_{max} \leq 17$ Gy is allowed) |
| Optic chiasm | $D_{max} \leq 37.5$ Gy |
| Optic nerves | $D_{max} \leq 37.5$ Gy |

comparable. The Analytical Anisotropic Algorithm (AAA) along with a grid resolution of 2.5 mm and heterogeneous corrections were adopted to arrive at dose calculations.

## 2.4 Plan comparison

Quantitative evaluation of the plans was performed by analysis of the dose-volume histograms (DVHs) extracted from the planning system with respect to target coverage, dose homogeneity and conformity, and OAR sparing. For the purpose of comparison, all plans were normalized to meet the same objectives with the 95% of the PTV-HA volume surrounded by the 100% isodose line. The dose distribution of the target was evaluated in terms of mean dose, $D_{2\%}$ and $D_{98\%}$ (dose received by 2% and 98% of target volume), conformity index (CI), prescription isodose/target volume (PITV) ratio, and homogeneity index (HI). CI was calculated using the equation:

$$CI = V_{t,ref}^2/(V_t \cdot V_{ref}) \quad (1)$$

according to Paddick (23). Here $V_{t,ref}$ represented the volume receiving a dose equal to or greater than the reference dose in the target volume, $V_t$ stood for the target volume, and $V_{ref}$ was the total volume covered by a dose equal to or greater than the reference dose. The reference dose was the 95% of the prescription dose in this study. CI ranged from 0 to 1, and the higher the CI, the better the conformity of the target volume. For comparison and reference purposes, dose conformity was also quantified using PITV, defined as the prescription isodose volume divided by the target volume. Since target coverage was maintained at 95% in this study, the smaller PITV indicated better conformity and less radiation exposure to normal tissue. HI was defined as follows:

$$\mathrm{HI} = (D_{2\,\%} - D_{98\,\%})/D_{prescription} \quad (2)$$

where $D_{prescription}$ meant the prescription dose. The ideal value of HI was 0, which indicated a sharp dose fall between the neck region and tail region of the PTV-HA dose-volume histogram, with increasing values for the metric indicative of declining homogeneity throughout the volume.

Concerning the hippocampus, we considered the maximum, mean, and quintile ($D_{20\%}$ to $D_{100\%}$) doses to assess hippocampal sparing. The maximum doses of the lens, optic chiasm, and optic nerve were also reported. Moreover, an additional structure called non-tumor tissue (NT) consisting of body minus PTV was created. The integral dose (24) for non-tumor tissue was calculated according to the following formula as a measure of low dose in the periphery: Integral dose = Mean dose (Gy) × Volume ($cm^3$). Furthermore, the number of monitor units (MUs) required per fraction dose for the four techniques was also compared.

## 2.5 Quality assurance

Dose verifications were performed using the ArcCheck Phantom (Sun Nuclear Corporation, Melbourne, USA) to ensure the deliverability of each treatment plan. It is a cylindrical water-equivalent phantom for patient specific quality assurance (QA) with a three-dimensional array of 1386 diode detectors. The measured doses at the detectors plane were compared with the predicted dose distribution previously calculated in Eclipse planning system. Evaluation was based on gamma analysis by SNC patient software with criteria of 3% maximum dose difference and 2 mm distance to agreement as recommended by the AAPM TG 218 (25). A global normalization for the absolute dose was performed. The agreement between the measured dose distribution and calculated dose distribution was considered acceptable if the gamma indexes of at least 95% of the pixels with a dose value of ≥ 10% of the maximum dose were smaller than 1. The treatment delivery time was documented from first beam on to last beam off when the QA plan was delivered. The mean dose rates of VMAT in both delivery modes were also calculated. In addition, the measured data of all QA plans were collected by delivering at the machine in one session to minimize the impact of machine output rate on QA results.

## 2.6 Radiobiological indices

Biologically equivalent dose in 2-Gy fractions ($EQD_2$) to 40% of the bilateral hippocampi was computed using a hippocampal α/β value of 2 (26). The NTCP for neurocognitive function impairment of the hippocampus was assessed for all plans according to the model proposed by Gondi et al. (26). The model was based on the Lyman model and its formula was expressed as follows:

$$\mathrm{NTCP} = \frac{1}{\sqrt{2\pi}}\int_{-\infty}^{t} \exp(-u^2/2)du \quad (3)$$

where,

$$t = \frac{EQD_2(D_{40\,\%}) - TD_{50}}{mTD_{50}} \quad (4)$$

$EQD_2(D_{40\%})$ was $EQD_2$ received by 40% of bilateral hippocampal volume, $TD_{50}$ was the $EQD_2(D_{40\%})$ value corresponding to a 50% probability of neurocognitive decline, and m represented the slope of the dose-response curve. Moreover, $TD_{50}$ and m were estimated to be 14.88 Gy and 0.54 by Gondi et al. (26).

## 2.7 Statistical evaluation

All data were reported as mean and standard deviation. The Wilcoxon matched-pair signed-rank test, a non-parametric test, implemented in SPSS software version 22 (SPSS, IBM Corp, Armonk, NY), was used for statistical analysis, and the difference was considered statistically significant when $p< 0.05$.

# 3 Results

Details about DVH parameters averaged over all patients with regard to target coverage and OAR sparing are summarized in

Table 2 for the comparison of the two irradiation modes FF and FFF. As to four kinds of plans for a representative patient, the spatial isodose distributions with display of an axial, sagittal and coronal plane at the level of hippocampus are presented in Figures 1 and 2, and the DVHs involving the PTV-HA, hippocampus and lens are showed in Figure 3.

## 3.1 Target coverage

It could be seen in Table 2 that the $D_{2\%}$, $D_{98\%}$, $D_{mean}$, HI, CI, and PITV were improved significantly for the VMAT planning techniques if flattening filter free beams were used, and the corresponding p values were all less than 0.001. On the contrary, the dose volume parameters of IMRT-FF plans were either slightly better or not significantly different compared to IMRT-FFF plans. It was worth noting that the removal of flattening filter had a greater impact on VMAT plans than IMRT. In addition, VMAT plans were remarkably superior compared to IMRT plans.

## 3.2 OARs sparing

The maximum and minimum doses of hippocampus for VMAT-FFF were 15.14 ± 0.50 Gy and 9.37 ± 0.39 Gy, which were significantly lower than the corresponding values of VMAT-

TABLE 2 Comparison of dose distributions of PTV-HA and OARs for VMAT and IMRT with the two irradiation modes FFF and FF.

| Variable | VMAT-FFF | VMAT-FF | p[a] | IMRT-FFF | IMRT-FF | p[b] |
|---|---|---|---|---|---|---|
| PTV-HA | | | | | | |
| $D_{2\%}$ | 33.24 ± 0.44 | 33.66 ± 0.52 | <0.001 | 34.62 ± 0.57 | 34.57 ± 0.57 | 0.001 |
| $D_{98\%}$ | 27.11 ± 0.39 | 26.81 ± 0.40 | <0.001 | 27.30 ± 0.29 | 27.31 ± 0.31 | 0.074 |
| $D_{mean}$ | 31.74 ± 0.29 | 32.11 ± 0.38 | <0.001 | 32.64 ± 0.36 | 32.54 ± 0.36 | <0.001 |
| HI | 0.19 ± 0.02 | 0.21 ± 0.02 | <0.001 | 0.22 ± 0.02 | 0.22 ± 0.02 | 0.016 |
| CI | 0.87 ± 0.02 | 0.85 ± 0.02 | <0.001 | 0.83 ± 0.02 | 0.83 ± 0.02 | 0.326 |
| PITV | 1.04 ± 0.02 | 1.07 ± 0.02 | <0.001 | 1.10 ± 0.02 | 1.10 ± 0.02 | 0.459 |
| Hippocampus | | | | | | |
| $D_{20\%}$ | 12.07 ± 0.58 | 12.93 ± 0.73 | <0.001 | 14.38 ± 0.38 | 14.09 ± 0.38 | <0.001 |
| $D_{40\%}$ | 11.46 ± 0.57 | 12.28 ± 0.72 | <0.001 | 13.89 ± 0.35 | 13.61 ± 0.35 | <0.001 |
| $D_{60\%}$ | 10.96 ± 0.54 | 11.73 ± 0.68 | <0.001 | 13.50 ± 0.35 | 13.23 ± 0.34 | <0.001 |
| $D_{80\%}$ | 10.45 ± 0.50 | 11.16 ± 0.64 | <0.001 | 13.09 ± 0.37 | 12.83 ± 0.34 | <0.001 |
| $D_{100\%}$ | 9.37 ± 0.39 | 9.98 ± 0.56 | <0.001 | 12.00 ± 0.39 | 11.87 ± 0.33 | 0.01 |
| $D_{mean}$ | 11.28 ± 0.51 | 12.07 ± 0.65 | <0.001 | 13.75 ± 0.34 | 13.48 ± 0.34 | <0.001 |
| $D_{max}$ | 15.14 ± 0.50 | 16.15 ± 0.58 | <0.001 | 17.51 ± 1.07 | 17.18 ± 1.03 | <0.001 |
| Lens L | | | | | | |
| $D_{max}$ | 6.91 ± 0.62 | 8.02 ± 0.73 | <0.001 | 7.80 ± 0.64 | 8.43 ± 0.74 | <0.001 |
| Lens R | | | | | | |
| $D_{max}$ | 6.95 ± 0.56 | 8.02 ± 0.71 | <0.001 | 8.02 ± 0.94 | 8.49 ± 0.95 | <0.001 |
| Optic chiasm | | | | | | |
| $D_{max}$ | 33.79 ± 0.68 | 34.19 ± 0.64 | 0.009 | 35.37 ± 0.55 | 35.24 ± 0.59 | 0.011 |
| Optic nerve L | | | | | | |
| $D_{max}$ | 31.47 ± 5.94 | 33.22 ± 1.11 | 0.002 | 32.79 ± 2.57 | 32.88 ± 2.54 | 0.019 |
| Optic nerve R | | | | | | |
| $D_{max}$ | 32.70 ± 1.14 | 33.28 ± 1.08 | 0.001 | 33.19 ± 2.41 | 33.30 ± 2.28 | 0.162 |
| NT | | | | | | |
| Integral dose | 31.55 ± 3.97 | 32.42 ± 4.02 | <0.001 | 32.04 ± 4.25 | 32.46 ± 4.42 | <0.001 |

The results of Wilcoxon matched-pair signed-rank test are also listed.
Dose values are given in Gy. Integral dose is given in $Gy*cm^3*10^3$. [a] p value denotes the results of Wilcoxon test between VMAT-FFF and VMAT-FF plans. [b] p value means the results of Wilcoxon test between IMRT-FFF and IMRT-FF plans.

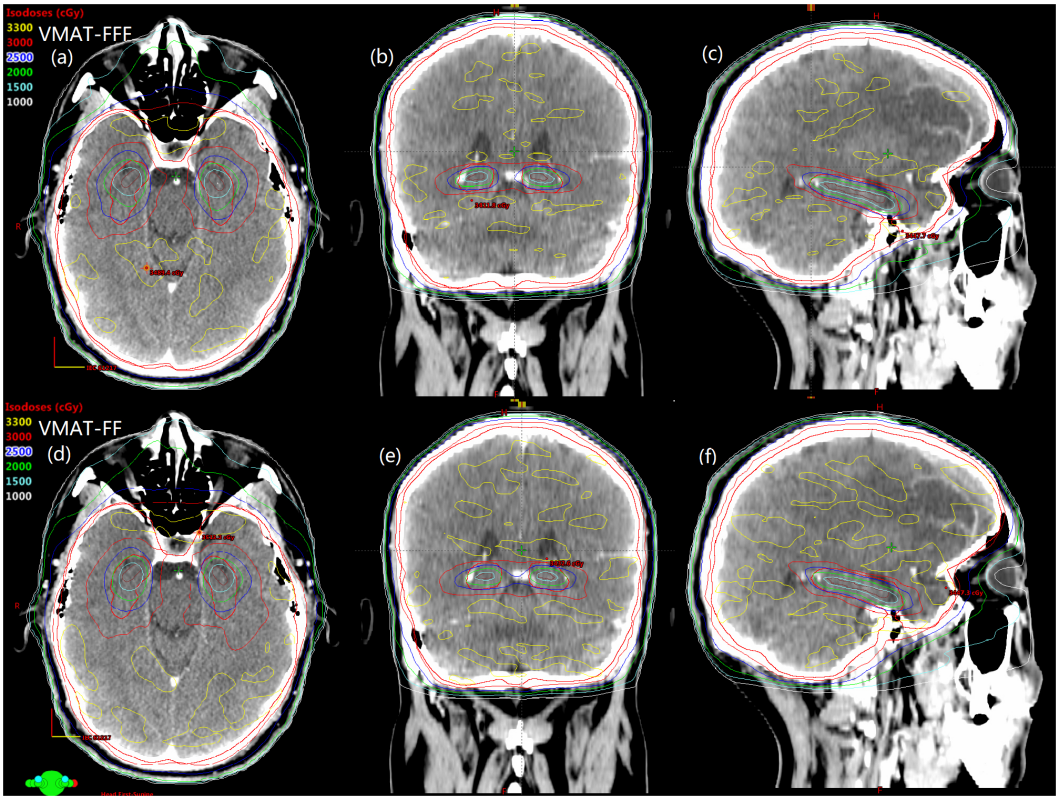


FIGURE 1
The comparison of spatial isodose distributions of VMAT-FFF **(A–C)** versus VMAT-FF **(D–F)** for a sample patient. Red contour represents the PTV-HA and brown contour represents the hippocampus.

FF, and the improvement of dose sparing for all the evaluation indicators involving the hippocampus in the VMAT-FFF was statistically significant compared with VMAT-FF. Dose constraints to hippocampus were reached for VMAT with or without the use of the FF, while the cumulative averages of $D_{max}$ and $D_{100\%}$ for hippocampus were 17.51 ± 1.07 Gy and 12.00 ± 0.39 Gy, 17.18 ± 1.03 Gy and 11.87 ± 0.33 Gy for IMRT-FFF and IMRT-FF, respectively, which did not meet the requirements for hippocampal sparing according to RTOG 0933 guidelines. For IMRT, the FF mode showed better results for hippocampus compared to the FFF, while the difference between the treatment modes was generally only about 2% even though statistically significant.

In addition to hippocampal sparing, the FFF technique also obviously reduced the doses to other OARs such as lens, optic chiasma, and optic nerve compared to FF mode with respect to VMAT (all $p< 0.05$). The maximum doses to left and right lenses in the VMAT-FFF plans on average were 6.91 ± 0.62 Gy and 6.95 ± 0.56 Gy, which were 13.8% and 13.3% lower than the corresponding values of VMAT-FF. A similar result can be found in the IMRT plans for lens. Concerning optic chiasma and optic nerve, $D_{max}$ was rather close between FF and FFF for IMRT. As for non-tumor tissue, FFF beams showed lower integral dose for both VMAT and IMRT compared with conventional beams.

In a word, the VMAT plans using FFF beams improved the homogeneity and conformity of the target and reduced OARs doses significantly keeping target coverage at the same level in comparison with the other three planning techniques.

## 3.3 NTCP for neurocognitive function impairment

Table 3 shows the computed NTCP for neurocognitive function impairment for the FFF and FF plans. The NTCP of VMAT-FFF plans was significantly lower than that of VMAT-FF plans. The opposite result was seen for IMRT technique, however the difference between FFF and FF plans was small.

## 3.4 Plan verification and efficiency

The monitor units, treatment time and passing rate of γ for each treatment modality, and the mean dose rates of VMAT plans are listed in Table 4. Meanwhile, Table 4 also shows the results of the Wilcoxon statistical test for between VMAT-FFF and VMAT-FF as well as between IMRT-FFF and IMRT-FF. The number of monitor units employed was dramatically reduced by 81.5% for VMAT-FFF compared with IMRT-FFF and 79.2% for VMAT-FF compared with IMRT-FF. Furthermore, FFF plans required more MUs than FF plans, with an increase of 19.2% for VMAT and 33.8% for IMRT. The mean treatment time was reduced by 26% for IMRT in FFF

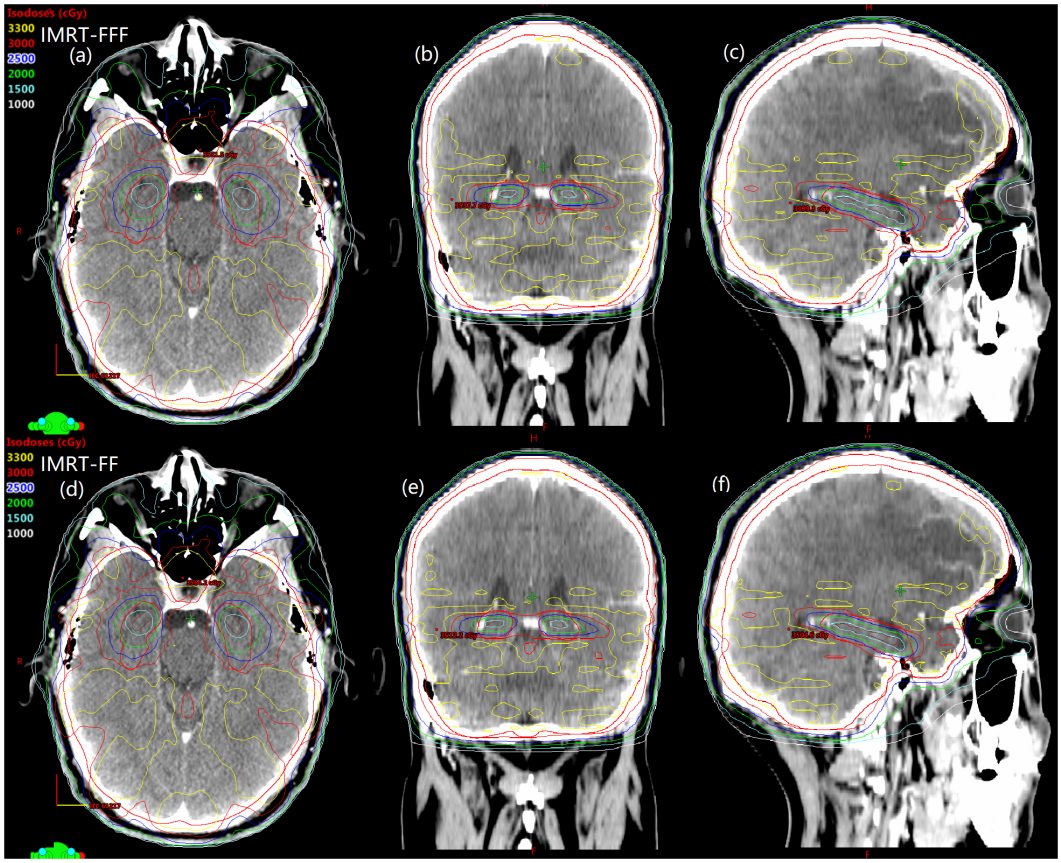


FIGURE 2
Spatial dose distributions in axial, coronal, sagittal views for one representative patient with avoidance of hippocampus during whole brain radiotherapy using IMRT-FFF **(A–C)** and IMRT-FF **(D–F)** techniques. PTV-HA and hippocampus are drawn in red and brown, respectively.

mode as compared to FF, but was almost the same in both irradiation modes in case of VMAT. Besides, VMAT took less treatment time than IMRT technique. As shown in Table 4, VMAT-FFF provided a higher mean dose rate than VMAT-FF, but both types of VMAT plans were well below their respective maximum dose rates. The analyzed data indicated that all 100 plans were clinically deliverable and passed the gamma evaluation. The gamma indices did not show any notable distinctions between FFF and FF for both VMAT and IMRT.

## 3.5 A volume-based analysis

The research results above showed that VMAT achieved significantly better plan quality than IMRT. There was little difference between FF and FFF plans for IMRT. Thus, the volume-based analysis was performed only for the VMAT technique. All values for PTV-HA (HI and CI), the hippocampus ($D_{100\%}$, $D_{mean}$, $D_{max}$ and NTCP), Lens L ($D_{max}$) and Lens R ($D_{max}$) in the three volume-dependent groups are provided in Table 5 for grouping according to hippocampal volume and Table 6 for grouping according to PTV-HA volume. The FF/FFF ratio was computed for all the parameters described above in the matched plans (e.g., $HI_{VMAT\text{-}FF}/HI_{VMAT\text{-}FFF}$). Then, the FF/FFF fraction for each group is plotted as a function of the corresponding volume, as shown in Figure 4 for grouping according to hippocampal volume and Figure 5 for grouping according to PTV-HA volume. In addition, the integral dose of NT is also considered for grouping based on PTV-HA volume. There is no significant trend in other dosimetric parameters with hippocampal and PTV-HA volumes, and the results are not shown.

There was a tendency for the conformity and homogeneity of PTV-HA to worsen and then improve with the increase in hippocampal volume. The homogeneity remained stable with increasing PTV-HA volume, while the conformity became better. The differences between FF and FFF for PTV-HA were larger in Group 1 and Group 6. With the increase in hippocampal volume, the $D_{100\%}$, $D_{mean}$ and NTCP of hippocampus gradually decreased, while $D_{max}$ gradually increased. All indices of the hippocampus showed little change among different PTV-HA volumes. The biggest difference between the two delivery modes was observed in Group 1 for all the evaluation parameters of the hippocampus when grouping was determined by hippocampal volume. However, the fluctuations of the FF/FFF values for hippocampus were not noticeable with changes in target volume. The lens had the lowest $D_{max}$ in cases with small hippocampal and target volumes. The benefit of FFF was slightly greater for small hippocampal and target volumes in terms of the left lens. However, the advantage of FFF was

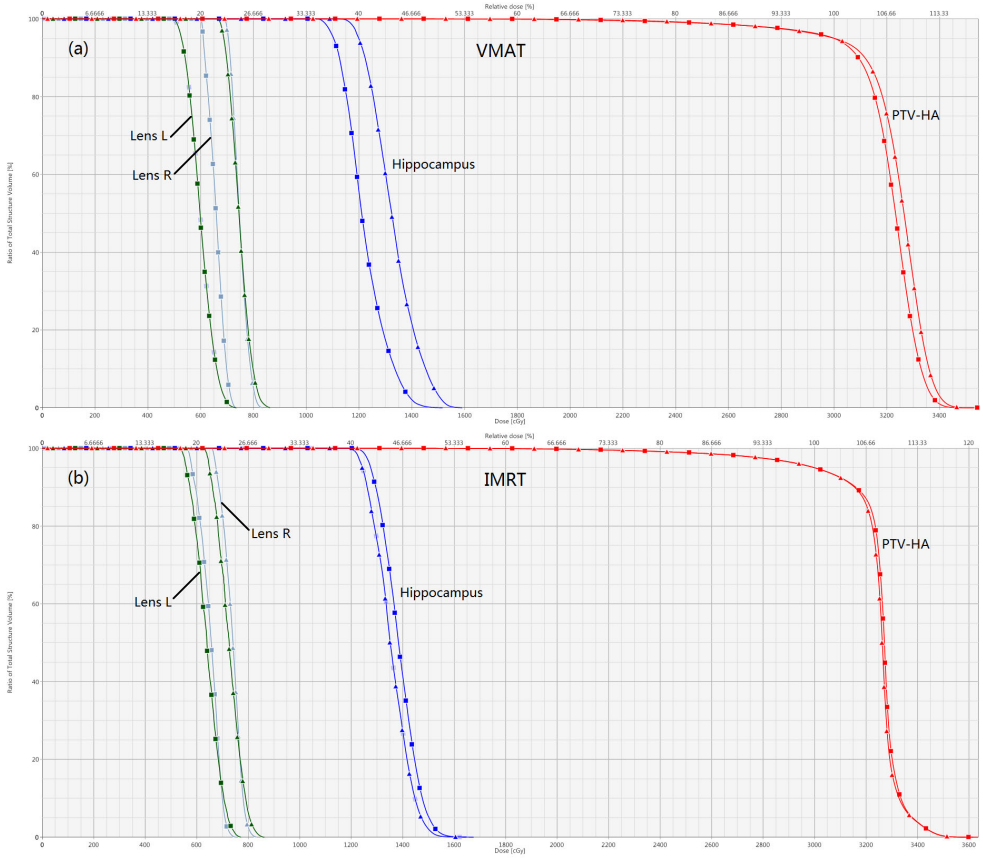


FIGURE 3
Normalized dose-volume histograms for a sample hippocampal-sparing WBRT patient. Comparisons of FFF versus FF for VMAT and IMRT are displayed in **(A, B)**, respectively. The lines with squares represent FFF plans, and the lines with triangles stand for FF plans. The optic chiasm and optic nerve are not shown for the sake of clarity.

greatest for medium hippocampal and target volumes in terms of the right lens. With the increase in target volume, the integral dose of NT also significantly increased, but the range of variation in the FF/FFF ratio was small.

## 4 Discussion

The flattening filter free delivery mode of a linear accelerator is not a new idea in radiation therapy but it has only recently become a reality for clinical routine. In this study, we presented the first evaluation of the potential of the flattening filter free mode in intensity modulated radiation therapy and volumetric modulated arc therapy for patients with hippocampal avoidance whole brain radiotherapy. In terms of target homogeneity and conformity, and OAR sparing, the VMAT-FFF has shown superior quality compared to the VMAT-FF, which can potentially reduce radiation induced inflammation in the hippocampus and its associated neurologic functional sequelae. For IMRT in this article, FFF beams led to similar plan quality compared to FF. IMRT-FFF had a lower dose to the lens while IMRT-FF achieved better hippocampal protection. Obviously, FFF mode is feasible and beneficial in whole brain radiotherapy with hippocampal avoidance, especially for VMAT. A planning study of right sided breast cancer indicated that VMAT-FFF achieved better target coverage and homogeneity than VMAT-FF with similar doses to the OARs while IMRT-FF showed better results regarding some parameters of OARs without compromising target coverage and homogeneity compared to IMRT-FFF (27). For gastric cancers (28) and patients with in-field recurrence of vertebral metastases (29), FFF plans

TABLE 3 Comparison of $EQD_2(D_{40\%})$ and NTCP for four types of plans.

| Parameters | VMAT-FFF | VMAT-FF | p[a] | IMRT-FFF | IMRT-FF | p[b] |
|---|---|---|---|---|---|---|
| $EQD_2(D_{40\%})$ | 9.02 ± 0.61 | 9.92 ± 0.8 | <0.001 | 11.78 ± 0.41 | 11.44 ± 0.41 | <0.001 |
| NTCP | 0.23 ± 0.02 | 0.27 ± 0.03 | <0.001 | 0.35 ± 0.02 | 0.34 ± 0.02 | <0.001 |

Dose values are given in Gy. [a] p value denotes the results of Wilcoxon test between VMAT-FFF and VMAT-FF plans. [b] p value means the results of Wilcoxon test between IMRT-FFF and IMRT-FF plans.

TABLE 4 Comparison of monitor units, treatment time, mean dose rate and the results of gamma analysis for four types of plans.

| Variable | VMAT-FFF | VMAT-FF | p[a] | IMRT-FFF | IMRT-FF | p[b] |
|---|---|---|---|---|---|---|
| Monitor units | 844 ± 35 | 708 ± 35 | <0.001 | 4561 ± 263 | 3409 ± 197 | <0.001 |
| Treatment time (min) | 3.10 ± 0.02 | 3.12 ± 0.02 | 0.56 | 6.90 ± 0.33 | 9.32 ± 0.46 | <0.001 |
| Mean dose rate (MU/min) | 337.6 ± 14.1 | 283.0 ± 13.9 | <0.001 | - | - | - |
| Passing rate of γ | 99.7 ± 0.4 | 99.8 ± 0.3 | 0.67 | 97.9 ± 0.7 | 97.6 ± 1.1 | 0.48 |

[a] p value denotes the results of Wilcoxon test between VMAT-FFF and VMAT-FF plans. [b] p value means the results of Wilcoxon test between IMRT-FFF and IMRT-FF plans.

significantly reduced the dose to the normal tissue, while maintaining target coverage, conformity and homogeneity comparable to FF plans for both IMRT and VMAT. However, differences in plan quality were insignificant between the two irradiation modes for carcinoma of the hypopharynx/larynx (20). It was worth mentioning that, for large and complex targets, such as advanced nasopharyngeal carcinoma (30), VMAT-FFF showed poorer conformity and homogeneity of the target compared to VMAT with traditional flattened beam, and VMAT-FF was more likely to result in a lower dose for most OARs. Based on previous researches, it can be concluded that it is not possible to generalize the results of planning studies for a specific combination of equipment and tumor site, and different targets must be investigated individually.

Mounting evidence imputes neurocognitive deficits in learning and memory after conventional WBRT to radiation induced inflammatory to the neural stem cell compartment in the hippocampus. Hence, the avoidance of hippocampus in the

TABLE 5 Summary of the results for parameters of PTV-HA, hippocampus and lens in three groups according to the hippocampal volume.

| | Parameters | | Group 1 | Group 2 | Group 3 |
|---|---|---|---|---|---|
| PTV-HA | HI | VMAT-FFF | 0.19 ± 0.02 | 0.20 ± 0.02 | 0.19 ± 0.03 |
| | | VMAT-FF | 0.21 ± 0.02 | 0.22 ± 0.02 | 0.21 ± 0.03 |
| | | p | 0.018 | 0.008 | 0.008 |
| | CI | VMAT-FFF | 0.87 ± 0.02 | 0.86 ± 0.02 | 0.87 ± 0.01 |
| | | VMAT-FF | 0.85 ± 0.03 | 0.84 ± 0.02 | 0.85 ± 0.02 |
| | | p | 0.018 | 0.008 | 0.008 |
| Hippocampus | $D_{100\%}$ | VMAT-FFF | 9.71 ± 0.39 | 9.34 ± 0.22 | 9.13 ± 0.36 |
| | | VMAT-FF | 10.46 ± 0.60 | 9.95 ± 0.45 | 9.62 ± 0.33 |
| | | p | 0.018 | 0.008 | 0.008 |
| | $D_{mean}$ | VMAT-FFF | 11.70 ± 0.45 | 11.31 ± 0.44 | 10.93 ± 0.38 |
| | | VMAT-FF | 12.63 ± 0.59 | 12.06 ± 0.62 | 11.64 ± 0.38 |
| | | p | 0.018 | 0.008 | 0.008 |
| | $D_{max}$ | VMAT-FFF | 14.83 ± 0.57 | 15.13 ± 0.49 | 15.40 ± 0.34 |
| | | VMAT-FF | 15.91 ± 0.57 | 16.09 ± 0.69 | 16.39 ± 0.43 |
| | | p | 0.018 | 0.008 | 0.008 |
| | NTCP | VMAT-FFF | 0.25 ± 0.02 | 0.23 ± 0.02 | 0.22 ± 0.02 |
| | | VMAT-FF | 0.30 ± 0.03 | 0.27 ± 0.03 | 0.25 ± 0.02 |
| | | p | 0.017 | 0.007 | 0.007 |
| Lens L | $D_{max}$ | VMAT-FFF | 6.60 ± 0.79 | 6.96 ± 0.42 | 7.10 ± 0.60 |
| | | VMAT-FF | 7.85 ± 0.96 | 8.02 ± 0.51 | 8.14 ± 0.79 |
| | | p | 0.018 | 0.008 | 0.008 |
| Lens R | $D_{max}$ | VMAT-FFF | 6.71 ± 0.70 | 6.96 ± 0.40 | 7.11 ± 0.56 |
| | | VMAT-FF | 7.69 ± 0.83 | 8.13 ± 0.41 | 8.16 ± 0.83 |
| | | p | 0.018 | 0.008 | 0.008 |

Dose values are given in Gy. p value denotes the results of Wilcoxon test between VMAT-FFF and VMAT-FF plans.

course of WBRT treatments has been proposed to achieve prospective neurocognitive benefits, and continued researches have been placed on this area. Using helical tomotherapy and linear accelerator-based IMRT technique, Gondi et al. have reported their preliminary experience and have presented excellent results with hippocampal-sparing whole-brain radiotherapy for patients with brain metastases (31). The hippocampus was spared by helical tomotherapy, which was administered at a median dose of 5.5 Gy and a maximum dose of 12.8 Gy. The hippocampus was spared by noncoplanar IMRT based on linac, resulting in a median dose of 7.8 Gy and a maximum dose of 15.3 Gy. It has previously been reported that the mean and maximum doses to hippocampus respectively were 11.2 ± 0.3 Gy, and 15.6 ± 0.4 Gy with 90.5% of the target volume surrounded by the prescription dose isoline, exhibited by intensity-modulated arc therapy approach for whole brain radiotherapy patients with sparing hippocampus (32). Volumetric modulated arc therapy plans with two full coplanar arcs generated by Auto-Planning engine offered 91.5% coverage for target and 16 Gy of the maximum dose to the hippocampus (33). For VMAT-FFF in this study, the maximum dose in the hippocampus was 15.14 ± 0.50 Gy, when the plans were established at 95% of the volume of PTV-HA to achieve 100% of the prescribed dose. Therefore, compared with previously published researches utilizing VMAT technique, the VMAT plans using FFF beams can attain comparable or lower dose to hippocampus with better target coverage.

Keeping the mean hippocampus dose below 12 Gy out of 30 Gy in 10 fractions prescription is recommended to improve

TABLE 6 Summary of the results for parameters of PTV-HA, hippocampus, lens and NT in three groups according to the PTV-HA volume.

| | Parameters | | Group 4 | Group 5 | Group 6 |
|---|---|---|---|---|---|
| PTV-HA | HI | VMAT-FFF | 0.19 ± 0.02 | 0.19 ± 0.01 | 0.19 ± 0.03 |
| | | VMAT-FF | 0.21 ± 0.02 | 0.21 ± 0.02 | 0.21 ± 0.03 |
| | | P | 0.008 | 0.012 | 0.012 |
| | CI | VMAT-FFF | 0.85 ± 0.01 | 0.87 ± 0.01 | 0.88 ± 0.01 |
| | | VMAT-FF | 0.83 ± 0.01 | 0.85 ± 0.01 | 0.87 ± 0.01 |
| | | p | 0.008 | 0.012 | 0.012 |
| Hippocampus | $D_{100\%}$ | VMAT-FFF | 9.28 ± 0.22 | 9.35 ± 0.58 | 9.47 ± 0.33 |
| | | VMAT-FF | 9.99 ± 0.52 | 9.91 ± 0.67 | 10.02 ± 0.55 |
| | | p | 0.008 | 0.012 | 0.012 |
| | $D_{mean}$ | VMAT-FFF | 11.20 ± 0.39 | 11.21 ± 0.74 | 11.45 ± 0.34 |
| | | VMAT-FF | 12.00 ± 0.61 | 11.99 ± 0.83 | 12.22 ± 0.55 |
| | | p | 0.008 | 0.012 | 0.012 |
| | $D_{max}$ | VMAT-FFF | 15.10 ± 0.56 | 15.32 ± 0.40 | 15.02 ± 0.54 |
| | | VMAT-FF | 16.04 ± 0.72 | 16.38 ± 0.45 | 16.05 ± 0.54 |
| | | p | 0.008 | 0.012 | 0.012 |
| | NTCP | VMAT-FFF | 0.23 ± 0.02 | 0.23 ± 0.03 | 0.24 ± 0.02 |
| | | VMAT-FF | 0.27 ± 0.03 | 0.27 ± 0.04 | 0.28 ± 0.03 |
| | | p | 0.007 | 0.011 | 0.011 |
| Lens L | $D_{max}$ | VMAT-FFF | 6.60 ± 0.61 | 7.32 ± 0.21 | 6.84 ± 0.72 |
| | | VMAT-FF | 7.72 ± 0.72 | 8.48 ± 0.43 | 7.89 ± 0.82 |
| | | P | 0.008 | 0.012 | 0.012 |
| Lens R | $D_{max}$ | VMAT-FFF | 6.74 ± 0.57 | 7.25 ± 0.32 | 6.87 ± 0.64 |
| | | VMAT-FF | 7.70 ± 0.65 | 8.51 ± 0.42 | 7.88 ± 0.80 |
| | | p | 0.008 | 0.012 | 0.012 |
| NT | Integral dose | VMAT-FFF | 29.84 ± 3.04 | 32.50 ± 4.73 | 32.52 ± 3.88 |
| | | VMAT-FF | 30.65 ± 2.89 | 33.49 ± 4.88 | 33.34 ± 3.97 |
| | | p | 0.008 | 0.012 | 0.012 |

Dose values are given in Gy. p value denotes the results of Wilcoxon test between VMAT-FFF and VMAT-FF plans.

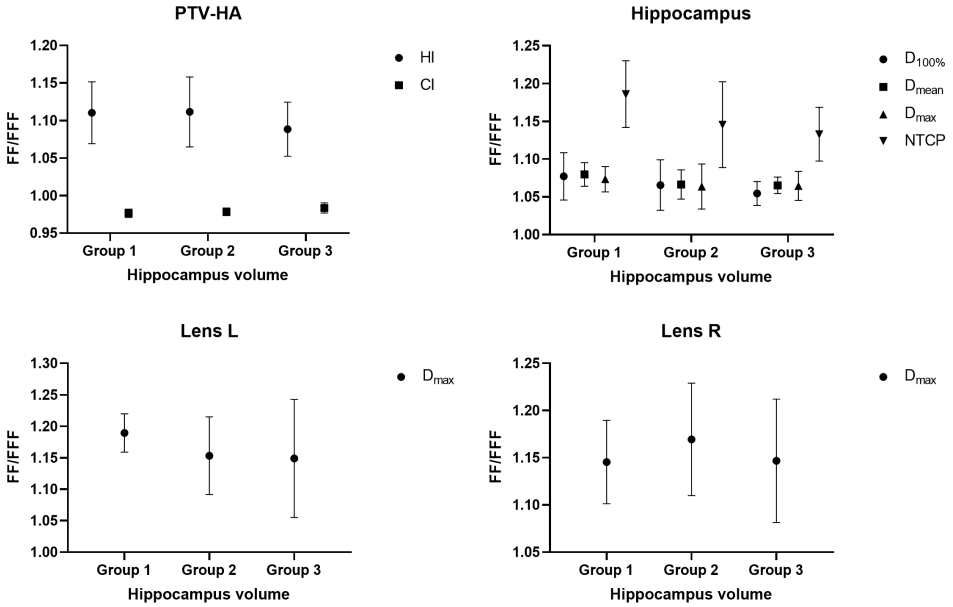


FIGURE 4
Ratio of FF and FFF plans for parameters of PTV-HA, hippocampus and lens plotted against hippocampal volume. All patients were stratified into three groups according to the hippocampal volume.

neurocognitive function (34). The treatment plan created by VMAT-FF was very close to the recommended value. The hippocampus $D_{mean}$ of VMAT-FFF plans was 11.28 ± 0.51 Gy, which was lower than the protocol requirement of 12 Gy. Nevertheless, neither IMRT-FFF nor IMRT-FF could satisfy the criteria.

Although some differences in the plan comparisons were statistically significant, the clinical relevance of these differences remains unclear. To address this issue to some extent, NTCP, an indication of the severity of damage to normal tissues, was calculated. The results of this study showed that VMAT-FFF had the lowest NTCP for impaired neurocognitive function, which was agreed well with the better sparing of hippocampus. It's worth noting that the slight differences, such as the maximum doses to optic nerve and optic chiasm, may not be clinically significant. Hence, the practical benefits of using FFF beams have yet to be verified by clinical results.

Hippocampal volume had a large effect on the planning parameters, as shown in Table 5. For example, the treatment planning with the small hippocampal volume resulted in the better dose distribution of target and lower $D_{max}$ values of hippocampus and lens. Therefore, accurate delineation of the hippocampus is necessary in order to achieve neuroprotective benefits. However, the hippocampus delineated varies greatly due to the differences in experience of radiation oncologist, quality of MRI, and the criteria for contouring of the hippocampus in different cancer centers. For instance, the volume of hippocampi was 2.68 ± 1.05 $cm^3$ in this study, whereas the value was 3.30 $cm^3$ described by Gondi et al. (31). Certainly, with the availability of the hippocampal atlas and continuing instruction, the delineation of hippocampus will become more accurate and uniform with time.

For VMAT, FFF beams achieved significantly better plan quality than FF beams over the entire range of hippocampal and target volumes. With the decrease in hippocampal volume, there will be an increase in the absolute difference between FFF and FF beams for the parameters of PTV-HA and the hippocampus. This finding can serve as a reference for selecting patients when utilizing the FFF technique for HA-WBRT. Nevertheless, the difference between FF and FFF seems to be insensitive to changes in target volume.

The analysis of the technical delivery parameters revealed that the number of MUs was higher for FFF compared to FF regardless of IMRT or VMAT, which was in line with these studies of advanced esophageal cancer (35) and prostate cancer (19). This effect is conceptually expected because the intensity of FFF beam decreases with the off-axis distance, which is evident in open beam dose profiles for larger fields (≥ 10 × 10 $cm^2$). Consequently, at the periphery of the larger target, additional MUs are required to gain a uniform dose distribution on account of the unflattened profile of the FFF beam. In addition, FFF plans generally have more modulation owing to the capability for higher MUs and the inherent beam profile shape itself. Furthermore, the higher amount of MUs and dose rate of FFF plan have raised concerns about radiation protection. In fact, the removal of FF gives rise to a significant decrease in neutron fluence and dose equivalent within the treatment room (36). The photon dose at the maze door in FFF mode is always lower than the dose measured in FF mode, regardless of the presence or absence of a water phantom and the size of the field opening (37). The required thickness of primary barriers is reduced by 8% when unflattened beams are used (38). Hence, existing shielding is usually adequate and surplus if instead of the standard flattened photon beams unflattened ones are used,

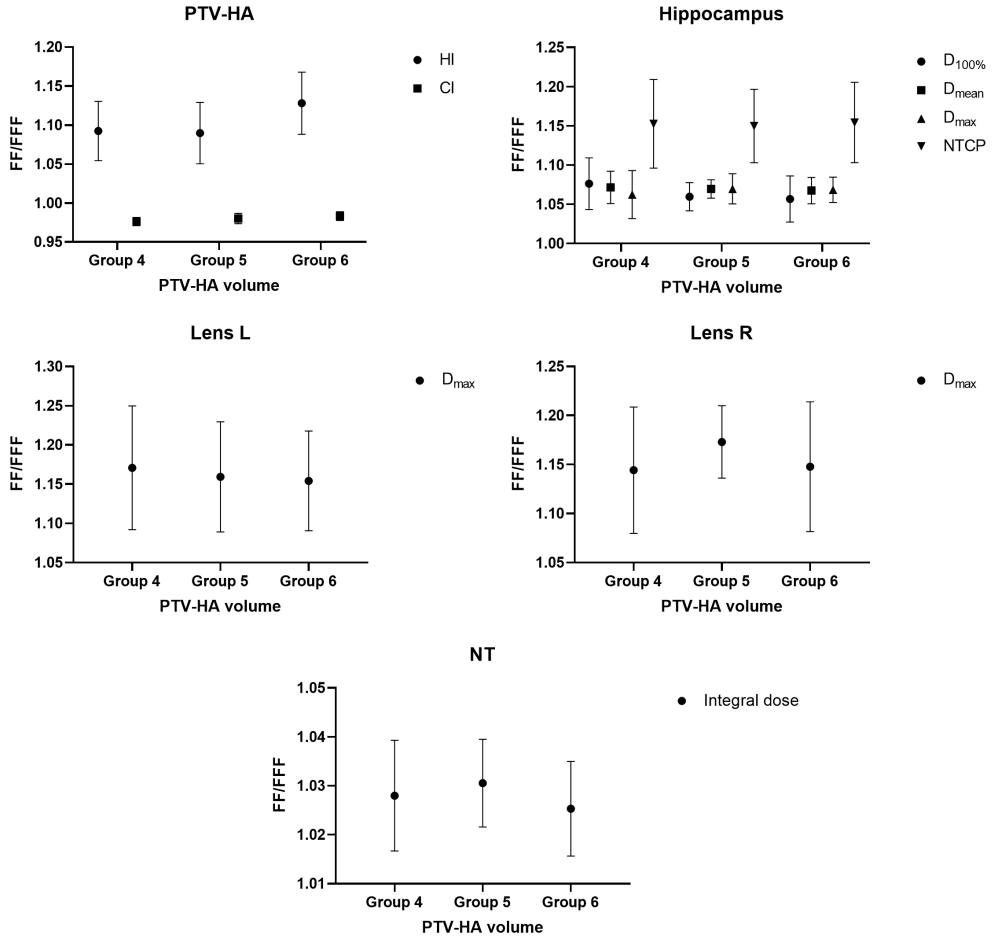


FIGURE 5
Ratio of FF and FFF plans for parameters of PTV-HA, hippocampus, lens and NT plotted against PTV-HA volume. All patients were stratified into three groups according to the PTV-HA volume.

which can reduce occupational exposure for staff, assuming a constant permitted dose per week. Although, an increased number of MUs with FFF was observed for IMRT, the treatment time was cut by 2.42 minutes because of the higher dose rate, improving patient stability and treatment accuracy. The time advantage of using FFF beams increases with increasing dose per fraction, which makes FFF beams especially attractive for stereotactic radiotherapy (39). However, compared to VMAT-FF, the use of the higher mean dose rate of VMAT-FFF did not translate into a time advantage due to the limited speed of the gantry rotation (4.8 degrees per second on the Trilogy). There was no statistical difference for the passing rate of γ between the FF and FFF, which was in accord with these studies of left-sided breast cancer (40) and prostate cancer (19). Moreover, the VMAT plans demonstrated better consistency between the calculated dose distributions and the measured dose distributions than the IMRT technique, which might be because IMRT had more MUs and more complex modulation.

In this study, FFF plans tended to show a significant reduction in dose to healthy tissue compared with standard FF plans in view of the integral dose of non-tumor tissue, which may lead to reducing the risk of long-term radiation-induced complications (41). Reason for this may be that the main source of photon scatter in the treatment head is eliminated by removing the flattening filter, leading to a reduction in the out-of-field dose. Linac head leakage was reduced by 52% by using 6MV FFF beam for IMRT prostate treatment demonstrated by Kragl et al. (17). Simultaneously, many studies have shown that the unflattened mode delivers a much lower peripheral dose (17, 42). Besides, on account of the elimination of beam hardening components from the flattening filter, the spectrum of the unflattened 6 MV beam is usually softer (43). According to Vassiliev et al., 6 MV FFF beam has a depth dose distribution that is comparable to that of conventional 4–5 MV beam (44). As a result, the dose to the skin may be slightly higher (45). The results of this study indicate for WBRT with hippocampal avoidance that the reduced head scattering and residual electron contamination are predominant in patient dose reduction and beam softening does not cause excessive phantom scattering, at short-to-medium distances from the field edges.

This study still has several limitations. For example, the number of patients is small, and this study is based on dosimetry and radiobiology rather than clinical outcomes. Hence, the practical benefits of the FFF plans need to be confirmed by long-term follow-up and a larger number of cases before the FFF mode is widely employed for HA-WBRT, which is the subject of further study.

Besides, due to the lack of measuring equipment in our institution, the integral dose was used to compare the out-of-field doses between FF and FFF beams in this paper. However, the peripheral doses are difficult to calculate correctly with the TPS, and the determination of peripheral doses by measurements of thermoluminescent dosimeters is more recommended (46, 47). In addition, several novel approaches have been proposed for HA-WBRT and have shown promising dosimetric advantages (48, 49). The combination of these methods and FFF techniques is expected to improve treatment plans, which also requires further investigation. Despite these limitations, our study will contribute to understanding the differences between the unflattened and flattened beams in whole-brain radiotherapy with hippocampal avoidance.

## 5 Conclusions

This study is the first to present evidence of the possible benefits of using FFF beams in HA-WBRT in terms of dosimetry and radiobiology, which is important to provide a new idea for improving the efficacy and neurocognitive side effects of HA-WBRT. VMAT with FFF beams achieved superior homogeneity and conformity of the target, better sparing of OARs, and lower NTCP of hippocampus with the similar treatment time compared to flat beams. The improvement resulting from the FFF technique in VMAT increased as the volume of the hippocampus decreased. IMRT-FFF provided comparable plan quality to IMRT-FF with the significantly reduced delivery time. Hence, FFF had a greater dosimetric effect on VMAT than IMRT. In addition, FFF beams showed a lower out-of-field dose, which may lead to reducing secondary cancer risk. FFF plans necessitated a significant increase in monitor units per fraction dose for both IMRT and VMAT, which was associated with the unflattened profile of FFF beams. The gamma scores of all plans were up to standard and no significant differences were detected between FF and FFF. Besides, VMAT showed considerable advantages over IMRT in terms of the plan quality, monitor units, treatment time and gamma indices. To sum up, VMAT-FFF offers the greatest dosimetric and radiobiological superiority, as well as the shortest treatment time compared to other techniques, so it may be considered the preferable therapeutic schedule for HA-WBRT.

## Data availability statement

The raw data supporting the conclusions of this article will be made available by the authors, without undue reservation.

## Ethics statement

The studies involving humans were approved by the ethics committee of Affiliated Hospital of Hebei University. The studies were conducted in accordance with the local legislation and institutional requirements. Written informed consent for participation was not required from the participants or the participants' legal guardians/next of kin in accordance with the national legislation and institutional requirements. Written informed consent was obtained from the individual(s) for the publication of any potentially identifiable images or data included in this article.

## Author contributions

FL: Conceptualization, Funding acquisition, Project administration, Writing – original draft. YP: Investigation, Methodology, Writing – review & editing. QL: Validation, Writing – review & editing. QZ: Data curation, Writing – review & editing. HS: Data curation, Writing – review & editing. SQ: Writing – review & editing. RZ: Writing – review & editing.

## Funding

The author(s) declare financial support was received for the research, authorship, and/or publication of this article. This work was supported by the Health Commission of Hebei Province, China (Grant number 20220630).

## Conflict of interest

The authors declare that the research was conducted in the absence of any commercial or financial relationships that could be construed as a potential conflict of interest.

## Publisher's note



## References

1. DeAngelis LM, Delattre J-Y, Posner JB. Radiation-induced dementia in patients cured of brain metastases. *Neurology* (1989) 39:789 LP–789. doi: 10.1212/WNL.39.6.789

2. Brown PD, Ballman KV, Cerhan JH, Anderson SK, Carrero XW, Whitton AC, et al. Postoperative stereotactic radiosurgery compared with whole brain radiotherapy for resected metastatic brain disease (NCCTG N107C/CEC·3): a multicentre,

randomised, controlled, phase 3 trial. *Lancet Oncol* (2017) 18:1049–60. doi: 10.1016/S1470-2045(17)30441-2

3. Monaco EA III, Faraji AH, Berkowitz O, Parry PV, Hadelsberg U, Kano H, et al. Leukoencephalopathy after whole-brain radiation therapy plus radiosurgery versus radiosurgery alone for metastatic lung cancer. *Cancer* (2013) 119:226–32. doi: 10.1002/cncr.27504

4. Scoville WB, Milner B. Loss of recent memory after bilateral hippocampal lesions. *J Neuropsychiatry Clin Neurosci* (2000) 12:103–13. doi: 10.1176/jnp.12.1.103-a

5. Raber J, Rola R, LeFevour A, Morhardt D, Curley J, Mizumatsu S, et al. Radiation-induced cognitive impairments are associated with changes in indicators of hippocampal neurogenesis. *Radiat Res* (2004) 162:39–47. doi: 10.1667/RR3206

6. Rola R, Raber J, Rizk A, Otsuka S, VandenBerg SR, Morhardt DR, et al. Radiation-induced impairment of hippocampal neurogenesis is associated with cognitive deficits in young mice. *Exp Neurol* (2004) 188:316–30. doi: 10.1016/j.expneurol.2004.05.005

7. Gondi V, Pugh SL, Tome WA, Caine C, Corn B, Kanner A, et al. Preservation of memory with conformal avoidance of the hippocampal neural stem-cell compartment during whole-brain radiotherapy for brain metastases (RTOG 0933): A phase II multi-institutional trial. *J Clin Oncol* (2014) 32:3810–6. doi: 10.1200/JCO.2014.57.2909

8. Ghia A, Tomé WA, Thomas S, Cannon G, Khuntia D, Kuo JS, et al. Distribution of brain metastases in relation to the hippocampus: implications for neurocognitive functional preservation. *Int J Radiat Oncol* (2007) 68:971–7. doi: 10.1016/j.ijrobp.2007.02.016

9. Tsai P-F, Yang C-C, Chuang C-C, Huang T-Y, Wu Y-M, Pai P-C, et al. Hippocampal dosimetry correlates with the change in neurocognitive function after hippocampal sparing during whole brain radiotherapy: a prospective study. *Radiat Oncol* (2015) 10:253. doi: 10.1186/s13014-015-0562-x

10. Verbakel WFAR, Cuijpers JP, Hoffmans D, Bieker M, Slotman BJ, Senan S. Volumetric intensity-modulated arc therapy vs. conventional IMRT in head-and-neck cancer: A comparative planning and dosimetric study. *Int J Radiat Oncol* (2009) 74:252–9. doi: 10.1016/j.ijrobp.2008.12.033

11. Wang B-H, Hua W, Gu X, Wang X-L, Li J, Liu L-Q, et al. Dosimetric study of different radiotherapy planning approaches for hippocampal avoidance whole-brain radiation therapy (HA-WBRT) based on fused CT and MRI imaging. *Australas Phys Eng Sci Med* (2015) 38:767–75. doi: 10.1007/s13246-015-0397-7

12. Benedek H, Lerner M, Nilsson P, Knöös T, Gunnlaugsson A, Ceberg C. The effect of prostate motion during hypofractionated radiotherapy can be reduced by using flattening filter free beams. *Phys Imaging Radiat Oncol* (2018) 6:66–70. doi: 10.1016/j.phro.2018.05.001

13. Navarria P, Ascolese AM, Mancosu P, Alongi F, Clerici E, Tozzi A, et al. Volumetric modulated arc therapy with flattening filter free (FFF) beams for stereotactic body radiation therapy (SBRT) in patients with medically inoperable early stage non small cell lung cancer (NSCLC). *Radiother Oncol* (2013) 107:414–8. doi: 10.1016/j.radonc.2013.04.016

14. Wu J, Song H, Li J, Tang B, Wu F. Evaluation of flattening-filter-free and flattening filter dosimetric and radiobiological criteria for lung SBRT: A volume-based analysis. *Front Oncol* (2023) 13:1108142. doi: 10.3389/fonc.2023.1108142

15. Dzierma Y, Nuesken FG, Palm J, Licht NP, Ruebe C. Planning study and dose measurements of intracranial stereotactic radiation surgery with a flattening filter-free linac. *Pract Radiat Oncol* (2014) 4:e109–16. doi: 10.1016/j.prro.2013.04.004

16. Bell K, Fleckenstein J, Nuesken F, Licht N, Rübe C, Dzierma Y. mARC treatment of Hypopharynx carcinoma with flat and flattening-filter-free beam energies – A planning study. *PloS One* (2016) 11:e0164616. doi: 10.1371/journal.pone.0164616

17. Kragl G, Baier F, Lutz S, Albrich D, Dalaryd M, Kroupa B, et al. Flattening filter free beams in SBRT and IMRT: Dosimetric assessment of peripheral doses. *Z Med Phys* (2011) 21:91–101. doi: 10.1016/j.zemedi.2010.07.003

18. Cashmore J. The characterization of unflattened photon beams from a 6 MV linear accelerator. *Phys Med Biol* (2008) 53:1933. doi: 10.1088/0031-9155/53/7/009

19. Treutwein M, Hipp M, Koelbl O, Dobler B. Volumetric-modulated arc therapy and intensity-modulated radiation therapy treatment planning for prostate cancer with flattened beam and flattening filter free linear accelerators. *J Appl Clin Med Phys* (2017) 18:307–14. doi: 10.1002/acm2.12168

20. Dobler B, Obermeier T, Hautmann MG, Khemissi A, Koelbl O. Simultaneous integrated boost therapy of carcinoma of the hypopharynx/larynx with and without flattening filter - a treatment planning and dosimetry study. *Radiat Oncol* (2017) 12:114. doi: 10.1186/s13014-017-0850-8

21. Duan S, Li C, Shi J, Ma Y, Zhang X, Huang J, et al. Synchronous bilateral breast carcinoma irradiation: A comparative investigation between flattened and unflattened beams. *Appl Radiat Isot* (2022) 181:110079. doi: 10.1016/j.apradiso.2021.110079

22. Sandrini ES, da Silva AX, da Silva CM. Evaluation of collimator rotation for volumetric modulated arc therapy lung stereotactic body radiation therapy using flattening filter free. *Appl Radiat Isot* (2018) 141:257–60. doi: 10.1016/j.apradiso.2018.05.026

23. Paddick I. A simple scoring ratio to index the conformity of radiosurgical treatment plans. Technical note. *J Neurosurg* (2000) 93:219–22. doi: 10.3171/jns.2000.93.supplement

24. D'Arienzo M, Masciullo SG, Sanctis VD, Osti MF, Chiacchiararelli L, Enrici RM. Integral dose and radiation-induced secondary Malignancies: comparison between stereotactic body radiation therapy and three-dimensional conformal radiotherapy. *Int J Environ Res Public Health* (2012) 9:4223–40. doi: 10.3390/ijerph9114223

25. Miften M, Olch A, Mihailidis D, Moran J, Pawlicki T, Molineu A, et al. Tolerance limits and methodologies for IMRT measurement-based verification QA: Recommendations of AAPM Task Group No. 218. *Med Phys* (2018) 45:e53–83. doi: 10.1002/mp.12810

26. Gondi V, Hermann BP, Mehta MP, Tomé WA. Hippocampal dosimetry predicts neurocognitive function impairment after fractionated stereotactic radiotherapy for benign or low-grade adult brain tumors. *Int J Radiat Oncol Biol Phys* (2012) 83:e487–93. doi: 10.1016/j.ijrobp.2011.10.021

27. Maier J, Knott B, Maerz M, Loeschel R, Koelbl O, Dobler B. Simultaneous integrated boost (SIB) radiation therapy of right sided breast cancer with and without flattening filter - A treatment planning study. *Radiat Oncol* (2016) 11:111. doi: 10.1186/s13014-016-0687-6

28. Bhushan M, Yadav G, Tripathi D, Kumar L, Kishore V, Dewan A, et al. Dosimetric analysis of unflattened (FFFB) and flattened (FB) photon beam energy for gastric cancers using IMRT and VMAT—a comparative study. *J Gastrointest Cancer* (2019) 50:408–19. doi: 10.1007/s12029-018-0080-9

29. Dobler B, Khemissi A, Obermeier T, Hautmann MG, Katsilieri Z, Kölbl O. Re-irradiating spinal column metastases using IMRT and VMAT with and without flattening filter - a treatment planning study. *Radiat Oncol* (2016) 11:33. doi: 10.1186/s13014-016-0603-0

30. Zhuang M, Zhang T, Chen Z, Lin Z, Li D, Peng X, et al. Advanced nasopharyngeal carcinoma radiotherapy with volumetric modulated arcs and the potential role of flattening filter-free beams. *Radiat Oncol* (2013) 8:120. doi: 10.1186/1748-717X-8-120

31. Gondi V, Tolakanahalli R, Mehta MP, Tewatia D, Rowley H, Kuo JS, et al. Hippocampal-sparing whole-brain radiotherapy: A "How-to" Technique using helical tomotherapy and linear accelerator–based intensity-modulated radiotherapy. *Int J Radiat Oncol* (2010) 78:1244–52. doi: 10.1016/j.ijrobp.2010.01.039

32. Pokhrel D, Sood S, Lominska C, Kumar P, Badkul R, Jiang H, et al. Potential for reduced radiation-induced toxicity using intensity-modulated arc therapy for whole-brain radiotherapy with hippocampal sparing. *J Appl Clin Med Phys* (2015) 16:131–41. doi: 10.1120/jacmp.v16i5.5587

33. Wang S, Zheng D, Zhang C, Ma R, Bennion NR, Lei Y, et al. Automatic planning on hippocampal avoidance whole-brain radiotherapy. *Med Dosim* (2017) 42:63–8. doi: 10.1016/j.meddos.2016.12.002

34. Chang J, Perez-Andujar A, Hossain S, Higby C, Ahmad S, Barani IJ, et al. Estimation of the incident probability of brain metastases in hippocampal-sparing whole-brain radiation. *Int J Radiat Oncol* (2014) 90:S312–3. doi: 10.1016/j.ijrobp.2014.05.1041

35. Nicolini G, Ghosh-Laskar S, Shrivastava SK, Banerjee S, Chaudhary S, Agarwal JP, et al. Volumetric modulation arc radiotherapy with flattening filter-free beams compared with static gantry IMRT and 3D conformal radiotherapy for advanced esophageal cancer: A feasibility study. *Int J Radiat Oncol Biol Phys* (2012) 84:553–60. doi: 10.1016/j.ijrobp.2011.12.041

36. Najem MA, Abolaban FA, Podolyák Z, Spyrou NM. Neutron production from flattening filter free high energy medical linac: A Monte Carlo study. *Radiat Phys Chem* (2015) 116:176–80. doi: 10.1016/j.radphyschem.2015.01.040

37. Tóth ÁÁ, Dragojlović LD, Ignjatov NV, Krmar M. Photon dose at the maze entrance door: The comparison of flattening filter and flattening filter free working modes. *Phys Med* (2018) 49:1–4. doi: 10.1016/j.ejmp.2018.04.007

38. Jank J, Kragl G, Georg D. Impact of a flattening filter free linear accelerator on structural shielding design. *Z Med Phys* (2014) 24:38–48. doi: 10.1016/j.zemedi.2013.05.002

39. Lang S, Shrestha B, Graydon S, Cavelaars F, Linsenmeier C, Hrbacek J, et al. Clinical application of flattening filter free beams for extracranial stereotactic radiotherapy. *Radiother Oncol* (2013) 106:255–9. doi: 10.1016/j.radonc.2012.12.012

40. Koivumäki T, Heikkilä J, Väänänen A, Koskela K, Sillanmäki S, Seppälä J. Flattening filter free technique in breath-hold treatments of left-sided breast cancer: The effect on beam-on time and dose distributions. *Radiother Oncol* (2016) 118:194–8. doi: 10.1016/j.radonc.2015.11.032

41. Murray LJ, Thompson CM, Lilley J, Cosgrove V, Franks K, Sebag-Montefiore D, et al. Radiation-induced second primary cancer risks from modern external beam radiotherapy for early prostate cancer: impact of stereotactic ablative radiotherapy (SABR), volumetric modulated arc therapy (VMAT) and flattening filter free (FFF) radiotherapy. *Phys Med Biol* (2015) 60:1237–57. doi: 10.1088/0031-9155/60/3/1237

42. Cashmore J, Ramtohul M, Ford D. Lowering whole-body radiation doses in pediatric intensity-modulated radiotherapy through the use of unflattened photon beams. *Int J Radiat Oncol* (2011) 80:1220–7. doi: 10.1016/j.ijrobp.2010.10.002

43. Mesbahi A. Dosimetric characteristics of unflattened 6MV photon beams of a clinical linear accelerator: A Monte Carlo study. *Appl Radiat Isot* (2007) 65:1029–36. doi: 10.1016/j.apradiso.2007.04.023

44. Vassiliev ON, Titt U, Pönisch F, Kry SF, Mohan R, Gillin MT. Dosimetric properties of photon beams from a flattening filter free clinical accelerator. *Phys Med Biol* (2006) 51:1907–17. doi: 10.1088/0031-9155/51/7/019

45. Guy CL, Karki K, Sharma M, Kim S. Clinically relevant investigation of flattening filter-free skin dose. *J Appl Clin Med Phys* (2016) 17:140–8. doi: 10.1120/jacmp.v17i6.6307

46. Dzierma Y, Bell K, Palm J, Nuesken F, Licht N, Rübe C. mARC vs. IMRT radiotherapy of the prostate with flat and flattening-filter-free beam energies. *Radiat Oncol* (2014) 9:250. doi: 10.1186/s13014-014-0250-2

47. Bell K, Dzierma Y, Palm J, Nuesken F, Licht N, Rübe C. mARC prostate treatment planning with Varian Eclipse for flat vs. FFF beams. *Phys Med* (2016) 32:474–8. doi: 10.1016/j.ejmp.2016.02.011

48. Xue J, Jin S, Zhang H, Zou K, Sheng J, Tang J, et al. A simplified non-coplanar volumetric modulated arc therapy for the whole brain radiotherapy with hippocampus avoidance. *Front Oncol* (2023) 13:1143564. doi: 10.3389/fonc.2023.1143564

49. Shen J, Bender E, Yaparpalvi R, Kuo H-C, Basavatia A, Hong L, et al. An efficient Volumetric Arc Therapy treatment planning approach for hippocampal-avoidance whole-brain radiation therapy (HA-WBRT). *Med Dosim* (2015) 40:205–9. doi: 10.1016/j.meddos.2014.11.007

frontiers | Frontiers in Oncology

TYPE Review
PUBLISHED 24 January 2024
DOI 10.3389/fonc.2024.1298605



OPEN ACCESS

EDITED BY
Timothy James Kinsella,
Brown University, United States

REVIEWED BY
Uma Goyal,
Banner Health, United States
Paul Stephen Rava,
UMass Memorial Medical Center,
United States

*CORRESPONDENCE
Tomas Kazda
tomas.kazda@mou.cz

RECEIVED 21 September 2023
ACCEPTED 08 January 2024
PUBLISHED 24 January 2024

CITATION
Pospisil P, Hynkova L, Hnidakova L, Maistryszinova J, Slampa P and Kazda T (2024) Unilateral hippocampal sparing during whole brain radiotherapy for multiple brain metastases: narrative and critical review. *Front. Oncol.* 14:1298605. doi: 10.3389/fonc.2024.1298605



# Unilateral hippocampal sparing during whole brain radiotherapy for multiple brain metastases: narrative and critical review

Petr Pospisil[1,2], Ludmila Hynkova[1,2], Lucie Hnidakova[1,2], Jana Maistryszinova[1,2], Pavel Slampa[1,2] and Tomas Kazda[1,2]*

[1]Department of Radiation Oncology, Masaryk Memorial Cancer Institute, Brno, Czechia, [2]Department of Radiation Oncology, Faculty of Medicine, Masaryk University, Brno, Czechia

**Background:** The landscape of brain metastases radiotherapy is evolving, with a shift away from whole-brain radiotherapy (WBRT) toward targeted stereotactic approaches aimed at preserving neurocognitive functions and maintaining overall quality of life. For patients with multiple metastases, especially in cases where targeted radiotherapy is no longer feasible due to widespread dissemination, the concept of hippocampal sparing radiotherapy (HA_WBRT) gains prominence.

**Methods:** In this narrative review we explore the role of the hippocampi in memory formation and the implications of their postradiotherapy lateral damage. We also consider the potential advantages of selectively sparing one hippocampus during whole-brain radiotherapy (WBRT). Additionally, by systematic evaluation of relevant papers published on PubMed database over last 20 years, we provide a comprehensive overview of the various changes that can occur in the left or right hippocampus as a consequence of radiotherapy.

**Results:** While it is important to note that various neurocognitive functions are interconnected throughout the brain, we can discern certain specialized roles of the hippocampi. The left hippocampus appears to play a predominant role in verbal memory, whereas the right hippocampus is associated more with visuospatial memory. Additionally, the anterior part of the hippocampus is more involved in episodic memory and emotional processing, while the posterior part is primarily responsible for spatial memory and pattern separation. Notably, a substantial body of evidence demonstrates a significant correlation between post-radiotherapy changes in the left hippocampus and subsequent cognitive decline in patients.

**Conclusion:** In the context of individualized palliative radiotherapy, sparing the unilateral (specifically, the left, which is dominant in most individuals) hippocampus could expand the repertoire of strategies available for adapted

WBRT in cases involving multiple brain metastases where stereotactic radiotherapy is not a viable option. Prospective ongoing studies assessing various memory-sparing radiotherapy techniques will define new standard of radiotherapy care of patients with multiple brain metastases.

KEYWORDS

whole brain radiotherapy, hippocampus, unilateral, brain metastases, neurocognitive function

## 1 Introduction

Brain metastases (BM) are the most common intracranial tumors in adults, accounting for more than half of all brain tumors. The incidence of BM is steadily increasing, primarily due to advances in comprehensive cancer care, better control of extracranial disease through improved systemic therapy, and enhanced detection of small metastases using more easily accessible magnetic resonance imaging. It is estimated that BM occur in up to 30 percent of adult patients with solid malignancies (1). Consequently, the prevalence and incidence of BM are continuously rising, making BM a significant social and health problem. Until recently, due to limited therapeutic options, BM were typically treated in a standardized manner, with whole-brain radiotherapy (WBRT) being the primary treatment for decades. Current treatments for BM include surgery, stereotactic radiosurgery (SRS), WBRT, chemotherapy, and modern targeted therapy (2).

Although the role of WBRT in patients with brain metastases has evolved in recent years, and its usage has decreased, WBRT remains a crucial tool in the standard treatment for the majority of patients with multiple BM (3). While radiotherapy has made significant advancements in general, WBRT itself has not seen substantial changes in recent decades. It has long been recognized that WBRT can lead to serious, irreversible side effects on the central nervous system. Neurocognitive dysfunction has become an increasingly relevant concern in patients with BM who receive WBRT. Preserving a good quality of life (QoL) for as long as possible and minimizing potential iatrogenic side effects of treatment are currently top priorities, not only in palliative medicine (4).

Although cognitive impairment in patients with BM is likely influenced by multiple factors, post-radiation changes in the hippocampus are considered one of the primary factors affecting neurocognitive function (NCF), particularly memory, and ultimately overall QoL (5–7). This article presents multiple clinical and preclinical data on radiation-induced damage to neural progenitor cells located in the subgranular zone of the hippocampus and its impact on radiation-induced neurocognitive decline, specifically in terms of short-term memory formation and recall (8). Additionally, by systematic evaluation of relevant papers published on PubMed database over last 20 years, we provide a comprehensive overview of the various changes that can occur in the left or right hippocampus as a consequence of radiotherapy with consideration of the potential benefits of sparing unilateral hippocampus during WBRT in patients with multiple brain metastases (presented in section 4.2 and 4.3 after necessary gradual description of relevant implicatons).

## 2 Hippocampus – basic overview

Due to bilateral brain symmetry, the hippocampus is situated in each cerebral hemisphere. It can be simplified that if there is unilateral damage to the hippocampus, with the structure in the other hemisphere remaining intact, memory functions of the brain can generally remain almost normal (9). Conversely, severe damage to both hippocampi in both hemispheres can lead to significant difficulties in forming new memories. Nevertheless, clinical observations and numerous studies demonstrate that damage to different regions of the hippocampus can result in specific memory disorders. For instance, verbal memory retention is most likely associated with the anterior part of the left hippocampus, while the right hippocampus plays a more prominent role in executive functions and regulation during verbal memory retrieval. The posterior part of the left hippocampus could then be linked to verbal memory capacity (10). The findings of our previous research are consistent with these observations, as discussed in further details (11, 12).

The hippocampus does not appear to have a uniform structure along its longitudinal axis. There is evidence of differences in both structure and function. The anterior part of the hippocampus is preferentially connected to the amygdala and orbitofrontal cortex and is believed to be mainly involved in episodic memory and the mediation of anxiety-related behaviors. In contrast, the posterior part of the hippocampus is preferentially connected to the retrosplenial and posterior parietal cortex and is thought to be especially engaged in memory and spatial navigation (13). Other parts of the brain (amygdala, fornix, etc.) are involved in the neurocognitive function in the complex brain organization.

In addition to the functional distinctions between the anterior and posterior hippocampus, there is substantial evidence regarding the lateralization of hippocampal functioning, highlighting that the roles of the right and left hippocampus are not identical. This knowledge is derived from findings in patients with unilateral hippocampal lesions, including those with conditions such as schizophrenia and mild cognitive impairment, as well as individuals who have undergone unilateral hippocampal resection as a treatment for epilepsy. In broad terms, it can be asserted that spatial memory is primarily associated with the right hippocampus, while episodic memory is linked to the left hippocampus.

Furthermore, gender differences in hippocampal lateralization during spatial tasks have been observed, with greater activation on the left in females and on the right in males. This discrepancy is likely attributed to the fact that females tend to rely more on verbal strategies, whereas males exhibit a preference for nonverbal spatial strategies (14). Additionally, several other studies discussed below have described varying clinical significance in the postradiotherapy changes between the left and right hippocampus.

It has been shown that radiation-induced microstructural changes in the brain, which can subsequently lead to cognitive impairment, occur soon after radiation exposure. These alterations may occur without obvious radiographic manifestations and may be detectable, for example, by diffusion tensor imaging (DTI) as white matter changes. Further information about radiation damages can be provided by MR perfusion a diffusion-weighted imaging (DWI). MR spectroscopy (MRS) is able to evaluate radiation-induced brain injury by assessing the metabolic concentrations at the molecular levels (15, 16).

## 3 Laterality in hippocampal function

Much of the information on this topic has been gleaned from non-oncology patients or healthy volunteers. Patients with BM possess unique characteristics; their cognitive and neurological functions may be influenced by the oncology disease itself, typically resulting in a poor prognosis and short life expectancy. The primary treatment goal is to enhance or sustain the quality of life. The view of this issue from the point of view of radiation oncology must be somewhat different from, for example, epilepsy surgery. In neurobiology, it is understood that explicit memory is primarily housed in the brain's temporal lobes, specifically within the hippocampus, as well as in the amygdala and neocortex.

While both episodic and spatial memory rely on the hippocampus, distinctions in these functions suggest partial separation and distinct structural neural foundations, as well as varying connections with other brain regions. Notably, the anterior and posterior hippocampus exhibit differences in structure and connectivity within the brain. Some studies suggest that the posterior hippocampus plays a greater role in spatial memory, whereas the anterior hippocampus is primarily associated with episodic memory (17, 18).

In addition to the functional differences between the anterior and posterior hippocampi, numerous examples support the presence of lateralization in hippocampal functions, meaning that the left and right hippocampus serve distinct functions. Much of this evidence is derived from studies involving patients with unilateral hippocampal lesions and unilateral hippocampal resections. Research on patients who have undergone resection of the left hippocampus for the treatment of epilepsy suggests impairment verbal memory tasks, specifically affecting learning and retention of story content, word recognition, recall, and verbal associative memory (19–21). In contrast, resections of the right hippocampus and parahippocampal cortex lead to deficits in visuospatial tasks (22). This aligns with findings of lateralized hippocampal activation in functional neuroimaging studies. Lateralization of hippocampal function is also evident in spatial memory, depending on whether verbalizable stimuli or abstract nonverbal stimuli are employed. This suggests possible differences in different cognitive strategies. These results provide support for the concept of functional lateralization within specific aspects of spatial memory (23).

Consequently, it can be inferred that the previous hypothesis of strictly lateralized organization of brain functions, with verbal memory components residing exclusively in the left hemisphere and spatial memory components solely in the right hemisphere, may not be so pronounced (24). Thus, with the advancement of cognitive neuroscience, the idea of strict structural specificity is now being questioned (25).Thus, the specific neurocognitive functions attributed to the left and right hippocampus are not as clear-cut as a following Figure 1 might suggest. While there are some general trends in terms of lateralization of functions in the brain, the hippocampus is a complex structure, and many functions involve both sides working together. Additionally, individual differences, as gender aspects, can play a significant role.

Conversely, the recovery and compensation of memory functions represent a demonstration of a particular functional plasticity within the brain (26). For instance, memory deficits typically associated with the contralateral temporal lobe function in patients with unilateral hippocampal sclerosis may show improvement after surgery (27). However, in patients with brain tumors, who are further burdened by oncological treatments, including radiation injury, it is not possible to assume the same ability for compensation.

From a radiotherapy perspective, the feasibility of sparing both hippocampi, only the right hippocampus, or only the left hippocampus is often influenced by the presence or proximity of individual BM within the hippocampus. The consideration of which functions are associated with each hippocampus is secondary in this context. Conversely, the discussed differences in lateralization are a significant factor to consider when contemplating unilateral hippocampal investigation in WBRT as discussed below. In this scenario, one of the hippocampi remains covered by full dose of radiation while only the other is protected. This experimental approach may offer greater sparing possibilities when focusing on a single hippocampus, along with improved rest of the brain irradiation (28).

### 3.1 Radiotherapy and hippocampus

The side effects of radiotherapy on the brain are highly specific to the tissues and structures involved. This specificity arises from

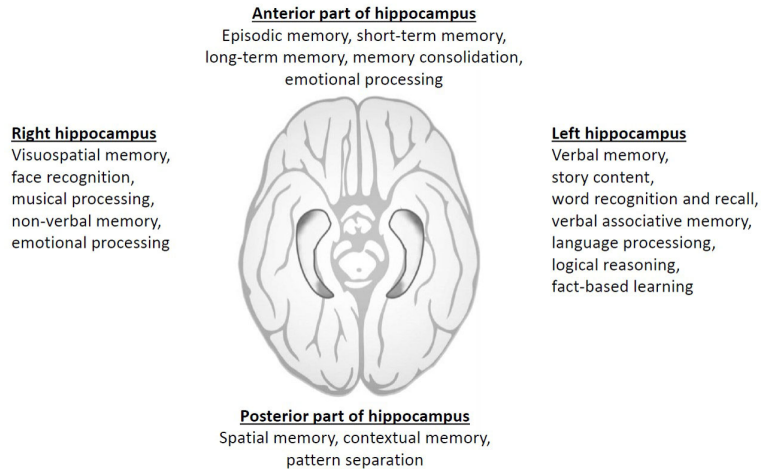


FIGURE 1
Summary of simplified division of different neurocognitive domains according to hippocampal location and laterality.

the combined impact of radiation on brain vasculature, neuroglial cells, and their precursors, including stem cells. Radiation-induced inflammatory effects and the disruption of the blood-brain barrier also play a role (29).

The radiation-induced inflammatory response leads to an increased activation of microglia, which release cytokines like tumor necrosis factor-alpha and interleukin-1 beta. Radiation is particularly cytotoxic to proliferating neuroglial progenitor cells, disrupting both gliogenesis and neurogenesis and resulting in a reduction in the number of newly formed neurons. One region in the brain known for its neurogenic potential is the hippocampus, specifically the subgranular zone of the hippocampal gyrus dentatus, housing a niche of neural stem cells crucial for memory formation. In our previous work, we hypothesized that the loss of neuronal cells in the hippocampal region that occurs after irradiation can be measured by changes in N-acetylaspartate (NAA) concentration using MRS. Our results showed that after whole brain radiotherapy (WBRT), there was a decrease in NAA concentration in both hippocampi, and these changes were associated with a decline in cognitive function as assessed by a battery of neurocognitive tests focused on memory, including the Auditory Verbal Learning Test and the Short Test of Visual-Spatial Memory-Revised. We observed a moderate positive correlation between the decrease in NAA concentration in the left hippocampus and some subtests related to verbal memory (12). A radiation technique employing intensity-modulated RT (IMRT) to administer a therapeutic dose to the entire brain region while sparing the bilateral hippocampi is known as hippocampal avoidance whole brain radiotherapy (HA-WBRT) (30–33).

In a pivotal phase II trial (RTOG 0933), HA-WBRT in BM patients was linked to the preservation of tested cognitive function and reported quality of life compared to historical controls (31). Subsequently, the results of a randomized phase III study (NRG CC001, published in 2020) comparing HA-WBRT plus memantine, the N-methyl-D-aspartate (NMDA) receptor antagonist, to WBRT plus memantine in 518 BM patients demonstrated a significantly lower risk of cognitive failure (adjusted hazard ratio, 0.74; P = .02) with hippocampal sparing, while there was no difference in intracranial progression or overall survival. HA-WBRT in combination with memantine can now be considered a new standard of care for the treatment of multiple brain metastases (34).

However, the planning process for HA-WBRT is significantly more labor-intensive compared to traditional WBRT. The key challenge lies in accurately defining the target volume and identifying critical structures and organs at risk (OAR), such as the hippocampus and hippocampal-avoiding zones (33). To address this, a consensus-based atlas for contouring in Neuro-Oncology can help reduce inter- and intra-observer delineation variability (35). Recently, an MRI-based OAR autosegmentation atlases are developed as well. Autosegmentation allows for high-quality contouring in a limited time frame. The accuracy of hippocampal contouring in the HA-WBRT technique is enhanced through automatic hippocampal segmentation using multitasking learning (36).

Other areas that may be relatively sensitive to radiation include periventricular regions (such as the subventricular zone) and white matter tracts containing oligodendrocyte precursor cells. These areas are relevant to brain neuroplasticity, which pertains to the brain's ability to establish or modify connections with other brain regions. Neuroplasticity is an essential property, particularly for brain injury recovery, among other functions.

The importance of preserving intact white matter integrity in maintaining cognitive function has also been highlighted in a secondary analysis of the RTOG 0933 trial. In their study, Bovi et al. established a correlation between neurocognitive decline and the pretreatment volume of MRI-determined white matter injury. They found a positive correlation (r = 0.54, P <.05) between a larger volume of pretreatment white matter injury and declines in recognition, as assessed by the Hopkins Verbal Learning Test-Revised (37).

A recently published prospective longitudinal trial assessed associations between changes in amygdala morphometry and

functional outcomes in patients with primary brain tumors receiving radiation therapy. Radiation dependent atrophy in bilateral amygdalae was associated with poorer memory, mood, and emotional well-being.

Advanced radiotherapeutic techniques such as volumetric modulated arc therapy (VMAT) enable the simultaneous sparing of other limbic brain structures involved in cognitive function for patients undergoing WBRT. While hippocampal sparing is already common practice in many cancer centers, the feasibility of extending this approach has, thus far, only been tested at the planning study level. The process of preparing a radiation plan is more time-consuming, and the homogeneity of radiation with respect to PTV (Planning Target Volume) dose coverage may be lower. Implementing an extended sparing approach for certain brain regions carries the risk of potentially impacting oncologic outcomes, including intracranial control and subsequent overall survival. Therefore, prospective studies are deemed necessary (38).

On the other hand, as advancements in stereotactic radiotherapy delivery continue, one might argue that preserving various other parts of the brain is safe, even in cases with multiple brain metastases (e.g., more than 15 lesions), especially when regular brain MR imaging follow-ups are conducted (38). The left and right hippocampus, left and right amygdala, fornix, and corpus callosum are crucial neurocognitive structures, and it is reasonable to assume that sparing all of them is essential to maximize the preservation of neurocognitive function. Indeed, in the NRG CC001 study, approximately 50% of patients treated with HA-WBRT and memantine experienced neurocognitive decline (34). It is conceivable that sparing more than just the hippocampi is necessary, as is being explored in the concept of Memory Avoidance WBRT, currently under evaluation in an ongoing phase II clinical trial (39). The Memory Avoidance region encompasses the left and right hippocampus, left and right amygdala, fornix, and corpus callosum, with constraints set at D100% ≤ 9 Gy and D0.03 cm3 ≤ 16 Gy in standard prescription of 30Gy in 10 fractions. In a dosimetry study involving ten enrolled patients (none of whom had brain metastases within the memory sparing region), only two of them failed to meet the constraints for achieving near-maximal dose sparing, as priority was given to target coverage and homogeneity of target irradiation. Utilizing modern LINAC-based volumetric modulated arc therapy, it is indeed possible to create a homogeneous treatment plan while preserving all critical neurocognitive function-related structures (40). For the further development of this intriguing and innovative technique of Memory Sparing-WBRT, the evaluation of post-treatment neurocognitive function and the assessment of the risk of local failure will be crucial.

## 3.2 Laterality of hippocampal changes after RT

Designing appropriate strategies to reduce radiation dose to the hippocampus would be enhanced if suitable imaging methods could be discovered to detect hippocampal damage *in vivo* in patients with brain tumors after cranial irradiation. Magnetic resonance imaging is a widely utilized neuroimaging method and is also employed in cognitive neuroscience. It can be utilized to assess regional morphology and physiology, including pathological issues, in the entire brain or in its individual components.

An example would be hippocampal volume measured by structural MRI. The utility of this method has been clinically validated, as seen in conditions such as Alzheimer's disease, temporal lobe epilepsy, and traumatic brain injury (40, 41). However, this technique has not yet been successfully employed as a biomarker for radiation-induced hippocampal volume loss (42). There is a notable correlation between the reduction in hippocampal volume and the administered radiation dose to the hippocampus. Nevertheless, at the lowest doses, the hippocampi appear to exhibit an adaptive increase in volume, suggesting a potential neuroplasticity effect. Consequently, it may be advisable to shield at least one hippocampus by administering the lowest feasible dose to preserve cognitive functions (43).

Recently, a systematic review was published, and a behavioral meta-analysis was conducted on the association between cognitive outcomes and multimodal MRI imaging in childhood medulloblastoma (MB) survivors. As summarized in the article, several studies have explored the link between hippocampal volume changes following radiotherapy and memory function (44). One study reported that smaller hippocampal volumes were associated with poorer verbal associative memory (45), while another study found a correlation between right hippocampal volume and learning, attention, and memory (42). In one of the included studies, significantly lower ADC (Apparent Diffusion Coefficient) levels were observed in the hippocampi of MB patients compared to the control group. This study highlights impaired hippocampal microstructure, which may lead to decreased memory performance in patients treated for MB.

The association between hippocampal volume and memory functions was also validated in the opposite direction, as demonstrated by a positive correlation between grey matter volume in the posterior hippocampus of London taxi drivers and their spatial memory, along with their navigational abilities (46).

Other studies show different changes occurring in the left and right hippocampus after irradiation as discussed below (Table 1).

PubMed database was used on 20 July 2023 to extract scientific articles describing different postradiotherapy changes in the leff, versus right hippocampus (Figure 2). Out of 108 identified articles, total of 18 studies was further evaluated (Table 1).

In patients whose left hippocampus received a mean dose of 30.7 Gy and 31 Gy, respectively, a statistically significant decrease in mean total performance quotient score of >10% was observed at 3 and 5 years after fractionated RT (benign, low-grade juvenile tumors), but no significant correlation was found with the doses received by the right hippocampus (51).

Higher doses to the left hippocampus can lead to significant impairment of verbal learning and memory; high doses to the left hippocampus and other structures on the left side of the brain (left temporal lobe, left frontal lobe, etc.) can result in impairment of verbal fluency, executive functions, and working memory speed as shown in a cross-sectional study of 78 primary brain tumor patients after radiotherapy (50).

TABLE 1 Summary of studies reporting different post-radiotherapy changes in left vs. right hippocampal region.

| Author, year | Diagnosis | Number of patients | observation | Laterality of greater changes |
|---|---|---|---|---|
| Yang, 2022 (47) | Glioblastoma | 133 | Mean left hippocampus dose was significantly associated with post-radiotherapy decline in MMSE scores ($p = 0.005$), while the right hippocampus not. | L |
| van der Weide, 2022 (48) | Low grade gliomas | 17 | The subgroup with left-sided tumors performed significantly lower on verbal tests. In the subgroup with right-sided tumors, RT dose in the left cerebrum was related to lower verbal memory performance | L |
| Qiu, 2021 (49) | Nasopharyngeal carcinoma | 146 | RT-associated progressive radial diffusivity reduction in the left cingulate angular bundle correlated with progressive cognitive impairment post-RT | L |
| Haldbo-Classen, 2020 (50) | Primary brain tumors | 78 | High RT dose to the left hippocampus associated with impaired verbal learning and memory ($p = 0.04$). RT dose to the left hippocampus, left temporal lobe, left frontal lobe and total frontal lobe associated with verbal fluency impairment ($p < 0.05$) and doses to the thalamus and the left frontal lobe with impaired executive functioning | L |
| Goda, 2020 (51) | Benign or low-grade brain tumors | 48 | A mean dose of ≤30 Gy to the left hippocampus as a dose constraint for preserving intelligence quotient is suggested | L |
| Tringale, 2019 (52) | Primary brain tumors | 27 | Higher mean dose to the left temporal pole white matter was significantly associated with decreased fractional anisotropy. | L |
| Shi, 2018 (53) | Nasopharyngeal carcinoma | 56 | Compared to pre-treatment group, cortical volumes of gray matter were significantly smaller in the left hippocampus, the right pulvinar and the right middle temporal gyrus | L |
| Raghubar, 2018 (54) | Pediatric brain tumor | 26 | Word Pair delayed recall was significantly associated with whole brain and right hippocampus mean dose, Integral biological effective dose, and Generalized equivalent uniform dose; and left hippocampus Generalized equivalent uniform dose | L/R |
| Zureick, 2018 (55) | Pediatric brain tumor | 70 | A higher left hippocampal V20GyE (percentage of the volume of a particular anatomical region receiving at least a 20 gray equivalent) was correlated with a score decline in all 4 measures. | L |
| Kim, 2018 (56) | Primary brain tumors | 26 | The mean dose of the left hippocampus and bilateral hippocampi were significantly higher in patients showing deterioration of the Seoul Verbal Learning Test for total recall and Recognition than in those without deterioration. | L |
| Pospisil, 2017 (12) | Brain metastases | 35 | Moderate positive correlation was observed between left hippocampal N-acetyl aspartat concentration decrease and Auditory Verbal Learning Test_total recall decline as well as with delayed recall decline. No correlation between right hippocampus h-tNAA and memory decline (AVLT) was observed. | L |
| Simo, 2016 (57) | Brain metastases from small cell lung cancer | 22 | decrease in gray matter over time in the right subcortical regions, bilateral insular cortex, and superior temporal gyrus plus in the right parahippocampal gyrus and hippocampus | R |
| Bodensohn, 2016 (58) | High grade gliomas | 44 | In the 'verbal memory test' lower percentile ranks were achieved in left-sided tumors compared to right-sided tumors. a correlation was detected between decreased figural recognition and the radiation dose to the left hippocampus | L |
| Tsai, 2015 (59) | Brain metastases | 40 | dosimetric parameters specific to left sided hippocampus exerted an influence on immediate recall of verbal predicting patients' neurocognitive decline after receiving HS-WBRT | L |
| Farjam, 2015 (60) | Low-grade glioma or benign tumor | 27 | vascular dose response in the left hippocampus of females correlated significantly with changes in memory function at 6 and 18-months post radiotherapy | L |
| Greenberger, 2014 (61) | Pediatric patients with low-grade gliomas | 32 | subgroup analysis indicated some significant decline in neurocognitive outcomes for young children (<7 years) and those with significant dose to the left temporal lobe/hippocampus | L |
| Peiffer, 2013 (62) | Primary brain tumor | 57 | Regions of adult neurogenesis primarily predicted cognition at %v40 (percent of region of interest receiving 40 Gy) except for the right hippocampus which predicted at %v10 | R |
| Redmond, 2013 (63) | Pediatric primary brain tumors and controls | 74 | significant relationship between reduced performance on verbal learning and increasing dose to the cerebrum and reduced performance on visual perception and increasing dose to the left temporal lobe | L |

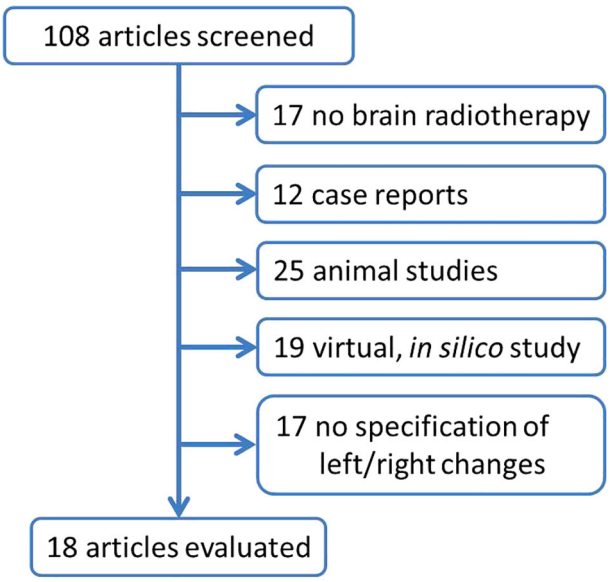


FIGURE 2
Flowchart summarizing the selection of studies describing different postradiotherapy changes in left vs. right hippocampal region. The search terms ,,hippocamp*", ,,radioth*", irrad*, left and right were used to search papers published during last 20 years (since 2003). In total, 108 articles was received using he search terms ,, ("hippocamp*"[All Fields]) AND ((radioth*) OR (irrad*)) AND ((left) OR (right))" with limitation for english written papers. Abstracts were reviewed and articles describing the other than brain cancer, case report, animal studies, virtual, in silico studies, studies with no specification of left vs. right changes were excluded.

In a prospective study, Zureick et al. explored the correlation between cognitive function and the dose received by the hippocampus in pediatric patients after proton irradiation. The results revealed a significant decrease in scores for delayed verbal memory and a borderline decrease for immediate verbal memory. However, no significant change was observed in scores for immediate and delayed visual memory. Furthermore, they identified a correlation between higher V20GyE (volume receiving 20 GyE or equivalent) on the left hippocampus and a decline in memory scores. Based on these findings, it is advisable to consider investigating the left hippocampus in pediatric brain tumor patients during proton/photon radiation therapy (55).

In other study, 40 cancer patients underwent HA-WBRT, and their neurocognitive functions were assessed before and four months after treatment. The results indicated stable hippocampus-dependent memory but significant associations between certain radiation doses to the hippocampus and verbal memory preservation. Specifically, lower radiation doses to the left hippocampus were linked to preserved immediate verbal memory (59).

In another study, eighty patients aged at least 6 years but less than 21 years with low-grade glioma were treated with RT to 54 Gy. On multivariate regression, after accounting for hydrocephalus, decline in short-delay recall was associated with the volume of right or left hippocampus receiving 40 Gy (V40 Gy) (64). This is an example of studies, where no difference between left and right postradiotherapy changes is presented.

## 3.3 Concept of unilateral hippocampal sparing

There is sufficient evidence supporting the crucial role of the hippocampus in both episodic and spatial memory functions. Numerous reports have documented that bilateral damage to this structure leads to severe memory impairments, often resulting in severe amnesia (9). Notably, the randomized NRG-CC001 trial demonstrated a reduced incidence of memory impairment when both hippocampi were spared during WBRT.

Whether the hippocampus sustains damage or protection during radiotherapy, such changes typically affect both hippocampi. Maintaining the integrity of both hippocampi is considered essential for normal cognitive function. However, the precise involvement of the dominant and non-dominant hemispheres' hippocampi in specific neurocognitive functions remains incompletely understood. From a radiobiological perspective, the hippocampus cannot be viewed as a solely serial or parallel organ. In cases where there is evidence of metastatic involvement in one hippocampus, it is advisable to consider at least a unilateral or partial sparing of the hippocampal region possibly even just the amygdala region (65–67). This approach represents a compromise, aiming to preserve neurocognitive functions partially while achieving more uniform irradiation of the brain region. Such an approach could significantly expand the indications for hippocampal avoidance whole-brain radiation therapy (HA WBRT), even for patients with unilateral hippocampal metastasis involvement or metastases in close proximity to the hippocampi.

In cases where patients have multiple brain metastases, particularly when these are unfortunately situated within memory-related structures (as previously discussed regarding Memory Sparing WBRT), it may be advisable to consider sparing at least one hippocampal region. To be more specific, given the higher frequency of post-radiotherapy changes in the left hippocampus, a strategy involving the sparing of the dominant left hippocampus during WBRT could be considered as an alternative approach in the palliative radiotherapy of multiple BM.

## 3.4 Clinical implications and future directions

In our previous in-silico virtual planning study involving 10 patients, we developed radiation therapy treatment plans that incorporated unilateral left hippocampal sparing. Our aim was twofold: first, to maintain the same dosimetry for the left hippocampus as typically achieved in both hippocampal-avoiding WBRT to demonstrate improvements in brain target coverage, and second, to achieve the same left hippocampal dosimetry as usual but with only unilateral left hippocampal sparing to illustrate the potential for further reducing radiation dose to the spared left hippocampus (28).

With the implementation of unilateral left hippocampal sparing, we were able to achieve a significant reduction in brain radiotherapy homogeneity index. This approach also led to a decrease in near-maximal dose (D2%) to the brain and an

increase in the near-minimal dose (D98%), thereby improving overall brain radiation dosage. Alternatively, by maintaining similar brain coverage, we could significantly reduce the radiation doses deposited in the left (spared) hippocampus (28).

Figure 3 illustrates the case of 47-year old women with melanoma, who developed multifocal brain metastases presented supra- and infratentorially. One metastasis was presented in the close proximity to the right hippocampus. Unilateral left hippocampal sparing WBRT was performed with dose prescription to planning target volume 30Gy in 10 fractions. Dose within left hippocampus was reduced to D0.03Gy = 18.64Gy and to D100% = 9.65Gy.

The concept of partial hippocampal sparing in whole-brain radiation therapy (WBRT) has also been proposed by McKay et al. (66) and Sapienza et al. (65). Their work supports the idea of unilateral hippocampal sparing as a compromise approach. Additionally, their research suggests the potential for expanding the indications of hippocampal avoidance WBRT to include patients with unilateral metastatic involvement in the hippocampus.

The only currently ongoing and recruiting trial that focuses on unilateral hippocampal sparing during radiotherapy is NCT04801342, titled "Neurocognitive Outcome of Bilateral or Unilateral Hippocampal Avoidance WBRT With Memantine for Brain Metastases". This phase 2 trial, conducted by researchers from National Taiwan University Hospital, involves enrolling patients with brain metastases located outside a 5-mm margin around either hippocampus (68). Patients are then randomized into two groups: the experimental arm, which receives unilateral hippocampal sparing WBRT plus memantine, and the active comparator arm, which undergoes bilateral hippocampal sparing WBRT plus memantine. In both cases, the prescribed dose is 10 fractions of 3.0 Gy each. The primary outcome of this study is the assessment of the decline in the Hopkins Verbal Learning Test-Revised (HVLT-R) memory score, which includes the sum of total recall and recognition index, measured from baseline to 6 months after the initiation of radiotherapy.

## 4 Conclusion

In summary, the human hippocampus plays a critical role in both intact episodic memory and spatial memory. Previous research indicates that there are notable structural and functional distinctions between the anterior and posterior regions of the hippocampus, reflecting differences in their connectivity to other brain regions. The posterior hippocampus is closely connected to the posterior parahippocampal cortex, which is involved in spatial function. This connectivity suggests that the posterior hippocampus is primarily responsible for spatial memory.

Conversely, the anterior hippocampus is associated with the perirhinal cortex, anterior temporal cortex, and amygdala, implying its involvement in episodic memory processes. It is worth noting that the activation pattern for episodic memory tasks is somewhat less distinct and tends to be more distributed in the left anterior hippocampus. However, the lateralization of activation may depend on the extent to which the task allows for the use of verbal strategies.

In essence, spatial tasks predominantly engage the right posterior hippocampus, while the engagement of the left anterior hippocampus is more prominent in episodic memory tasks, although this can vary based on the specific demands of the task, particularly in terms of verbal processing.

Differences in functional distribution along the longitudinal axis of the hippocampus, as well as lateral differences, could potentially account for sex differences in memory function. These distinctions might then manifest as variations in behavior between genders. However, the underlying neural mechanisms responsible for these sex differences remain largely unexplored. Gaining insight into the neural basis of sex differences in memory functions would not only

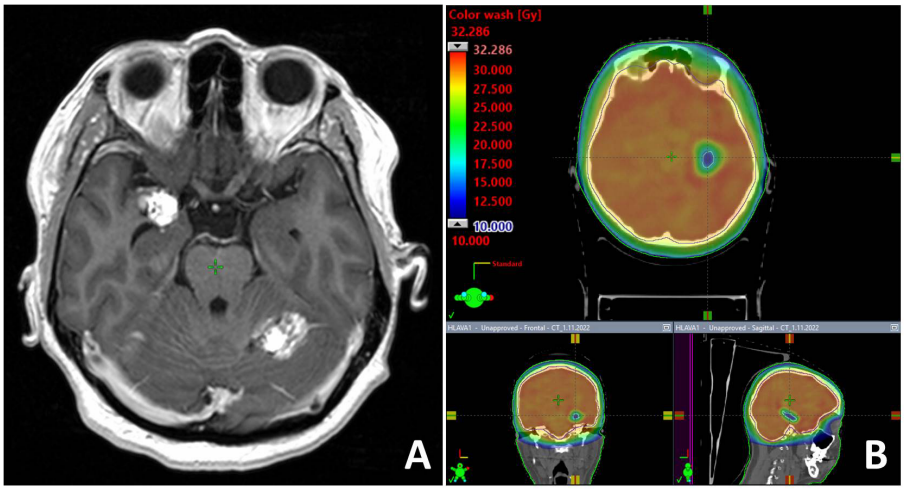


FIGURE 3
T1-weighted contrast enhancing MR examination with one metastasis located close to the right hippocampus **(A)**. Unilateral hippocampal sparing radiotherapy technique **(B)** was employed in the palliative RT.

contribute to our theoretical understanding of hippocampal function but also hold potential clinical significance. Notably, gender disparities in spatial memory performance are evident in variations in hippocampal activation patterns. Functional MRI studies have revealed greater right-sided activation in the posterior hippocampus among males. Furthermore, gender differences in the impact of unilateral hippocampal resection as a treatment for epilepsy have been observed, indicating that men and women may respond differently in terms of memory effects to this procedure.

Many patients with multiple BM are not suitable candidates for stereotactic radiotherapy, often due to the limited availability of advanced radiotherapy facilities and systems. Given that post-radiotherapy changes in the left hippocampus are more frequently associated with post-radiotherapy neurocognitive decline, the concept of unilateral left (dominant) hippocampal sparing has been proposed.

In addition to ongoing prospective clinical phase II trial (NCT04801342), it will be essential to routinely document specific doses administered to the left and right hippocampus. This documentation will help in comparing pre- and post-radiotherapy neurocognitive function. Determining the dominant hemisphere is crutial as well. Meanwhile, on an individual patient basis, unilateral (left, dominant) hippocampal sparing could expand the range of modifications available for whole-brain radiation therapy in multiple brain metastases unamenable for stereotactic radiotherapy.

## Author contributions

TK: Conceptualization, Funding acquisition, Supervision, Writing – original draft, Writing – review & editing. PP: Writing – original draft, Writing – review & editing. LHy: Data curation, Investigation, Writing – review & editing. LHn: Data curation, Investigation, Writing – review & editing. JM: Data curation, Investigation, Writing – review & editing. PS: Conceptualization, Supervision, Writing – review & editing.

## Funding

The author(s) declare financial support was received for the research, authorship, and/or publication of this article. This work was financially supported by the Ministry of Health of the Czech Republic, grant no. NV18-03-00469, and conceptual Development of Research Organization MMCI 00209805. Supported by the project National Institute for Cancer Research (Programme EXCELES, ID Project No. LX22NPO5102)—Funded by the European Union—Next Generation EU.

## Conflict of interest

The authors declare that the research was conducted in the absence of any commercial or financial relationships that could be construed as a potential conflict of interest.

## Publisher's note



## References

1. Gavrilovic IT, Posner JB. Brain metastases: epidemiology and pathophysiology. *J Neurooncol* (2005) 75(1):5–14. doi: 10.1007/s11060-004-8093-6

2. Le Rhun E, Guckenberger M, Smits M, Dummer R, Bachelot T, Sahm F, et al. EANO Executive Board and ESMO Guidelines Committee. Electronic address: clinicalguidelines@esmo.org. EANO-ESMO Clinical Practice Guidelines for diagnosis, treatment and follow-up of patients with brain metastasis from solid tumours. *Ann Oncol* (2021) 32(11):1332–47. doi: 10.1016/j.annonc.2021.07.016

3. Wen PY. Controversies in neuro-oncology: role of whole-brain radiation therapy in the treatment of newly diagnosed brain metastases. *Neuro Oncol* (2015) 17(7):915. doi: 10.1093/neuonc/nov102

4. Matsui JK, Perlow HK, Upadhyay R, McCalla A, Raval RR, Thomas EM, et al. Advances in radiotherapy for brain metastases. *Surg Oncol Clin N Am* (2023) 32 (3):569–86. doi: 10.1016/j.soc.2023.02.007

5. Laack NN, Brown PD. Cognitive sequelae of brain radiation in adults. *Semin Oncol* (2004) 31(5):702–13. doi: 10.1053/j.seminoncol.2004.07.013

6. Monje ML, Mizumatsu S, Fike JR, Palmer TD. Irradiation induces neural precursor-cell dysfunction. *Nat Med* (2002) 8(9):955–62. doi: 10.1038/nm749

7. Lehrer EJ, Jones BM, Dickstein DR, Green S, Germano IM, Palmer JD, et al. The cognitive effects of radiotherapy for brain metastases. *Front Oncol* (2022) 12:893264. doi: 10.3389/fonc.2022.893264

8. Gondi V, Tomé WA, Mehta MP. Why avoid the hippocampus? A comprehensive review. *Radiother Oncol* (2010) 97(3):370–6. doi: 10.1016/j.radonc.2010.09.013

9. Di Gennaro G, Grammaldo LG, Quarato PP, Esposito V, Mascia A, Sparano A, et al. Severe amnesia following bilateral medial temporal lobe damage occurring on two distinct occasions. *Neurol Sci* (2006) 27(2):129–33. doi: 10.1007/s10072-006-0614-y

10. Sozinova EV, Kozlovskiy SA, Vartanov AV, Skvortsova VB, Pirogov YA, Anisimov NV, et al. The role of hippocampal parts in verbal memory and activation processes. *Int J Psychophysiol* (2008) 69(3):312. doi: 10.1016/j.ijpsycho.2008.05.328

11. Pospisil P, Kazda T, Bulik M, Dobiaskova M, Burkon P, Hynkova L, et al. Hippocampal proton MR spectroscopy as a novel approach in the assessment of radiation injury and the correlation to neurocognitive function impairment: initial experiences. *Radiat Oncol* (2015) 10:211. doi: 10.1186/s13014-015-0518-1

12. Pospisil P, Kazda T, Hynkova L, Bulik M, Dobiaskova M, Burkon P, et al. Post-WBRT cognitive impairment and hippocampal neuronal depletion measured by *in vivo* metabolic MR spectroscopy: Results of prospective investigational study. *Radiother Oncol* (2017) 122(3):373–9. doi: 10.1016/j.radonc.2016.12.013

13. Strange BA, Witter MP, Lein ES, Moser EI. Functional organization of the hippocampal longitudinal axis. *Nat Rev Neurosci* (2014) 15(10):655–69. doi: 10.1038/nrn3785

14. Frings L, Wagner K, Unterrainer J, Spreer J, Halsband U, Schulze-Bonhage A. Gender-related differences in lateralization of hippocampal activation and cognitive strategy. *Neuroreport* (2006) 17(4):417–21. doi: 10.1097/01.wnr.0000203623.02082.e3

15. Chapman C, Zhu T, Nazem-Zadeh M, Tao Y, Buchtel HA, Tsien CI, et al. Diffusion tensor imaging predicts cognitive function change following partial brain radiotherapy for low-grade and benign tumors. *Radiother Oncol* (2016) 120(2):234–40. doi: 10.1016/j.radonc.2016.06.021

16. Bobek-Billewicz B, Stasik-Pres G, Majchrzak H, Zarudzki L. Differentiation between brain tumor recurrence and radiation injury using perfusion, diffusion-weighted imaging and MR spectroscopy. *Folia Neuropathol* (2010) 48(2):81–92.

17. Zeidman P, Maguire EA. Anterior hippocampus: the anatomy of perception, imagination and episodic memory. *Nat Rev Neurosci* (2016) 17(3):173–82. doi: 10.1038/nrn.2015.24

18. Kühn S, Gallinat J. Segregating cognitive functions within hippocampal formation: a quantitative meta-analysis on spatial navigation and episodic memory. *Hum Brain Mapp* (2014) 35(4):1129–42. doi: 10.1002/hbm.22239

19. Frisk V, Milner B. The role of the left hippocampal region in the acquisition and retention of story content. *Neuropsychologia* (1990) 28(4):349–59. doi: 10.1016/0028-3932(90)90061-R

20. Baxendale SA. The role of the hippocampus in recognition memory. *Neuropsychologia* (1997) 35(5):591–8. doi: 10.1016/s0028-3932(96)00123-6

21. Mayer V, Yates AJ. Intellectual changes following temporal lobectomy for psychomotor epilepsy; preliminary communication. *J Neurol Neurosurg Psychiatry* (1955) 18(1):44–52. doi: 10.1136/jnnp.18.1.44

22. Bohbot VD, Kalina M, Stepankova K, Spackova N, Petrides M, Nadel L. Spatial memory deficits in patients with lesions to the right hippocampus and to the right parahippocampal cortex. *Neuropsychologia* (1998) 36(11):1217–38. doi: 10.1016/s0028-3932(97)00161-9

23. Barkas LJ, Henderson JL, Hamilton DA, Redhead ES, Gray WP. Selective temporal resections and spatial memory impairment: cue dependent lateralization effects. *Behav Brain Res* (2010) 208(2):535–44. doi: 10.1016/j.bbr.2009.12.035

24. Glikmann-Johnston Y, Saling MM, Chen J, Cooper KA, Beare RJ, Reutens DC. Structural and functional correlates of unilateral mesial temporal lobe spatial memory impairment. *Brain* (2008) 131(Pt 11):3006–18. doi: 10.1093/brain/awn213

25. Saling MM. Verbal memory in mesial temporal lobe epilepsy: beyond material specificity. *Brain* (2009) 132(Pt 3):570–82. doi: 10.1093/brain/awp012

26. Helmstaedter C, Elger CE. Functional plasticity after left anterior temporal lobectomy: reconstitution and compensation of verbal memory functions. *Epilepsia* (1998) 39(4):399–406. doi: 10.1111/j.1528-1157.1998.tb01392.x

27. Baxendale S, Thompson PJ, Duncan JS. Improvements in memory function following anterior temporal lobe resection for epilepsy. *Neurology* (2008) 71(17):1319–25. doi: 10.1212/01.wnl.0000319699.04265.fd

28. Kazda T, Vrzal M, Prochazka T, Dvoracek P, Burkon P, Pospisil P, et al. Left hippocampus sparing whole brain radiotherapy (WBRT): A planning study. *BioMed Pap Med Fac Univ Palacky Olomouc Czech Repub* (2017) 161(4):397–402. doi: 10.5507/bp.2017.031

29. Rola R, Raber J, Rizk A, Otsuka S, VandenBerg SR, Morhardt DR, et al. Radiation-induced impairment of hippocampal neurogenesis is associated with cognitive deficits in young mice. *Exp Neurol* (2004) 188(2):316–30. doi: 10.1016/j.expneurol.2004.05.005

30. Megias D, Phillips M, Clifton-Hadley L, Harron E, Eaton DJ, Sanghera P, et al. Dose specification for hippocampal sparing whole brain radiotherapy (HS WBRT): considerations from the UK HIPPO trial QA programme. *Br J Radiol* (2017) 90 (1071):20160829. doi: 10.1259/bjr.20160829

31. Gondi V, Pugh SL, Tome WA, Caine C, Corn B, Kanner A, et al. Preservation of memory with conformal avoidance of the hippocampal neural stem-cell compartment during whole-brain radiotherapy for brain metastases (RTOG 0933): a phase II multi-institutional trial. *J Clin Oncol* (2014) 32(34):3810–6. doi: 10.1200/JCO.2014.57.2909

32. Leskinen S, Shah HA, Yaffe B, Schneider SJ, Ben-Shalom N, Boockvar JA, et al. Hippocampal avoidance in whole brain radiotherapy and prophylactic cranial irradiation: a systematic review and meta-analysis. *J Neurooncol* (2023) 163(3):515–27. doi: 10.1007/s11060-023-04384-6

33. Kazda T, Jancalek R, Pospisil P, Sevela O, Prochazka T, Vrzal M, et al. Why and how to spare the hippocampus during brain radiotherapy: the developing role of hippocampal avoidance in cranial radiotherapy. *Radiat Oncol* (2014) 9:139. doi: 10.1186/1748-717X-9-139

34. Brown PD, Gondi V, Pugh S, Tome WA, Wefel JS, Armstrong TS, et al. Hippocampal avoidance during whole-brain radiotherapy plus memantine for patients with brain metastases: phase III trial NRG oncology CC001. *J Clin Oncol* (2020) 38(10):1019–29. doi: 10.1200/JCO.19.02767

35. Eekers DBP, Di Perri D, Roelofs E, Postma A, Dijkstra J, Aithkumar T, et al. Update of the EPTN atlas for CT- and MR-based contouring in Neuro-Oncology. *Radiother Oncol* (2021) 160:259–65. doi: 10.1016/j.radonc.2021.05.013

36. Qiu Q, Yang Z, Wu S, Qian D, Wei J, Gong G, et al. Automatic segmentation of hippocampus in hippocampal sparing whole brain radiotherapy: A multitask edge-aware learning. *Med Phys* (2021) 48(4):1771–80. doi: 10.1002/mp.14760

37. Bovi JA, Pugh SL, Sabsevitz D, Robinson CG, Paulson E, Mehta MP, et al. Pretreatment volume of MRI-determined white matter injury predicts neurocognitive decline after hippocampal avoidant whole-brain radiation therapy for brain metastases: secondary analysis of NRG oncology radiation therapy oncology group 0933. *Adv Radiat Oncol* (2019) 4(4):579–86. doi: 10.1016/j.adro.2019.07.006

38. Mehta P, Janssen S, Fahlbusch FB, Schmid SM, Gebauer J, Cremers F, et al. Sparing the hippocampus and the hypothalamic- pituitary region during whole brain radiotherapy: a volumetric modulated arc therapy planning study. *BMC Cancer* (2020) 20(1):610. doi: 10.1186/s12885-020-07091-x

39. Perlow HK, Nalin AP, Ritter AR, Addington M, Ward A, Liu M, et al. Tips-06 advancing beyond the hippocampus to preserve cognition for patients with brain metastases: dosimetric results from a phase 2 trial of memory-avoidance whole brain radiotherapy. *Neurooncol Adv* (2023) 5(Suppl 3):iii35. doi: 10.1093/noajnl/vdad070.137

40. Kovacevic S, Rafii MS, Brewer JB. Alzheimer's Disease Neuroimaging Initiative. High-throughput, fully automated volumetry for prediction of MMSE and CDR decline in mild cognitive impairment. *Alzheimer Dis Assoc Disord* (2009) 23(2):139–45. doi: 10.1097/WAD.0b013e318192e745

41. Farid N, Girard HM, Kemmotsu N, Smith ME, Magda SW, Lim WY, et al. Temporal lobe epilepsy: quantitative MR volumetry in detection of hippocampal atrophy. *Radiology* (2012) 264(2):542–50. doi: 10.1148/radiol.12112638

42. Riggs L, Bouffet E, Laughlin S, Laperriere N, Liu F, Skocic J, et al. Changes to memory structures in children treated for posterior fossa tumors. *J Int Neuropsychol Soc* (2014) 20(2):168–80. doi: 10.1017/S135561771300129X

43. Le Fèvre C, Cheng X, Loit MP, Keller A, Cebula H, Antoni D, et al. Role of hippocampal location and radiation dose in glioblastoma patients with hippocampal atrophy. *Radiat Oncol* (2021) 16(1):112. doi: 10.1186/s13014-021-01835-0

44. Wauters M, Uyttebroeck A, De Waele L, Sleurs C, Jacobs S. Neuroimaging biomarkers and neurocognitive outcomes in pediatric medulloblastoma patients: a systematic review. *Cerebellum* (2021) 20(3):462–80. doi: 10.1007/s12311-020-01225-4

45. Decker AL, Szulc KU, Bouffet E, Laughlin S, Chakravarty MM, Skocic J, et al. Smaller hippocampal subfield volumes predict verbal associative memory in pediatric brain tumor survivors. *Hippocampus* (2017) 27(11):1140–54. doi: 10.1002/hipo.22758

46. Maguire EA, Spiers HJ, Good CD, Hartley T, Frackowiak RS, Burgess N. Navigation expertise and the human hippocampus: a structural brain imaging analysis. *Hippocampus* (2003) 13(2):250–9. doi: 10.1002/hipo.10087

47. Yang F, Dinakaran D, Heikal AA, Yaghoobpour Tari S, Ghosh S, Amanie J, et al. Dosimetric predictors of toxicity in a randomized study of short-course vs conventional radiotherapy for glioblastoma. *Radiother Oncol* (2022) 177:152–7. doi: 10.1016/j.radonc.2022.10.016

48. van der Weide HL, Kłos J, Langendijk JA, Brouwer CL, Sinnige PF, Borra RJH, et al. Clinical relevance of the radiation dose bath in lower grade glioma, a cross-sectional pilot study on neurocognitive and radiological outcome. *Clin Transl Radiat Oncol* (2022) 33:99–105. doi: 10.1016/j.ctro.2022.02.001

49. Qiu Y, Guo Z, Lin X, Li J, Li Z, Han L, et al. Standard radiotherapy for patients with nasopharyngeal carcinoma results in progressive tract-specific brain white matter alterations: A one-year follow-up via diffusion tensor imaging. *Radiother Oncol* (2021) 159:255–64. doi: 10.1016/j.radonc.2021.03.039

50. Haldbo-Classen L, Amidi A, Lukacova S, Wu LM, Oettingen GV, Lassen-Ramshad Y, et al. Cognitive impairment following radiation to hippocampus and other brain structures in adults with primary brain tumours. *Radiother Oncol* (2020) 148:1–7. doi: 10.1016/j.radonc.2020.03.023

51. Goda JS, Dutta D, Krishna U, Goswami S, Kothavade V, Kannan S, et al. Hippocampal radiotherapy dose constraints for predicting long-term neurocognitive outcomes: mature data from a prospective trial in young patients with brain tumors. *Neuro Oncol* (2020) 22(11):1677–85. doi: 10.1093/neuonc/noaa076

52. Tringale KR, Nguyen TT, Karunamuni R, Seibert T, Huynh-Le MP, Connor M, et al. Quantitative imaging biomarkers of damage to critical memory regions are associated with post-radiation therapy memory performance in brain tumor patients. *Int J Radiat Oncol Biol Phys* (2019) 105(4):773–83. doi: 10.1016/j.ijrobp.2019.08.003

53. Shi L, Du FL, Sun ZW, Zhang L, Chen YY, Xie TM, et al. Radiation-induced gray matter atrophy in patients with nasopharyngeal carcinoma after intensity modulated radiotherapy: a MRI magnetic resonance imaging voxel-based morphometry study. *Quant Imaging Med Surg* (2018) 8(9):902–9. doi: 10.21037/qims.2018.10.09

54. Raghubar KP, Lamba M, Cecil KM, Yeates KO, Mahone EM, Limke C, et al. Dose-volume metrics and their relation to memory performance in pediatric brain tumor patients: A preliminary study. *Pediatr Blood Cancer* (2018) 65(9):e27245. doi: 10.1002/pbc.27245

55. Zureick AH, Evans CL, Niemierko A, Grieco JA, Nichols AJ, Fullerton BC, et al. Left hippocampal dosimetry correlates with visual and verbal memory outcomes in survivors of pediatric brain tumors. *Cancer* (2018) 124(10):2238–45. doi: 10.1002/cncr.31143

56. Kim KS, Wee CW, Seok JY, Hong JW, Chung JB, Eom KY, et al. Hippocampus-sparing radiotherapy using volumetric modulated arc therapy (VMAT) to the primary brain tumor: the result of dosimetric study and neurocognitive function assessment. *Radiat Oncol* (2018) 13(1):29. doi: 10.1186/s13014-018-0975-4

57. Simó M, Vaquero L, Ripollés P, Gurtubay-Antolin A, Jové J, Navaro A, et al. Longitudinal brain changes associated with prophylactic cranial irradiation in lung cancer. *J Thorac Oncol* (2016) 11(4):475–86. doi: 10.1016/j.jtho.2015.12.110

58. Bodensohn R, Corradini S, Ganswindt U, Hofmaier J, Schnell O, Belka C, et al. A prospective study on neurocognitive effects after primary radiotherapy in high-grade glioma patients. *Int J Clin Oncol* (2016) 21(4):642–50. doi: 10.1007/s10147-015-0941-1

59. Tsai PF, Yang CC, Chuang CC, Huang TY, Wu YM, Pai PC, et al. Hippocampal dosimetry correlates with the change in neurocognitive function after hippocampal sparing during whole brain radiotherapy: a prospective study. *Radiat Oncol* (2015) 10:253. doi: 10.1186/s13014-015-0562-x

60. Farjam R, Pramanik P, Aryal MP, Srinivasan A, Chapman CH, Tsien CI, et al. A radiation-induced hippocampal vascular injury surrogate marker predicts late

neurocognitive dysfunction. *Int J Radiat Oncol Biol Phys* (2015) 93(4):908–15. doi: 10.1016/j.ijrobp.2015.08.014

61. Greenberger BA, Pulsifer MB, Ebb DH, MacDonald SM, Jones RM, Butler WE, et al. Clinical outcomes and late endocrine, neurocognitive, and visual profiles of proton radiation for pediatric low-grade gliomas. *Int J Radiat Oncol Biol Phys* (2014) 89 (5):1060–8. doi: 10.1016/j.ijrobp.2014.04.053

62. Peiffer AM, Leyrer CM, Greene-Schloesser DM, Shing E, Kearns WT, Hinson WH, et al. Neuroanatomical target theory as a predictive model for radiation-induced cognitive decline. *Neurol* (2013) 80(8):747–53. doi: 10.1212/WNL.0b013e318283bb0a

63. Redmond KJ, Mahone EM, Terezakis S, Ishaq O, Ford E, McNutt, et al. Association between radiation dose to neuronal progenitor cell niches and temporal lobes and performance on neuropsychological testing in children: a prospective study. *Neuro Oncol* (2013) 15(3):360–9. doi: 10.1093/neuonc/nos303

64. Acharya S, Wu S, Ashford JM, Tinkle CL, Lucas JT, Qaddoumi I, et al. Association between hippocampal dose and memory in survivors of childhood or adolescent low-grade glioma: a 10-year neurocognitive longitudinal study. *Neuro Oncol* (2019) 21(9):1175–83. doi: 10.1093/neuonc/noz068

65. Sapienza LG, Ludwig MS, Mandel JJ, Nguyen DH, Echeverria AE. Could patients benefit from whole-brain radiotherapy with unilateral hippocampus sparing? *Rep Pract Oncol Radiother* (2021) 26(3):454–6. doi: 10.5603/RPOR.a2021.0059

66. McKay MJ, Hassan SZ, Sanderson C, Thomas A, McKay MJ, Chindewere A. Partial hippocampal sparing whole brain radiotherapy in a patient with bilateral Malignant melanoma metastases to the hippocampus: a case report. *Precis Cancer Med* (2021) 4:39. doi: 10.21037/pcm-21-23

67. Unnikrishnan S, Karunamuni R, Salans MA, Gudipati S, Qian AS, Yu J, et al. Dose-dependent atrophy in bilateral amygdalae and nuclei after brain radiation therapy and its association with mood and memory outcomes on a longitudinal clinical trial. *Int J Radiat Oncol Biol Phys* (2023) 117(4):834–45. doi: 10.1016/j.ijrobp.2023.05.026

68. CLINICAL TRIALS. GOV. *Neurocognitive outcome of bilateral or unilateral hippocampal avoidance WBRT with memantine for brain metastases* (2021). Available at: https://classic.clinicaltrials.gov/ct2/show/study/NCT04801342?term=radiotherapy&recrs=a&cond=Brain+Metastases&draw=3.

frontiers | Frontiers in Oncology

TYPE Original Research
PUBLISHED 14 February 2024
DOI 10.3389/fonc.2024.1339126



OPEN ACCESS

EDITED BY
Xiangpan Li,
Renmin Hospital of Wuhan University, China

REVIEWED BY
Fuli Zhang,
People's Liberation Army General Hospital, China
Ma Yangguang,
The First Affiliated Hospital of Zhengzhou University, China
Bo Jiang,
Tianjin Medical University Cancer Institute and Hospital, China

*CORRESPONDENCE
Zhiqiang Liu
zhiqiang.liu@cicams.ac.cn
Hui Yan
hui.yan@cicams.ac.cn

†These authors have contributed equally to this work

RECEIVED 15 November 2023
ACCEPTED 26 January 2024
PUBLISHED 14 February 2024

CITATION
Huang P, Shang J, Hu Z, Liu Z and Yan H (2024) Predicting voxel-level dose distributions of single-isocenter volumetric modulated arc therapy treatment plan for multiple brain metastases.
*Front. Oncol.* 14:1339126.
doi: 10.3389/fonc.2024.1339126



# Predicting voxel-level dose distributions of single-isocenter volumetric modulated arc therapy treatment plan for multiple brain metastases

Peng Huang†, Jiawen Shang†, Zhihui Hu, Zhiqiang Liu* and Hui Yan*

Department of Radiation Oncology, National Cancer Center/National Clinical Research Center for Cancer/Cancer Hospital, Chinese Academy of Medical Sciences and Peking Union Medical College, Beijing, China

**Purpose:** Brain metastasis is a common, life-threatening neurological problem for patients with cancer. Single-isocenter volumetric modulated arc therapy (VMAT) has been popularly used due to its highly conformal dose and short treatment time. Accurate prediction of its dose distribution can provide a general standard for evaluating the quality of treatment plan. In this study, a deep learning model is applied to the dose prediction of a single-isocenter VMAT treatment plan for radiotherapy of multiple brain metastases.

**Method:** A U-net with residual networks (U-ResNet) is employed for the task of dose prediction. The deep learning model is first trained from a database consisting of hundreds of historical treatment plans. The 3D dose distribution is then predicted with the input of the CT image and contours of regions of interest (ROIs). A total of 150 single-isocenter VMAT plans for multiple brain metastases are used for training and testing. The model performance is evaluated based on mean absolute error (MAE) and mean absolute differences of multiple dosimetric indexes (DIs), including ($D_{max}$ and $D_{mean}$) for OARs, ($D_{98}$, $D_{95}$, $D_{50}$, and $D_2$) for PTVs, homogeneity index, and conformity index. The similarity between the predicted and clinically approved plan dose distribution is also evaluated.

**Result:** For 20 tested patients, the largest and smallest MAEs are 3.3% $\pm$ 3.6% and 1.3% $\pm$ 1.5%, respectively. The mean MAE for the 20 tested patients is 2.2% $\pm$ 0.7%. The mean absolute differences of $D_{98}$, $D_{95}$, $D_{50}$, and $D_2$ for PTV60, PTV52, PTV50, and PTV40 are less than 2.5%, 3.0%, 2.0%, and 3.0%, respectively. The prediction accuracy of OARs for $D_{max}$ and $D_{mean}$ is within 3.2% and 1.2%, respectively. The average DSC ranges from 0.86 to 1 for all tested patients.

**Conclusion:** U-ResNet is viable to produce accurate dose distribution that is comparable to those of the clinically approved treatment plans. The predicted results can be used to improve current treatment planning design, plan quality, efficiency, etc.

KEYWORDS

multiple brain metastases, volumetric modulated arc therapy, radiotherapy, deep learning, dose prediction

# 1 Introduction

Brain metastasis is the cancer that occurs when cancer cells from their original sites spread to the brain. The typical tumor sites causing brain metastasis are the lung, breast, colon, and kidney. Brain metastases could be single or multiple tumor sites in the brain (1, 2). The brain metastases could cause pressure on the brain. Also, the function of the surrounding brain tissue could be changed by the tumor. The symptoms of brain metastases include memory loss, seizures, headaches, etc. (3). The traditional treatment methods for brain metastases are surgery, whole-brain radiotherapy (WBRT), three-dimensional conformal radiation therapy (3D-CRT), hypo-fractionated stereotactic radiotherapy (SRT), and single-fraction stereotactic radiosurgery (SRS) (4–7).

WBRT and 3D-CRT have been traditionally used for the treatment of multiple brain metastases. However, WBRT can cause cognitive dysfunction or dementia, while 3D-CRT takes a long time to treat multiple brain metastases (8–10). In SRS/SRT, a higher accuracy of patient positioning is required. Recently, the developments of image-guided radiotherapy (IGRT) and volumetric modulated arc therapy (VMAT) techniques have provided precise target localization and quick dose delivery for patients under radiotherapy. The introduction of VMAT not only takes a short time in treatment delivery but also shows a highly conformal dose comparable to conventional SRS/SRT (11, 12). The treatment of brain metastases using VMAT has been accepted as a routine treatment modality in recent years (13, 14).

Compared to multiple-isocenter VMAT, single-isocenter VMAT is popular due to its quick and accurate beam delivery for the treatment of multiple brain metastases (15–17). However, to achieve an ideal dose distribution, a set of suitable plan optimization parameters (dose constraints and their weighting factors) is needed prior to the optimization of the treatment plan. Also, planners have to adjust these parameters manually during plan optimization, which usually takes several hours. To address this issue, knowledge-based planning (KBP) was proposed (18, 19) in the last decade. They implemented plan automation through optimization algorithms or templates from previously treated patients. These methods can partially reduce the effort involved in parameter fine-tuning but still require human involvement (20). Recently, the research interest in KBP has transitioned from classic machine learning methods to modern deep learning methods (21–25). Unlike classic machine learning methods, modern deep learning methods can directly learn features from the original data and predict 3D doses with high precision.

The recent development of the dose prediction model is mostly based on the U-Net structure, which consists of an encoder and decoder with skip connections. 2D U-Net was first applied to prostate IMRT plans by Nguyen et al. (21). After that, many efforts were made. Residual learning was introduced to the dose prediction model by several researchers (22–25), while dense connectivity was used to enhance feature representation capability by other researchers in their models (26–28). In addition, other types of networks, such as Resnet (27, 29, 30) and GAN (31–33), are also used for dose prediction. So far, the deep U-net-like architecture and its variants with various types of residual or dense blocks become the mainstream structure for dose prediction (34–38).

With the successful applications of deep learning models in predicting dose distribution for many primary tumor sites such as the lung (25, 26), head-and-neck (23, 28, 33, 34), and prostate (21, 35), it is interesting to investigate this application for brain metastasis. In the study, a deep U-net architecture (30), previously successfully applied to predict dose distribution for head-and-neck cancer patients, is used as the base model in predicting the dose distribution of the VMAT plan for brain metastasis. The rest of this paper is organized as follows: In Methods, the patient data, prediction model, and experimental settings are introduced in detail. In Results, the prediction accuracy of the deep learning model is evaluated by comparing it with the dose distribution of the clinically approved plans. Finally, the advantages and disadvantages of the prediction model are discussed, and future work is prospected in the Discussions.

# 2 Methods

## 2.1 Patient data

The dataset consists of 150 single-isocenter VMAT treatment plans designed for multiple brain metastases patients treated in our

institute during 2019–2022. All patient plans are made by medical physicists and approved by radiation oncologists for clinical treatment. The number of tumors in each patient is varied from one to four. PTVs include PTV60 for 31 patients, PTV52 for 41 patients, PTV50 for 34 patients, and PTV40 for 44 patients. Primary OARs include body, brain stem, spinal cord, left lens, right lens, left optic nerve, right optic nerve, and optic chiasm.

The 150 patient plans are randomly divided into three sets: 100 for training sets, 30 for validation sets, and 20 for testing sets. These VMAT plans are designed with two arcs and delivered with 6 MV beam energy. The input images are all rescaled to 256 × 256 × 21 matrixes (7 for CT images, 7 for contour image, and 7 channels for target prescriptions), and the output image is 256 × 256 × 1 matrixes (dose distributions on each slice). This study was conducted in accordance with the Declaration of Helsinki (as revised in 2013). This study was approved by the ethics committee of the National Cancer Center/Cancer Hospital, Chinese Academy of Medical Sciences, and Peking Union Medical College. The committee waived the written informed consent because this is a retrospective study.

## 2.2 Prediction model

The U-net with residual network (U-ResNet) model incorporating residual convolutional and de-convolutional blocks is shown in Figure 1. It consists of contracting and expansive paths. The contracting path follows convolutional layers and stacked building blocks of Identity-Block and Conv-Block to extract multiscale patient-specific features, doubling the number of feature maps at each step. The expansive path at each step consists of a de-convolutional block that halves the number of feature maps and concatenation with the corresponding feature map from the contracting path. The network ends with one de-convolution with 1 × 1 filters replacing 3 × 3 filters.

In the training and validation process, the training samples are augmented by randomly flipping, rotating, scaling, or shifting. The model is trained from scratch with the layer kernel weights initialized using Xavier uniform initialization. Adam optimizer (39) with a batch size of 4 is used for optimization. The initial learning rate (LR) is 1e −4, and the LR is reduced to 20% of its original value if the validation loss does not improve after 10 epochs. The training process is also stopped if the validation loss does not improve after 20 epochs. The model with the best performance on the validation samples is obtained for testing. The proposed network is implemented in Keras with TensorFlow as the backend on a workstation equipped with two NVIDIA GeForce 2080 Ti GPUs. The training process for a single model takes around 20 h. The prediction process for one case takes less than 1 s.

## 2.3 Model evaluation

The mean absolute error (MAE) is used to evaluate the accuracy of the predicted 3D dose distribution. It is the average error over all voxels of the body and is defined as Equation 1:

$$\mathrm{MAE}_k = \frac{1}{N_k}\sum_{i=1}^{N_k}|D_P - D_T| \times 100\,\% \tag{1}$$

Where $N_k$ is the number of total voxels belonging to the $k$th structure. $D_P$ and $D_T$ are the predicted and ground-truth (or calculated) doses of the $i$th voxel. The voxel doses were normalized by the value of the prescription dose. Several traditional dosimetry indexes (DIs) ($D_{\max}$, $D_{\mathrm{mean}}$ for OARs and $D_{98}$, $D_{95}$, $D_{50}$, and $D_2$ for PTVs), conformity index (CI), and homogeneity index (HI) are also evaluated.

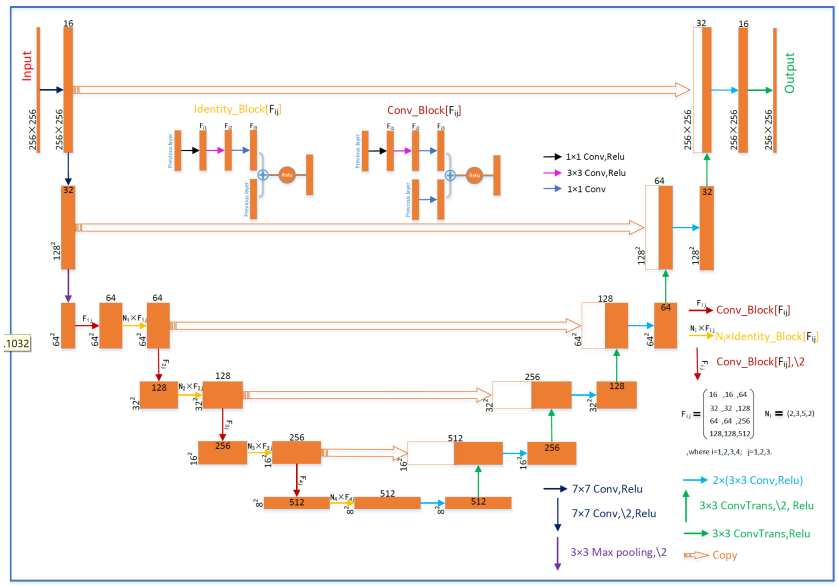


FIGURE 1
Schematic diagram of the deep U-net architecture.

CI formula is defined as Equation 2:

$$\mathrm{CI} = \frac{V_{T,\mathrm{ref}}}{V_T} \times \frac{V_{T,\mathrm{ref}}}{V_{\mathrm{ref}}} \quad (2)$$

$V_{T,\mathrm{ref}}$ is the volume of the target volume at which the received dose is equal to or greater than the reference dose; $V_T$ is the volume of the target volume; $V_{\mathrm{ref}}$ is the volume at which the received dose is equal to or greater than the reference dose. The closer the value of CI is to 1, the better the target is covered. HI formula is defined as Equation 3:

$$\mathrm{HI} = \frac{D_2 - D_{98}}{D_{50}} \quad (3)$$

where $D_n$ represents the minimum radiation dose received by $n$% of the volume of the radiation area. The closer the value of HI to 0, the better the uniformity of the target dose. In addition, the absolute differences in DI between predicted and clinically approved plans are evaluated as follows: $|\delta \mathrm{DI}| = |\mathrm{DI}_{\mathrm{clinical}} - \mathrm{DI}_{\mathrm{Predicted}}|$.

The dice similarity coefficient (DSC) between dose distributions is also evaluated and defined as Equation 4:

$$\mathrm{DSC}(A, B) = \frac{2|A \cap B|}{|A| + |B|} \quad (4)$$

where A represents the clinical isodose volume and B denotes the predicted isodose volume.

# 3 Results

## Dose difference

The MAE plot for all 20 tested patients is shown in Figure 2. The largest and smallest MAEs are 3.3% ± 3.6% and 1.3% ± 1.5% within the patient's body, respectively. The largest and smallest MAEs are 5.2% ± 4.0% and 2.1% ± 1.7% within the targets, respectively. The average MAE is 2.2% ± 0.7% (relative to the prescription of PTV) within the body, and the average MAE is 3.6% ± 1.0% within targets.

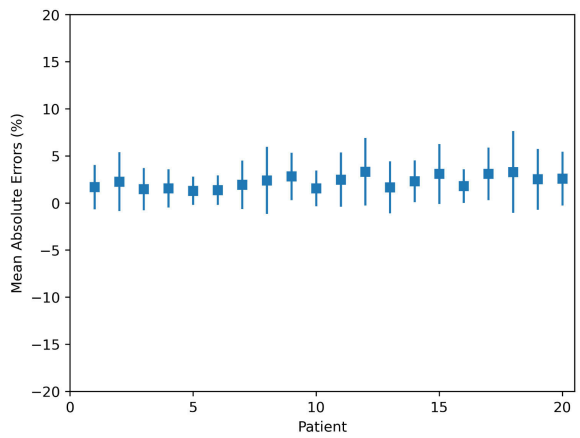


FIGURE 2
Mean absolute errors within the body for 20 tested patients.

## Dosimetric index

For PTVs with multiple prescription doses, the dosimetric indexes are shown in Table 1. On average, the absolute differences of $D_{98}$, $D_{95}$, $D_{50}$, and $D_2$ for PTV60, PTV52, PTV50, and PTV40 are less than 2.5%, 3.0%, 2.0%, and 3.0%, respectively. There are no significant differences between predicted and clinically approved plan doses for PTVs. There are no significant differences from the predicted results for HI and CI. Regarding OARs, the dosimetric indexes of $D_{\mathrm{max}}$ and $D_{\mathrm{mean}}$ are shown in Table 2. The prediction accuracy for $D_{\mathrm{max}}$ and $D_{\mathrm{mean}}$ is between 3.2% and 1.2%. Six OARs for $D_{\mathrm{max}}$ and eight for $D_{\mathrm{mean}}$ were predicted within 2%. There is no significant difference between clinical and predicted results. For certain patients, the $D_{\mathrm{max}}$ and $D_{\mathrm{mean}}$ of OARs are close to 0, as they are far from PTV. This causes a large standard deviation of dosimetric results for these OARs. In general, the dosimetric indexes predicted by the model well match those from the clinically approved plans.

The examples of two patients' DVHs are presented in Figure 3. The clinical and predicted DVHs are shown in solid and dashed lines, respectively. Case 1 has two prescription doses (5,250 cGY and 6,000 cGy) and more OARs, while case 2 has one prescription dose (4,800 cGy) and three OARs. For OARs, the maximal dose discrepancy is presented in the higher dose region of the brain stem in both cases. For PTV, the maximal dose discrepancy is presented in the higher dose region of PTV5250 in case 1 and the lower dose region of PTV4800 in case 2.

## Volumes similarity

The dice similarity coefficients between predicted and clinically approved plan doses for the different isodose volumes are calculated. As shown in Figure 4, the DSC versus isodose volumes for 20 tested patients are presented. The black curve denotes the averaged DSC curve, which usually ranges from 0 to 1, with 1 standing for ideal match. The averaged DSC for the different isodose volumes ranges from 0.86 to 1.

Corresponding to the cases shown in Figure 3, their clinical and predicted dose maps in 2D slices are presented in Figure 5. In the first and second columns, the clinical and predicted dose maps in axial view are displayed with a color wash pattern. The different images between the first and second columns are presented in the third column. For case 1, the predicted doses are higher than the clinical doses in two small regions on the left and right sides of PTV. For case 2, the predicted doses are less than the clinical doses on the left-bottom sides of PTV. Overall, the predicted and clinical doses are highly consistent.

# 4 Discussions

In this study, an advanced deep learning model is applied to predict 3D dose distribution based on our clinical dataset. As far as we know, there is no deep learning model used in predicting the dose of VMAT plans for multiple brain metastases. Using 150 brain

10.3389/fonc.2024.1339126

TABLE 1 Statistics of dosimetric indexes for PTVs of 20 tested patients.

| PTVs | Dosimetric indexes | Clinically approved | Model predicted | \|δDI\| | *p*-value |
|---|---|---|---|---|---|
| PTV60 | $D_{98}$ (Gy) | 60.1 ± 1.0 | 58.9 ± 1.5 | 2.1% ± 2.1% | 0.054 |
| | $D_{95}$ (Gy) | 60.7 ± 0.8 | 59.5 ± 1.2 | 2.2% ± 1.9% | 0.063 |
| | $D_{50}$ (Gy) | 62.8 ± 1.2 | 62.4 ± 1.0 | 1.9% ± 2.0% | 0.541 |
| | $D_2$ (Gy) | 65.0 ± 2.3 | 64.9 ± 1.5 | 2.5% ± 1.4% | 0.947 |
| | HI | 0.1 ± 0.0 | 0.1 ± 0.0 | 0.0% ± 0.0 | 0.336 |
| | CI | 1.0 ± 0.0 | 1.0 ± 0.0 | 0.0% ± 0.0 | 0.282 |
| PTV52 | $D_{98}$ (Gy) | 50.7 ± 0.7 | 49.4 ± 1.8 | 3.0% ± 1.2% | 0.142 |
| | $D_{95}$ (Gy) | 52.2 ± 0.1 | 51.3 ± 0.9 | 1.8% ± 1.5% | 0.116 |
| | $D_{50}$ (Gy) | 57.1 ± 0.8 | 56.1 ± 0.7 | 2.1% ± 1.4% | 0.104 |
| | $D_2$ (Gy) | 60.5 ± 2.1 | 59.7 ± 1.6 | 2.0% ± 1.9% | 0.271 |
| | HI | 0.2 ± 0.0 | 0.2 ± 0.0 | 0.0% ± 0.0 | 0.657 |
| | CI | 1.0 ± 0.0 | 0.9 ± 0.0 | 0.0% ± 0.0 | 0.087 |
| PTV50 | $D_{98}$ (Gy) | 49.0 ± 0.6 | 48.2 ± 0.4 | 1.4% ± 2.0% | 0.489 |
| | $D_{95}$ (Gy) | 50.3 ± 0.4 | 49.3 ± 0.3 | 2.0% ± 1.4% | 0.295 |
| | $D_{50}$ (Gy) | 55.5 ± 0.5 | 54.7 ± 0.2 | 1.5% ± 0.7% | 0.208 |
| | $D_2$ (Gy) | 59.4 ± 0.8 | 59.4 ± 0.6 | 0.2% ± 0.2% | 0.627 |
| | HI | 0.2 ± 0.0 | 0.2 ± 0.0 | 0.0% ± 0.0 | 0.391 |
| | CI | 1.0 ± 0.0 | 0.9 ± 0.0 | 0.0% ± 0.0 | 0.353 |
| PTV40 | $D_{98}$ (Gy) | 38.3 ± 0.6 | 37.9 ± 0.4 | 1.0% ± 1.2% | 0.207 |
| | $D_{95}$ (Gy) | 40.0 ± 0.1 | 39.4 ± 0.8 | 1.6% ± 1.6% | 0.225 |
| | $D_{50}$ (Gy) | 43.3 ± 1.1 | 43.6 ± 0.3 | 2.6% ± 1.6% | 0.741 |
| | $D_2$ (Gy) | 45.9 ± 1.6 | 46.5 ± 0.4 | 3.0% ± 1.1% | 0.400 |
| | HI | 0.2 ± 0.0 | 0.2 ± 0.0 | 0.0% ± 0.0 | 0.453 |
| | CI | 1.0 ± 0.0 | 0.9 ± 0.0 | 0.0% ± 0.0 | 0.350 |

TABLE 2 Statistics of dosimetric metrics for OARs in 20 tested patients.

| | Dmax (Gy) | | | | Dmean (Gy) | | | |
|---|---|---|---|---|---|---|---|---|
| OARs and body | Clinically approved | Model predicted | \|δDI\| (%) | *p*-value | Clinically approved | Model predicted | \|δDI\| (%) | *p*-value |
| Brain stem | 4.7 ± 4.8 | 4.2 ± 4.9 | 2.8 ± 2.1 | 0.247 | 1.1 ± 1.1 | 1.1 ± 1.6 | 0.9 ± 1.0 | 0.990 |
| Spinal cord | 0.7 ± 1.7 | 0.7 ± 1.6 | 0.6 ± 1.3 | 0.961 | 0.1 ± 0.2 | 0.0 ± 0.1 | 0.1 ± 0.2 | 0.113 |
| Center lens | 0.6 ± 0.8 | 0.8 ± 1.0 | 0.7 ± 0.7 | 0.076 | 0.4 ± 0.7 | 0.6 ± 0.9 | 0.6 ± 0.5 | 0.219 |
| Right lens | 0.8 ± 0.9 | 0.7 ± 0.8 | 0.6 ± 0.6 | 0.450 | 0.5 ± 0.7 | 0.4 ± 0.5 | 0.6 ± 0.5 | 0.248 |
| Center optic nerve | 1.7 ± 3.0 | 1.4 ± 2.5 | 0.9 ± 0.9 | 0.161 | 1.1 ± 2.1 | 1.0 ± 1.9 | 0.7 ± 0.6 | 0.302 |
| Right optic nerve | 1.3 ± 1.5 | 1.1 ± 1.6 | 1.2 ± 1.1 | 0.233 | 0.7 ± 1.0 | 0.6 ± 1.1 | 0.8 ± 0.8 | 0.508 |
| Optic chiasm | 3.7 ± 4.5 | 3.8 ± 6.0 | 1.8 ± 3.2 | 0.857 | 1.3 ± 2.0 | 1.2 ± 2.0 | 1.2 ± 1.4 | 0.789 |
| Body | 60.2 ± 7.3 | 59.4 ± 7.5 | 3.2 ± 2.5 | 0.137 | 1.6 ± 1.1 | 1.6 ± 1.0 | 0.3 ± 0.2 | 0.705 |

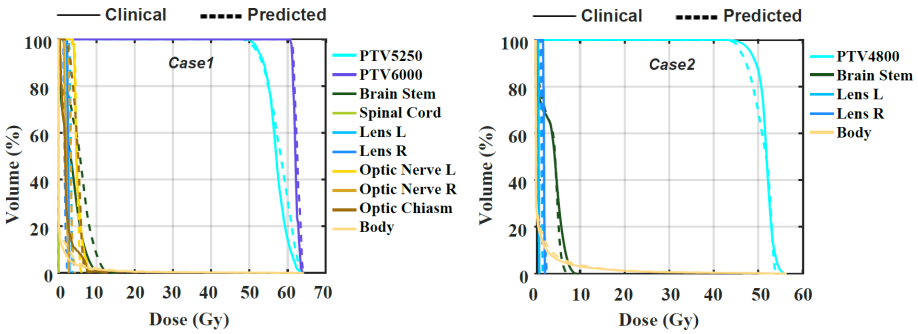


FIGURE 3
The comparison of the clinical and predicted DVHs for two cases.

metastases from VMAT plans, the U-ResNet model exhibits accurate dose distribution and high efficiency. As shown in Table 1, the mean prediction errors range from 1.9% to 2.5%, 1.8% to 3.0%, 0.2% to 2.0%, and 1.0% to 3.0% for PTV60, PTV52, PTV50, and PTV40, respectively. For the absolute value of the PTV dose, the mean value of the predicted plan doses is slightly less than that of the clinically approved plan doses. This may be due to the inclusion of various target prescriptions in a single model, where the varying combinations of prescriptions may impact the prediction accuracy of the target dose. The limited number of samples and larger variation of tumor sites may be another reason. There is no significant difference in dosimetric indexes between clinically approved and predicted plan doses. Although the results demonstrate that the prediction accuracy is acceptable for clinical use, there is still a certain room for improvement.

Although U-ResNet succeeded in dose prediction, as reported by many researchers, there is still a lot of room for improvement. The receptive field would be enlarged increasingly by the stacked multiple convolution layers in the decoder. However, the network's capability to catch features in multiscale resolution could be limited. The predicted voxel dose is affected not only by the neighboring voxels but also by the spatial distribution between PTVs and OARs. Thus, to extract multiscale features from the image simultaneously, the introduction of pyramid blocks is needed. We will test the model with the modules in a serial or parallel manner in the future, which could further improve the performance of the prediction model.

There are several challenges to this study. First, it is difficult to collect hundreds of VMAT plans with similar locations and shapes of tumor mass for model learning. In the case of multiple brain metastases, the number of tumor masses and their locations could vary considerably among patients. The limited number of samples and larger variation of tumor sites and shapes will make it hard to learn a solid pattern for a learning model. A more effective model or strategy is needed in dealing with such situations for multiple brain metastases. Second, the introduction of U-ResNet increases the

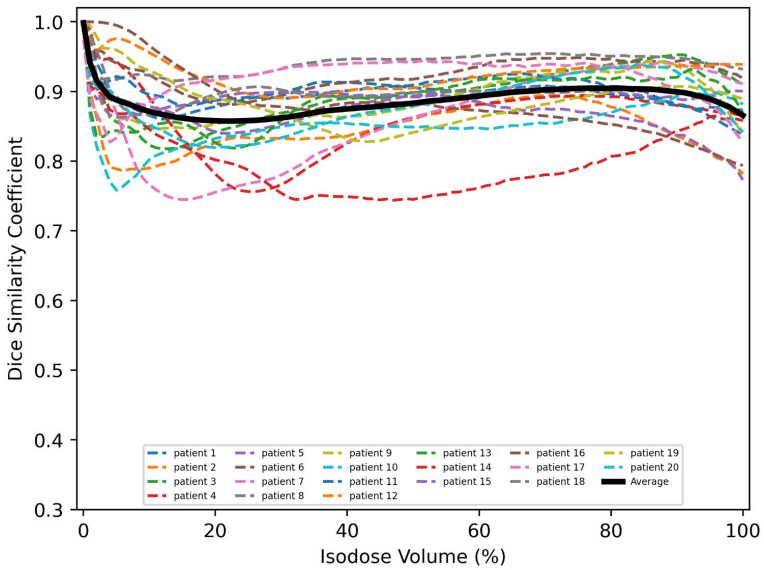


FIGURE 4
Similarity between clinical and predicted isodose distributions for 20 tested patients.

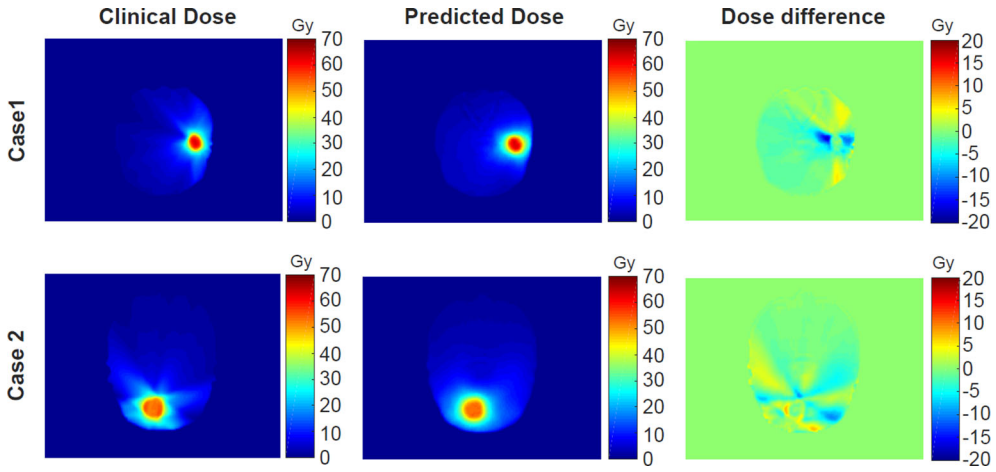


FIGURE 5
The comparison of the clinical and predicted dose maps for two cases.

complexity and time of model training. As tested, the time on model training is about 20 h on a workstation equipped with two NVIDIA GeForce 2080Ti GPUs. In the future, we plan to further fine-tune the basic 3D model and build a more memory-efficient mechanism for higher performance.

## 5 Conclusions

In this work, we evaluated a deep-learning model for 3D voxel-by-voxel dose prediction. It is capable of producing accurate dose distribution of VMAT plans for multiple brain metastases. As an improvement over the single U-Net or ResNet, it is a powerful model that can automatically correlate ROI voxel with dose voxel to achieve high-precise 3D dose prediction. The predicted results can be used to improve current treatment planning design, plan quality, and efficiency.

## Data availability statement

The original contributions presented in the study are included in the article/supplementary material. Further inquiries can be directed to the corresponding authors.

## Author contributions

PH: Conceptualization, Methodology, Writing – original draft. JS: Methodology, Software, Validation, Writing – original draft. ZH: Data curation, Formal Analysis, Validation, Writing – review & editing. ZL: Funding acquisition, Project administration, Resources, Writing – review & editing. HY: Conceptualization, Funding acquisition, Supervision, Writing – review & editing.

## Funding

The author(s) declare financial support was received for the research, authorship, and/or publication of this article. This work is supported by the Special Research Fund for Central Universities, Peking Union Medical College, CAMS Innovation Fund for Medical Sciences (CIFMS) (2022-I2M-C&T-B-075), the Beijing Hope Run Special Fund of Cancer Foundation of China (LC2021B01), the Natural Science Foundation (NSF) of China (No. 11975312), and the Beijing Municipal Natural Science Foundation (7202170).

## Conflict of interest

The authors declare that the research was conducted in the absence of any commercial or financial relationships that could be construed as a potential conflict of interest.

## Publisher's note

# References


1. Soffietti R, Ruda R, Mutani R. Management of brain metastases. *J Neurol*. (2002) 249:1357–69. doi: 10.1007/s00415-002-0870-6

2. Zimm S, Wampler GL, Stablein D, Hazra T, Young HF. Intracerebral metastases in solid-tumor patients: natural history and results of treatment. *Cancer*. (1981) 48:384–94. doi: 10.1002/1097-0142(19810715)48:2<384::AID-CNCR2820480227>3.0.CO;2-8

3. Posner JB. *Neurologic complications of cancer*. Philadelphia, PA: FA Davies (1995).

4. Soffietti R, Costanza A, Laguzzi E, Nobile M, Rudà R. Radiotherapy and chemotherapy of brain metastases. *J Neurooncol*. (2005) 75:31–42. doi: 10.1007/s11060-004-8096-3

5. Richards CM, Khuntia D, Mehta MP. Therapeutic management of metastatic brain tumors. *Crit Rev Oncol Hematol*. (2007) 61:70–8. doi: 10.1016/j.critrevonc.2006.06.012

6. Shibamoto Y, Sugie C, Iwata H. Radiotherapy for metastatic brain tumors. *Int J Clin Oncol*. (2009) 14:281–8. doi: 10.1007/s10147-009-0915-2

7. Caffo M, Barresi V, Caruso G, Cutugno M, la Fata G, Venza M, et al. Innovative therapeutic strategies in the treatment of brain metastases. *Int J Mol Sci*. (2013) 14:2135–74. doi: 10.3390/ijms14012135

8. Kocher M, Soffietti R, Abacioglu U, Villà S, Fauchon F, Baumert BG, et al. Adjuvant whole-brain radiotherapy versus observation after radiosurgery or surgical resection of one to three cerebral metastases: results of the EORTC 22952-26001 study. *J Clin Oncol*. (2011) 29:134–41. doi: 10.1200/JCO.2010.30.1655

9. Boehling NS, Chang EL, Ma LJ, Phan N, Yeung R, Sahga A. Stereotactic radiosurgery for brain metastases: current status and future directions. *J Radiat Oncol*. (2012) 1:245–53. doi: 10.1007/s13566-012-0043-x

10. Fowler JF, Welsh JS, Howard SP. Loss of biological effect in prolonged fraction delivery. *Int J Radiat Oncol Biol Phys*. (2004) 59:242–9. doi: 10.1016/j.ijrobp.2004.01.004

11. Wolff HA, Wagner DM, Christiansen H, Hess CF, Vorwerk H. Single fraction radiosurgery using Rapid Arc for treatment of intracranial targets. *Radiat Oncol*. (2010) 5:77. doi: 10.1186/1748-717X-5-77

12. Clark GM, Popple RA, Young PE, Fiveash JB. Feasibility of single-isocenter volumetric modulated arc radiosurgery for treatment of multiple brain metastases. *Int J Radiat Oncol Biol Phys*. (2010) 76:296–302. doi: 10.1016/j.ijrobp.2009.05.029

13. Mayo CS, Ding L, Addesa A, Kadish S, Fitzgerald TJ, Moser R. Initial experience with volumetric IMRT (RapidArc) for intracranial stereotactic radiosurgery. *Int J Radiat Oncol Biol Phys*. (2010) 75:253–9. doi: 10.1016/j.ijrobp.2009.10.005

14. Teoh M, Clark CH, Wood K, Whitaker S, Nisbet A. Volumetric modulated arc therapy: a re- view of current literature and clinical use in practice. *Br Inst Radiol*. (2011) 84:967–96. doi: 10.1259/bjr/22373346

15. Iwai Y, Ozawa S, Ageishi T, Pellegrini R, Yoda K. Feasibility of single-isocenter, multi-arc non-coplanar volumetric modulated arc therapy for multiple brain tumors using a linear accelerator with a 160-leaf multileaf collimator: a phantom study. *J Radiat Res*. (2014) 55:1015–20. doi: 10.1093/jrr/rru042

16. Kang J, Ford EC, Smith K, Wong J, McNutt TR. A method for optimizing LINAC treatment geometry for volumetric modulated arc therapy of multiple brain metastases. *Med Phys*. (2010) 37:4146–54. doi: 10.1118/1.3455286

17. Clark GM, Popple RA, Prendergast BM, Spencer SA, Thomas EM, Stewart JG, et al. Plan quality and treatment planning technique for single isocenter cranial radiosurgery with volumetric modulated arc therapy. *Pract Radiat Oncol*. (2012) 2:306–13. doi: 10.1016/j.prro.2011.12.003

18. Good D, Lo J, Lee WR, Wu QJ, Yin FF, Das SK. A knowledge-based approach to improving and homogenizing intensity modulated radiation therapy planning quality among treatment centers: an example application to prostate cancer planning. *Int J Radiat Oncol Biol Phys*. (2013) 87:176–81. doi: 10.1016/j.ijrobp.2013.03.015

19. Nwankwo O, Mekdash H, Sihono DS, Wenz F, Glatting G. Knowledge-based radiation therapy (KBRT) treatment planning versus planning by experts: validation of a KBRT algorithm for prostate cancer treatment planning. *Radiat Oncol*. (2015) 10:111. doi: 10.1186/s13014-015-0416-6

20. Shiraishi S, Moore KL. Knowledge-based prediction of three-dimensional dose distributions for external beam radiotherapy. *Med Phys*. (2016) 43:378. doi: 10.1118/1.4938583

21. Nguyen D, Long T, Jia X, Lu W, Gu X, Iqbal Z, et al. A feasibility study for predicting optimal radiation therapy dose distributions of prostate cancer patients from patient anatomy using deep learning. *Sci Rep*. (2019) 9:1076. doi: 10.1038/s41598-018-37741-x

22. Jiang D, Yan H, Chang N, Li T, Mao R, Du C, et al. Convolutional neural network-based dosimetry evaluation of esophageal radiation treatment planning. *Med Phys*. (2020) 47:4735–42. doi: 10.1002/mp.14434

23. Fan J, Wang J, Chen Z, Hu C, Zhang Z, Hu W. Automatic treatment planning based on three-dimensional dose distribution predicted from deep learning technique. *Med Phys*. (2019) 46:370–81. doi: 10.1002/mp.13271

24. Chen X, Men K, Li Y, Yi J, Dai J. A feasibility study on an automated method to generate patient-specific dose distributions for radiotherapy using deep learning. *Med Phys*. (2019) 46:56–64. doi: 10.1002/mp.13262

25. Kearney V, Chan JW, Haaf S, Descovich M, Solberg TD. DoseNet: a volumetric dose prediction algorithm using 3D fully-convolutional neural networks. *Phys Med Biol*. (2018) 63:235022. doi: 10.1088/1361-6560/aaef74

26. Barragán-Montero AM, Nguyen D, Lu W, Lin MH, Norouzi-Kandalan R, Geets X, et al. Three-dimensional dose prediction for lung IMRT patients with deep neural networks: robust learning from heterogeneous beam configurations. *Med Phys*. (2019) 46:3679–91. doi: 10.1002/mp.13597

27. Zhang J, Liu S, Yan H, Li T, Mao R, Liu J. Predicting voxel-level dose distributions for esophageal radiotherapy using densely connected network with dilated convolutions. *Phys Med Biol*. (2020) 65:205013. doi: 10.1088/1361-6560/aba87b

28. Nguyen D, Jia X, Sher D, Lin MH, Iqbal Z, Liu H, et al. 3D radiotherapy dose prediction on head and neck cancer patients with a hierarchically densely connected U-net deep learning architecture. *Phys Med Biol*. (2019) 64:065020. doi: 10.1088/1361-6560/ab039b

29. Yan H, Liu S, Zhang J, Liu J, Li T. Utilizing pre-determined beam orientation information in dose prediction by 3D fully-connected network for intensity modulated radiotherapy. *Quant Imaging Med Surg*. (2021) 11:4742–52. doi: 10.21037/qims-20-1076

30. Liu Z, Fan J, Li M, Yan H, Hu Z, Huang P, et al. A deep learning method for prediction of three-dimensional dose distribution of helical tomotherapy. *Med Phys*. (2019) 46:1972–83. doi: 10.1002/mp.13490

31. Babier A, Mahmood R, McNiven AL, Diamant A, Chan TCY. Knowledge-based automated planning with three-dimensional generative adversarial networks. *Med Phys*. (2020) 47:297–306. doi: 10.1002/mp.13896

32. Zhan B, Xiao J, Cao C, Peng X, Zu C, Zhou J, et al. Multi-constraint generative adversarial network for dose prediction in radiotherapy. *Med Image Anal*. (2022) 77:102339. doi: 10.1016/j.media.2021.102339

33. Gu X, Strijbis VIJ, Slotman BJ, Dahele MR, Verbakel WFAR. Dose distribution prediction for head-and-neck cancer radiotherapy using a generative adversarial network: influence of input data. *Front Oncol*. (2023) 13:1251132. doi: 10.3389/fonc.2023.1251132

34. Osman AFI, Tamam NM, Yousif YAM. A comparative study of deep learning-based knowledge-based planning methods for 3D dose distribution prediction of head and neck. *J Appl Clin Med Phys*. (2023) 24:e14015. doi: 10.1002/acm2.14015

35. Kadoya N, Kimura Y, Tozuka R, Tanaka S, Arai K, Katsuta Y, et al. Evaluation of deep learning-based deliverable VMAT plan generated by prototype software for automated planning for prostate cancer patients. *J Radiat Res*. (2023) 64:842–9. doi: 10.1093/jrr/rrad058

36. Gronberg MP, Gay SS, Netherton TJ, Rhee DJ, Court LE, Cardenas CE. Technical Note: Dose prediction for head and neck radiotherapy using a three-dimensional dense dilated U-net architecture. *Med Phys*. (2021) 48:5567–73. doi: 10.1002/mp.14827

37. Gronberg MP, Beadle BM, Garden AS, Skinner H, Gay S, Netherton T, et al. Deep learning-based dose prediction for automated, individualized quality assurance of head and neck radiation therapy plans. *Pract Radiat Oncol*. (2023) 13:e282–91. doi: 10.1016/j.prro.2022.12.003

38. Gronberg MP, Jhingran A, Netherton TJ, Gay SS, Cardenas CE, Chung C, et al. Deep learning-based dose prediction to improve the plan quality of volumetric modulated arc therapy for gynecologic cancers. *Med Phys*. (2023) 50:6639–48. doi: 10.1002/mp.16735

39. Kingma DP, Ba J. Adam: A method for stochastic optimization. *arXiv:1412.6980* (2014).

frontiers | Frontiers in Oncology

TYPE Review
PUBLISHED 08 May 2024
DOI 10.3389/fonc.2024.1338225



OPEN ACCESS

EDITED BY
Yirui Zhai,
Chinese Academy of Medical Sciences and Peking Union Medical College, China

REVIEWED BY
Mirek Fatyga,
Mayo Clinic Arizona, United States
Bin Wang,
Sun Yat-sen University Cancer Center (SYSUCC), China
Songbing Qin,
The First Affiliated Hospital of Soochow University, China

*CORRESPONDENCE
Yong Yin
yinyongsd@126.com

RECEIVED 14 November 2023
ACCEPTED 19 April 2024
PUBLISHED 08 May 2024

CITATION
Du S, Gong G, Liu R, Meng K and Yin Y (2024) Advances in determining the gross tumor target volume for radiotherapy of brain metastases.
*Front. Oncol.* 14:1338225.
doi: 10.3389/fonc.2024.1338225



# Advances in determining the gross tumor target volume for radiotherapy of brain metastases

Shanshan Du[1,2], Guanzhong Gong[2], Rui Liu[2], Kangning Meng[2] and Yong Yin[1,2]*

[1]Department of Oncology, Affiliated Hospital of Southwest Medical University, Luzhou, Sichuan, China, [2]Department of Radiation Oncology Physics and Technology, Shandong Cancer Hospital and Institute, Shandong First Medical University and Shandong Academy of Medical Sciences, Jinan, China

Brain metastases (BMs) are the most prevalent intracranial malignant tumors in adults and are the leading cause of mortality attributed to malignant brain diseases. Radiotherapy (RT) plays a critical role in the treatment of BMs, with local RT techniques such as stereotactic radiosurgery (SRS)/stereotactic body radiotherapy (SBRT) showing remarkable therapeutic effectiveness. The precise determination of gross tumor target volume (GTV) is crucial for ensuring the effectiveness of SRS/SBRT. Multimodal imaging techniques such as CT, MRI, and PET are extensively used for the diagnosis of BMs and GTV determination. With the development of functional imaging and artificial intelligence (AI) technology, there are more innovative ways to determine GTV for BMs, which significantly improve the accuracy and efficiency of the determination. This article provides an overview of the progress in GTV determination for RT in BMs.

KEYWORDS

**brain metastases, MRI, GTV, delineation, artificial intelligence**

## 1 Introduction

Brain metastases (BMs) are the most frequent intracranial malignant tumors in adults; among patients with malignant tumors, the incidence rate of BMs in adults is 10%–30%, and that in children is 6%–10% (1). The leading tumor type resulting in BMs is lung cancer, accounting for approximately 20%, followed by melanoma, breast cancer, etc. (1). Notably, the incidence of BMs surpasses that of primary brain tumors, making them the primary cause of mortality from malignant brain diseases (2).

The treatment methods for BMs include whole-brain radiotherapy (WBRT), stereotactic radiosurgery (SRS)/stereotactic body radiotherapy (SBRT), surgery, and systemic therapy (3). In recent years, an increasing amount of clinical evidence supports the application of local RT techniques such as SRS/SBRT in BMs (4). Accurate determination of the gross tumor target volume (GTV) is crucial for ensuring the

efficacy of SRS/SBRT. With the development of advanced imaging technology and information science and technology, the use of multimodal imaging technology and artificial intelligence (AI) to improve the accuracy of GTV determination in BMs has become a popular research direction.

## 2 RT for BMs

Radiotherapy (RT) serves as the primary treatment method for BMs. Objective studies have shown that patients with symptomatic BMs typically have a median overall survival (OS) of just 1 month without treatment. However, treatment with glucocorticosteroids alone, such as dexamethasone, can extend the median OS to 2 months (5). Lagerwaard et al. (6) reported that patients who received different doses of WBRT experienced an extended median OS of 3–6 months and a 1-year survival rate of 10%.

WBRT is the standard treatment for multiple BMs (7). However, WBRT often results in delayed adverse events including leukoencephalopathy, associated cognitive dysfunction, cerebral atrophy, and radionecrosis. Cognitive dysfunction is reported in approximately 10%–20% of patients undergoing WBRT (8). To avoid radiation damage to normal brain tissue, local RT methods such as SRS/SBRT have been developed. Multiple international clinical trials support SRS as the preferred treatment for BM patients with one to four metastases (9–12). The JLGK0901 (4) study revealed that patients with five to 10 BMs achieved comparable treatment results with patients with two to four BMs by receiving SRS treatment; the median OS all reached 10.8 months. Therefore, SRS could be considered an alternative treatment for multiple BMs instead of WBRT.

SRS/SBRT requires precise GTV determination and accurate dose delivery, which are directly related to the therapeutic efficacy and prognosis. The small size of BMs and their unclear enhancement affect lesion detection and visibility of tumor boundaries, which are the key challenges that need to be addressed in GTV determination for BMs.

## 3 Advances in GTV determination of BMs based on multimodal imaging

### 3.1 Computed tomography-based GTV determination in BMs

#### 3.1.1 Single-energy CT-based determination

Computed tomography (CT) simulation images serve as the primary foundation for GTV determination in BMs. CT offers high spatial resolution, minimal distortion, and sensitivity to features such as bleeding, calcification, and structural changes in the surrounding skull of BMs. The linear relationship between the CT value and tissue electron density is the basis for dose calculations in RT planning (12) (Figure 1).

However, single-energy CT (SECT) is susceptible to bone artifacts, peri-tumor edematous areas, and fibrosis, limiting its use in GTV determination in BMs. Emerging CT technologies provide a reliable means to improve the precision of GTV determination.

#### 3.1.2 Dual-energy computed tomography-based determination

Dual-energy computed tomography (DECT) improves the signal-noise ratio (SNR) and contrast-noise ratio (CNR) of intracranial abnormal metal deposits, iodine contrast, normal brain tissue, and abnormal lesions, resulting in superior image quality (13). DECT reduces the beam hardening artifacts caused by the skull through a special reconstruction algorithm, improving the image quality of posterior fossa tumors and improving BM imaging (14).

DECT shows greater image enhancement at low tube voltages (15). Karino et al. (16) analyzed energy spectral images of virtual monochromatic images (VMI) with energy levels ranging from 40 to 140 KeV in increments of 1 keV gradient and found that a VMI of 63 KeV significantly improved the overall image quality and BM boundary display. Kraft et al. (17) further compared the differences between 63 keV reconstructed VMI and 120 kV CT in BM imaging and confirmed that the image quality of VMI was significantly

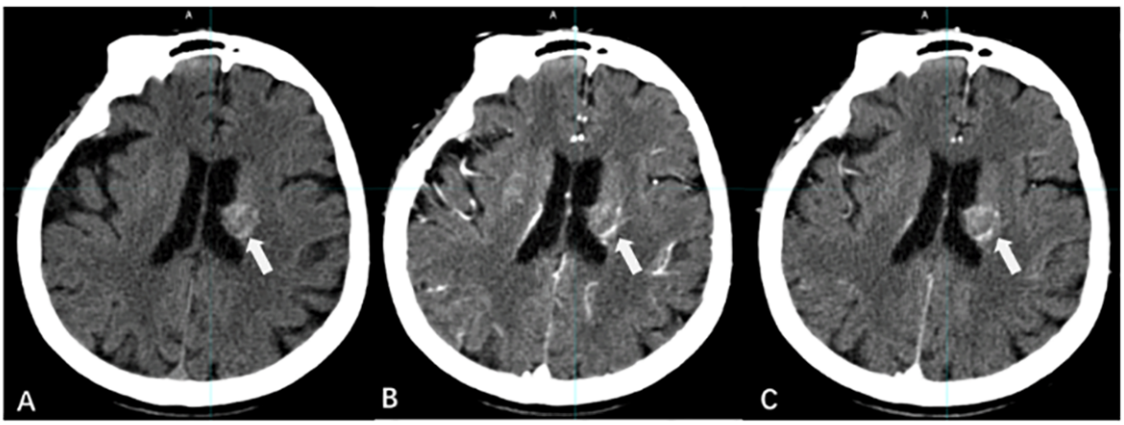


FIGURE 1
CT imaging manifestations of BMs. [**(A)** CT scan without contrast; **(B)** CT contrast scan in arterial phase; **(C)** CT contrast scan in vein phase].

better than that of conventional CT, which could improve the reliability and accuracy of GTV determination in BMs.

## 3.2 Multisequence MR-based GTV determination in BMs

Compared with CT, magnetic resonance (MR) provides high soft tissue resolution, clear differentiation between tumors and tissue edema, and avoids radiation injury. MR is thus indispensable for diagnosing, planning treatment, and posttreatment monitoring of brain tumors (18).

Contrast-enhanced MRI (CE-MRI) with gadolinium (Gd)-based contrast serves as the gold standard for identifying BMs (19). However, the contrast of the enhanced region of BMs in CE-MRI is affected by various factors, including the characteristics of the blood–brain barrier (BBB), magnetic field strength, concentration of Gd-based contrast agent (GBCA), relaxivity properties, time elapsed since injection, and the MR imaging technique (20). Derks et al. (12) found that 3T MR was more sensitive than 1.5 T MR in the diagnosis of small-volume BMs with diameters < 5 mm.

Cheng et al. (21) found that 7T MR improved visualization of small structures and subtle brain tumor lesions compared to 3T MR, which had significant potential for the diagnosis, treatment, and monitoring of BMs. However, the increase in magnetic field strength also leads to greater magnetization artifacts, which affects the GTV determination of BMs.

CE-T1WI and T2/Fluid-attenuated inversion recovery (FLAIR) are the most commonly used sequences in MR simulations of BMs (22).

### 3.2.1 CE-T1WI-based determination

There are differences in the imaging of BMs on T1WI with different imaging bases. A comparative analysis of the detection rates of BMs using enhanced spin-echo (SE) and gradient-echo (GRE) sequences by Suh et al. (23) revealed that, with a layer thickness of 1 mm, 3D SE images had a 20.6% higher detection rate than 3D GRE images. Additionally, for lesions with diameters less than 5 mm, 3D SE images exhibited a 30.1% higher detection rate than 3D GRE images. For the detection of BMs, especially lesions less than 5 mm in size, 3D SE-enhanced images with a 1-mm-layer slice thickness are more suitable.

Whether delayed enhancement MRI can improve the detection rate of BMs has been controversial (Figure 2). Cohen et al. (24) concluded that the detection rate of BMs by delayed CE-MRI is related to lesion volume. For larger BMs, delayed CE-MRI is not more advantageous than immediate postcontrast-enhanced imaging; however, for lesions with diameters ≤ 5 mm, delayed CE-MRI improves the detection rate of lesions and increases the display of tumor boundaries, especially when the delay time is more than 10 min (25–28).

Chen et al. (29) investigated the effect of CE-MRI with different delay times on the generation of small-volume BMs, and the results showed that compared with 10 min after contrast agent injection, the metastatic volumes at 1, 3, and 5 min decreased by 31.6%, 18.5%, and 10.1%, respectively, and the metastatic volumes at 18

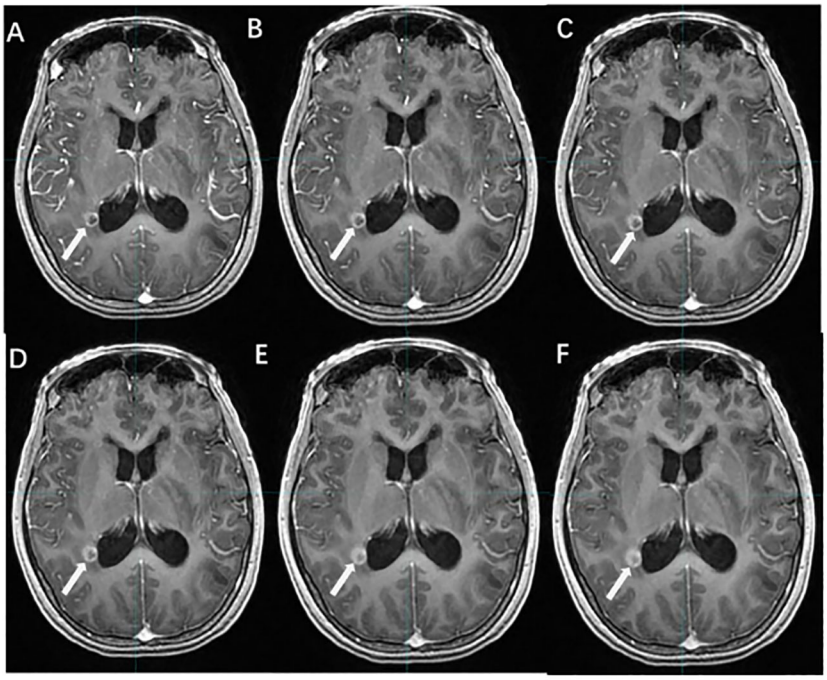


FIGURE 2
The effect of time-delayed contrast-enhanced T1WI on the visualization of BMs. [**(A–F)** The BM manifest on contrast-enhanced T1WI at 1, 3, 5, 10, 18, and 20 min after Gd-DTPA injection].

and 20 min increased by only 8% and 10%, respectively. Therefore, CE-MRI with a delay time of more than 10 min should be a routine modality for the detection and border display of small-volume BMs.

Several studies have demonstrated that high-dose Gd-based contrast agents (GBCA) improve the demonstration of BMs, and the use of triple-dose contrast agents increases the detection of BMs < 5 mm by 65.6%; however, it also increases the risk of patient complications and the cost of the examination (26, 30–33).

### 3.2.2 T2/FLAIR-based determination

Unlike CE-T1WI, T2/FLAIR uses a low concentration of GBCA to enhance the lesion, and the contrast agent required to enhance the lesion is only one-fourth of that required for CE-T1WI (34, 35). Several studies have demonstrated that CE-T2/FLAIR is superior in detecting leptomeningeal metastases, small-volume lesions, and lesions located in superficial areas of the brain (36, 37) (Figure 3).

There were differences in the detection rate and enhancement degree of BMs between CE-T2/FLAIR and CE-T1WI. Jin et al. (38) suggested that this was related to the vascular permeability and microvascular density around the lesions of BMs. In lesions with higher density or greater damage to the BBB, the venous leakage of the contrast medium increased, resulting in a large accumulation of GBCA in the extracellular space. The enhancement effect of T2 reduced the degree of enhancement of the lesions and even led to negative enhancement. Thus, the degree of CE-T2/FLAIR enhancement was negatively associated with vascular permeability and demonstrated superior enhancement in BMs with low vascular permeability. CE-T2/FLAIR is an effective supplement to CE-T1WI, and the combined application of the two improves the detection and determination accuracy of BMs (39).

## 3.3 PET-based GTV determination of BMs

Positron emission tomography (PET) is a noninvasive imaging technique used to assess the biological function and metabolism of tumors. 18F fluorodeoxyglucose (18F-FDG) is the most widely used PET tracer, but normal brain tissue also shows high glucose uptake, which affects the GTV determination of BMs (40). Compared to 18F-FDG, the uptake of radiolabeled amino acids is lower, allowing them to cross the intact BBB, revealing BMs beyond CE MRI, and providing new insights for delineating biological targets in BMs (41).

### 3.3.1 PET/CT

PET/CT is used to obtain information on tumor biology and metabolism, which is valuable for determining biological GTVs. However, it has limitations in detecting BMs, especially for small-volume BMs. Factors such as lower FDG uptake by small BMs and the lower spatial resolution of PET/CT affect image quality, while the high uptake of inflammatory tissue reduces diagnostic specificity (42). In a study of more than 900 patients with BMs from lung cancer, Li et al. (43) found that CE-MRI had a higher sensitivity than FDG PET/CT for diagnosing BMs in patients (77% vs. 21%).

PET/CT is primarily used to detect extracranial lesions and is not highly sensitive for BMs, especially those with small volumes. Therefore, PET/CT is often complemented by the combination of enhanced MRI or CT (Figure 4).

### 3.3.2 PET/MR

PET/MRI has the advantage of simultaneously capturing both structural and functional aspects of tumors, which enhances RT planning and the assessment of treatment response (44). By combining high-resolution soft tissue PET with MRI, PET/MR provides a reliable basis for precise GTV determination in BMs.

Singnurkar et al. (45) compared the clinical performance of FDG PET/MR with FDG PET/CT in tumor imaging. FDG PET/MR was found to be similar to FDG PET/CT in detecting local lymph nodes and distant metastases but superior in assessing the local extent of tumors. Similarly, another study by Sekine et al. (46) demonstrated a 6.7% improvement in PET/MR imaging compared to PET/CT for occult tumors, including brain tumors.

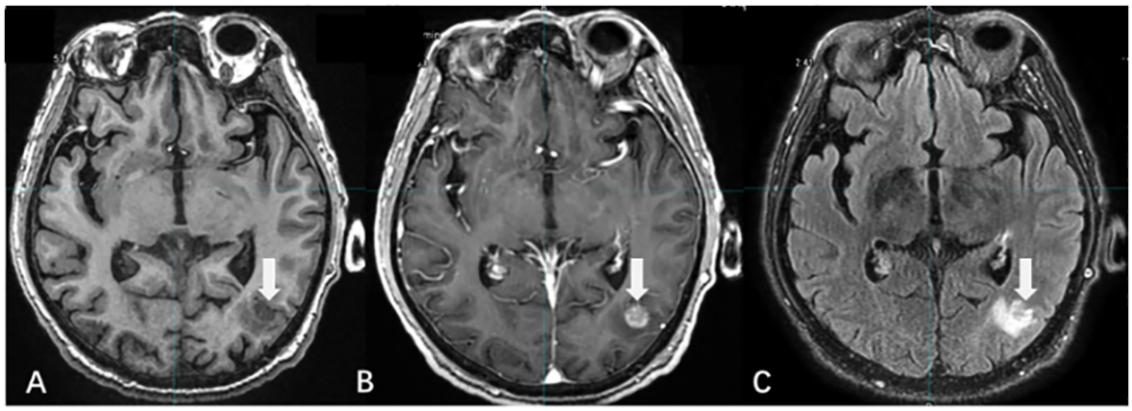


FIGURE 3
The display differences of BMs among T1WI, T1WI+C, and T2/FLAIR. [**(A)** T1WI without contrast; **(B)** CE-T1WI; **(C)** CE-T2/FLAIR].

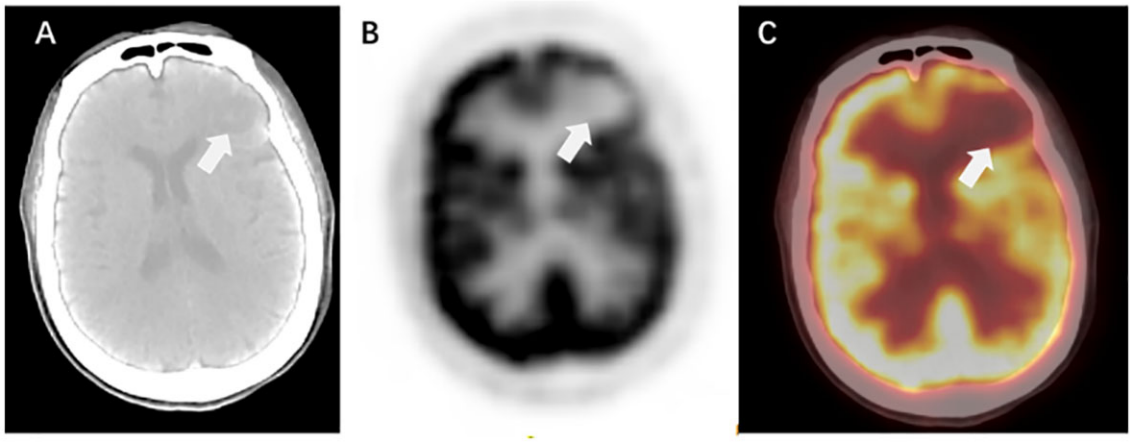


FIGURE 4
PET/CT manifestations of BMs. [**(A)** CT without contrast; **(B)** PET; **(C)** PET/CT].

## 3.4 CT/MRI fusion

CT provides crucial anatomical information and electron density data for RT planning and dose calculation, but it lacks sufficient soft tissue contrast, making it unreliable to determine GTV only based on CT alone (47). MRI provides high soft tissue resolution, enabling differentiation between active tumors and edematous tissue. The fusion of CT and MRI images combines the advantages of both modalities. However, differences in the underlying principles of CT and MRI imaging modalities, poor reproducibility of body fixation, poor accuracy of patient positioning, interlayer differences in layer thicknesses of images from different modalities, and tumor regression due to treatment all contribute to the poor quality of CT/MRI fusion images, which affects the visualization of the BMs and the accuracy of the GTV determination.

Few controlled studies of the volume and dosimetric effects of CT/MRI fusion in BMs' GTVs have been reported. However, in general, CT/MRI fusion can improve the determination accuracy of GTV in BMs, allowing for personalized treatment options, organ preservation, or functional avoidance. Moreover, it facilitates intensification and dose escalation strategies (Figure 5).

# 4 The future direction of GTV determination in BMs

## 4.1 AI-based detection of BMs and automatic segmentation of GTVs

AI is trained and validated on large datasets to provide automated tools to assist physicians in accurately and quickly

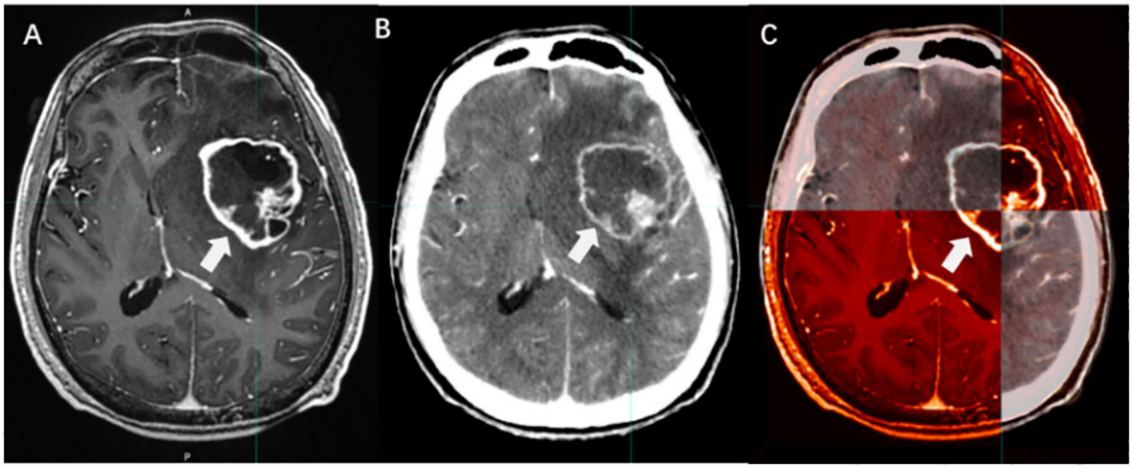


FIGURE 5
The boundary determination of BMs applying CT/MRI fusion. [**(A)** CE-T1WI images; **(B)** Enhanced CT images; **(C)** CT/MRI fusion].

detecting BMs in large-scale medical imaging datasets. Manually determining BMs' GTVs is time-consuming and challenging, and autosegmentation significantly enhances efficiency and precision. Deep learning models, such as convolutional neural networks (CNN), have shown promising results in BM image segmentation. Since 2018, AI-based contouring has evolved from classical machine learning (cML) to deep learning (DL). Cho et al. (48) conducted a systematic review of the literature on BM detection based on machine learning. The detection rates of BMs in the cML and DL groups were 88.7% and 90.1%, respectively. The DL group had a lower false-positive rate per patient than the cML group (10 vs. 135), indicating a clear advantage for DL. Deep learning models are adaptable and resilient in handling complex lesion shapes and indistinct boundaries through substantial labeled image data assimilation.

CNN-based AI has gained widespread acceptance for the screening and identification of BMs. Grovik et al. (49) conducted a study evaluating a CNN deep learning method for the automatic detection and segmentation of BMs using multisequence MRI. The results showed an average sensitivity of 83% for detecting BMs, indicating remarkable accuracy. However, the network's ability to detect BMs was related to lesion size. It was shown that by using the optimal probability threshold (average sensitivity = 83%), the network showed an average false-positive rate of 8.3 (no size limit) and 3.4 (10 $mm^3$ size limit) lesions per case, with the highest sensitivity and lowest numbers of false positives in patients with few metastases.

Zhou et al. (50) developed a DL single-shot detector (SSD) algorithm based on CE T1WI to detect BMs. For the test group, the sensitivity of the baseline SSD was 81%; the sensitivity was 98% for metastases ≥ 6 mm in diameter. The combined algorithm of feature fusion (FF) and SSD developed by Amemiya et al. (51) revealed that the FF and baseline SSDs showed an overall sensitivity of 86.0% and 83.8% and a positive predictive value (PPV) of 46.8% and 45.2%, respectively. Thus, FF SSD significantly improved the small lesion detection without reducing the overall PPV. Li et al. (52) introduced a two-stage deep learning model designed for automatic BM detection and segmentation, achieving a detection sensitivity rate of 91%.

With more data availability and technological advancements, AI is expected to become a crucial tool for diagnosing and treating BMs. However, there are still challenges in brain tumor imaging research related to AI technology. Modeling requires large datasets from multiple centers. However, subjectivity can be introduced during the preprocessing stage when physicians manually segment the images. This necessitates high requirements for consistency in image data quality. Therefore, most AI models for BMs are still in the research stage, and their clinical application requires thorough validation.

## 4.2 Functional MRI in GTV determination of BMs

With the development of functional imaging, biology-guided RT has gradually become part of clinical practice. Biologic target volumes refer to regions within the target volume with varying radiosensitivities, determined by various tumor biological factors, including hypoxia, blood supply, proliferation, apoptosis, cell cycle regulation, infiltration, and metastatic properties. Tumor hypoxia is common in RT due to abnormalities in the tumor vasculature. Hypoxic cells are highly resistant to RT, resulting in a relative lack of local tumor doses. Therefore, identifying and quantifying tumor hypoxia is crucial for improving the effectiveness of RT.

Functional MRI, including dynamic contrast-enhanced MRI (DCE-MRI) and dynamic susceptibility contrast-perfusion-weighted imaging (DSC-PWI), can identify, quantify, and spatially map areas of hypoxia before treatment and track hypoxia changes during radiation (53, 54). It can help improve the radiation dose to the hypoxic RT-resistance area through dose engraving and protect the organ at risk (OAR), and it should be incorporated into the practice of radiotherapy in BMs (55, 56).

Functional MR imaging techniques, such as PWI, diffusion-weighted imaging (DWI), and magnetic resonance spectroscopy, provide clinical insight into tumor metabolism, pathophysiology, and microcirculatory status, and they are increasingly used for GTV determination in BMs.

### 4.2.1 PWI

PWI can be categorized into two main types: those that use Gd contrast agents and those that do not. DSC and DCE, both based on Gd injections, efficiently evaluate vascular infiltration and neovascularization in the enhanced regions of BMs. DSC quantifies tumor vascular supply and is the most frequently employed PWI technique for brain tumor evaluation (57).

Arterial spin labeling (ASL) is a noninvasive method for examining blood flow changes in BMs without the use of paramagnetic contrast agents and without being influenced by the BBB. This imaging technique uses hydrogen protons present in arterial blood as endogenous tracers to provide accurate results. Soni et al. (58) conducted a quantitative comparison of perfusion values acquired through ASL and DSC in brain tumors, demonstrating a favorable degree of agreement. As a result, ASL, as a noninvasive test, exhibits greater potential for broad utilization.

Hou et al. (54) used MR-3D-ASL to map cerebral blood flow to determine the high-perfused GTV ($GTV_H$) versus the low-perfused GTV ($GTV_L$). Their findings revealed an uneven distribution of perfusion within BMs and variations in intratumoral and intertumoral perfusion between tumors with and without necrosis. Dose escalation to low-perfusion areas with RT resistance should be performed by reducing the dose boost volume so that the dose to the target area is targeted and distributed according to blood perfusion. Hou et al. (59) further designed three RT plans based on CBF measurements. When compared to the conventional plan, the dose painting plan exhibited that the $D_{2\%}$, $D_{98\%}$ (doses to 2% and 98% volume of the PTV), and the mean dose increased by 20.50%, 19.32%, and 19.60% in the low-perfusion region, respectively. Therefore, 3D-ASL-guided dose painting effectively increases the radiation dose to the low-perfusion subregion without increasing the dose to the OAR, and subregion identification and segmentation based on the differences in blood perfusion in the GTV are of great clinical significance (Figure 6).

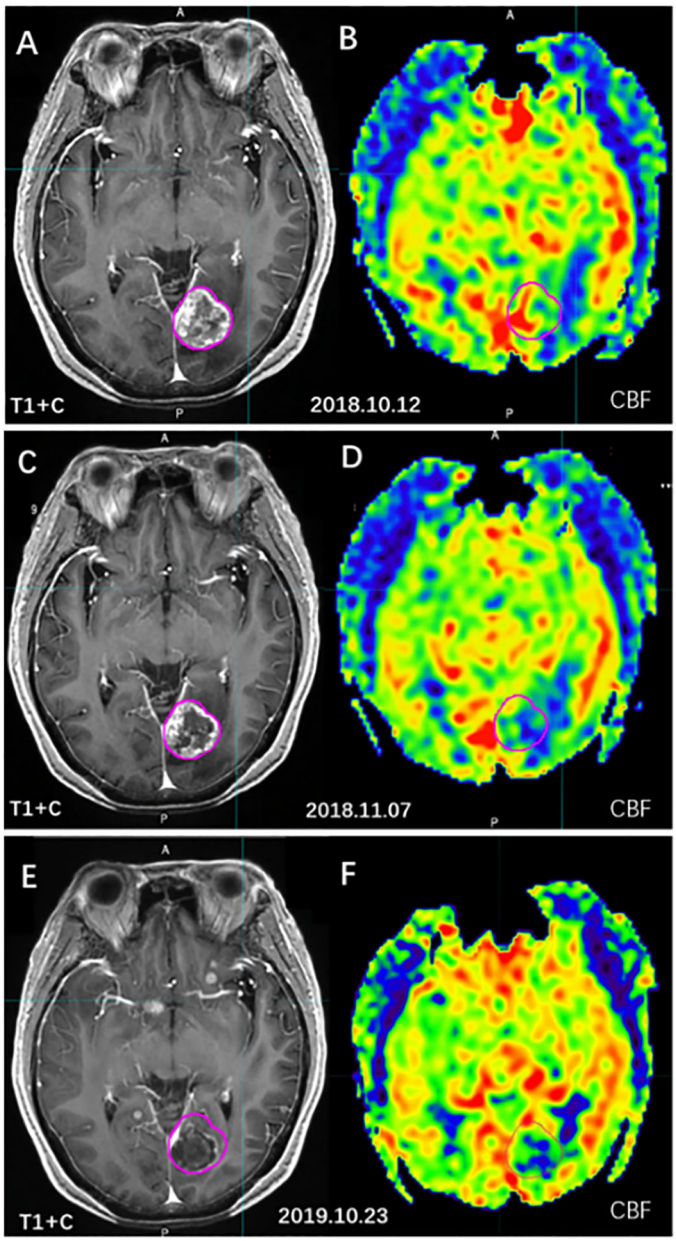


FIGURE 6
The cerebral blood volume variation of BMs before and after radiotherapy. [**(A, C, E)** T1WI+C images; **(B, D, F)** 3D-ASL cerebral blood volume images; **(A, B)** before radiotherapy; **(C, D)** 4 weeks after radiotherapy; **(E, F)** 1 year after radiotherapy].

### 4.2.2 DWI

Conventional MRI sequences have limitations in distinguishing between infiltrating tumors and vasogenic edema. Apparent diffusion coefficient (ADC) values can measure the extent to which water molecules are restricted in healthy brain tissue and central nervous system lesions. On high b-valued DWI, BMs appear as high-intensity signals with low ADC values, which can distinguish tumor and edema.

A study conducted by Zhong et al. (60) identified differences in the ADC values between patients with and without BMs. An ADC value of $0.837 \times 10^{-3}$ mm/s was found to be critical for distinguishing BMs from nonbrain metastases, yielding a sensitivity of 83.7% and a specificity of 69.2%, resulting in a high BM detection rate. However, DWI has low resolution and is prone to magnetization artifacts, and its clinical application in BMs is still mainly qualitative. The study of GTV determination of BMs based on DWI is still under investigation.

## 5 Conclusion and prospects

Accurate target determination is the primary premise for ensuring the efficacy of local RT for BMs. How to improve the accuracy of GTV determination is one of the key issues in

improving the efficacy of SRS/SBRT. With the progression of functional imaging technology and AI, methods such as MRI and PET provide more comprehensive data analysis concerning tumor size, infiltration depth, internal microenvironment, and chemical composition within BMs, which provides a feasible method for further improving the detection of BMs and the precision of GTV determination and provides a broad perspective for the clinical application of individualized RT.

## Author contributions

SD: Writing – original draft. GG: Writing – review & editing. RL: Writing – original draft. KM: Writing – original draft. YY: Writing – review & editing.

## Funding

The author(s) declare financial support was received for the research, authorship, and/or publication of this article. This work was supported in part by the Taishan Scholars Project of Shandong Province (Grant No. ts201712098).

## Acknowledgments

The authors acknowledge the assistance of Shandong Cancer Hospital and Institute (Shandong Cancer Hospital) in the preparation of the manuscript.

## Conflict of interest

The authors declare that the research was conducted in the absence of any commercial or financial relationships that could be construed as a potential conflict of interest.

## Publisher's note



## References

1. Noh T, Walbert T. Brain metastasis: clinical manifestations, symptom management, and palliative care. *Handb Clin Neurol*. (2018) 149:75–88. doi: 10.1016/B978-0-12-811161-1.00006-2

2. Deshpande K, Buchanan I, Martirosian V, Neman J. Clinical perspectives in brain metastasis. *Cold Spring Harb Perspect Med*. (2020) 10:a037051. doi: 10.1101/cshperspect.a037051

3. Garsa A, Jang JK, Baxi S, Chen C, Akinniranye O, Hall O, et al. Radiation therapy for brain metastases: A systematic review. *Pract Radiat Oncol*. (2021) 11:354–65. doi: 10.1016/j.prro.2021.04.002

4. Yamamoto M, Serizawa T, Shuto T, Akabane A, Higuchi Y, Kawagishi J, et al. Stereotactic radiosurgery for patients with multiple brain metastases (JLGK0901): a multi-institutional prospective observational study. *Lancet Oncol*. (2014) 15:387–95. doi: 10.1016/S1470-2045(14)70061-0

5. Den RB, Andrews DW. Radiotherapy for brain metastases. *Neurosurg Clin N Am*. (2011) 22:37–44, vi. doi: 10.1016/j.nec.2010.08.001

6. Lagerwaard FJ, Levendag PC, Nowak PJ, Eijkenboom WM, Hanssens PE, Schmitz PI. Identification of prognostic factors in patients with brain metastases: a review of 1292 patients. *Int J Radiat Oncol Biol Physics*. (1999) 43:795–803. doi: 10.1016/s0360-3016(98)00442-8

7. Brown PD, Ahluwalia MS, Khan OH, Asher AL, Wefel JS, Gondi V. Whole-brain radiotherapy for brain metastases: evolution or revolution? *J Clin Oncol*. (2018) 36:483–+. doi: 10.1200/jco.2017.75.9589

8. Narita Y, Sato S, Kayama T. Review of the diagnosis and treatment of brain metastases. *Jpn J Clin Oncol*. (2022) 52:3–7. doi: 10.1093/jjco/hyab182

9. Kayama T, Sato S, Sakurada K, Mizusawa J, Nishikawa R, Narita Y, et al. Effects of surgery with salvage stereotactic radiosurgery versus surgery with whole-brain radiation therapy in patients with one to four brain metastases (JCOG0504): A phase III, noninferiority, randomized controlled trial. *J Clin Oncol*. (2018) 36:3282–+. doi: 10.1200/jco.2018.78.6186

10. Mahajan A, Ahmed S, McAleer MF, Weinberg JS, Li J, Brown P, et al. Post-operative stereotactic radiosurgery versus observation for completely resected brain metastases: a single-centre, randomised, controlled, phase 3 trial. *Lancet Oncol*. (2017) 18:1040–8. doi: 10.1016/s1470-2045(17)30414-x

11. Brown PD, Ballman KV, Cerhan JH, Anderson SK, Carrero XW, Whitton AC, et al. Postoperative stereotactic radiosurgery compared with whole brain radiotherapy for resected metastatic brain disease (NCCTG N107C/CEC·3): a multicentre, randomised, controlled, phase 3 trial. *Lancet Oncol*. (2017) 18:1049–60. doi: 10.1016/s1470-2045(17)30441-2

12. Derks S, van der Veldt AAM, Smits M. Brain metastases: the role of clinical imaging. *Br J Radiol*. (2022) 95:20210944. doi: 10.1259/bjr.20210944

13. Chiro GD, Brooks RA, Kessler RM, Johnston GS, Jones AE, Herdt JR, et al. Tissue signatures with dual-energy computed tomography. *Radiol*. (1979) 131:521–3. doi: 10.1148/131.2.521

14. Hwang WD, Mossa-Basha M, Andre JB, Hippe DS, Culbertson S, Anzai Y. Qualitative comparison of noncontrast head dual-energy computed tomography using rapid voltage switching technique and conventional computed tomography. *J Comput Assist Tomogr*. (2016) 40:320–5. doi: 10.1097/RCT.0000000000000350

15. Johnson TR, Krauss B, Sedlmair M, Grasruck M, Bruder H, Morhard D, et al. Material differentiation by dual energy CT: initial experience. *Eur Radiol*. (2007) 17:1510–7. doi: 10.1007/s00330-006-0517-6

16. Karino T, Ohira S, Kanayama N, Wada K, Ikawa T, Nitta Y, et al. Determination of optimal virtual monochromatic energy level for target delineation of brain metastases in radiosurgery using dual-energy CT. *Br J Radiol*. (2020) 93:20180850. doi: 10.1259/bjr.20180850

17. Kraft J, Lutyj P, Grabenbauer F, Strohle SP, Tamihardja J, Razinskas G, et al. Assessment of dual-energy computed tomography derived virtual monoenergetic imaging for target volume delineation of brain metastases. *Radiother Oncol*. (2023) 187:109840. doi: 10.1016/j.radonc.2023.109840

18. Fink JR, Muzi M, Peck M, Krohn KA. Multimodality brain tumor imaging: MR imaging, PET, and PET/MR imaging. *J Nucl Med*. (2015) 56:1554–61. doi: 10.2967/jnumed.113.131516

19. Essig M, Anzalone N, Combs SE, Dorfler A, Lee SK, Picozzi P, et al. MR imaging of neoplastic central nervous system lesions: review and recommendations for current practice. *AJNR Am J Neuroradiol*. (2012) 33:803–17. doi: 10.3174/ajnr.A2640

20. Danieli L, Riccitelli GC, Distefano D, Prodi E, Ventura E, Cianfoni A, et al. Brain tumor-enhancement visualization and morphometric assessment: A comparison of MPRAGE, SPACE, and VIBE MRI techniques. *AJNR Am J Neuroradiol*. (2019) 40:1140–8. doi: 10.3174/ajnr.A6096

21. Cheng K, Duan Q, Hu J, Li C, Ma X, Bian X, et al. Evaluation of postcontrast images of intracranial tumors at 7T and 3T MRI: An intra-individual comparison study. *CNS Neurosci Ther*. (2023) 29:559–65. doi: 10.1111/cns.14036

22. Tong E, McCullagh KL, Iv M. Advanced imaging of brain metastases: from augmenting visualization and improving diagnosis to evaluating treatment response. *Front Neurol*. (2020) 11:270. doi: 10.3389/fneur.2020.00270

23. Suh CH, Jung SC, Kim KW, Pyo J. The detectability of brain metastases using contrast-enhanced spin-echo or gradient-echo images: a systematic review and meta-analysis. *J Neurooncol*. (2016) 129:363–71. doi: 10.1007/s11060-016-2185-y

24. Cohen-Inbar O, Xu Z, Dodson B, Rizvi T, Durst CR, Mukherjee S, et al. Time-delayed contrast-enhanced MRI improves detection of brain metastases: a prospective

validation of diagnostic yield. *J Neurooncol*. (2016) 130:485–94. doi: 10.1007/s11060-016-2242-6

25. Kang KM, Choi SH, Hwang M, Yoo RE, Yun TJ, Kim JH, et al. Application of Synthetic MRI for Direct Measurement of Magnetic Resonance Relaxation Time and Tumor Volume at Multiple Time Points after Contrast Administration: Preliminary Results in Patients with Brain Metastasis. *Korean J Radiol*. (2018) 19:783–91. doi: 10.3348/kjr.2018.19.4.783

26. Kushnirsky M, Nguyen V, Katz JS, Steinklein J, Rosen L, Warshall C, et al. Time-delayed contrast-enhanced MRI improves detection of brain metastases and apparent treatment volumes. *J Neurosurg*. (2016) 124:489–95. doi: 10.3171/2015.2.JNS141993

27. Jeon JY, Choi JW, Roh HG, Moon WJ. Effect of imaging time in the magnetic resonance detection of intracerebral metastases using single dose gadobutrol. *Korean J Radiol*. (2014) 15:145–50. doi: 10.3348/kjr.2014.15.1.145

28. Russell EJ, Geremia GK, Johnson CE, Huckman MS, Ramsey RG, Washburn-Bleck J, et al. Multiple cerebral metastases: detectability with Gd-DTPA-enhanced MR imaging. *Radiol*. (1987) 165:609–17. doi: 10.1148/radiology.165.3.3317495

29. Chen M, Wang P, Guo Y, Yin Y, Wang L, Su Y, et al. The effect of time delay for magnetic resonance contrast-enhanced scan on imaging for small-volume brain metastases. *NeuroImage Clin*. (2022) 36:103223. doi: 10.1016/j.nicl.2022.103223

30. Runge VM, Wells JW, Williams NM. Magnetic resonance imaging of an experimental model of intracranial metastatic disease. A study of lesion detectability. *Invest Radiol*. (1994) 29:1050–6. doi: 10.1097/00004424-199412000-00007

31. Yuh WT, Fisher DJ, Runge VM, Atlas SW, Harms SE, Maravilla KR, et al. Phase III multicenter trial of high-dose gadoteridol in MR evaluation of brain metastases. *AJNR Am J Neuroradiol*. (1994) 15:1037–51.

32. Runge VM, Wells JW, Nelson KL, Linville PM. MR imaging detection of cerebral metastases with a single injection of high-dose gadoteridol. *J Magnetic Resonance Imaging: JMRI*. (1994) 4:669–73. doi: 10.1002/jmri.1880040509

33. Yuh WT, Tali ET, Nguyen HD, Simonson TM, Mayr NA, Fisher DJ. The effect of contrast dose, imaging time, and lesion size in the MR detection of intracerebral metastasis. *AJNR Am J Neuroradiol*. (1995) 16:373–80.

34. Jin T, Ge M, Huang R, Yang Y, Liu T, Zhan Q, et al. Utility of contrast-enhanced T2 FLAIR for imaging brain metastases using a half-dose high-relaxivity contrast agent. *AJNR Am J Neuroradiol*. (2021) 42:457–63. doi: 10.3174/ajnr.A6931

35. Oguz KK, Cila A. Rim enhancement of meningiomas on fast FLAIR imaging. *Neuroradiology*. (2003) 45:78–81. doi: 10.1007/s00234-002-0914-8

36. Fukuoka H, Hirai T, Okuda T, Shigematsu Y, Sasao A, Kimura E, et al. Comparison of the added value of contrast-enhanced 3D fluid-attenuated inversion recovery and magnetization-prepared rapid acquisition of gradient echo sequences in relation to conventional postcontrast T1-weighted images for the evaluation of leptomeningeal diseases at 3T. *AJNR Am J Neuroradiol*. (2010) 31:868–73. doi: 10.3174/ajnr.A1937

37. Seong M, Park S, Kim ST, Park SG, Kim YK, Kim HJ, et al. Diagnostic accuracy of MR imaging of patients with leptomeningeal seeding from lung adenocarcinoma based on 2017 RANO proposal: added value of contrast-enhanced 2D axial T2 FLAIR. *J Neurooncol*. (2020) 149:367–72. doi: 10.1007/s11060-020-03617-2

38. Jin T, Zhang H, Liu X, Kong X, Makamure J, Chen Z, et al. Enhancement degree of brain metastases: correlation analysis between enhanced T2 FLAIR and vascular permeability parameters of dynamic contrast-enhanced MRI. *Eur Radiol*. (2021) 31:5595–604. doi: 10.1007/s00330-020-07625-8

39. Ahn SJ, Chung TS, Chang JH, Lee SK. The added value of double dose gadolinium enhanced 3D T2 fluid-attenuated inversion recovery for evaluating small brain metastases. *Yonsei Med J*. (2014) 55:1231–7. doi: 10.3349/ymj.2014.55.5.1231

40. Chen W. Clinical applications of PET in brain tumors. *J Nucl Med*. (2007) 48:1468–81. doi: 10.2967/jnumed.106.037689

41. Langen KJ, Galldiks N. Update on amino acid PET of brain tumours. *Curr Opin Neurol*. (2018) 31:354–61. doi: 10.1097/WCO.0000000000000574

42. Galldiks N, Langen KJ, Albert NL, Chamberlain M, Soffietti R, Kim MM, et al. PET imaging in patients with brain metastasis-report of the RANO/PET group. *Neuro Oncol*. (2019) 21:585–95. doi: 10.1093/neuonc/noz003

43. Li Y, Jin G, Su D. Comparison of Gadolinium-enhanced MRI and 18FDG PET/PET-CT for the diagnosis of brain metastases in lung cancer patients: A meta-analysis of 5 prospective studies. *Oncotarget*. (2017) 8:35743–9. doi: 10.18632/oncotarget.16182

44. Guo L, Wang G, Feng Y, Yu T, Guo Y, Bai X, et al. Diffusion and perfusion weighted magnetic resonance imaging for tumor volume definition in radiotherapy of brain tumors. *Radiat Oncol*. (2016) 11:123. doi: 10.1186/s13014-016-0702-y

45. Singnurkar A, Poon R, Metser U. Comparison of 18F-FDG-PET/CT and 18F-FDG-PET/MR imaging in oncology: a systematic review. *Ann Nucl Med*. (2017) 31:366–78. doi: 10.1007/s12149-017-1164-5

46. Sekine T, Barbosa FG, Sah BR, Mader CE, Delso G, Burger IA, et al. PET/MR outperforms PET/CT in suspected occult tumors. *Clin Nucl Med*. (2017) 42:e88–95. doi: 10.1097/RLU.0000000000001461

47. Popp I, Weber WA, Combs SE, Yuh WTC, Grosu AL. Neuroimaging for radiation therapy of brain tumors. *Topics Magnetic Resonance Imaging: TMRI*. (2019) 28:63–71. doi: 10.1097/rmr.0000000000000198

48. Cho SJ, Sunwoo L, Baik SH, Bae YJ, Choi BS, Kim JH. Brain metastasis detection using machine learning: a systematic review and meta-analysis. *Neuro Oncol*. (2021) 23:214–25. doi: 10.1093/neuonc/noaa232

49. Grovik E, Yi D, Iv M, Tong E, Rubin D, Zaharchuk G. Deep learning enables automatic detection and segmentation of brain metastases on multisequence MRI. *J Magn Reson Imaging*. (2020) 51:175–82. doi: 10.1002/jmri.26766

50. Zhou Z, Sanders JW, Johnson JM, Gule-Monroe MK, Chen MM, Briere TM, et al. Computer-aided detection of brain metastases in T1-weighted MRI for stereotactic radiosurgery using deep learning single-shot detectors. *Radiol*. (2020) 295:407–15. doi: 10.1148/radiol.2020191479

51. Amemiya S, Takao H, Kato S, Yamashita H, Sakamoto N, Abe O. Feature-fusion improves MRI single-shot deep learning detection of small brain metastases. *J Neuroimaging*. (2022) 32:111–9. doi: 10.1111/jon.12916

52. Li R, Guo Y, Zhao Z, Chen M, Liu X, Gong G, et al. MRI-based two-stage deep learning model for automatic detection and segmentation of brain metastases. *Eur Radiol*. (2023) 33:3521–31. doi: 10.1007/s00330-023-09420-7

53. Jensen R, Salzman K, Schabel M. Preoperative dynamic contrast-enhanced mri correlates with molecular markers of hypoxia and vascularity in specific areas of intratumoral microenvironment and is predictive of patient outcome. *Neuro-Oncology*. (2014) 16:iii13. doi: 10.1093/neuonc/nou206.47

54. Hou C, Gong G, Wang L, Su Y, Lu J, Yin Y. Study of sub-region segmentation of brain metastases based on magnetic resonance perfusion imaging. *Chin J Radiat Oncol*. (2021) 30:1047–53. doi: 10.3760/cma.j.cn113030-20200613-00306

55. Li M, Zhang Q, Yang K. Role of MRI-based functional imaging in improving the therapeutic index of radiotherapy in cancer treatment. *Front Oncol*. (2021) 11:645177. doi: 10.3389/fonc.2021.645177

56. Djan I, Petrovic B, Erak M, Nikolic I, Lucic S. Radiotherapy treatment planning: benefits of CT-MR image registration and fusion in tumor volume delineation. *Vojnosanit Pregl*. (2013) 70:735–9. doi: 10.2298/vsp110404001d

57. Scola E, Desideri I, Bianchi A, Gadda D, Busto G, Fiorenza A, et al. Assessment of brain tumors by magnetic resonance dynamic susceptibility contrast perfusion-weighted imaging and computed tomography perfusion: a comparison study. *Radiol Med*. (2022) 127:664–72. doi: 10.1007/s11547-022-01470-z

58. Soni N, Dhanota DPS, Kumar S, Jaiswal AK, Srivastava AK. Perfusion MR imaging of enhancing brain tumors: Comparison of arterial spin labeling technique with dynamic susceptibility contrast technique. *Neurol India*. (2017) 65:1046–52. doi: 10.4103/neuroIndia.NI_871_16

59. Hou C, Yin H, Gong G, Wang L, Su Y, Lu J, et al. A novel approach for dose painting radiotherapy of brain metastases guided by mr perfusion images. *Front Oncol*. (2022) 12:828312. doi: 10.3389/fonc.2022.828312

60. Zhong Y, Yang Q, Liu Z, Wang Y, Li L, Wen J, et al. The value of MRI plain scan and DWI in the diagnosis of brain metastases. *Chin J Cancer*. (2021) 43:466–71. doi: 10.3760/cma.j.cn112152-20190313-00153

frontiers | Frontiers in Oncology

TYPE Original Research
PUBLISHED 12 June 2024
DOI 10.3389/fonc.2024.1333642



OPEN ACCESS

EDITED BY
Timothy James Kinsella,
Brown University, United States

REVIEWED BY
Stefano Vagge,
Ente Ospedaliero Ospedali Galliera, Italy
Andrew Wenhua Ju,
East Carolina University, United States
Susanne Rogers,
Aarau Cantonal Hospital, Switzerland

*CORRESPONDENCE
Dalong Pang
dalong.pang@gunet.georgetown.edu

RECEIVED 05 November 2023
ACCEPTED 21 May 2024
PUBLISHED 12 June 2024

CITATION
Niu Y, Rashid A, Lee J-m, Carrasquilla M, Conroy DR, Collins BT, Satinsky A, Unger KR and Pang D (2024) Comparative analysis of plan quality and delivery efficiency: ZAP-X vs. CyberKnife for brain metastases treatment. *Front. Oncol.* 14:1333642. doi: 10.3389/fonc.2024.1333642



# Comparative analysis of plan quality and delivery efficiency: ZAP-X vs. CyberKnife for brain metastases treatment

Ying Niu, Abdul Rashid, Jui-min Lee, Michael Carrasquilla, Dylan R. Conroy, Brian T. Collins, Andrew Satinsky, Keith R. Unger and Dalong Pang*

Department of Radiation Medicine, Georgetown University Hospital, Washington, DC, United States

**Purpose/Objectives:** ZAP-X, a novel and dedicated radiosurgery (SRS) system, has recently emerged, while CyberKnife has solidified its position as a versatile solution for SRS and stereotactic body radiation therapy over the past two decades. This study aims to compare the dosimetric performance and delivery efficiency of ZAP-X and CyberKnife in treating brain metastases of varying target sizes, employing circular collimation.

**Methods and materials:** Twenty-three patients, encompassing a total of 47 brain metastases, were included in the creation of comparative plans of ZAP-X and CyberKnife for analysis. The comparative plans were generated to achieve identical prescription doses for the targets, while adhering to the same dose constraints for organs at risk (OAR). The prescription isodose percentage was optimized within the range of 97–100% for each plan to ensure effective target-volume coverage. To assess plan quality, indices such as conformity, homogeneity, and gradient (CI, HI, and GI) were computed, along with the reporting of total brain volumes receiving 12Gy and 10Gy. Estimated treatment time and monitor units (MUs) were compared between the two modalities in evaluating delivery efficiency.

**Results:** Overall, CyberKnife achieved better CI and HI, while ZAP-X exhibited better GI and a smaller irradiated volume for the normal brain. The superiority of CyberKnife's plan conformity was more pronounced for target size less than 1 cc and greater than 10 cc. Conversely, the advantage of ZAP-X's plan dose gradient was more notable for target sizes under 10 cc. The homogeneity of ZAP-X plans, employing multiple isocenters, displayed a strong correlation with the target's shape and the planner's experience in placing isocenters. Generally, the estimated treatment time was similar between the two modalities, and the delivery efficiency was significantly impacted by the chosen collimation sizes for both modalities.

**Conclusion:** This study demonstrates that, within the range of target sizes within the patient cohort, plans generated by ZAP-X and CyberKnife exhibit comparable plan quality and delivery efficiency. At present, with the current platform of the two modalities, CyberKnife outperforms ZAP-X in terms of conformity and homogeneity, while ZAP-X tends to produce plans with a more rapid dose falloff.

KEYWORDS

**stereotactic radiosurgery, brain metastases, CyberKnife, ZAP-X, plan quality, delivery efficiency**

# 1 Introduction

Brain metastases are the most prevalent cancerous lesions in the brain, with an estimated incidence rate of 20–40% among cancer patients (1–3). Radiotherapy serves as a viable treatment option for metastatic brain tumors, either as a primary solution or in combination with systemic chemotherapy. Historically, whole brain radiotherapy (WBRT) was the standard approach for patients with or without surgery. However, due to concerns regarding toxicity, WBRT is now commonly deferred (4, 5). As a focal technique that minimizes damage to surrounding healthy tissues, stereotactic radiosurgery (SRS) has emerged as a preferred management option for brain metastases of patients (6). Numerous studies have highlighted the advantages of using SRS or adding SRS to WBRT for brain metastases, such as improved local control, comparable survival rates, and reduced cognitive deterioration (7–9). Consequently, there has been a steady increase in the percentage of patients receiving SRS treatment (10, 11).

The advantages of SRS treatment stem from the dosimetric characteristics of its plans, specifically the steep dose gradient and high dose conformity, which enable dose intensification beyond the capabilities of conventional treatments (12–14). SRS is offered as a treatment solution by various radiation modalities, including cobalt-60 based systems like the Gamma Knife (15, 16), as well as systems with specially equipped linear accelerators (Linacs), such as the Varian Edge (Varian, Palo Alto, CA, USA) (17), Brainlab Novalis (Brainlab, Munich, Germany) (18), CyberKnife (Accuray Inc. Sunnyvale, California) (19) and the more recently developed ZAP-X (ZAP Surgical, San Carlos, CA) (20).

CyberKnife, a robotic radiosurgery system, was introduced commercially in the late 1990's. Its standout advantage lies in its ability to deliver non-coplanar radiation fields with ease and real-time tumor tracking. Initially developed for treating intracranial lesions, CyberKnife has expanded to treat lesions throughout the body, benefiting thousands of patients worldwide (21). The system features a compact 6-MV X-band Linac and a versatile robotic arm equipped with six joints, allowing for both rotational and translational movement of the radiation source (22). The radiation source follows a predetermined path that connects multiple beam entry locations (i.e., nodes) on a virtual spherical surface. This unique configuration allows for radiation crossfire from nodes distributed across solid angles exceeding $2\pi$ steradians. Furthermore, the radiation beams can be precisely directed to non-isocentric directions from each node. CyberKnife possesses a source axial distance (SAD) ranging from 65 to 80 cm, with a dose rate of up to 1000 monitor unit per minute (MU/min). It offers a selection of fixed conical cones and variable circular collimators (i.e., IRIS$^{TM}$) with 12 different collimation diameters from 5 to 60 mm. The IRIS collimator is made of two banks of six tungsten segments, each creating a hexagonal aperture to produce a 12-sided field shape to approximate a circle (23). Notably, a recent addition to the system includes Multileaf collimator (MLC) technology (24). Frameless intracranial treatment is facilitated by the system's imaging guidance, which employs a pair of orthogonal room-mounted kV generators and panels. This imaging guidance provides reconstructed 3D coordinates of the patient's skull for precise initial setup and real-time tracking during treatment delivery. To enhance precision, a customized mesh face mask is prepared during simulation phase and is subsequently utilized for treatment. Prior to treatment initiation, any deviation in the initial setup is corrected through the controlled movement of robotic couch. Throughout the delivery of treatment, the real-time patient movement is compensated by the movement of robotic arm (25).

ZAP-X is a cutting-edge platform that emerged in the market just a few years ago. Rather than other SRS systems that require a shielded radiation vault, ZAP-X's standout feature is its self-contained, self-shielded design (26–28). Its primary focus is on the precise treatment of intracranial lesions without compromising versatility. ZAP-X incorporates a 2.7-MV S-band Linac, which is mounted on a gyroscope-like gantry with independent dual rotating axes, centered around a unique common isocenter. Notably, it offers delivery of non-coplanar radiation beams through moving the radiation source on a virtual spherical surface, covering approximately $2\pi$ steradians of solid angles. Additionally, ZAP-X features a compact 45 cm SAD and a dose rate of up to 1500 MU/min. It provides circular collimation with eight different diameters, ranging from 4 to 25 mm. The collimator size can be changed automatically during treatment through a novel tungsten wheel collimator (29). For imaging guidance, ZAP-X employs a gantry-mounted kV imaging system, allowing the capturing of images from specified angles to achieve precise initial skull alignment. This system also facilitates continuous image acquisition at predetermined intervals, ensuring seamless rotation of gantry during treatment delivery. Skull offsets are calculated by aligning the captured images with real-time generated Digitally Reconstructed Radiographs (DRRs). Based on these calculated offsets, the isocenter position is accurately corrected in patient's head using a patient couch equipped with translational movement capabilities. In line with Cyberknife, ZAP-X also utilizes a customized mesh face mask to support patient immobilization.

Both ZAP-X and CyberKnife utilize compact Linac designs and offer non-coplanar radiation delivery with a large range of beam geometry in terms of solid angle, which is crucial for achieving desired optimized plans in intracranial SRS. However, there are notable differences between the two systems. ZAP-X employs an isocentric technique with couch movement, allowing for the delivery of multiple isocenters within a single treatment. In contrast, CykerKnife delivers non-isocentric beams without requiring couch movement during treatment delivery. Both systems employ circular collimation, offering similar collimating sizes for lesions with small and intermediate volumes. However, CyberKnife offers larger collimator sizes to accommodate lesions with large volumes. It is worth mentioning that ZAP-X, with its shorter SAD and lower beam energy, exhibits characteristics that align more closely with Gamma Knife. A study conducted by Georg et al. focused on the peripheral dose fall-off of ZAP-X using various

detectors, and the results indicate that the beam characteristics of ZAP-X are more like those of Gamma Knife (30). The differences in machine characteristics between ZAP-X and CyberKnife may potentially impact their plan parameters, which motivates further investigation into the dosimetric comparison between these two modalities. Romanelli et al. conducted a preliminary dosimetric comparison of trigeminal neuralgia plans between ZAP-X and CyberKnife. They found that the two modalities yielded comparable plans for such functional treatment, and also highlighted the potential clinical value of ZAP-X in low dose region (31). Several studies have investigated the dosimetric characteristic of CyberKnife compared with other techniques, such as Gamma Knife and volumetric modulated arc therapy (VMAT) (32–35). However, to the best of our knowledge, no systematic study has been published comparing the dosimetric performance and delivery efficiency of ZAP-X and CyberKnife for brain metastases with varying target sizes. Therefore, our objective is to perform such a comparison, capitalizing on our extensive experience of CyberKnife SRS and more recent implementation of ZAP-X SRS since 2020.

# 2 Materials and methods

## 2.1 Patient cohort

In this study, a cohort of 23 patients who underwent treatment between 2018 and 2021 were selected. Among these patients, 12 received CyberKnife treatment and 11 patients received ZAP-X treatment. The cohort comprised a total of 47 lesions, which were treated using 28 individual treatment plans. Each plan targeted 1 to 6 metastases. Notably, the anatomical locations of the lesions were well distributed within the cohort, as evidenced by Table 1. Additionally, Table 2 provides an overview of the plan distribution concerning the number of lesions and the volume size of targets. The majority of plans (i.e., 89.3%) targeted 1 or 2 lesions. The plan distribution in terms of the sizes of the targeted lesions displayed a well-balanced representation. To facilitate comparison, an alternative ZAP-X/CyberKnife plan was generated for each original CyberKnife/ZAP-X treatment plan, ensuring attainment of the same clinical goal. The median prescription dose across the 28 plans was 24 Gy (i.e., range, 15–30 Gy), administered over 1 to 5 fractions.

## 2.2 Imaging and target delineation

The planning CT series was obtained with a slice thickness of no more than 1 mm. To aid in contouring, T1-weighted MRI images with or without contrast in 1 mm thickness were fused with the planning CT. Experienced radiation oncologists delineated the gross tumor volume (GTV) as well as the organs at risk (OARs). The target volume for all patients in the study was defined as the planning target volume (PTV), which incorporated setup margins. In this study, PTV was created from GTV using margins of 0 or 1 mm for all selected patients. The prescription dose for all patients was designated to the PTV. Normal brain tissue was defined as the entire brain excluding the PTV.

TABLE 1 Summary of tumor locations (47 lesions).

| | | n | n (%) |
|---|---|---|---|
| Frontal | Left | 4 | 8.5% |
| | Right | 7 | 14.9% |
| Temporal | Left | 4 | 8.5% |
| | Right | 3 | 6.4% |
| Parieto-occipital | Left | 6 | 12.8% |
| | Right | 10 | 21.3% |
| Cerebellar | Left | 5 | 10.6% |
| | Right | 6 | 12.8% |
| Vermis | | 2 | 4.3% |

## 2.3 Treatment planning

ZAP-X planning was performed using the dedicated ZAP-X treatment planning system (referred to as "ZAP-X TPS"). The ZAP-X TPS incorporates a sphere packing scheme with inverse planning (36) and supports both manual and automatic isocenter placement. Considering the compact design of ZAP-X, a simulation is conducted for each determined isocenter position from sphere packing to establish a safety zone for gantry movement, ensuring collision-free delivery based on a conservative patient model with appropriate size and margins. Subsequently, all available beam angles for all isocenter positions are determined, forming a pool for inverse planning. In the inverse planning process, the weights of the beams in the pool are optimized using linear and quadratic programing, based on the planner's defined constraints. For each isocenter, the optimized beams with non-zero MUs are connected

TABLE 2 Statistics summary of 28 treatment Plans.

| | | No. of Plans | % of Plans |
|---|---|---|---|
| No. of Lesions per plan | 1 | 18 | 64.3% |
| | 2 | 7 | 25.0% |
| | 4 -6 | 3 | 10.7% |
| Total volume of plan | <1 cc | 9 | 32.1% |
| | [1 cc, 3 cc) | 7 | 25.0% |
| | [3 cc, 10 cc) | 7 | 25.0% |
| | >10 cc | 5 | 17.9% |
| Fraction No. of plan prescription | 1 | 12 | 42.9% |
| | 3 | 13 | 46.4% |
| | 5 | 3 | 10.7% |

to form a delivery path using the traveling salesman algorithm, minimizing delivery time while avoiding collision. In cases where the target is small and regular in shape, the isocenters are typically placed at the center of targets with suitable collimator sizes. For larger or irregularly shaped targets, multiple isocenters are employed, with each isocenter covering the target partially. These multiple isocenters are typically positioned near the boundary of the target to minimize the overlaps between shots within target, resulting in a desired plan uniformity.

Treatment planning for CyberKnife was performed using the Accuray Precision 2.0 treatment planning system (referred to as "CyberKnife TPS") on the CyberKnife VSI platform. In this study, all plans were generated using the variable IRIS$^{TM}$ collimator for the range of tumor size in this study. The CyberKnife TPS offers both short and full paths with different numbers of nodes, and for this study, the full path with a larger number of nodes was utilized. The VOLO optimizer, operating under the inverse planning scheme, was employed (37). The CyberKnife TPS allows for manual or automatic selection of initial collimator sizes for optimization. The choice of collimator sizes depends on the target sizes and the planner's preference for conformity and homogeneity. Planners can choose to activate multiple collimator sizes to maximize dose-profile sculpting capabilities or select a minimal number of collimator sizes to streamline computational efficiency without compromising plan quality. Within the CyberKnife TPS, the "target boundary distance" option allows targeting of beams at a specific distance from the delineated target boundary. This parameter can be adjusted by the planner to emphasize either homogeneity or conformity. In this study, a target boundary distance within 5 mm outward was commonly employed.

ZAP-X and CyberKnife treatment planning systems share several design features. One notable feature is the ability to create multiple hollow contour sets, known as "shells", which provide control over plan conformity and dose falloff. Planner can adjust the objectives and penalties assigned to these shells to fine-tune plan quality in inverse planning. In this study, the CyberKnife planer typically generated three sets of shells to manage spillages at different dose levels (e.g., 3 mm, 10 mm, and 20 mm from target boundary for high, middle, and low dose regions, respectively). The sizes of these shells were adjustable based on the planer's preference. In contrast, the ZAP-X TPS offers predetermined shell sizes to planers, including 0 mm, 1 mm, 5 mm, and 10 mm from the target boundary. Another shared feature is that both systems support the ray-tracing algorithm in dose calculation for tissue heterogeneity, although CyberKnife TPS offers the additional option of Monte Carlo dose calculation. For this study, we employed the ray-tracing algorithm for dose calculation in both treatment planning systems.

In this study, the primary objective for both ZAP-X and CyberKnife plans was to achieve target-volume coverage between 97–100% while determining the prescribed isodose percentage (PIP) relative to the maximum dose. Additionally, stringent adherence to the dose constraints specified in the AAPM TG101 guidelines was maintained for all OARs (38). Special emphasis was placed on minimizing the extent of low dose regions to prevent any 30% isodose regions from extending beyond the immediate target vicinity.

## 2.4 Comparison metrics

Dose conformity of each plan was assessed using the Radiation Therapy Oncology Group (RTOG) conformity index (CI) and the modified Paddick conformity index (nCI) defined as follows:

$$CI = \frac{V_{Rx}}{V_T} \tag{1}$$

$$nCI = \frac{V_T \times V_{Rx}}{(V_{T,\,Rx})^2} \tag{2}$$

Herein, $V_T$ is the planning target volume, $V_{Rx}$ is the total volume covered by prescription dose, and $V_{T,\,Rx}$ is the partial volume of target covered by prescription dose.

Dose homogeneity was assessed for each target, with the homogeneity index (HI) defined by the equation,

$$HI = \frac{D_{max}}{D_{Rx}} \tag{3}$$

where $D_{max}$ is the maximum dose to the target and $D_{Rx}$ is the prescription dose.

The dose fall-off was assessed for each plan using the prescription isodose volume, i.e., $V_{x\,\%\,Rx}$, which represents the volume receiving at least x% of prescription dose. Two commonly used gradient indices (GI) are calculated as follows:

$$GI50\,\% = \frac{V_{50\,\%\,RX}}{V_{100\,\%\,Rx}} \tag{4}$$

$$GI25\,\% = \frac{V_{25\,\%\,RX}}{V_{100\,\%\,Rx}} \tag{5}$$

In addition, two more surrogates were also calculated as follows,

$$R50\,\% = \frac{V_{50\,\%\,RX}}{V_T} \tag{6}$$

$$R25\,\% = \frac{V_{25\,\%\,RX}}{V_T} \tag{7}$$

The R50% and R25% indices are useful for evaluating dose fall-off performance while accounting for differences in conformity. These indices express the ratios of absolute irradiated volumes to the target volume, which allows for a more accurate assessment of dose fall-off without the influence of variations in conformity.

V12 and V10, which are the volumes of normal brain tissue receiving at least 12 Gy and 10 Gy, were reported for plan comparison as predictors of brain necrosis for single-fraction treatments (39).

The delivery efficiency was evaluated with estimated treatment time of each fraction from TPS and MU coefficient defined as the following,

$$C\_MU = \frac{MU/Fx}{Rx \times V_T} \tag{8}$$

The estimated treatment time was calculated as the dry run time plus estimated patient setup and imaging time interval. For

CyberKnife, the patient initial setup time was set as 5 minutes in TPS, and the imaging time interval is 1 minute. For ZAP-X, the patient initial setup time is also 5 minutes, and there is no imaging time interval needed because ZAP-X imaging tracking does not interrupt treatment delivery.

To assess the difference of indices and parameters between the ZAP-X and CyberKnife plans, the two tailed t-test was performed, and a P value less than 0.05 was considered to indicate statistical significance.

## 3 Results

Table 3 provides a summary of the comparison for conformity, homogeneity, dose falloff and delivery efficiency of all plans and targets between ZAP-X and CyberKnife. The results indicate that the CyberKnife system demonstrated statistically significant better CI and nCI (see Equations (1) and (2)) compared to ZAP-X(p values shown in Table 3). However, there is no significant difference in target-volume coverage between the two modalities. On average, CyberKnife plans exhibited statistically significant smaller HI (see Equation (3)), while the ZAP-X plans showed a lower minimum dose, higher mean dose and higher maximum dose, indicating greater dose heterogeneity within the targets. Conversely, the ZAP-X plans demonstrated better dose falloff, as indicated by the GI50%, GI25%, R50% and R25% indices (see Equations (4–7)), which reflect the benefits in the medium and low dose regions. Additionally, the ZAP-X plans achieved significantly smaller irradiated volume of normal brain tissues, as evidenced by the V12 and V10 parameters, while the mean dose to whole brain remained comparable between the two modalities. In terms of delivery efficiency, there was no significant difference in the estimated treatment time between modalities, although ZAP-X plans generally required fewer MUs compared to CyberKnife plans.

The comparison of plan conformity was further refined based on target sizes. Figure 1 illustrates the graphical comparison of CI for plans generated by ZAP-X and CyberKnife across various target size ranges. The overall findings indicate that CyberKnife plans exhibit superior conformity compared to ZAP-X plans. Particularly, for very small tumors (< 1 cc), CyberKnife achieved significantly smaller CI values than ZAP-X. Among the 9 plans evaluated, the mean CI values for ZAP-X and CyberKnife were 1.53 and 1.38, respectively. However, the difference in CI was less pronounced for intermediate-sized tumors. Among the 14 plans with medium-sized targets (between 1 cc and 10 cc), the mean CI values for ZAP-X and CyberKnife were 1.38 and 1.31, respectively. Conversely, for large tumors (> 10 cc), the disparity in CI became more significant. Among the 5 plans assessed, the mean CI values for ZAP-X and CyberKnife were 1.34 and 1.19, respectively.

Figure 2 presents a detailed comparison of isodose volumes at various percentage levels, ranging from 100% to 10%, with small increments. The analysis included 23 plans with target volumes less than 10 cc, with a median volume size of 1.70 cc, ranging from 0.15 cc to 8.67 cc. Across three target size ranges demonstrated in Figure 2, CyberKnife consistently outperformed ZAP-X in terms of V100%, demonstrating superior conformity. For targets smaller

TABLE 3 Comparison of dosimetry indices and parameters for plan quality and delivery efficiency.

| | | Cyberknife | ZAP-X | p *Value* |
|---|---|---|---|---|
| | | *Median (range)* | *Median (range)* | |
| Conformity | CI | 1.28 (1.10–1.76) | 1.41 (1.19 - 1.86) | <0.001 |
| | nCI | 1.30 (1.10–1.76) | 1.41 (1.20 - 1.88) | <0.001 |
| | Coverage(%) | 99.87 (97.22 -100) | 99.64 (98.46–100) | 0.90 |
| Homogeneity | HI | 1.19 (1.07 - 1.27) | 1.39 (1.13 - 2.00) | < 0.0001 |
| | Dmin (%$D_{Rx}$)* | 1.00 (0.92 -1.11) | 0.95 (0.81 - 1.01) | < 0.0001 |
| | Dmean (%$D_{Rx}$) | 1.11 (1.04 - 1.15) | 1.23 (1.09 - 1.44) | < 0.0001 |
| Dose falloff | GI50% | 5.27 (3.39 - 8.98) | 3.14 (2.70 - 3.81) | < 0.0001 |
| | GI25% | 16.53 (8.17 - 31.02) | 11.72 (7.76 - 18.64) | < 0.0001 |
| | R50% | 6.86 (3.95 - 12.85) | 4.53 (3.57 - 5.48) | < 0.0001 |
| | R25% | 20.04 (10.18 - 41.70) | 16.49 (10.90 - 25.20) | < 0.001 |
| Normal brain | V12 (cc) ** | 4.34 (1.23 – 20.84) | 1.84 (0.51 – 13.64) | < 0.01 |
| | V10 (cc) | 6.05 (1.73 – 29.46) | 2.69 (0.71 – 21.17) | < 0.01 |
| Whole brain | Dmean (cGy) | 116 (28 - 484) | 111 (24- 445) | 0.93 |
| Delivery efficiency | C_MU(MU/(cGy·cc))*** | 2.75 (0.26 - 9.68) | 1.84 (0.31–6.81) | < 0.001 |
| | Tx Time/Fx (mins) | 28 (17–51) | 26 (16–65) | 0.99 |

* The minimum and mean doses of target are presented as percentages of the prescription dose.
** The V12 and V10 of Normal brain tissue were calculated and compared for 12 plans with single fraction, all other parameters were compared for 28 plans.
*** The coefficient C_MU is defined in Equation (8).

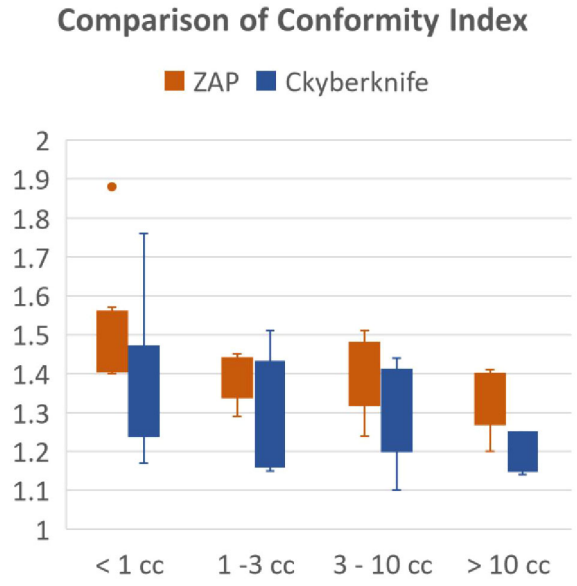


FIGURE 1
The results of the modified Paddick conformity index were compared using box plots, which were divided into four separate target size ranges.

than 1 cc, ZAP-X exhibited better dose fall-off from V90% to V10% compared to CyberKnife. For targets larger than 1 cc but less than 10 cc, ZAP-X showed statistically significant superiority over CyberKnife from V90% to V40%. However, no noticeable differences were observed between the two modalities in the low-dose range (V25% to V10%) for targets between 1 cc and 10 cc. Analyzing the 14 plans with target volumes between 1 cc and 10 cc, the mean R25% values for ZAP-X and CyberKnife were 17.1 and 20.6, respectively, with a p-value of 0.096. Additionally, there were five plans with a target-volume range larger than 10 cc, not depicted in Figure 2, with a median volume size of 21.96 cc, ranging from 14.44 cc to 25.83 cc. Comparing the dose falloff performance between ZAP-X and CyberKnife for these five plans, the mean R50% values were 4.55 and 4.38, respectively, with a p-value of 0.66. The mean R25% values for the two modalities were 14.6 and 13.1, respectively, with a p-value of 0.33. These findings indicate that there are no observable differences in both the medium and low-dose regions between the two modalities for targets larger than 10 cc.

Figure 3 displays a comparison of the HI results for all lesions treated with CyberKnife and ZAP-X. The results are presented as histograms, representing the percentage of targets within each HI range. In the CyberKnife plans, all targets achieved an HI value of less than 1.3. Conversely, the ZAP-X plans exhibited a broader distribution of HI values, with 83% of targets having an HI less than 1.6, and 64% of targets with an HI less than 1.5. Notably, the HI distributions differed between the ZAP-X targets treated with a single isocenter and those treated with multiple isocenters. Among all ZAP-X targets, 55.3% were covered by a single isocenter, with a median HI value of 1.31, and 92.3% of these targets achieved an HI less than 1.5. For the remaining 44.7% of targets treated with multiple isocenters, 71.4% of them exhibited an HI greater than 1.5.

In Figure 4, a comparative analysis of dose distributions for a small target in the skull base is presented. The optimized beam orientations of the two modalities are influenced by the target's location, resulting in distinct dosimetric characteristics. The cut views of 2D dose distribution reveal that ZAP-X benefits from its posterior beams, which offer the shortest radiological paths to the target. On the other hand, CyberKnife relies on its lateral and superior beams. The ZAP-X plan utilized a single 12.5 mm collimator size isocenter, resulting in 99.3% target-volume coverage, a CI of 1.40, a HI of 1.45, and a GI50% of 2.81. In contrast, the CyberKnife plan employed collimation sizes of 10 and 12.5 mm, achieving 100% target-volume coverage, a CI of 1.48, an HI of 1.23, and a GI50% of 5.56. Additional plan parameters related to delivery efficiency can be found in Table 4 under plan ID 5.

Figure 5 presents a postoperative case with a large target volume. For ZAP-X, a total of 12 isocenters were used with collimation sizes ranging from 15 to 25 mm. The strategic placement of most isocenters near the boundary of the target volume aimed to achieve optimal plan uniformity. The resulting ZAP-X plan demonstrated excellent performance with 99.7% target-volume coverage, a CI of 1.19, a HI of 1.52, and a GI50% of 3.02. In comparison, the CyberKnife plan achieved 98.7% target-volume coverage, a CI of 1.14, an HI of 1.22, and a GI50% of 3.95. Further details on delivery efficiency and other plan parameters can be found in Table 4 under plan ID 16.

Table 4 provides a comparison of plan parameters for all plans targeting a single lesion within the cohort. The plans are listed in ascending order based on the sizes of the target volumes. Strong correlations were observed between the MU numbers of the plans with the target volume sizes, also, with the selected collimator sizes. In this study, most selected collimator sizes for both modalities were 10 mm or larger, with none smaller than 7.5 mm. CyberKnife plans consistently employed a minimum collimator size of 10 mm across all cases. Additionally, for target sizes less than 3 cc, a single collimator size of 10 mm was frequently utilized for CyberKnife plans. Conversely, the chosen minimal collimator size for ZAP-X plans varied based on the specific target size and shape. For very small lesions (plans with IDs 1 to 5 in Table 4), both modalities employed similar collimator size ranges. ZAP-X exhibited a slight improvement in delivery efficiency, requiring 15.8% fewer MUs and 2.4 minutes less in estimated delivery time, on average, compared to CyberKnife. However, these differences did not reach statistical significance (p=0.27 and 0.08, respectively). For lesions with intermediate sizes up to 3 cc (plans with IDs 6 to 11 in Table 4), CyberKnife plans utilized smaller maximal collimator sizes compared to ZAP-X. For these cases, ZAP-X demonstrated notable delivery efficiency, necessitating 44.3% fewer MUs and 8.2 minutes less in estimated delivery time, with statistically significant differences observed (p=0.007/0.002). In the cases of target sizes exceeding 3 cc (plans with IDs 12 to 18 in Table 4), the largest 25 mm collimator size of ZAP-X is frequently selected, while the maximum collimator size for CyberKnife plans reached up to 30 mm. ZAP-X exhibited a 12.6% reduction in MUs without statistical significance (p=0.40), but a statistically significant average increase of 6 minutes in estimated delivery time (p=0.02) compared to CyberKnife.

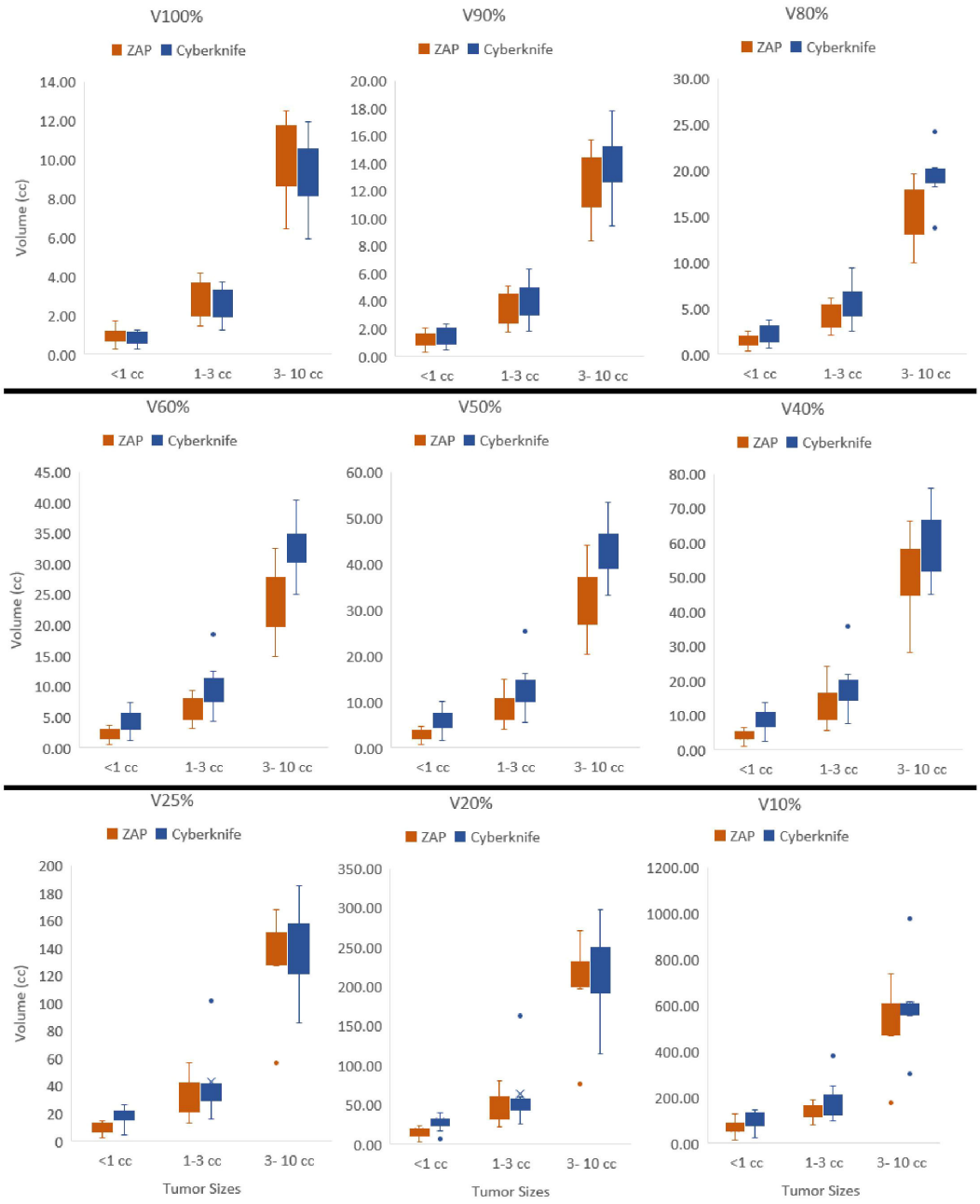


FIGURE 2
Isodose volumes were displayed as box plots comparing two modalities, i.e., V100%, V90%, V80%, V60%, V50%, V40%, V25%, V20% and V10% are the volumes enclosed by 100%, 90%, 80%, 60%, 50%, 40%, 25%, 20% and 10% of isodose surfaces normalized with prescription dose. The results were divided into three separate target size bins, i.e.,<1cc, 1–3cc and 3–10cc.

## 4 Discussions

This study presents a systematic comparison of treatment plans between ZAP-X and CyberKnife. The findings indicate that both modalities can generate treatment plans with acceptable plan quality, as shown in Table 1. In general (without considering the impact of target size), CyberKnife outperforms ZAP-X in terms of plan conformity and homogeneity, whereas ZAP-X demonstrates superior performance in dose gradient. The treatment delivery efficiency is comparable between the two modalities. Furthermore, the study reveals a correlation between dosimetry performance and delivery in relation to the target size, as illustrated in Figures 1, 2, Table 4. Specifically, for small target sizes (<1 cc), CyberKnife exhibits significant advantages in plan conformity, while ZAP-X excels in dose gradient. However, for larger target sizes, the respective advantages become less apparent.

CyberKnife employs non-isocentric beam delivery, utilizing gantry pivoting with a robotic arm to enhance flexibility. This unique feature enables the generation of highly conformal and uniform treatment plans, as evidenced by Figures 1, 3, particularly

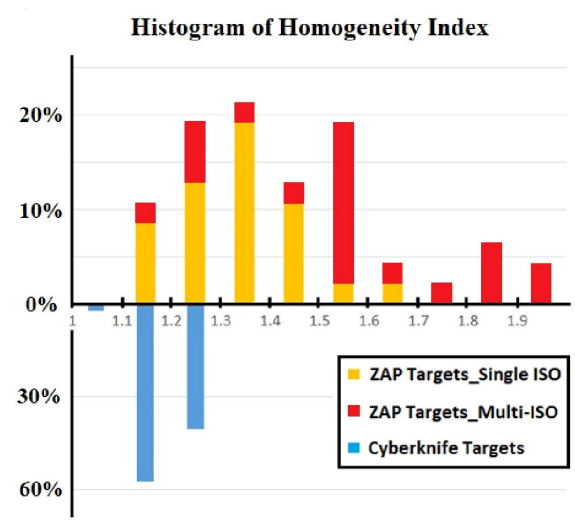


FIGURE 3
The comparison of HI was performed using differential histogram. The range of HI value is from 1.0 to 2.0 with bins of 0.1 for all 47 lesions. For each of bin of ZAP-X histogram, the targets covered by single and multiple isocenters were differentiated by different colors.

for cases involving irregular or large volumes, as illustrated in Figure 5. The CyberKnife TPS supports the creation of plans with strategically directed non-isocentric beams near the target's boundary. This approach ensures that the prescribed isodose line conforms to the target volume's surface curvature, while minimizing beam overlap within the target, thereby enhancing plan homogeneity (40), as demonstrated in Figures 5B, C.

In contrast, ZAP-X utilizes an isocentric technique that lacks the gantry pivoting flexibility seen in CyberKnife. Instead, it relies on sphere packing, similar to Gamma Knife, to address complex cases, taking advantages of its beam geometry with large solid angles. Notably, ZAP-X exhibits greater capability than Gamma Knife in manipulating shot shape by delivering optimized sparsely distributed beams to an isocenter. In cases involving multiple isocenters, once the isocenters with appropriate collimator sizes are positioned, all candidate beams associated with the isocenters are simultaneously optimized. The planning process typically involves iterative adjustments, such as manual fine-tuning of isocenter positions and collimator sizes combined with inverse planning guided by updated dose constraints. While the planner can steer the optimizer by adjusting the dose constraints, the determination of isocenter positions and collimator sizes is crucial for achieving the desired plan quality in many situations.

Generally, if multiple isocenters are placed more peripherally on the target, the resulting plan tends to exhibit improved homogeneity, as demonstrated in Figure 5B. However, due to the overlap of neighboring shots, hotspots may be unavoidable, as depicted in Figure 5C. Planners prioritize target coverage and conformity while allowing for compromises in plan homogeneity, which explains for the variation in HI values of ZAP-X plans with multiple isocenters, ranging from 1.1 to 2.0, as depicted in Figure 3.

In Figure 3, we also present an interesting finding regarding the comparison of HI-value distributions between ZAP-X plans of single isocenter and plans with multiple isocenters. It is observed that plans utilizing a single isocenter have yielded better HI values compared to plans with multiple isocenters. The median HI value of the single isocenter plans is close to that of CyberKnife. As depicted in Figure 4, in this study, a commonly employed strategy in ZAP-X planning is to use a single isocenter with a collimator size that closely matches the target diameter. This approach often leads to achieving an acceptable CI, particularly when dealing with regular target shapes. In the plans with a single isocenter, the HI value is determined by the prescribed isodose line based on desired target coverage and plan conformity, which is influenced by the flatness, shape and dose falloff of shot with optimized beams.

Although ZAP-X and CyberKnife both possess large number of spatial nodes covering solid angles for radiation crossfire exceeding $2\pi$, their respective available scopes of beam orientations differ significantly, i.e., the scope of beam orientation of ZAP-X are quite similar to Gamma Knife, whereas CyberKnife possesses the scope covering entire anterior hemisphere, however, posterior beams are restricted in access due to the limited conch height. As depicted in Figure 4, these difference in beam orientations may lead to different characteristics in dosimetry, and such difference may be influenced by the anatomical location of target.

Although ZAP-X and CyberKnife both utilize a large number of spatial nodes to cover solid angles exceeding $2\pi$ steradians for radiation crossfire, they differ in terms of their available scopes of beam orientations. ZAP-X exhibits a beam orientation scope similar to that of Gamma Knife, while CyberKnife has a scope nearly covering the entire anterior hemisphere. However, CyberKnife's access to posterior beams is limited due to the restricted couch height. This difference in beam orientations can result in discernible differences in dosimetric characteristics as depicted in Figure 4, and ultimately lead to variations in plan quality, particularly when considering the specific anatomical location of the target.

Tables 1, 4 provide evidence that, overall, ZAP-X demonstrates superior delivery efficiency in terms of MU numbers compared to CyberKnife within the studied cohort. It is important to consider that several factors can influence the MU numbers of plans using different modalities. For example, as indicated in Table 5, ZAP-X has a higher output per MU than CyberKnife at the same collimator size, while CyberKnife beams possess better penetrability, evidenced by the comparison of TPRs. However, as summarized in Table 4, the key determinant affecting the MU numbers among plans is often the selection of different collimation size ranges during plan creation. For plans with intermediate target sizes (i.e., plans with ID 6–11 in Table 4), CyberKnife planners, drawing from their experience, typically avoid selecting collimators larger than 10 mm. Conversely, for larger target volumes, CyberKnife benefits from the availability of larger collimator sizes that are not available on ZAP-X. On average, across the entire cohort, no significant difference in estimated treatment time is observed between the two systems, as the movement time of the gantry dominates the total delivery time for both modalities. Consequently, small variations in MU numbers are unlikely to result in discernable differences in delivery time.

It is important to note that this study focuses solely on the systems with circular collimation and does not include the MLC

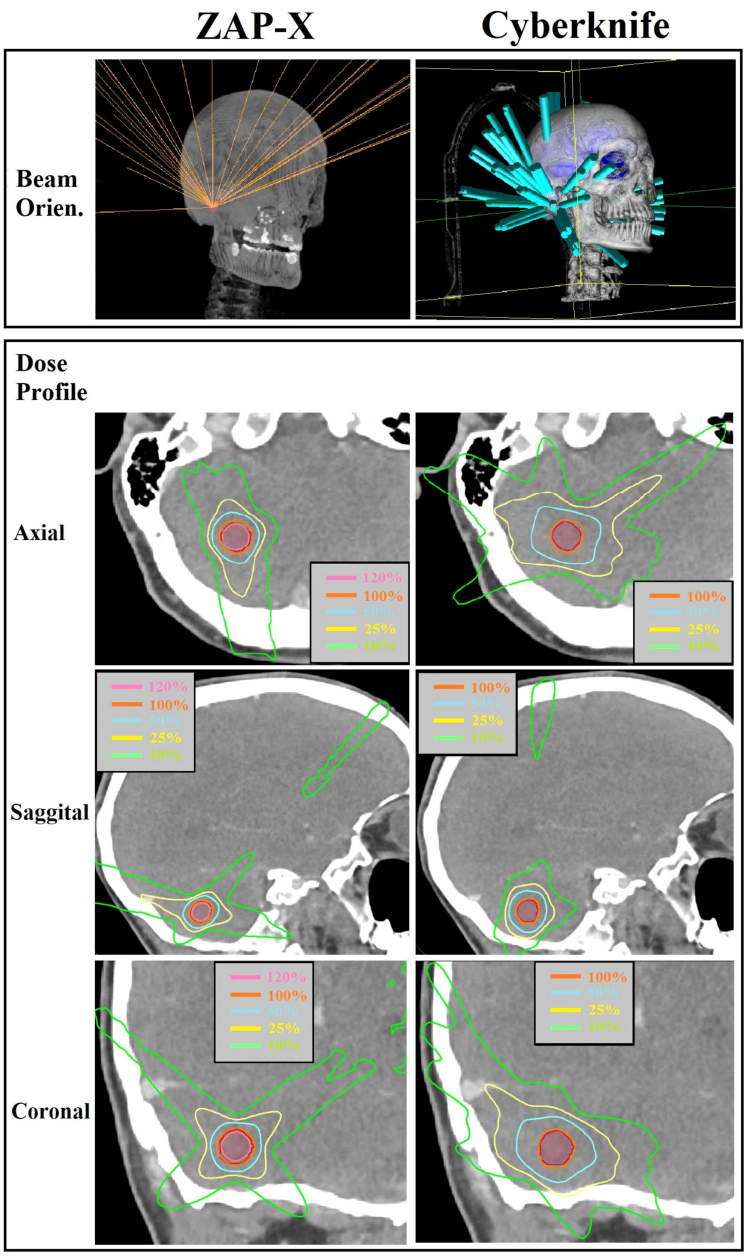


FIGURE 4
Visual comparison of beam orientation and multiplanar dose distributions between ZAP-X and CyberKnife for a representative case with small target volume (i.e., 0.84 cc). The 100% isodose line was normalized to prescribed dose.

version of CyberKnife. Additionally, it should be emphasized that the dosimetric characteristics highlighted in this study do not directly reflect the machine characteristics of the two systems, but rather the differences in dosimetric performance between the two modalities within the specific clinical implementation. These differences are influenced by machine characteristics, preferred clinical goals, and the current treatment planning capacities. The planning strategy employed in our study for both ZAP-X and CyberKnife prioritized target coverage, conformity and sparing of OARs. For plan homogeneity, a prescription isodose percentage (PIP) higher than 75% was desirable for CyberKnife plans, while PIP was maximized for ZAP-X without compromising conformity. Efforts were also made to balance dose falloff, treatment time, and other factors. Under the context of such clinical implementation, the extent of advantages of CyberKnife/ZAP-X plans in terms of plan homogeneity/dose falloff may be determined by the PIP chosen for planning and should not be concluded as a machine characteristic. Lee et al. (41) suggested that choosing a lower PIP can improve the dose falloff of CyberKnife plans while maintaining the desired plan conformity. As widely recognized in the radiosurgery community, the Gamma-knife employs a lower prescription isodose percentage, typically set at 50%, compared to the CyberKnife, which often uses 75% or higher. This is due to the machine characteristics and sphere packing technique of the

TABLE 4 Comparison of beam parameters and delivery efficiency of ZAP-X/Cyberknife for 18 plans with a single target.

| Plan ID | Target Vol.(cc) | ZAP-X ISO No. | ZAP-X/Cyberknife* | | | |
|---|---|---|---|---|---|---|
| | | | Collimator Size Range(mm)** | Beam No.*** | Tx Time (mins) | C_MU (MU/(cGy•cc)) |
| 1 | 0.15 | 1 | (7.5,7.5)/(10,10) | 36/42(39) | 18/19 | 20/18 |
| 2 | 0.42 | 1 | (10,10)/(10,10) | 35/90(40) | 19/24 | 6.7/8.0 |
| 3 | 0.47 | 1 | (10,10)/(10,10) | 32/97(49) | 16/20 | 6.8/9.1 |
| 4 | 0.48 | 1 | (12.5,12.5)/(10,10) | 33/32(24) | 16/19 | 3.5/8.2 |
| 5 | 0.84 | 1 | (12.5,12.5)/(10,12.5) | 36/51(32) | 18/17 | 3.6/5.8 |
| 6 | 0.89 | 5 | (10,15)/(10,10) | 51/114(39) | 18/23 | 3.3/7.2 |
| 7 | 0.92 | 1 | (15,15)/(10,10) | 48/82(31) | 16/27 | 2.7/5.5 |
| 8 | 1.1 | 3 | (10,12.5)/(7.5,10) | 70/100(49) | 23/27 | 4.3/6.1 |
| 9 | 1.13 | 2 | (10,12.5)/(10,10) | 48/129(37) | 21/28 | 2.7/4.0 |
| 10 | 2.76 | 1 | (20,20)/(10,10) | 33/200(57) | 16/28 | 0.7/1.7 |
| 11 | 2.9 | 3 | (10,25)/(10,10) | 52/104(20) | 22/31 | 1.5/2.6 |
| 12 | 4.86 | 4 | (12.5,25)/(10,20) | 34/104(45) | 20/23 | 0.47/0.93 |
| 13 | 8.41 | 5 | (15,25)/(10,20) | 92/190(59) | 32/26 | 0.60/0.69 |
| 14 | 8.67 | 10 | (12.5,25)/(10,25) | 100/114(46) | 35/25 | 0.81/0.69 |
| 15 | 14.44 | 10 | (15,25)/(10,20) | 114/190(48) | 36/34 | 0.43/0.60 |
| 16 | 21.96 | 12 | (15,25)/(10,30) | 197/192(66) | 43/31 | 0.33/0.27 |
| 17 | 22.94 | 12 | (20,25)/(10,30) | 122/185(44) | 40/32 | 0.31/0.33 |
| 18 | 25.83 | 9 | (15,20)/(10,30) | 190/180(46) | 38/31 | 0.34/0.26 |

*All parameters are listed with the order ZAP-X/Cyberknife. ** The range is presented as the value of (min, max) *** The node number of each Cyberknife plan is in parenthesis.

Gamma-knife. In this study, it was demonstrated that ZAP-X, in some situations, can produce plans that approach the homogeneity achieved by CyberKnife, unlike the Gamma-knife.

The CyberKnife treatment planning system has undergone significant evolution and improvement over the last twenty years, transitioning from the initial forward planning scheme with isocentric sphere packing technique to the current, more sophisticated inverse planning scheme with non-isocentric technique. On the other hand, ZAP-X utilizes sphere packing to achieve conformal coverage of the target, and the dependence on planner experience remains a limitation of the current planning capacities for ZAP-X. The introduction of a more sophisticated optimization algorithm that allows for automatic placement of isocenters with proper collimator sizes based on the shape and size of the target is likely to further enhance plan quality.

The potential for enhancing plan quality with ZAP-X extends beyond algorithmic advancements alone. While intuitively increasing the number of isocenters in ZAP-X plans could potentially improve plan quality, practical limitations must be considered. Currently, skull position verification using kV imaging is required for each isocenter, which can significantly increase delivery time when more isocenters are added. In this study, the goal was to strike a balance between plan quality and treatment time by minimizing the number of isocenters in ZAP-X plans. However, it is anticipated that advancements in machine characteristics, such as increased gantry speed, improved imaging processes for skull alignment between isocenters, and the ability to dynamically adjust collimation during each isocenter delivery, have the potential to enhance delivery efficiency (42). These improvements, along with sophisticated planning schemes, hold the promise of achieving improved conformity and homogeneity in ZAP-X plans, bringing them closer to the levels achieved by CyberKnife.

In addition to machine characteristics that affect delivery behavior, the beam characteristics of different modalities can also have an impact on plan quality. As aforementioned, ZAP-X differentiates itself from CyberKnife with its lower beam energy, which is similar to Gamma Knife. Additionally, when considering a single beam, ZAP-X has a short SAD, which theoretically results in larger beam divergence and a sharper beam penumbra. These unique features have the potential to influence dosimetric performance, particularly in terms of dose falloff and peripheral

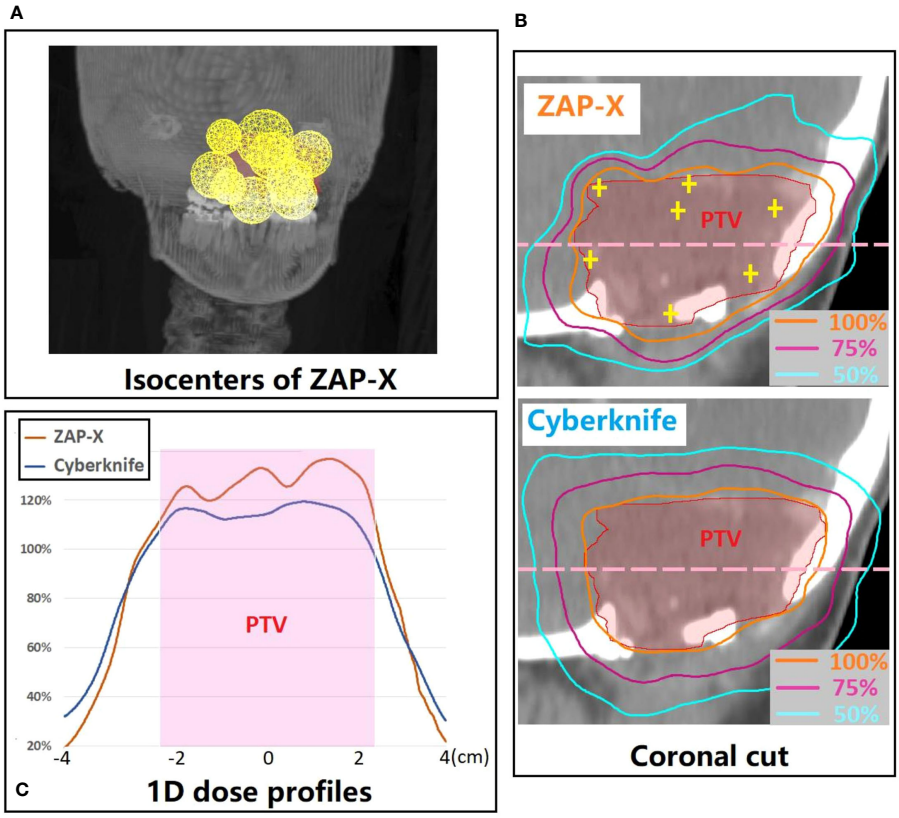


FIGURE 5
**(A)** 3D visualization of the isocenter positions in the ZAP-X plan for a representative postoperative case with large PTV (i.e., 21.96 cc). **(B)** A coronal cut view which demonstrates the difference in dose distribution between ZAP-X and Cyberknife. The yellow cross-hairs indicate the isocenter positions of ZAP-X plan projected at the view. **(C)** Comparison of 1D dose profiles between modalities along the pink dash line in **(B)**. The 100% isodose line was normalized to prescribed dose.

dose. Further studies are needed to thoroughly investigate the dosimetric impact of these specific beam characteristics on plan quality.

This study has limitations regarding the inclusion of cases involving multiple lesions planned in a single treatment plan. As depicted in Table 2, only three plans were generated for treating more than three lesions simultaneously. It is crucial to acknowledge that CyberKnife provides IRIS collimator sizes up to 60 mm, which holds the potential for improved delivery efficiency and plan quality in cases with multiple lesions. Further research is warranted to comprehensively compare the performance of these two modalities in treating multiple lesions within a single plan.

TABLE 5 Comparison of output and TPR@5cm for each collimator size using in planning.

| Collimator Size(mm) | ZAP/Cyberknife* | |
|---|---|---|
| | Output (cGy/MU) | TPR@5 cm % |
| 30 | NA/0.98 | NA/89.6 |
| 25 | 1.00/0.97 | 79.0/88.1 |
| 20 | 0.99/0.96 | 78.1/87.3 |
| 15 | 0.98/0.94 | 77.1/86.1 |
| 12.5 | 0.97/0.92 | 76.5/85.6 |
| 10 | 0.95/0.89 | 75.8/84.4 |
| 7.5 | 0.92/0.80 | 75.3/83.3 |

*Parameters are listed with the order ZAP-X/Cyberknife; outputs of IRIS$^{TM}$ collimation are listed for Cyberknife; machine output of Cyberknife was calibrated with 60 mm fixed cone.

## 5 Conclusions

Our study demonstrates that both ZAP-X and CyberKnife with circular collimation are capable of generating plans with equivalent dosimetric outcomes for patients with brain metastases of various sizes. Both modalities effectively achieve adequate dose coverage for the PTVs. While CyberKnife plans generally exhibit greater conformity and homogeneity, ZAP-X plans demonstrate a faster dose falloff. In terms of delivery efficiency, ZAP-X outperforms CyberKnife in terms of MU numbers, whereas the estimated delivery times of both systems are comparable. It is important to consider that the planning strategy employed for CyberKnife in this study was specific to a particular clinical implementation, utilizing a high PIP. Additionally, it is worth acknowledging that ZAP-X represents the first generation of the SRS platform, and its current planning and delivery scheme may have inherent limitations. However, as the technology continues to evolve and improve, it is

anticipated that ZAP-X will unlock its full potential and deliver even better dosimetric performance.

## Data availability statement

The original contributions presented in the study are included in the article/supplementary material, Further inquiries can be directed to the corresponding author.

## Author contributions

YN: Writing – review & editing, Writing – original draft, Visualization, Validation, Resources, Project administration, Methodology, Investigation, Formal analysis, Data curation, Conceptualization. AR: Writing – review & editing, Methodology, Investigation, Data curation, Conceptualization. JL: Writing – review & editing, Methodology, Investigation, Data curation, Conceptualization. MC: Writing – review & editing, Conceptualization. DC: Writing – review & editing, Conceptualization. BC: Writing – review & editing, Conceptualization. AS: Writing – review & editing, Conceptualization. KU: Writing – review & editing, Conceptualization. DP: Writing – review & editing, Supervision, Resources, Project administration, Methodology, Investigation, Conceptualization.

## Funding

The author(s) declare that no financial support was received for the research, authorship, and/or publication of this article.

## Acknowledgments

The authors would like to thank Siyuan Lei (Department of Radiation Medicine, MedStar Georgetown University Hospital) for her assistance in CyberKnife planning.

## Conflict of interest

The authors declare that the research was conducted in the absence of any commercial or financial relationships that could be construed as a potential conflict of interest.

## Publisher's note

All claims expressed in this article are solely those of the authors and do not necessarily represent those of their affiliated organizations, or those of the publisher, the editors and the reviewers. Any product that may be evaluated in this article, or claim that may be made by its manufacturer, is not guaranteed or endorsed by the publisher.

## References

1. Nayak L, Lee EQ, Wen PY. Epidemiology of brain metastases. *Curr Oncol Rep*. (2012) 14:48–54. doi: 10.1007/s11912-011-0203-y

2. Bradley KA, Mehta MP. Management of brain metastases. *Semin Oncol*. (2004) 31:693–701. doi: 10.1053/j.seminoncol.2004.07.012

3. Patchell RA. The management of brain metastases. *Cancer Treat Rev*. (2003) 29:533–40. doi: 10.1016/S0305-7372(03)00105-1

4. Chang E, Wefel J, Hess K, Allen P, Lang F, Kornguth D, et al. Neurocognition in patients with brain metastases treated with radiosurgery or radiosurgery plus whole-brain irradiation: a randomized controlled trial. *Lancet Oncol*. (2009) 10:1037–44. doi: 10.1016/S1470-2045(09)70263-3

5. Brown PD, Jaeckle K, Ballman KV, Farace E, Cerhan JH, Anderson SK, et al. Effect of radiosurgery alone vs radiosurgery with whole brain radiation therapy on cognitive function in patients with 1 to 3 brain metastases: a randomized clinical trial. *JAMA*. (2016) 316:401–9. doi: 10.1001/jama.2016.9839

6. Soliman H, Das S, Larson DA, Sahgal A. Stereotactic radiosurgery (SRS) in the modern management of patients with brain metastases. *Oncotarget*. (2016) 7:12318–30. doi: 10.18632/oncotarget.v7i11

7. Aoyama H, Shirato H, Tago M, Nakagawa K, Toyoda T, Hatano K, et al. Stereotactic radiosurgery plus whole-brain radiation therapy vs stereotactic radiosurgery alone for treatment of brain metastases: a randomized controlled trial. *JAMA*. (2006) 295:2483–91. doi: 10.1001/jama.295.21.2483

8. Yamamoto M, Serizawa T, Higuchi Y, Sato Y, Kawagishi J, Yamanaka K, et al. A multi-institutional prospective observational study of stereotactic radiosurgery for patients with multiple brain metastases (JLGK0901 Study Update): irradiation-related complications and long-term maintenance of mini-mental state examination scores. *Int J Radiat Oncol Biol Phys*. (2017) 99:31–40. doi: 10.1016/j.ijrobp.2017.04.037

9. Soffietti R, Kocher M, Abacioglu UM, Villa S, Fauchon F, Baumert BG, et al. A European Organization for Research and Treatment of Cancer phase III trial of adjuvant whole-brain radiotherapy versus observation in patients with one to three brain metastases from solid tumors after surgical resection or radiosurgery: quality-of-life results. *J Clin Oncol*. (2013) 31:65–72. doi: 10.1200/JCO.2011.41.0639

10. Modh A, Burmeister C, Elshaikh MA, Siddiqui F, Siddiqui S, Shah MM, et al. Radiation utilization trends in the treatment of brain metastases from non-small cell lung cancer. *Int J Radiat Oncol Biol Phys*. (2017) 99:E94. doi: 10.1016/j.ijrobp.2017.06.815

11. Kann BH, Park HS, Johnson SB, Chiang VL, Yu JB. Radiosurgery for brain metastases: Changing practice patterns and disparities in the United States. *J Natl Compr Canc Netw*. (2017) 15:1494–502. doi: 10.6004/jnccn.2017.7003

12. Lutz W, Winston KR, Maleki N. A system for stereotactic radiosurgery with a linear accelerator. *Int J Radiat Oncol Biol Phys*. (1988) 14:373–81. doi: 10.1016/0360-3016(88)90446-4

13. Podgorsak EB, Olivier A, Pla M, Lefebvre PY, Hazel J. Dynamic stereotactic radiosurgery. *Int J Radiat Oncol Biol Phys*. (1988) 14:115–26. doi: 10.1016/0360-3016(88)90059-4

14. Kim J, Jin JY, Walls N, Nurushev T, Movsas B, Chetty IJ, et al. Image-guided localization accuracy of stereoscopic planar and volumetric imaging methods for stereotactic radiation surgery and stereotactic body radiation therapy: a phantom study. *Int J Radiat Oncol Biol Phys*. (2011) 79:1588–96. doi: 10.1016/j.ijrobp.2010.05.052

15. Jawahar A, Matthew RE, Minagar A, Shukla D, Zhang JH, Willis BK, et al. Gamma knife surgery in the management of brain metastases from lung carcinoma: a retrospective analysis of survival, local tumor control, and freedom from new brain metastasis. *J Neurosurg*. (2004) 100:842–7. doi: 10.3171/jns.2004.100.5.0842

16. Sadik ZHA, Beerepoot LV, Hanssens PEJ. Efficacy of gamma knife radiosurgery in brain metastases of primary gynecological tumors. *J Neurooncol*. (2019) 142:283–90. doi: 10.1007/s11060-019-03094-2

17. Ohira S, Ueda Y, Akino Y, Hashimoto M, Masaoka A, Hirata T, et al. HyperArc VMAT planning for single and multiple brain metastases stereotactic radiosurgery: a new treatment planning approach. *Radiat Oncol*. (2018) 13:13. doi: 10.1186/s13014-017-0948-z

18. Shah AP, Meeks DT, Willoughby TR, Ramakrishna N, Warner CJ, Swanick CW, et al. Intrafraction motion during frameless radiosurgery using Varian HyperArc™ and BrainLab Elements™ immobilization systems. *J Radiosurg SBRT*. (2020) 7:149–56.

19. Adler JRJr, Chang SD, Murphy MJ, Doty J, Geis P, Hancock SL. The CyberKnife: a frameless robotic system for radiosurgery. *Stereotact Funct Neurosurg*. (1997) 69:124–8. doi: 10.1159/000099863

20. Pan L, Qu B, Bai J, Huang L, Wang J, Wang C, et al. The Zap-X radiosurgical system in the treatment of intracranial tumors: A technical case report. *Neurosurgery*. (2021) 88:E351–5. doi: 10.1093/neuros/nyaa550

21. Kurup G. CyberKnife: A new paradigm in radiotherapy. *J Med Phys*. (2010) 35:63–4. doi: 10.4103/0971-6203.62194

22. Wong KH, Dieterich S, Tang J, Cleary K. Quantitative measurement of CyberKnife robotic arm steering. *Technol Cancer Res Treat*. (2007) 6:589–94. doi: 10.1177/153303460700600601

23. Kilby W, Naylor M, Dooley JR, Maurer CR, Sayeh S. A technical overview of the CyberKnife system. *Handb robotic image-guided Surg*. (2020) 2:15–38. doi: 10.1016/B978-0-12-814245-5.00002-5

24. McGuinness CM, Gottschalk AR, Lessard E, Nakamura JL, Pinnaduwage D, Pouliot J, et al. Investigating the clinical advantages of a robotic linac equipped with a multileaf collimator in the treatment of brain and prostate cancer patients. *J Appl Clin Med Phys*. (2015) 16:284–95. doi: 10.1120/jacmp.v16i5.5502

25. Adler JR Jr, Murphy MJ, Chang SD, Hancock SL. Image-guided robotic radiosurgery. *Neurosurgery*. (1999) 44:1299–306. doi: 10.1227/00006123-199906000-00079

26. Weidlich GA, Schneider MB, Adler JR. Self-shielding analysis of the Zap-X system. *Cureus*. (2017) 9:e1917. doi: 10.7759/cureus.1917

27. Weidlich GA, Bodduluri M, Achkire Y, Lee C, Adler JR Jr. Characterization of a novel 3 megavolt linear accelerator for dedicated intracranial stereotactic radiosurgery. *Cureus*. (2019) 11:e4275. doi: 10.7759/cureus.4275

28. Weidlich GA, Schneider MB, Simcic V, Oostman Z, Adler JR Jr. Self-shielding for the ZAP-X®: revised characterization and evaluation. *Cureus*. (2021) 13:e13660. doi: 10.7759/cureus.13660

29. Weidlich GA, Schneider MB, Adler JR. Characterization of a novel revolving radiation collimator. *Cureus*. (2018) 10:e2146. doi: 10.7759/cureus.2146

30. Weidlich GA, Chung W, Kolli S, Thirunarayanan I, Loysel T. Characterization of the ZAP-X® Peripheral dose fall-off. *Cureus*. (2021) 13:e13972. doi: 10.7759/cureus.13972

31. Romanelli P, Chuang C, Meola A, Bodduluri RM, Adler JR Jr. ZAP-X: A novel radiosurgical device for the treatment of trigeminal neuralgia. *Cureus*. (2020) 12:e8324. doi: 10.7759/cureus.8324

32. Sio TT, Jang S, Lee SW, Curran B, Pyakuryal AP, Sternick ES. Comparing gamma knife and CyberKnife in patients with brain metastases. *J Appl Clin Med Phys*. (2014) 15:4095. doi: 10.1120/jacmp.v15i1.4095

33. Vergalasova I, Liu H, Alonso-Basanta M, Dong L, Li J, Nie K, et al. Multi-institutional dosimetric evaluation of modern day stereotactic radiosurgery (SRS) treatment options for multiple brain metastases. *Front Oncol*. (2019) 9:483. doi: 10.3389/fonc.2019.00483

34. Zhang S, Yang R, Shi C, Li J, Zhuang H, Tian S, et al. Noncoplanar VMAT for brain metastases: A plan quality and delivery efficiency comparison with coplanar VMAT, IMRT, and cyberKnife. *Technol Cancer Res Treat*. (2019) 18:1533033819871621. doi: 10.1177/1533033819871621

35. El Shafie RA, Tonndorf-Martini E, Schmitt D, Celik A, Weber D, Lang K, et al. Single-isocenter volumetric modulated arc therapy vs. CyberKnife M6 for the stereotactic radiosurgery of multiple brain metastases. *Front Oncol*. (2020) 10:568. doi: 10.3389/fonc.2020.00568

36. Adler JR, Schweikard A, Achkire Y, Blanck O, Bodduluri M, Ma L, et al. Treatment planning for self-shielded radiosurgery. *Cureus*. (2017) 9:e1663. doi: 10.7759/cureus.1663

37. Schüler E, Lo A, Chuang CF, Soltys SG, Pollom EL, Wang L. Clinical impact of the VOLO optimizer on treatment plan quality and clinical treatment efficiency for CyberKnife. *J Appl Clin Med Phys*. (2020) 21:38–47. doi: 10.1002/acm2.12851

38. Benedict SH, Yenice KM, Followill D, Galvin JM, Hinson W, Kavanagh B, et al. Stereotactic body radiation therapy: the report of AAPM Task Group 101. *Med Phys*. (2010) 37:4078–101. doi: 10.1118/1.3438081

39. Minniti G, Clarke E, Lanzetta G, Osti MF, Trasimeni G, Bozzao A, et al. Stereotactic radiosurgery for brain metastases: analysis of outcome and risk of brain radionecrosis. *Radiat Oncol*. (2011) 6:48. doi: 10.1186/1748-717X-6-48

40. Lin YW, Lin KH, Ho HW, Lin HM, Lin LC, Lee SP, et al. Treatment plan comparison between stereotactic body radiation therapy techniques for prostate cancer: non-isocentric CyberKnife versus isocentric RapidArc. *Phys Med*. (2014) 30:654–61. doi: 10.1016/j.ejmp.2014.03.008

41. Lee SW, Jang S, Pyakuryal AP, Chang K, Sio TT. The impact of CyberKnife's prescription isodose percentage on intracranial target planning. *J Appl Clin Med Phys*. (2014) 15:5081. doi: 10.1120/jacmp.v15i5.5081

42. Niu Y, Lee J, Gardner E, Rashid A, Pang D. (2023). Investigating benefits of dynamic collimation using novel revolving collimator in stereotactic radiosurgery, in: *Poster presented at The American Association of Physicists in Medicine 65th annual meeting*, Houston, TX, July 23–27

frontiers | Frontiers in Oncology

TYPE Original Research
PUBLISHED 13 August 2024
DOI 10.3389/fonc.2024.1333245



OPEN ACCESS

EDITED BY
Yirui Zhai,
Chinese Academy of Medical Sciences and Peking Union Medical College, China

REVIEWED BY
Christoph Straube,
Technical University of Munich, Germany
Michael Schulder,
Hofstra University, United States

*CORRESPONDENCE
Philipp Reinhardt
philipp.reinhardt@insel.ch

†These authors have contributed equally to this work and share first authorship

‡These authors have contributed equally to this work and share last authorship

RECEIVED 04 November 2023
ACCEPTED 24 July 2024
PUBLISHED 13 August 2024

CITATION
Reinhardt P, Ahmadli U, Uysal E, Shrestha BK, Schucht P, Hakim A and Ermiş E (2024) Single versus multiple fraction stereotactic radiosurgery for medium-sized brain metastases (4-14 cc in volume): reducing or fractionating the radiosurgery dose? *Front. Oncol.* 14:1333245. doi: 10.3389/fonc.2024.1333245



# Single versus multiple fraction stereotactic radiosurgery for medium-sized brain metastases (4-14 cc in volume): reducing or fractionating the radiosurgery dose?

Philipp Reinhardt[1*†], Uzeyir Ahmadli[2†], Emre Uysal[3], Binaya Kumar Shrestha[1], Philippe Schucht[4], Arsany Hakim[3‡] and Ekin Ermiş[1‡]

[1]Department of Radiation Oncology, Inselspital, Bern University Hospital and University of Bern, Bern, Switzerland, [2]University Institute of Diagnostic and Interventional Neuroradiology, Inselspital, University Hospital and University of Bern, Bern, Switzerland, [3]Department of Radiation Oncology, Prof. Dr. Cemil Tascioglu City Hospital, Istanbul, Türkiye, [4]Department of Neurosurgery, Inselspital, Bern University Hospital, University of Bern, Bern, Switzerland

**Background and purpose:** Stereotactic radiosurgery (SRS) of brain metastases (BM) and resection cavities is a widely used and effective treatment modality. Based on target lesion size and anatomical location, single fraction SRS (SF-SRS) or multiple fraction SRS (MF-SRS) are applied. Current clinical recommendations conditionally recommend either reduced dose SF-SRS or MF-SRS for medium-sized BM (2–2.9 cm in diameter). Despite excellent local control rates, SRS carries the risk of radionecrosis (RN). The purpose of this study was to assess the 12-months local control (LC) rate and 12-months RN rate of this specific patient population.

**Materials and methods:** This single-center retrospective study included 54 patients with medium-sized intact BM (n=28) or resection cavities (n=30) treated with either SF-SRS or MF-SRS. Follow-up MRI was used to determine LC and RN using a modification of the "Brain Tumor Reporting and Data System" (BT-RADS) scoring system.

**Results:** The 12-month LC rate following treatment of intact BM was 66.7% for SF-SRS and 60.0% for MF-SRS (p=1.000). For resection cavities, the 12-month LC rate was 92.9%% after SF-SRS and 46.2% after MF-SRS (p=0.013). For intact BM, RN rate was 17.6% for SF-SRS and 20.0% for MF-SRS (p=1.000). For resection cavities, RN rate was 28.6% for SF-SRS and 20.0% for MF-SRS (p=1.000).

**Conclusion:** Patients with intact BM showed no statistically significant differences in 12-months LC and RN rate following SF-SRS or MF-SRS. In patients with resection cavities the 12-months LC rate was significantly better following SF-SRS, with no increase in the RNFS.

KEYWORDS

brain metastases, stereotactic radiosurgery, multiple fraction SRS, single fraction SRS, radionecrosis, MRI, response assessment, recurrence

# Introduction

Brain metastases (BM) commonly occur in solid cancers and are a significant cause of morbidity and mortality (1, 2). Due to the increasing incidence of BM over the past few decades, the true prevalence may be underestimated (3). This increase can be attributed to the growing number of cancer survivors as well as improved identification of BM through the use of modern imaging modalities (3, 4).

Historically, whole brain radiation therapy (WBRT) was the backbone in the treatment of BM (5). Toxicity, especially neurocognitive decline after WBRT, prompted investigations of more focal therapies to spare normal brain tissue. Randomized trials showed the safety and efficacy of local radiotherapy, known as stereotactic radiosurgery (SRS) (6–9). With the growing evidence for its usefulness over the past decade, SRS alone has become the standard of care for patients with a good performance status and a limited number of newly diagnosed BM (10).

Despite the excellent local control (LC), especially in small BM treated with single fraction SRS (SF-SRS), physicians must consider the risk of radionecrosis (RN) (11). For large BM (>3 cm in diameter), the benefit of SRS in terms of LC must be weighed against the risk of RN. The Radiation Therapy Oncology Group (RTOG) conducted the phase 1 90-05 trial to estimate the maximum tolerated dose for SF-SRS in previously irradiated patients (12). The authors proposed reducing the radiosurgical dose depending on tumor size and recommended 18 Gy for tumors with diameters of 2–3 cm. In the meantime multi-fraction radiosurgery (MF-SRS) regimes have been introduced (13–15). MF-SRS has been widely utilized as an alternative to reduce the risk of RN. The latest clinical practice guideline from the American Society for Radiation Oncology (ASTRO) recommends that lesions >3 to 4 cm in diameter should be treated with MF-SRS whereas, for small lesions (< 2 cm), SF-SRS is preferred (16). For patients with medium-sized BM (2.0–2.9 cm in diameter) the guideline made no clear recommendation and SF-SRS or MF-SRS is conditionally recommended.

The primary aim of this single-center, retrospective study was to investigate the incidence of local failure (LF) and RN after SF-SRS (1×18 Gy) and MF-SRS (3×8 Gy, 5×6 Gy) in patients with intact BM and resection cavities with target volumes ranging from 4 $cm^3$ (2 cm in diameter) to 14 $cm^3$ (3 cm in diameter).

# Materials and methods

## Eligibility

This retrospective study was approved by the local ethics committee (Cantonal Ethics Committee Bern, Switzerland, KEK BE 2023-00223). To be eligible, patients had to be treated with SRS between 08/2014 and 01/2022, aged ≥ 18 years, and have histologically confirmed systemic malignancy, with intact BM or resection cavities measuring between 4 $cm^3$ (2 cm in diameter) and 14 $cm^3$ (3 cm in diameter). Adequate magnetic resonance imaging (MRI) follow-up was also a prerequisite (including at least pre- and post-contrast T1, T2 and diffusion-weighted imaging [DWI]).

## Treatment and dosimetric parameters

A commercial stereotactic mask fixation device was used to immobilize patients in the supine position. Post-contrast enhanced T1- and T2-weighted MRI (1 mm thick) and computed tomography (CT) images (0.75 mm thick) were acquired. CT and MRI scans were registered in the treatment planning system (Accuracy, Precision Treatment Planning) for target volume and normal tissue delineation. Using the post-contrast enhanced T1 sequence and T2 sequence, the gross tumor volume (GTV) for intact metastases was manually delineated. The planning tumor volumes (PTVs) for intact BM were generated by a zero-margin expansion of the GTV. The postoperative rim of enhancement at the edge of the resection cavity and the resection cavity itself were included in the GTV of the resected BM. For resection cavities, the GTV was expanded with a 2 mm margin to the PTV. Surgical tracts and the attached dura was included into the PTV. For patients who received SF-SRS, 1×18 Gy was prescribed. MF-SRS was performed with either 24 Gy in 3 fractions or 30 Gy in 5 fractions. Biologically effective dose (BED) with an $\alpha/\beta$ of 12 Gy corresponded to 45 Gy for SF-SRS and 40 Gy (3×8 Gy) to 45 Gy (5×6 Gy) for MF-SRS. None of the patients had received previous a WBRT and only 9 had undergone previous SRS targeting a different lesion. Treatment plans were generated using Multiplan treatment planning software version 5.3 or Precision version 1.3 (Accuray. Sunnyvale, CA). The Cyberknife Robotic Radiosurgery System (Accuray, Sunnyvale, CA) was used to deliver the radiation.

To evaluate the risk of RN rates, healthy brain tissue receiving 10 Gy for single-fraction (V10 Gy), 20 Gy for three fractions (V20 Gy) and 30 Gy for five fractions (V30 Gy) were retrospectively generated, using a structure of brain minus PTV. These parameters were not employed during the optimization of the initial treatment plan. Furthermore, a dose gradient index (GI), which quantifies the dose falloff, was retrospectively calculated by using the formula: the volume corresponding to half of the prescription isodose divided by the prescription isodose volume (17). The GI threshold of "3" was used to objectively measure the plan quality (17).

## Follow-up data and radiologic measures

Data were collected during routine clinical procedures (diagnosis, treatment, and follow-up [FU]) and were available via the clinical information system and picture archiving and communication system (PACS) of the Inselspital, Bern University Hospital. All patients had undergone serial MRI every 3–6 months. Our institution's standardized MRI protocol was followed for imaging acquisition. Images were obtained either on a 1.5T (Magnetom Aera or Avanto, Siemens Healthineers, Erlangen, Germany) or a 3T MR scanner (Magnetom Vida or Skyra, Siemens Healthineers, Erlangen, Germany). However, external MRI exams were also considered for evaluation if the inclusion criteria were fulfilled. The standard brain tumor MRI protocol in our institution included pre- and post-contrast sequences. Pre-contrast sequences include sagittal T1w Sampling Perfection with Application optimized Contrasts using different flip angle Evolution (SPACE), axial fluid-attenuated inversion recovery (FLAIR) and axial DWI. Post-contrast sequences (after intravenous injection of 0.1 mmol/kg gadolinium-based agent) included axial susceptibility weighted imaging (SWI), axial T2w, and sagittal fat-saturated T1 SPACE and coronal fat-saturated FLAIR. DWI was acquired at b values of 0 and 1000 with an automatically calculated apparent diffusion coefficient (ADC) map.

Single ratings of the images were performed by two board-certified neuroradiologists at baseline and during FU (Supplementary Table 1). Baseline imaging was the last MRI before SRS. All lesions were scored using the Brain Tumor Reporting and Data System (BT-RADS) (18). To adapt this classification system for the evaluation of BM, the changes based on T2/FLAIR images without enhancement, which are usually used to evaluate non-enhancing gliomas, were not considered as a marker for progression or response. As the primary endpoint was LF, lesions outside the radiation field were separately evaluated. T1/T2 mismatch (19) and central diffusion restriction (20) were taken into consideration to help in differencing between tumor recurrence and radiation necrosis (Figures 1, 2).

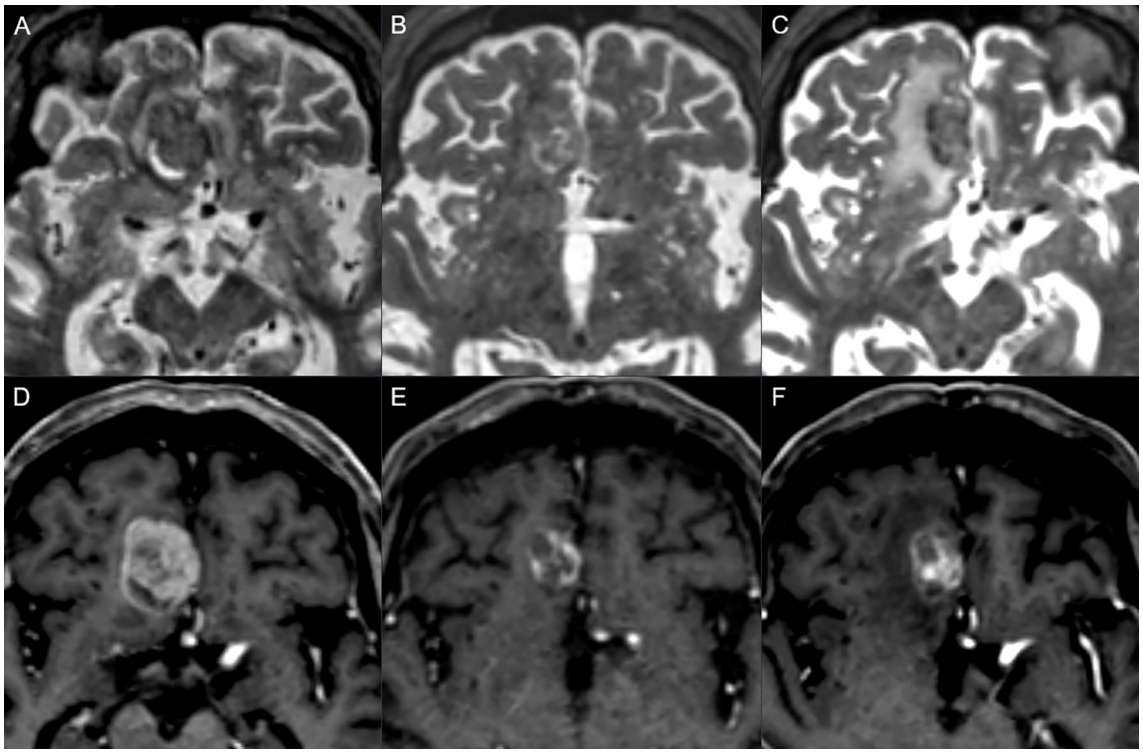


FIGURE 1
Follow-up example showing progression: axial T2w (upper row) and post-contrast axial T1w (lower row) in a 78-year-old man with metastatic melanoma. Baseline images **(A, D)** show right frontal metastasis, mostly solid with small peripheral cystic changes. Three months after stereotactic radiotherapy **(B, E)** a reduction of the contrast enhancement and the overall diameter was seen with a T1/T2 mismatch, scored as BT-RADS 1. Six months later **(C, F)** there was an increase in the contrast enhancement, representing an increase in the solid part of the lesion with a T1/T2 matching, scored as BT-RADS 3c.

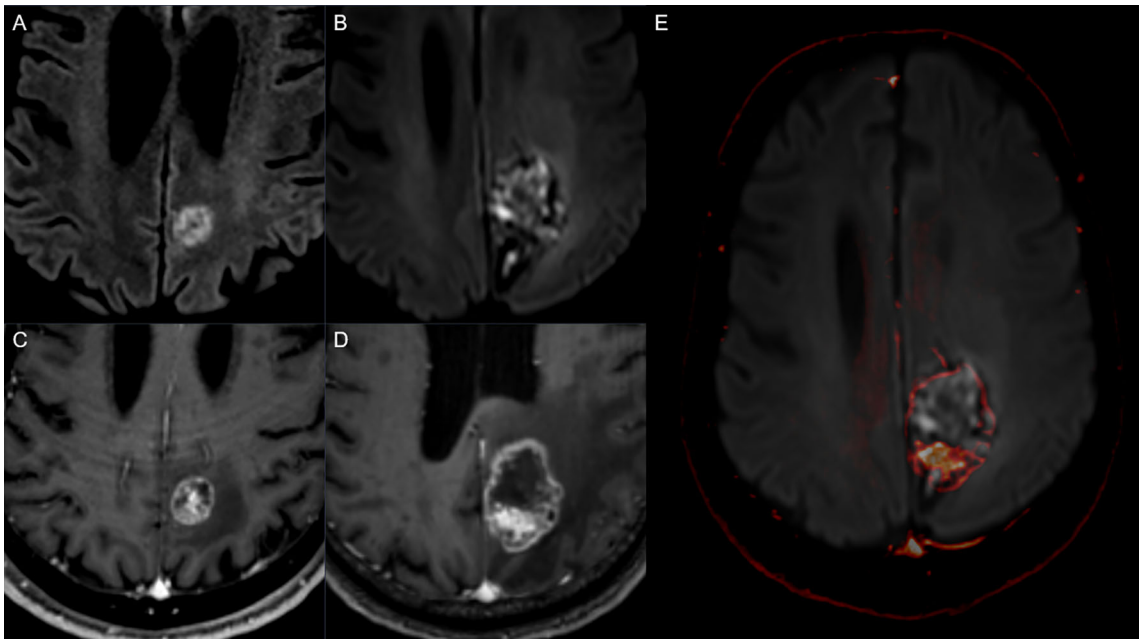


FIGURE 2
Follow up example showing radionecrosis: Diffusion-weighted MRI sequences (upper row) and post-contrast T1w (lower row) in a 69-year-old man with metastatic non-small cell lung cancer. Baseline imaging **(A, C)** shows left parietal metastasis, mostly solid. Three months after stereotactic radiotherapy **(B, D)** there was an increase in the overall diameter of the lesion with ring enhancement and central diffusion restriction as seen on the fused image **(E)** (post-contrast T1 superimposed on DWI, see arrow). The increase in diameter was attributed to the radionecrosis and scored as BT-RADS 3a.

The following were evaluated: change in diameter of the enhancing lesion, new enhancing lesion outside the radiation field, and mass effect. LF or RN was defined depending on the score, (Supplementary Table 1). Lesions classified as 3b showed simultaneous signs of LF and RN and could not always be categorized as one or the other. If local salvage treatment was applied to a lesion previously scored as 3b, we defined this as an event in terms of LF without RN. If no local salvage treatment was applied and further MRI FU was performed, this lesion was defined as intermediate 3b with signs of LF and RN.

## Endpoints

The primary endpoint was defined as 12-months LC rate after SRS (defined as time between date of last SRS and suspected LF detected by MRI). Secondary endpoints were RN rate WBRT-free survival (WBRT-FS) and overall survival (OS).

## Statistical analysis

Categorical variables were presented numerically (as a percentage). Continuous variables were reported as median (range). Patient survival was calculated from the time of BM diagnosis and obtained using Kaplan-Meier analysis. For 12-month LC, patients who failed within 12 months and patients who did not fail for at least 12 months were analyzed. Chi-square test or Fisher exact test, where appropriate, were used to compare categorical variables between groups. A p-value of less than 0.05 was deemed statistically significant. Statistical analyses were performed using IBM SPSS Statistics for Windows, version 26 (IBM Corp., Armonk, N.Y., USA).

# Results

## Patient characteristics and treatment

We included 54 patients with 58 BM. Two-thirds of the patients were men, and the median age was 63 years (range 37–89 years). NSCLC (50%) and melanoma (21%) were the most common primary cancers, followed by breast cancer (9%). SRS was performed on 28 intact BM and 30 resection cavities. SF-SRS was administered to 22 of the patients with intact BM, and 6 received MF-SRS. Of the patients with resection cavities, 16 received SF-SRS and 14 MF-SRS. The majority of patients (72.4%) received some form of systemic treatment before, concomitant or after SRS. Among those who had undergone systemic treatment, the most common modalities were chemotherapy (47.4%) and immunotherapy (39.5%). Details of the patient characteristics and treatments are provided in Table 1.

10.3389/fonc.2024.1333245

TABLE 1 Patient characteristics and treatment .

| | | All (n=58) | Range or % | Intact BM (n=28) | | | | Resection cavity (n=30) | | | |
|---|---|---|---|---|---|---|---|---|---|---|---|
| | | | | SF-SRS (n=22; 79%) | | MF-SRS (n=6; 21%) | | SF-SRS (n=16; 53%) | | MF-SRS (n=14; 47%) | |
| Age | Median (range) | 63 | 37–89 | 63 | 50–78 | 58 | 52–89 | 62 | 52–77 | 66 | 37–82 |
| Sex | Male | 38 | 65.5 | 15 | 68% | 3 | 50% | 10 | 63% | 10 | 71% |
| | Female | 20 | 34.5 | 7 | 32% | 3 | 50% | 6 | 38% | 4 | 29% |
| KPS | ≥90 | 43 | 75.4 | 19 | 86% | 3 | 50% | 13 | 81% | 8 | 57% |
| | <90 | 14 | 24.6 | 2 | 9% | 3 | 50% | 3 | 19% | 6 | 43% |
| Primary cancer | NSCLC | 29 | 50.0 | 9 | 41% | 2 | 33% | 13 | 81% | 5 | 36% |
| | Melanoma | 12 | 20.7 | 3 | 14% | 1 | 17% | 2 | 13% | 6 | 43% |
| | Breast cancer | 5 | 8.6 | 1 | 5% | 2 | 33% | 1 | 6% | 1 | 7% |
| | Colorectal cancer | 4 | 6.9 | 2 | 9% | 0 | 0% | 0 | 0% | 2 | 14% |
| | Renal cell cancer | 3 | 5.2 | 3 | 14% | 0 | 0% | 0 | 0% | 0 | 0% |
| | Other | 5 | 8.6 | 4 | 18% | 1 | 17% | 0 | 0% | 0 | 0% |
| Status of primary cancer | Controlled | 24 | 41.4 | 10 | 45% | 3 | 50% | 7 | 44% | 4 | 29% |
| | Uncontrolled | 13 | 22.4 | 5 | 23% | 1 | 17% | 1 | 6% | 6 | 43% |
| | Newly diagnosed | 21 | 36.2 | 7 | 32% | 2 | 33% | 8 | 50% | 4 | 29% |
| BM number | Single | 28 | 48.3 | 7 | 32% | 2 | 33% | 9 | 56% | 10 | 71% |
| | Multiple | 30 | 51.7 | 15 | 68% | 4 | 67% | 7 | 44% | 4 | 29% |
| Systemic treatment | Before SRS | 24 | 41,4 | 12 | 55% | 3 | 50% | 3 | 19% | 6 | 43% |
| | After SRS | 16 | 27,6 | 4 | 18% | 2 | 33% | 9 | 56% | 1 | 7% |
| | Concomitant | 2 | 3,4 | 0 | 0% | 0 | 0% | 0 | 0% | 2 | 14% |
| | No | 16 | 27,6 | 6 | 27% | 1 | 17% | 4 | 25% | 5 | 36% |
| Medical therapy | Chemotherapy | 18 | 31,0 | 7 | 32% | 0 | 0% | 8 | 50% | 3 | 21% |
| | Targeted therapy | 5 | 8,6 | 5 | 23% | 0 | 0% | 0 | 0% | 0 | 0% |
| | İmmunotherapy | 15 | 25,9 | 3 | 14% | 3 | 50% | 3 | 19% | 6 | 43% |
| | Hormontherapy | 3 | 5,2 | 0 | 0% | 2 | 33% | 1 | 6% | 0 | 0% |
| | No | 16 | 27,6 | 6 | 27% | 1 | 17% | 4 | 25% | 5 | 36% |
| | missing | 1 | 1,7 | 1 | 5% | 0 | 0% | 0 | 0% | 0 | 0% |
| SF-SRS | 1×18 Gy (BED=50,4) | 38 | 65.5 | 22 | 100% | 0 | 0% | 16 | 100% | 0 | 0% |
| MF-SRS | 3×8 Gy (BED=43,2) | 8 | 13.8 | 0 | 0% | 2 | 33% | 0 | 0% | 6 | 43% |
| | 5×6 Gy (BED=48) | 12 | 20.7 | 0 | 0% | 4 | 67% | 0 | 0% | 8 | 57% |
| Prescribed isodose line | Median (range) | 76.5 | 54.8–81.0 | 61.50 | 54,8-80,0 | 66.00 | 60,0-75,9 | 79.5 | 60,0-80,0 | 78.7 | 59,0-81,0 |
| Conformity index | Median (range) | 1.18 | 1.05–1.81 | 1.18 | 1.07–1.81 | 1.20 | 1.11–1.37 | 1.12 | 1.05–1.32 | 1.14 | 1.07–1.22 |
| Heterogeneity index | Median (range) | 1.29 | 1.14–1.82 | 1.50 | 1.14–1.82 | 1.51 | 1.32–1.67 | 1.26 | 1.25–1.67 | 1.26 | 1.23–1.69 |
| PTV in cc (mean, range) | Median (range) | 7.2 | 4.1–13.1 | 5.77 | 4.06–9.53 | 8.70 | 4.84–13.05 | 7.81 | 5.01–9.40 | 9.66 | 5.99–12.64 |

KPS, Karnofsky Performance Scale; NSCLC, non-small cell lung cancer; BM, brain metastases; SRS, stereotactic radiosurgery; SF-SRS, single fraction stereotactic radiosurgery; MF-SRS, multiple fraction stereotactic radiosurgery.

## Local control intact BM

After a median FU of 21 months, LF occurred in 9 (32.1%) patients. The 12-month LC rate was 65.2%. There was no significant difference between the two fractionation schemes, with a 12-month LC rate of 66.7% for SF-SRS and 60% for MF-SRS (p=1.000) (Table 2). A higher LC rate was observed in patients with NSCLC compared to those with other primary tumors (100% vs. 42.9%, p=0.007) (Supplementary Table 2). Furthermore, the LC rate of patients with synchronous BM was higher than that of patients with metachronous BM (100% vs. 46.7%, p=0.019). The 12-month LC rate was found to be unaffected by the administered systemic treatment (SF-SRS p=1.000; MF-SRS not applicable) (Supplementary Table 3). Furthermore, no significant difference was found according to the type of systemic treatment (SF-SRS p=0.213, MF-SRS p=0.100) (Supplementary Table 3). In addition, patients with severe BM symptoms exhibited a significantly lower 12-month LC rate than those with mild or no symptoms (0% vs 85.7% vs 75.0%; p=0.014). A higher prescribed isodose line (IDL) (cutoff IDL >60%) demonstrated a statistically higher 12-month LC rate (p=0.023).

## Local control resection cavities

LF occurred in 9 patients after a median FU of 18 months. The 12-month LC rate was 70.4%. The 12-month LC rate was significantly higher in patients undergoing SF-SRS (92.9%) than those treated with MF-SRS (46.2%) (p=0.013) (Table 2). No significant difference was found in the administration of systemic treatment (SF-SRS p=0.286; MF-SRS p=0.592) or the type of systemic treatment (SF-SRS p=0.500; MF-SRS p=0.476) (Supplementary Table 4). No other factors were associated with significant differences in 12-month LC.

## Radionecrosis

At 6 and 12 months, the RN rates for patients with intact BM were 11.1% and 18.2%, respectively, and 3.4% and 25% for patients with resection cavities. For intact BM, 12-months RN rate was 17.6% for SF-SRS and 20.0% for MF-SRS (p=1.000). For resection cavities, 12-months RN rate was 28.6% for SF-SRS and 20.0% for MF-SRS (p=1.000) (Table 2). No difference was found for the 12-month RN rate between SF-SRS and MF-SRS in either group. The treatment planning for intact BM with HI <1.65 (0.0% vs 40%, p=0.029) and IDL >60% (0.0% vs 40.0%, p=0.029) was associated with lower 12-months RN rate. (Supplementary Table 2). The results demonstrated no statistically significant difference in 12-month RN rates between a GI of <3 vs >3 (20% vs 25%, p=1.000).

Upon further analyses, the 12-month RN rate was examined for V10 Gy, V20 Gy and V30 Gy in relation to the number of fractions. There was no statistical difference in RN rates for brain minus PTV volume receiving 10 Gy, 20 Gy and 30 Gy for one, three and five fractions with a threshold volume of ≥10cc (21.4% vs 22.2%, p=1.000) (Supplementary Table 5).

## Whole brain radiotherapy free survival

Salvage WBRT rates 6 and 12 months after SRS were 3.7% and 9.5% for patients with intact BM, and 23.3% and 27.6% for those with a resected cavity, respectively (Table 2). There was no relationship between fractionation and WBRT in either group (Supplementary Figure 1).

## Overall survival

OS rates after 6 and 12 months were 96.4% and 71.4% in the patients with intact BM, and 96.7% and 80.0% in those with a resection cavity, respectively. There were no statistically significant differences between fractionation and OS in either group (Supplementary Figure 2).

# Discussion

The results of this single-center retrospective study showed no significant difference between SF-SRS and MF-SRS regarding the

TABLE 2 Overview of results at 12-month follow-up after treatment of intact brain metastases and resection cavities according to fractionation scheme.

| | Intact BM (n=28) | | p | Cavity (n=30) | | p |
|---|---|---|---|---|---|---|
| | SF-SRS (n=22) | MF-SRS (n=6) | | SF-SRS (n=16) | MF-SRS (n=14) | |
| OS | 68.2% | 83.3% | 0.416 | 87.5% | 71.4% | 0.845 |
| LC rate | 66.7% | 60.0% | 1.000 | 92.9% | 46.2% | 0.013 |
| DBFFS | 68.2% | 60.0% | 0.563 | 56.3% | 64.3% | 0.984 |
| DBF rates | 36.8% | 40.0% | 1.000 | 43.8% | 38.5% | 0.774 |
| WBRT-FS | 90.2% | 100% | 0.354 | 68.8% | 78.6% | 0.578 |
| WBRT rates | 12.5% | 0% | 1.000 | 31.3% | 23.1% | 0.697 |
| RN rates | 17.6% | 20.0% | 1.000 | 28.6% | 20.0% | 1.000 |

BM, brain metastases, OS, overall survival, LC, local control, DBFFS, distant brain failure-free survival, DBF, distant brain failure, WBRT-FS, whole brain radiotherapy free survival, WBRT, whole brain radiotherapy, RN, radionecrosis.

12-months LC and 12-months RN in patients with medium-sized intact BM. In patients with resection cavities, however, those who underwent SF-SRS showed a significantly better 12-months LC rate, with no difference in 12-months RN rate. The prescribed dose for SF-SRS is based on the landmark RTOG 90-05 trial, which provides a recommendation for unresected brain metastasis based on the lesion size (12). Following the single-dose regimen of RTOG 90-05, Vogelbaum et al. performed a retrospective study to determine the LC for different intact BM sizes (21). Their results showed a significant benefit in terms of LC of SRS performed with 24 Gy (for BM ≤ 20mm) compared to 18 Gy (for BM 21–30 mm) and 15 Gy (for BM 31–40 mm) (p = 0.0005). LC rates at 1 year in the 24 Gy, 18 Gy and 15 Gy groups were 85%, 49% and 45%, respectively. The authors concluded that LC was proportional to the prescribed dose. The worse LC in patients with larger BM led to the investigation of MF-SRS. Few retrospective studies have evaluated different dose and fractionation regimes in patients with intact brain metastasis. Minniti et al. retrospectively analyzed 289 patients with 343 BM >2 cm in diameter (13). Depending on the size, patients with SF-SRS received either 18 Gy (2–3 cm) or 15–16 Gy (>3 cm). For MF-SRS, 3 × 9 Gy were used, and 53% of the lesions were <3 cm. When compared to BM treated with SF-SRS, lesions treated with MF-SRS showed a significantly higher 1-year LC (91% vs 77%, p=0.01). Additionally, following the administration of MF-SRS, the 1-year incidence of RN was significantly lower (18% vs 9%, p=0.01). These results were confirmed by Chon et al. (22) who analyzed SF-SRS and MF-SRS in patients with BM of 2.5 to 3 cm in diameter. MF-SRS was administered with a median cumulative dose of 35 Gy over 5 fractions, whereas SF-SRS was administered with a median dose of 20 Gy. Both the RN rate after 14 months of FU (29.9% vs 5.3%, p=0.001) and the 1-year LC rate (66.6% vs 92.4%, p=0.028) were significantly better in the MF-SRS-treated group. A meta-analysis comparing SF-SRS and MF-SRS for the definitive and postoperative treatment of BM was published by Lehrer et al. (23). BM were divided into 2 groups based on size (group A: 4–14 $cm^3$ or 2–3 cm in diameter; group B: >14 $cm^3$ or >3 cm in diameter). For patients with intact BM in group A, the results demonstrated no difference in 1-year LC between SF-SRS and MF-SRS (77.1% vs 92.9%, p=0.18). However, the incidence of RN in this group was considerably reduced following MF-SRS (23.1% vs 7.3%, p=0.003). Furthermore, in patients with resection cavities, the authors found no significant difference in the 1-year LC (only group B was assessed, 62.4% vs 85.7%, p=0.13) between SF-SRS and MF-SRS. The rates of RN were comparable, with no statistically significant difference (7.3% vs 7.5%; p=0.85). A small single-center retrospective study by Donovan et al. (24) looked at RN after SF-SRS (1×24 Gy) and MF-SRS (3×7 Gy). They included 22 patients with 62 BM and a median lesion volume of 0.67ml. There was no difference in the RN rate related to either the maximum dose (OR 1.0, 95% CI: 0.9–1.1), the fractionation scheme (OR 1.0, 95% CI: 0.3–3.6) or a prior WBRT (OR 0.4, 95% CI: 0.2–1.2). However, larger target volumes were associated with an increased risk of RN (OR 3.1, 95% CI: 1.0–9.6).

The dose applied to the 10 cc of healthy brain tissue is a valuable marker for RN. For single-fraction SRS brain volumes receiving 10 Gy and for three and five fraction SRT brain volumes receiving 20Gy and 30 Gy, respectively, have been shown to be predictive for symptomatic necrosis (25–27). In our study, we could not demonstrate any difference in12-month RN rates for the volume cutoff of 10cc with different fractionation schemes.

Our study revealed no difference in OS between SF-SRS and MF-SRS although our results for LFFS and RNFS contradicted those of the earlier studies. A recently published retrospective study by Ostdiek-Wille et al. (28) with a large number of patients, however, supports our results. In their examination of 6961 patients from the National Cancer Database, the median survival times did not differ significantly (10.9 months following SF-SRS and 11.3 months following MF-SRS [p=0.31]).

To our knowledge, no study has so far compared SF-SRS and MF-SRS for treatment of medium-sized resection cavities. We might anticipate an association between radiation dosage and LC for various fractionation schemes, according to a few data from retrospective studies (29–31). However, a recently published summary recommended SF-SRS of higher than 16 Gy or MF-SRS 3 × 8 Gy or > 27.5 Gy in 5 fractions to improve local cavity control (32).

Despite the benefit in terms of LC after postoperative SRS compared to surgery alone, the rate of leptomeningeal disease (LMD) is high and causes significant morbidity without an effective treatment opportunity (33). It is hypothesized that tumor seeding during surgical resection leads to leptomeningeal tumor spread. A few retrospective studies evaluated the efficiency of preoperative SRS in BM (34, 35). Recently, a meta-analysis by Dharnipragada et al. compared pre- and postoperative SRS in BM (36). Both groups were balanced with no significant difference in tumor size distribution. The results demonstrated a significant difference in the rates of local recurrence after one year, with 11% in the preoperative SRS group and 17.5% in the postoperative SRS group (p=0.014). Additionally, the rate of LMD was significantly lower in patients treated with preoperative SRS, with 4.4% vs. 12.3% (p=0.019). No difference was found in terms of RN and OS. Despite these promising results, the optimal fractionation remains undefined. Currently, randomized prospective trials investigating the role of preoperative SRS (37, 38). The results are awaited and could potentially have a significant impact on clinical practice.

The benefits of MF-SRS for treatment of medium-sized intact BM were not supported by the findings of our single-center retrospective study but our study had several limitations. First, due to our inclusion criteria, only a small patient group could be included in this retrospective analysis. Second, the recommendation for prescription of MF-SRS for larger BM has changed in recent years. Data collected in the past revealed a connection between BED and LC. According to Wiggenraad et al. (39), $BED_{12}$ for SRS in intact BM should be at least 40 Gy. Remick et al. (14) also showed an improvement in LC with a $BED_{10} \geq 50$ Gy. As stated by Minniti et al. (13) the current recommended scheme for MF-SRS in BM is 27 Gy in 3 fractions. In our investigation, either 30 Gy in 5 fractions ($BED_{12}$ = 45 Gy) or 24 Gy in 3 fractions ($BED_{12}$ = 40 Gy) was used in MF-SRS. The lower BED might be less effective and could lead to a lower LFFS. Third, our groups were not well-balanced, and the treated target volumes in the SF-SRS group were smaller than those in the MF-SRS group. Fourth, it is difficult to compare studies since

there is no definition of a medium-sized BM. Most studies assessed the BM size based on the diameter on axial MRI slices. Additionally, target volumes were substantially larger when an extra GTV to PTV margin was applied. In our opinion, only perfectly spherical lesions would be appropriate for this 2D assessment. We therefore used a 3D measurement to determine the BM size in accordance with the GTV. In contrast, no margin was provided to expand the GTV to the PTV in intact BM. For future research, a consistent definition of "medium-sized" BM is needed. Furthermore, the differentiation of LF and RN is challenging. Without a histological confirmation, the MRI-based findings could be misleading. According to our modification of the BT-RADS scoring system, lesions that scored 3b simultaneously showed characteristics of LF and RN. Therefore, the incidence of LC and RN in our analysis could have been overestimated. Additionally, there is a known limitation of using only conventional imaging in the differentiation between tumor and necrosis. The inclusion of advanced imaging could potentially be beneficial to distinguish RN from LF but was not feasible in our study.

Overall, there is so far no evidence from prospective trials evaluating SF- and MF-SRS in patients with medium-sized intact BM and resection cavities. Currently, two prospective trials are recruiting patients to answer this question (NCT05160818, NCT03697343).

## Conclusion

Our results showed no difference in LC or RN following treatment with SF-SRS and MF-SRS for intact BM. In patients with resection cavities, SF-SRS resulted in significantly better LC, without increasing RNFS.

## Data availability statement

The original contributions presented in the study are included in the article/Supplementary Material. Further inquiries can be directed to the corresponding author.

## Ethics statement

The studies involving humans were approved by Cantonal Ethics Committee Bern, Switzerland. The studies were conducted in accordance with the local legislation and institutional requirements. Written informed consent for participation was not required from the participants or the participants' legal guardians/next of kin in accordance with the national legislation and institutional requirements.

## Author contributions

PR: Conceptualization, Data curation, Writing – original draft, Writing – review & editing. UA: Data curation, Writing – review & editing. EU: Formal analysis, Visualization, Writing – review & editing. BS: Data curation, Writing – review & editing. PS: Data curation, Writing – review & editing. AH: Data curation, Writing – review & editing. EE: Conceptualization, Data curation, Writing – review & editing.

## Funding

The author(s) declare that no financial support was received for the research, authorship, and/or publication of this article.

## Conflict of interest

The authors declare that the research was conducted in the absence of any commercial or financial relationships that could be construed as a potential conflict of interest.

## Publisher's note



## Supplementary material

The Supplementary Material for this article can be found online at: https://www.frontiersin.org/articles/10.3389/fonc.2024.1333245/full#supplementary-material

## References

1. Nayak L, Lee EQ, Wen PY. Epidemiology of brain metastases. *Curr Oncol Rep*. (2012) 14:48–54. doi: 10.1007/s11912-011-0203-y

2. Lamba N, Wen PY, Aizer AA. Epidemiology of brain metastases and leptomeningeal disease. *Neuro Oncol*. (2021) 23:1447. doi: 10.1093/neuonc/noab101

3. Berghoff AS, Schur S, Füreder LM, Gatterbauer B, Dieckmann K, Widhalm G, et al. Descriptive statistical analysis of a real life cohort of 2419 patients with brain metastases of solid cancers. *ESMO Open*. (2016) 1:e000024. doi: 10.1136/esmoopen-2015-000024

4. Sacks P, Rahman M. Epidemiology of brain metastases. *Neurosurg Clinics NA*. (2020) 31:481–8. doi: 10.1016/j.nec.2020.06.001

5. Aizer AA, Lamba N, Ahluwalia MS, Aldape K, Boire A, Brastianos PK, et al. Brain metastases: A Society for Neuro-Oncology (SNO) consensus review on current management and future directions. *Neuro Oncol*. (2022) 24:1613–46. doi: 10.1093/neuonc/noac118

6. Aoyama H, Shirato H, Tago M, Nakagawa K, Toyoda T, Hatano K, et al. Stereotactic radiosurgery plus whole-brain radiation therapy vs stereotactic

radiosurgery alone for treatment of brain metastases: a randomized controlled trial. *JAMA*. (2006) 295:2483–91. doi: 10.1001/jama.295.21.2483

7. Chang EL, Rey J, Wefel S, Hess KR, Allen PK, Lang FF, et al. Articles Neurocognition in patients with brain metastases treated with radiosurgery or radiosurgery plus whole-brain irradiation: a randomised controlled trial. *Lancet Oncol*. (2009) 10:1037–44. doi: 10.1016/S1470

8. Kocher M, Soffietti R, Abacioglu U, Villà S, Fauchon F, Baumert BG, et al. Adjuvant whole-brain radiotherapy versus observation after radiosurgery or surgical resection of one to three cerebral metastases: Results of the EORTC 22952-26001 study. *J Clin Oncol*. (2011) 29:134–41. doi: 10.1200/JCO.2010.30.1655

9. Sahgal A, Aoyama H, Kocher M, Neupane B, Collette S, Tago M, et al. Phase 3 trials of stereotactic radiosurgery with or without whole-brain radiation therapy for 1 to 4 brain metastases: Individual patient data meta-analysis. *Int J Radiat Oncol Biol Phys*. (2015) 91:710–7. doi: 10.1016/j.ijrobp.2014.10.024

10. Palmer JD, Trifiletti DM, Gondi V, Chan M, Minniti G, Rusthoven CG, et al. Multidisciplinary patient-centered management of brain metastases and future directions. *Neurooncol Adv*. (2020) 2:1–17. doi: 10.1093/noajnl/vdaa034

11. Minniti G, Clarke E, Lanzetta G, Osti MF, Trasimeni G, Bozzao A, et al. Stereotactic radiosurgery for brain metastases: Analysis of outcome and risk of brain radionecrosis. *Radiat Oncol*. (2011) 6:1–9. doi: 10.1186/1748-717X-6-48

12. Shaw E, Scott C, Souhami L, Dinapoli R, Kline R, Loeffler J, et al. Single dose radiosurgical treatment of recurrent previously irradiated primary brain tumors and brain metastases: final report of RTOG protocol 90-05. *Int J Radiat Oncol Biol Phys*. (2000) 47:291–8. doi: 10.1016/S0360-3016(99)00507-6

13. Minniti G, Scaringi C, Paolini S, Lanzetta G, Romano A, Cicone F, et al. Single-fraction versus multifraction (3 × 9 gy) stereotactic radiosurgery for large (>2 cm) brain metastases: A comparative analysis of local control and risk of radiation-induced brain necrosis. *Int J Radiat Oncol Biol Phys*. (2016) 95:1142–8. doi: 10.1016/j.ijrobp.2016.03.013

14. Remick JS, Kowalski E, Khairnar R, Sun K, Morse E, Cherng HRR, et al. A multi-center analysis of single-fraction versus hypofractionated stereotactic radiosurgery for the treatment of brain metastasis. *Radiat Oncol*. (2020) 15:1–11. doi: 10.1186/s13014-020-01522-6

15. Yan M, Holden L, Wang M, Soliman H, Myrehaug S, Tseng CL, et al. Gamma knife icon based hypofractionated stereotactic radiosurgery (GKI-HSRS) for brain metastases: impact of dose and volume. *J Neurooncol*. (2022) 159:705–12. doi: 10.1007/s11060-022-04115-3

16. Gondi V, Bauman G, Bradfield L, Burri SH, Cabrera AR, Cunningham DA, et al. Radiation therapy for brain metastases: an ASTRO clinical practice guideline. *Pract Radiat Oncol*. (2022) 12:P265–82. doi: 10.1016/j.prro.2022.02.003

17. Paddick I, Lippitz B. A simple dose gradient measurement tool to complement the conformity index. *J Neurosurg*. (2006) 105 Supplement:194–201. doi: 10.3171/sup.2006.105.7.194

18. Weinberg BD, Gore A, Shu HKG, Olson JJ, Duszak R, Voloschin AD, et al. Management-based structured reporting of posttreatment glioma response with the brain tumor reporting and data system. *J Am Coll Radiol*. (2018) 15:767–71. doi: 10.1016/j.jacr.2018.01.022

19. Kano H, Kondziolka D, Lobato-Polo J, Zorro O, Flickinger JC, Lunsford LD. T1/T2 matching to differentiate tumor growth from radiation effects after stereotactic radiosurgery. *Neurosurgery*. (2010) 66:486–91. doi: 10.1227/01.NEU.0000360391.35749.A5

20. Hainc N, Alsafwani N, Gao A, O'Halloran PJ, Kongkham P, Zadeh G, et al. The centrally restricted diffusion sign on MRI for assessment of radiation necrosis in metastases treated with stereotactic radiosurgery. *J Neurooncol*. (2021) 155:325–33. doi: 10.1007/s11060-021-03879-4

21. Vogelbaum MA, Angelov L, Lee SY, Li L, Barnett GH, Suh JH. Local control of brain metastases by stereotactic radiosurgery in relation to dose to the tumor margin. *J Neurosurg*. (2006) 104:907–12. doi: 10.3171/jns.2006.104.6.907

22. Chon H, Yoon KJ, Lee D, Kwon DH, Cho YH. Single-fraction versus hypofractionated stereotactic radiosurgery for medium-sized brain metastases of 2.5 to 3 cm. *J Neurooncol*. (2019) 145:49–56. doi: 10.1007/s11060-019-03265-1

23. Lehrer EJ, Peterson JL, Zaorsky NG, Brown PD, Sahgal A, Chiang VL, et al. Single versus multifraction stereotactic radiosurgery for large brain metastases: an international meta-analysis of 24 trials. *Int J Radiat OncologyBiologyPhys*. (2019) 103:618–30. doi: 10.1016/j.ijrobp.2018.10.038

24. Donovan EK, Parpia S, Greenspoon JN. Incidence of radionecrosis in single-fraction radiosurgery compared with fractionated radiotherapy in the treatment of brain metastasis. *Curr Oncol*. (2019) 26:e328–33. doi: 10.3747/co.26.4749

25. Faruqi S, Ruschin M, Soliman H, Myrehaug S, Zeng KL, Husain Z, et al. Adverse radiation effect after hypofractionated stereotactic radiosurgery in 5 daily fractions for surgical cavities and intact brain metastases. *Int J Radiat Oncol Biol Phys*. (2020) 106:772–9. doi: 10.1016/j.ijrobp.2019.12.002

26. Upadhyay R, Ayan AS, Jain S, Klamer BG, Perlow HK, Zoller W, et al. Dose-volume tolerance of the brain and predictors of radiation necrosis after 3-fraction radiosurgery for brain metastases: A large single-institutional analysis. *Int J Radiat Oncol Biol Phys*. (2024) 118:275–84. doi: 10.1016/j.ijrobp.2023.07.040

27. Milano MT, Grimm J, Niemierko A, Soltys SG, Moiseenko V, Redmond KJ, et al. Single- and multifraction stereotactic radiosurgery dose/volume tolerances of the brain. *Int J Radiat Oncol Biol Phys*. (2021) 110:68–86. doi: 10.1016/j.ijrobp.2020.08.013

28. Ostdiek-Wille GP, Amin S, Wang S, Zhang C, Lin C. Single fraction stereotactic radiosurgery and fractionated stereotactic radiotherapy provide equal prognosis with overall survival in patients with brain metastases at diagnosis without surgery at primary site. *PeerJ*. (2023) 11:e15357. doi: 10.7717/peerj.15357

29. Brown PD, Ballman KV, Cerhan JH, Anderson SK, Carrero XW, Whitton AC, et al. Postoperative stereotactic radiosurgery compared with whole brain radiotherapy for resected metastatic brain disease (NCCTG N107C/CEC·3): a multicentre, randomised, controlled, phase 3 trial. *Lancet Oncol*. (2017) 18:1049–60. doi: 10.1016/S1470-2045(17)30441-2

30. Mahajan A, Ahmed S, McAleer MF, Weinberg JS, Li J, Brown P, et al. Post-operative stereotactic radiosurgery versus observation for completely resected brain metastases: a single-centre, randomised, controlled, phase 3 trial. *Lancet Oncol*. (2017) 18:1040–8. doi: 10.1016/S1470-2045(17)30414-X

31. Iorio-Morin C, Masson-Côté L, Ezahr Y, Blanchard J, Ebacher A, Mathieu D. Early Gamma Knife stereotactic radiosurgery to the tumor bed of resected brain metastasis for improved local control: Clinical article. *J Neurosurg*. (2014) 121 Suppl_2:69–74. doi: 10.3171/2014.7.GKS141488

32. Minniti G, Niyazi M, Andratschke N, Guckenberger M, Palmer JD, Shih HA, et al. Current status and recent advances in resection cavity irradiation of brain metastases. *Radiat Oncol*. (2021) 16:1–14. doi: 10.1186/s13014-021-01802-9

33. Johnson MD, Avkshtol V, Baschnagel AM, Meyer K, Ye H, Grills IS, et al. Surgical resection of brain metastases and the risk of leptomeningeal recurrence in patients treated with stereotactic radiosurgery. *Int J Radiat Oncol Biol Phys*. (2016) 94:537–43. doi: 10.1016/j.ijrobp.2015.11.022

34. Patel KR, Burri SH, Asher AL, Crocker IR, Fraser RW, Zhang C, et al. Comparing preoperative with postoperative stereotactic radiosurgery for resectable brain metastases: A multi-institutional analysis. *Neurosurgery*. (2016) 79:279–85. doi: 10.1227/NEU.0000000000001096

35. Prabhu RS, Dhakal R, Vaslow ZK, Dan T, Mishra MV, Murphy ES, et al. Preoperative radiosurgery for resected brain metastases: the PROPS-BM multicenter cohort study. *Int J Radiat Oncol Biol Phys*. (2021) 111:764–72. doi: 10.1016/j.ijrobp.2021.05.124

36. Dharnipragada R, Dusenbery K, Ferreira C, Sharma M, Chen CC. Preoperative versus postoperative radiosurgery of brain metastases: A meta-analysis. *World Neurosurg*. (2024) 182:35–41. doi: 10.1016/j.wneu.2023.10.131

37. Ginzac A, Dupic G, Brun L, Molnar I, Casile M, Durando X, et al. Preoperative stereotactic radiosurgery for brain metastases: the STEP study protocol for a multicentre, prospective, phase-II trial. *BMC Cancer*. (2021) 21. doi: 10.1186/s12885-021-08602-0

38. Das S, Faruqi S, Nordal R, Starreveld Y, Kelly J, Bowden G, et al. multicenter, randomized controlled trial of preoperative versus postoperative stereotactic radiosurgery for patients with surgically resectable brain metastases. *BMC Cancer*. (2022) 22. doi: 10.1186/s12885-022-10480-z

39. Wiggenraad R, De Kanter AV, Kal HB, Taphoorn M, Vissers T, Struikmans H. Dose–effect relation in stereotactic radiotherapy for brain metastases. A systematic review. *Radiother Oncol*. (2011) 98:292–7. doi: 10.1016/j.radonc.2011.01.011

# Frontiers in Oncology

**Advances knowledge of carcinogenesis and tumor progression for better treatment and management**

The third most-cited oncology journal, which highlights research in carcinogenesis and tumor progression, bridging the gap between basic research and applications to imrpove diagnosis, therapeutics and management strategies.

---

## Discover the latest Research Topics

See more →


**Frontiers**

Avenue du Tribunal-Fédéral 34
1005 Lausanne, Switzerland
frontiersin.org

**Contact us**

+41 (0)21 510 17 00
frontiersin.org/about/contact